RESIDUAL STRESSES AND HEAT TREATMENTS FOR METALLIC WELDED COMPONENTS.

ABDUL GHANI AL-OLABI
B.Eng., M.Eng.

SUPERVISOR

Prof. M.S.J.HASHMI

DUBLIN CITY UNIVERSITY

SCHOOL OF MECHANICAL AND MANUFACTURING ENGINEERING

PH.D **JANUARY 1994**

RESIDUAL STRESSES AND HEAT TREATMENTS FOR METALLIC WELDED COMPONENTS.

BY

ABDUL GHANI AL-OLABI
(B.Eng, M.Eng)

This thesis is submitted as the fulfilment of the requirement for the award of Doctor of philosophy to :

DUBLIN CITY UNIVERSITY

Sponsoring Establishment :

Dublin City University

January 1994

DECLARATION

I hereby certify that this material, which I now submit for assessment on the programme of study leading to the award of PhD in Engineering is entirely my own work and has not been taken from the work of others save and to the extent that such work has been cited and acknowledged within the text of my work.

Signed: 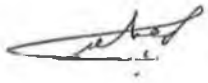

Candidate

Date: 7/1/1994

ACKNOWLEDGEMENTS

I would specially like to thank my **parents** who strongly supported and encouraged me to finish this thesis. This work is dedicated to them.

I would also like to express my appreciation to **Prof. M.S.J.Hashmi, Head Of The School Of Engineering** for his helpful supervision and guidance during the course of this project.

I would also like to acknowledge the help of the following: Mr. G.Dardes, Mr. G.Kenny and Mr. M.Fleming of EOLAS; Mr. L.MaCarthy, Mr. J.Walsh and Mr. G.Toyrrell in Airmotive Ireland; Prof. E.R.Petty, Dr. M.J.Pomeroy and Dr. R.Ramesh in University of Limerick; Mr. L.Domican, Mr. T.Walsh, Mr. S.Doherty and Mr. I.Hooper the workshop technicians in our School. I would also like to thank Ms. Lesley Lawlor for her help and patient.

Finally, I would like to thank all my friends who lent support and encouragement while the thesis was being written.

RESIDUAL STRESSES AND HEAT TREATMENTS FOR METALLIC WELDED COMPONENTS.

A.G.OLABI, B.Eng., M.Eng.

ABSTRACT

This investigation was carried out with the aim of studying the effect of Post Weld Heat Treatment (PWHT) on the microstructure and the mechanical properties of different types of metallic components. The objective was to reduce or eliminate the residual stress in these components without compromising the strength.

Two types of welded materials, AISI-410 and AISI-1020 were fully investigated. In order to optimize the heat treatment conditions, different PWHTs were applied by varying the soaking temperature, heating rate, soaking time duration and cooling rate.

To assess the effect of these different heat treatment schemes on the mechanical properties, micro-hardness, tensile strength and notched impact tests have been employed on these welded joints. Metallurgical testing has also been carried out to assess the change in the metal microstructure before and after the heat treatments.

A hole drilling method has been used to estimate the magnitude and distribution of residual stresses before and after applying these different kinds of heat treatments.

Finite element method has also been used to study the effect of residual stresses on these welded components. To carry out this work a finite element program LUSAS was employed with the objective of studying the effect of the length and width of the welding on the mechanical properties.

The results show that there is a substantial reduction in the residual stresses with a good improvement in the mechanical properties for certain schemes of PWHTs.

TABLE OF CONTENT

CHAPTER ONE

INTRODUCTION

1.1 WELDING (HISTORICAL AND TYPES)

Welding is the most important way to join metals. It is the only way to join two or more pieces of metal to make them act as one piece. Welding is widely used to manufacture or repair all products made of metal. It is defined by the American Welding Society, as a localized coalescence of metals. This coalescence is brought about by the application of heat, with or without the fusion, by the addition of filler metal or the application of pressure.

Since more than 2000 years, welding was used to join small gold boxes which were made by pressure welding lap joints. During the iron age it appears that the Egyptians and other people in the Eastern Mediterranean area learned to weld pieces of iron together. During the middle ages different articles were produced which were welded by hammering. However, it was not until the early 19th century that welding as we know it today was discovered and used. During this period, two types of welding were discovered, the first was by acetylene and the second was by the production of an arc between two carbon electrodes using a battery. The period of 1877 to 1903 provided a great number of discoveries pertaining to welding. During this period gas welding and cutting and arc welding with the carbon arc were developed and resistance welding became a practical joining process.

In 1892 the arc metal process using a metal electrode was discovered and in 1900 Strohmeyer [1] introduced a coated metal electrode in Great Britain. Meanwhile, the resistance welding process was developed including seam welding and spot welding. During the period from about 1900 to 1918 oxyacetylene welding and cutting processes together with carbon arc

welding and metal arc welding processes were used primarily for repair and maintenance work. In 1920 Automatic welding was introduced, during the 1920s various different types of welding electrodes were developed and used for different kinds of metals.

During the 1930s tungsten inert gas welding was discovered using atmospheres of argon and helium. Submerged arc welding was used in the late 1930s and early 1940s. In 1948 gas shielded metal arc welding was successfully developed. In 1950s the Co2 was used as an inert gas. Electroslag welding process was used in 1958 and electro-moulding process was used in 1959 for the fabrication of welded diesel engine blocks. The plasma arc welding process, which is very similar to gas tungsten arc welding was invented by Robert Gage [2] in 1957. The electron beam welding process, which uses a focused beam of electrons as a heat source in a vacuum chamber, was developed in the late 1940s. In the last few years the process has gained widespread acceptance for welding, its popularity is increasing since recent developments have allowed it to be used without any need for the vacuum chamber. The newest of welding processes is laser welding, it has been used for cutting metals also. Additional welding processes and methods will be developed and as the need arises they will be adapted to metalworking requirements.

Welding is now the universally accepted method of permanently joining all metals. In some respects, it might be considered a mature industry but it is still a growing industry. The true impact of welding on the metalworking industry should be measured in the value of the parts produced by welding, the amount of money saved by the use of welding over other metal fabrication processes, and in the value of products made possible by welding. The application of welding processes have many advantages on producing the welded structures, which can be summarized as:

1 - High joint efficiency: The joint efficiency is defined as the percentage of the fracture strength of a joint to the fracture strength of the base plate. The values of joint

efficiency of welded joints are higher than riveted joints, it can be as high as 100%.

2 - Water and air tightness: A welded structure is ideal for situations which require water and air tightness such as submarine hulls and storage tanks.

3 - Weight saving: The weight of a hull structure can be reduced by as much as 10 - 20% if welding is used.

4 - No limit on thickness: It is very difficult to rivet plates that are more than 2 inches thick. In welded structures there is virtually no limit to thickness that may be employed.

5 - Simple structure design: In welded structures, members can be simply butted together or fillet welded. In riveted structures, complex joints are required.

6 - Reduction in the fabrication time: A welded structure can be fabricated in a short period of time and be less costly than riveted structures.

On the other hand, there are still some problems with the application of welding processes in producing the welded structures, which can be summarized as:

1 - Difficult to arrest fracture: Once the crack starts to propagate in a welded structure, it is very difficult to arrest it.

2 - Possibility of defects: Welds are often plagued with various types of defects including porosity, cracks, slag inclusion,etc.

3 - Sensitive to materials: Some materials are more difficult to weld than others.

4 - Lack of reliable NDT techniques: Although many non-destructive testing methods have been developed and are in use today, some are completely satisfactory in terms of cost and reliability for specific application only.

5 - Residual stress and distortion: Because of the non-uniform heating during welding, residual stress and distortion result after welding, which may lead to cracking and mismatching.

1.2 RESIDUAL STRESS IN WELDING COMPONENTS

Residual stresses in a structural materials or components are those stresses which exist in the object without the application of any service or other external loads. Manufacturing processes are the most common causes of residual stress. Virtually all manufacturing processes e.g. casting, welding, machining, forging,... etc. introduce residual stresses into the manufactured object.

In welding, under the effect of a sharp and localized thermal transient the base metal undergoes during welding a complex pattern of thermal expansions and shrinkages of metallurgical and of mechanical origins arises.

These stresses are located in the welded joint and in its direct vicinity. Generally they reach a level close to the yield strength of the metal, an external constraint having or not occurred during welding. Under conditions of multi-axial loadings, they can result in the brittle fracture of a welded joint. The residual stresses cause cracking and mismatching. High tensile residual stresses in areas near the weld cause fracture under certain condition.

Thermal or mechanical treatments are needed to reduce or suppress the welding residual stresses and to provide protection against the risk of initiation and propagation of brittle fracture

and component failure. In addition, it protects against the tendency of metal corrosion, and also against the dimensional instabilities producing deformation during further working of the component.

1.3 CRACK IN WELDED COMPONENTS

Residual stresses contribute to weld cracking. The restrained contraction of welded structures during cooling sets up tensile stresses in the joint and may cause one of the most serious of weld defects, which is crack. Weld cracking will occur during manufacturing operation of the weldment or shortly after the weldment is completed. Cracking may occur in the weld deposit, in the heat affected zone, or in both of these regions. It is either of the gross type, which is visible to the naked eye and is termed macrocracking, or is visible only under the microscope, in which case it is termed microcracking or microfissuring. Cracking that occurs during the solidification of the weld metal is known as solidification cracking or hot cracking. Embrittlement of the parent metal or heat affected zone may result in subsolidus or cold cracking. In solidification cracking there are two necessary preconditions for the occurrence of cracking during the weld thermal cycle, the metal must lack ductility, and the tensile stress developed as a result of contraction must exceed the corresponding fracture stress. The mechanical properties of the metal in the region of the solidus are therefore important in relation to solidification cracking. In general, cracking may occur for many reasons and may occur years after the weldment is completed. Restraint and residual stresses are the main reasons for weld cracking during the fabrication of a weldment. Weld restraint can come from several factors, one of the most important is the stiffness and rigidity of the weldment itself. Another factor involved is the rapid cooling of the weld deposit, if the base metals being joined are cold and the weld is relatively small it will cool extremely rapidly. So shrinkage will occur quickly and cracking can occur. Another reason for cracking is the content of carbon and other elements in the base metal when the weld is made with higher carbon or high alloy base metal. During welding the base metal is melted and mixed with the electrode to produce the weld

metal. The resulting weld metal has a higher carbon and alloy content, giving it a higher strength but low ductility and as it shrinks it may not have sufficient ductility to cause plastic deformation and therefore cracking may occur. Another factor is the hydrogen pick up in the weld metal. In the heat affected zone of the base metal, the presence of hydrogen in the arc atmosphere will cause it to be absorbed in the molten metal. As the metal cools it rejects the hydrogen and if there is sufficient restraint, cracking will occur.

1.4 POST WELD TREATMENTS AND THEIR EFFECTIVENESS

Stress relief heat treatment is defined as the uniform heating of a structure at a suitable temperature, holding at this temperature for a predetermined period of time, followed by uniform cooling. Stress relief heat treatment is usually performed below the critical temperature range (before the transformation to austenite). The temperature and time for post weld heat treatment depend on the type of material. The percentage relief of internal stresses is dependent on the material type, composition, or yield strength. In general, the application of PWHT below the critical temperature Ac_1 (723 °C for AISI-1020 and 773 °C for AISI-410) produces softening of the base metal and can also have an influence more or less pronounced on the resistance to the brittle failure. However, the effects are very different according to the grades and qualities, on the one hand, and according to the welding conditions on the other hand. The PWHT is usually applied with the aim to achieve the following improvements:

* Stress relief.
* Minimizing the susceptibility to crack formation particularly under the conditions which call for high notch toughness.
* To improve the dimensional stability.
* To decrease the heat affected zone (HAZ) hardness by decomposition of martensite and other supersaturated structures.
* To increase the resistance to corrosion.
* To remove cold cracking.

When a thermal stress relief treatment is employed to reduce residual stresses, other important properties must be taken into consideration such as the microstructure, tensile and impact strength. Thus, it is necessary to select the heat treatment procedure which will develop the desirable properties in the material, while at the same time providing the maximum stress relief.

1.5 REVIEW OF METHODS FOR MEASURING RESIDUAL STRESSES

During the 1950s, many aspects about the measurement of residual stresses have been reviewed by a number of investigators [3-6].

During the past few decades these techniques have been further developed to provide an accurate estimation of the residual stress in different types of components. The following sections will describe different techniques which are used for measuring the residual stresses.

1.5.1 SECTIONING TECHNIQUE

Sectioning technique in conjunction with electrical resistance strain gauges is one of the oldest but still useful techniques for measuring residual stress in plates. The principle of this technique is based on the fact that if a portion of a residually stressed body is cut away and the resulting deformation of the body is carefully measured, then the residual stress which existed at the component surface can be calculated.

In this technique, electrical strain gages have to be mounted on the surface of the test piece. Then, by gradual machining, a small piece of metal containing the gauges is removed from the structure. In this method as the specimen is machined, the resistance of the gauges changes, and the magnitude of strain is determined by measuring the change in resistance.

Different types of strain gauges can be used in this technique including single element gauges and rosettes with two, three or four elements.

Many investigators [7-8] have reviewed and recommended this method. This method can be considered as a simple and accurate method. However, it is a destructive method and gives the average stress for the area of the specimen from which the piece was removed.
Other investigators [9-11] applied this method to study the residual stress in components produced by welding, forming and casting.

1.5.2 HOLE-DRILLING TECHNIQUE

The hole drilling method has become a popular technique for determining surface residual stress in components. This method has been proposed by Mathar 1934 [12] and developed by Soete [13] and Suppiger et al, [14]. The principle of this method is based upon the fact that when a small hole is drilled in a plate the residual stress in areas outside the hole are partially relaxed. Residual stress that existed in the drilled area can then be determined by measuring the amount of stress relaxation that takes place in the area surrounding the drilled hole.

In this method, a special purpose strain gauge rosette is attached to the component at the point of interest, and then a small hole is produced into the component through the centre of the rosette. The production of the hole in the stressed components causes a stress relaxation in the area around the hole, which can be detected and measured by the surface mounted strain gauge rosette. Then the principal residual stresses and their directions can be computed by using appropriate equations. Many studies [15-19] have been carried out to modify and simplify these equations.

Other studies have been undertaken to investigate the effect of different parameters on this method. Chow and Cundiff [20] and Flaman [21] studied the effect of the drilling speed and

force on the results, these studies point out that with higher drilling speed and lower force one can get better results. Niku-Lari et al, [22], Flaman and Manning [23] and Flaman and Boag [24] studied the relation between the hole depth and the total relaxed strains.

In fact, the accuracy of this method is an important point, which has been studied by Bynum [25], Kabiri [26-27] and Wang [28-29]. These studies indicate that the hole drilling method gives accurate results with a tolerance of $\pm 4\%$, which can be considered as an acceptable value.

This method can be considered as a semi destructive method where a little damage could be caused to the test component but at the same time, this method must be used with utmost care. More detailed discussions about this method and its theory are given in chapter three.

1.5.3 X-RAY DIFFRACTION METHOD

This is one of the most widely used methods for evaluating residual stresses in components. The early articles have been written by Norton and Rosenthal [30-31] in 1944 about the application of x-ray diffraction method for measuring residual stresses nondestructively.

This method is based on the fact that the elastic strains in metals that have crystalline structures can be determined by measuring the lattice parameter (spacings between crystallographic lattice planes which are caused by stress) where the lattice parameter of the metal in the unstressed state is known or can be determined.

In general, when external or internal forces are applied to a structure made up of metallic crystals, the crystalline lattice is distorted, thus changing the interatomic distances when the deformation exceeds the elastic limit. Plastic deformation takes place as a result of slipping between the lattice planes. The change in the interatomic spacing is always directly proportional

to the stress. Due to the fact that the wavelengths of x-rays are of the same general order of the magnitude as the atomic spacings in metallic crystals, the short wavelength of x-ray makes it possible for the rays to penetrate the crystalline lattice to some extent and be reflected back from the atomic planes which they have penetrated.

More developments and new instruments [32-34] have been introduced during the last ten years which made this method more suitable for applications of residual stress measurements. Many investigators [35-36] have used this method for measuring residual stress, and satisfactory results have been obtained.

This method has wider applications auspiciously for the measurement of residual stresses in complicated shaped components. However, it needs considerable amount of time to measure the residual stress at each point, and hence is very tedious and likely to be inaccurate [37], especially in situations where high temperatures have distorted the atomic structure of the material.

1.5.4 NEUTRON DIFFRACTION METHOD

The early report about this method has been published in reference [38]. Many investigators [39-40] have developed and reviewed this method. The neutron diffraction method is very similar to the x-ray method for residual stress determination in that both measure the change in spacing between planes of atoms reflecting the neutron or x-ray beam. The change in spacing gives the strains in certain defined directions in the specimen and these, by use of appropriate material constants, are converted into corresponding stresses.

In neutron diffraction method much greater penetration (approximately 30 mm for steel) is possible, which makes this by for the best method for measuring the residual stress in the depth of the components. On the other hand, the resolution of the neutron diffraction [40] is not

as good as that of the x-ray diffraction. Authors of references [41-42] have used this method to measure the residual stresses which are present in components manufactured by different processes e.g. welding and forging.

1.5.5 ULTRASONIC METHOD

This method is based upon the principle that the velocity of sound waves in a metal component change when stresses are applied to the component. Hsu and Schse [43] have reviewed this method as an advanced non - destructive method for measuring residual stress. The only limitation for this method is that the metallurgical texture can affect the results.

Many developments have been made by Heyman [44], Hsu [45], Dike and Johnson [46] which suggest that significant improvement can be achieved in the application of this method. During the last few years more investigations have been carried out which increase the capability of this method for measuring the residual stress in the components.

1.5.6 BARKHAUSEN NOISE METHOD

Barkhausen noise method is a magnetic and completely non destructive method for measuring residual stress in components. In 1970, Pashley [47] published the first article about the application of this method for evaluating residual stress. During the past few years many developments [48, 49] have been made to improve the application of this method.

The principle of this method is that when a ferromagnetic is subjected to a magnetic field it becomes magnetized in a rapid series of tiny steps. These discontinuous changes in magnetization can be monitored with a sensitive electromagnetic detector. This measured signal, called Barkhausen Noise is influenced by the stresses in the materials. This method can be considered as a non-destructive and easy method to use. On the other hand, it is limited to

ferromagnetic materials and also the thickness of the materials may affect the results. This method has been used to measure the residual stress for different types of components. References [50, 51] present some results of measuring the residual stresses for different components.

1.6 REVIEW OF PREVIOUS WORK

1.6.1 MECHANICAL PROPERTIES AND THE APPLICATION OF PWHT

A large number of investigations have been carried out to study the effects of different parameters on the welded components. Many studies were carried out to evaluate the residual stress on the welded parts. Other studies were concerned on the application of the different types of treatments (mechanical and thermal) to reduce or diminish the residual stresses in the welded components. Many studies were also made to investigate the effect of post weld heat treatment (PWHT) on the reduction of the residual stress.

Vinokurov [52] discussed the mechanical aspect of stress relieving by heat treatment and non-heat treatment. He found that the heat treatment is the most effective method for relieving the residual stresses in the welded components. The post weld heat treatment has two aspects, first, relieving the negative stresses effect and second, improving the mechanical properties.

Krishnan and Rao [53] have studied the effect of PWHT on microstructural changes and ferrite content in austenitic weld metals. They applied three different heat temperature 600, 800 and 1000 °C and three different duration time 1, 10 and 100 hours. They used two different welding processes TIG and SAW. The results showed that the PWHTs and the heat input have affected the shape of the ferrite network, and the network transformed to globules in some of the PWHT conditions.

Bmankirski [54] has investigated the mechanical properties for welded joint on 20K sheet plate [GOST 5520-69] 40 mm thick. He has compared these properties under three conditions, (1) initial condition, (2) tempering [heating temperature 625+10°C, holding time 2 hrs, cooling in air], and (3) after vibration treatment [which was carried out at the resonance frequency of 24-32 Hz for a time of 20-25 min]. Welding was carried out by manual arc-welding process. The result detected that tempering reduced yield strength and hardness but increased impact toughness. Vibration loading resulted in slight increase of strength and reduced ductility.

Zhou [55] did an investigation which aimed to improve the mechanical properties of 2Cr13 steel welded joints and to avoid the distortion and welding crack. The mechanical properties tests have been applied on six different types of deposit metal. Different types of preheating temperatures have been used. The results show that the impact toughness of the welded joints decreases with the increase of the preheating temperature.

In reference [56] the author investigated the mechanical strength and fracture mechanics of [Crack Tip Opening Displacement] of welded joints. He used Submerged Arc Welding, the base metal was a modified steel TT St E36, the initial plate thickness was 60 mm and a wire electrode of type S3 was used. The welds were examined in the as-welded state and after stress relief annealing (570°C for 2.5 hrs). The investigation involved comparison between the tensile strength, yield strength, hardness, and impact energy for the plates and pipes before and after heat treatment. The paper also has discussed the characteristic of the heat affected zone in the welded component. The results show that in all cases, comparably lower fracture toughness characteristic values were obtained for the heat affected zone.

Akhtar [57] carried out an investigation to study the effect of different welding parameters which could lead to optimize the structural integrity of weldments made from 13/2 and 13/4 martensitic stainless steel base metals with austenitic 15/25 and a 50 per cent cobalt containing weld metals. He investigated the effect of weld metals and other different welding

variables such as, pre-heat, PWHT and heat input on the mechanical properties. Different mechanical tests have been carried out e.g. hardness variation, tensile strength, impact energy and corrosion fatigue for all these above conditions.

Salkin [58] reviewed the ideas and codes on stress relief heat treatments of welded components. The major points in his study are that the residual stresses are located in the welded joint and in its direct vicinity. Generally, reach a level close to the yield strength of the metal with or without constraint having occurred during welding.

The stress relief heat treatment generally, produces a softening of the base metal and can also have an influence on brittle fracture resistance. The stress relief heat treatment has a negligible effect on the coarse grain structure. Also, the residual stress heat treatment allows an increase of the endurance limit ranging from 10 - 15%. Also, he studied the effect of welding process which might have a high energy input. There is no evidence about any improvement as a result of the high energy input.

Adoyan, et al. [59] used a new form of specimen to assess the effect of welding technology and all types of external loading on the distortion of the structure. They used a disc shaped specimen which was made of St3 steel for a range of heat treatment temperatures between 250°C to 600°C for 3 hrs. The efficiency of stabilisation of dimensions by low temperature heat treatment (250°C) in distortion caused by the relaxation of the residual stresses is almost identical with that achieved in high temperature tempering (600°C).

Evans [60-67] did a series of investigations to study the effect of different parameters on the microstructure and properties of C-Mn welded metal deposits.

In reference [60], he investigated the effect of stress relieving on the microstructure and properties of C-Mn as welded metal deposits using different contents of C and Mn. Sixteen

different metal deposits have been used, all specimens were stress relieved at 580°C for 2 hrs. To evaluate the effect of stress relief heat treatment the investigator examined the metallographic and mechanical properties [hardness, tensile strength, impact]. The results show that this heat treatment has improved the notch impact and reduced the hardness and the tensile strength.

Evans [61-63] also studied the effects of Carbon, Silicon, Sulphur and Phosphorus on the microstructure and properties of C-Mn steels. Different kinds of testing have been carried out to evaluate the effects of C, Si, P, S on hardness, tensile strength, impact and metallography structure by changing the content of those elements C [0.05 - 0.15%], Si [0.20 - 0.90%], S [0.007 - 0.046%], and P [0.007 - 0.040%]. Heat treatments have been applied and all the above testings were carried out on specimens before and after heat treatment.
The results of these testings show that the hardness and tensile strength have increased by increasing the Carbon percentage. Whilst, the impact energy decreased. Also, by increasing the Phosphorous and Silicon percentage the hardness and the tensile strength have increased without any significant change on the impact energy. Whilst, the hardness, tensile strength and impact energy have decreased by increasing the Sulphur percentage.

In reference [64] he studied the effect of heat input on the microstructure and properties of shielded metal arc welding. The metallographic studies revealed that the structure of as deposited weld metal changed as heat input was increased. It was found that an increase of the bead size was accompanied by a decrease in the amount of acicular ferrite and a general coarsening of the microstructure. The tensile properties were reduced by increasing the heat input, and an optimum impact properties were achieved at approximately 2 KJ/m.

Evans, in reference [65-67] studied the effect of different factors on the microstructure and mechanical properties, he studied the effect of the interpass temperature, the electrode diameter and the welding position.

Toshioka [68] has reviewed the heat treatment deformation and residual stress which would be a result of some types of heat treatments.

In reference [69] the results of investigation on post weld treatments of steel pressure vessels were reported. The author described the conditions of applied heat treatment according to different regulations [Dutch, French, U.S, Japan]. He also mentioned all other kinds of treatments which are possible to affect stress relief in pressure vessels.

Another study has been undertaken by Bosansky, et al. [70] to investigate the effect of Niobium (Nb) and the influence of Molybdenum (Mo) on weld toughness as a function of stress relieving heat treatment. Different percentage of Niobium with and without Molybdenum with different conditions of stress relief heat treatment (different temperature and cooling time) were looked at, and good result was obtained for heat treatment at 580°C for 1 hr. Hardness measurements and Electron microscopy were used to define the difference between all the above conditions.

Fidler [71] investigated the influence of heat treatment on the residual stresses of AISI 316 welded components. He applied different types of heat treatments, four different soaking temperature 650, 750, 850 and 1050 °C and three different duration time 1, 10 and 100 hours. The results show that there is a sufficient reduction in the residual stresses after applying PWHT for 1 hours at 650 °C.

Other investigation has been carried out by Ito et. al. [72] to study the effect of chemical composition, cooling rate during welding, pre and post weld heat treatment on the toughness of the welded joint.

The author in reference [73] has reviewed the metallurgy of heat treatment of welded joints. He studied the effect of different type of stress relieving heat treatment for C-Mn steels.

His paper includes a comparison between the hardness variation for as welded and heat treated conditions. Also it included a comparison for the notch toughness of different heat treatment conditions. The results show that the most improvements in the microstructure and mechanical properties can be obtained by applying heat treatment with soaking temperature of 550 to 700°C.

Vitek et.al. [74] studied the microstructure of Fe-3Cr-1.5Mo-0.1V of thick section welded plates (102 mm thick). Electron beam welding has been used to carry out the welding. An optical and electronic microscope have been used in this testing. The structure varied between bainite and ferrite and after PWHT the microstructure was mostly tempered bainite.

Gauzzi and Missori [75] investigated the microstructural transformations in austenitic ferritic joints. They carried out hardness tests across the welding specimen in the as-welded condition and in the as-welded-tempered condition. Different types of pre-heating and PWHTs have been made for different types of filler metal.

Other investigation has been carried out by Takemoto et. al. [76] to study the effect of post weld cooling method (PWC) and PWHT on stress corrosion crack (SCC) of butt welded pipes of AISI 304. Stress relaxation method has been employed to estimate the residual stresses in the welded pipes. Comparisons were made between as welded conditions and after PWHT and PWC to assess the value of stresses which will cause the SCC. These comparisons also included the effect of the pipe diameters and thicknesses. The results show that there is a good improvement in the welded component after the application of PWC treatment.

Farrar [77] investigated the nature and kinetics of the phase transformation of metastable of delta-ferrite in two duplex stainless steel of the deposit metal. A microstructure testing has been carried out for these types of metals for as welded condition and after the application of two different schemes of PWHTs, at 700°C for 15 hrs and at 850°C for 8 hrs.

Zubchenko, et al. [78] investigated the effect of temperature and time conditions on hardening welded joints in 15Kh2MFA and 15Kh2NMFA steels and of their relaxation resistance. They also investigated the effect of temperature and heating time on the relaxation process of residual stresses in heat treatment. Different reheating temperatures were used, and the investigator looked into the relation between the chemical composition and the time duration.

Mashinson, et al. [79] carried out an investigation to study the impact toughness of high frequency of pipes welded joints of St-52 produced by controlled rolling and welding by high frequency welding. Heat treatment at 820-840 °C was carried out, a partial recrystallisation and equalisation in the HAZ has been obtained by the application of this heat treatment. The metal was completely recrystallised by heat treatment of 930-950 °C. In both conditions, it was possible to ensure stable impact toughness values of 20 J/cm^2.

Gill and Gnanamoorthy [80] investigated the effect of alloy composition on the transformation kinetics of delta ferrite in AISI 316 stainless steel weld metal. They found that the transformation kinetics of delta-ferrite depend mainly on the carbon content of the weld metal.

1.6.2 THE APPLICATION OF SPECIFIC TYPES OF TREATMENTS

A number of papers reported the effect of vibrational treatment on the residual stress as a new method which has some advantage. In reference [81] the results of a study on the application of vibratory stress relief process, instead of the heat treatment, has been reported. In this the author described it as a method of applying controlled low amplitude, low frequency vibrations in metal components to obtain dimensional stability and to control machining tolerances. This process has many advantages. It is an economical, fast and convenient method of reducing stress and is used during processing without causing metallurgical changes, movements, oxidation or scaling.

A vibratory stress relief system consists of a small electrically operated vibrator, an accelerometer to transmit the degree of vibration to a resonance readout, a motor control to speed up or slow down the rate of vibration, and r.p.m readout and an ammeter. The author mentioned the advantages and limitations of this process of treatment, and reported that most applications which require vibration take 10 to 20 min and use an average of 1/2 kW of power and the typical frequency range is 20 to 90 Hz. The application of the vibratory process has eliminated 68 percent of the thermal stresses developed during welding, assuring dimensional stability with the same degree of accuracy.

Olenin, et al. [82] have studied the effect of vibration treatment on reducing the residual stresses especially when the heat treatment can not be used or when the work piece is too large. In this paper the residual stress relief was determined on specimens of St3 steel in the form of sheets 300 mm long, 20-40 mm wide, and 2 mm thick. The reduction in residual stress was 50-55% and the duration of vibrational treatment in the optimum conditions was 20-25 min.

Thomas [83] gave a general idea about using vibration method for stress relieving. He called this method as Meta Lax. In this paper he described this method and how it works. This process is applicable to most kinds of the metals except copper and copper alloys. He also outlined the advantages of this process. Keller [84] also described the vibration method and their advantages.

Another work has been carried out by Merun and Olenin [85] to show that hydraulic treatment makes it possible to reduce the residual welding stresses by 50 - 70% for specimens produced from low carbon steels.

Hrivnak and Yushchenko [86] reviewed the principles of different types of mechanical stress-relief treatments. In their paper they discussed the effectiveness of these different methods of treatment, which could provide a high percentage of stress relief. Their studies concluded that

the mechanical stress relief treatment can not replace the heat treatment for its advantages in providing stress relief and improving the microstructure and mechanical properties of the welded components.

Many studies have been carried out to study the effectiveness and the designing of local heat treatment system. Bikur et. al. [87] developed a flexible water cooled inductor for local heat treatment, which would be applied for large welded structure. They described very briefly the design of this system. A very good saving in the energy and materials as the result of applying this type of heat treatment have been obtained.

Korol'Kov [88] studied the local heat treatment of welded joints in large spherical tanks with capacity of 2000 m^3 for the storage of liquid Ammonia. These tanks are fabricated from low alloy Silicon-Manganese steel 09G2S. The heat treatment procedures were by heating up to 600 - 650 °C at a rate of 200 °C/h holding at this temperature for 1 h and cooling to 200 °C at a rate not more than 150 °C/h. Then it kept to cool in the air. The residual stresses have reduced 3-4 times after the application of the above heat treatment. The temperature was monitored by using a thermoelectric transducer mounted on the welded seam. The local heating has been insulated with MVT mats of 80 mm thickness.

Another investigation [89] carried out in Russia to study the effect of heat treatment on the level of the residual stresses the authors applied two types of heat treatments on specimens of 100 mm thickness. The first type of heat treatment was by holding the specimen at 1050 °C for 2.8 hours with air or water cooling followed by stabilizing at 800 °C for 14 hours. The second type is tempering heat treatment by holding the specimen for 10 hours at 480 °C. Stress relaxation by sectioning method has been used to accomplish the residual stress measurements in this specimen. The results show that there is a good reduction in the residual stress after the second type of heat treatment, whilst the first type of heat treatment has slightly reduced the residual stresses in this specimen.

1.6.3 RESIDUAL STRESSES IN WELDED COMPONENTS

A number of researches have been carried out to study the residual stresses in the welded component and their effect, especially, in the HAZ. An investigation has been carried out by Wilson, et al. [90] to study the residual stresses and ductility in the welded structures. A series of specimens with two different sizes 5x7/8 in and 12x5/8 in have been used, each consisting of two plates connected with a longitudinal butt weld.

The residual stresses in the plates were determined by the relaxation method, it was found that the stresses in the HAZ were of the order of the yield point of the unaffected base metal. Also, they found that the welded specimens had a slightly higher ultimate strength and yield point and lower elongation and reduction of area than plates without welds.

Simpson [91] carried out experimental work to study the residual stress for AISI 304 stainless-steel pipe weldments. Two different methods have been employed to measure the residual stress, blind hole-drilling method and layer removal method.

Other investigation [92] has been carried out to estimate the temperature distribution generated during the arc welding of both the A36 steel and 6061 T6 aluminum structures. In this study, he determined the distribution of the heat temperature during welding along and across the welding line and in the depth of the specimen, for both types of metals.

Lamb, et al. [93] investigated the residual stresses in two laser surface melted stainless steels of AISI 316 and AISI 420. the residual stresses were measured by X-ray diffractometry. They applied stress relieving heat treatments. The results show that there is a great reduction in the residual stresses after applying the heat treatments.

Berghaus [94] investigated the residual stresses at small diffusion welds, of small stainless

steel tubes. The welding was carried out by employing diffusion welding. The residual stresses were measured at different points around the welds and the comparison was made between different weld current. He used the hole-drilling method and the sectioning method for measuring the residual stresses in these components.

Thomas [95, 96] reviewed the heat affected zone cracking in the austenitic stainless steel. In the first part of this review, he discussed the different types of HAZ cracks. In the second part, he reviewed and discussed the effect of welding variables, PWHTs and the composition on the HAZ crack. He also discussed the effect of other factors (strain, diffusion, grain size and back filling) on the HAZ crack.

An investigation [97] has been carried out at the University of Tenessee by Lundin, et al. to determine the stress relief cracking susceptibility of Cr-Mo alloys ranging in composition from 2.25Cr-1Mo to 12Cr-2Mo. Two heat treatment temperatures of 620 and 680 °C have been applied, the results showed that the higher chromium materials are not susceptible to stress-relief cracking, and by lowering heat treatment temperature and increasing the C, Si, V, P and Ti the susceptibility of the stress relief cracking is increased.

Leyda, et al. [98] have studied the stress rupture properties of different kinds of stainless steel welded components. They investigated the effect of PWHTs and welding processes on the stress rupture properties for 1.25Cr-0.5Mo, 2.25Cr-1Mo, stainless steel type 308 and Inconel 182.

Different studies have been carried out to develop a mathematical theory of heat distribution and residual stress valuation. An early research has been carried out by Rosenthal [99] to develop a mathematical theory of heat distribution during welding and cutting.

Masubuchi, et al. [100] did a series of investigations at M.I.T. to develop basic computer

programs which can be used for analysis and control of distortion of welded structures. They developed a computer program for studying the thermal stresses and metal movements during welding. One and two dimensional finite element programs have been developed. Experimental data were compared with analytical predictions by the one and two dimensional finite element programs. The results of this study showed that the simple 1-D program has proved to be adequate.

Tall [101] applied a numerical method to calculate the residual stresses produced in the individual plates due to welding. This computional method predicted results which are closer to those obtained by experimental method.

Due to the fast development and successful demonstration of the computer during the past few years, more research has been carried out to estimate the residual stress by the analytical solution especially, by using the finite element method. Lindgren [102] did a simulation of butt-welding of plates. An analytical technique was applied to study the temperature fields and the residual stresses. The thermal material properties were assumed to be independent (of the time) in the analytical solutions. The results of these analytical solution were similar to the results which have been obtained by finite element method.

Goldak, et al. [103] investigated the application of three dimensional finite element method to study the residual stress in butt-welded components. In their study they assumed that the geometry of half of the welded component is 10.16 x 10.16 x 1.27 cm and the material was carbon steel. The results show that the maximum value for the longitudinal stress is about 500 MPa.

Muraki, et al. [104, 105] studied the thermal stresses and metal movement during welding. They developed a finite element program to analyze these thermal stresses and carried out experimental work to study the residual stresses using 6061-T6 Aluminum alloy. Good

agreements were obtained between the experimental and analytical results.

Van Gulick [106] has applied the finite element method to study the residual stresses in the welded components. He used general purpose finite element program "ABAQUS 4.5".

Agapakis and Masubuchi [107] have developed one dimensional model finite element technique to study the distribution of the residual strain and stress after welding. They compared these analytical predictions by the experimental testing to the distribution of the residual stress for 304 stainless steel and HY-130 high strength steel. The experimental results show that there is a good correlation with the analytical predictions.

Kassmaul, et al. [108] studied the temperature distribution and the residual stresses for welded specimen of KS02. They determined the temperature distribution by both experimental and numerical calculation by using finite element package [Smart] to study the temperature and residual stress distribution. The results were in quite good agreement considering the high cost of the computing, which would be reduced with more improvement of the personal computer.

Majorana, et al. [109] presented the procedure for the determination of the thermal and the mechanical stress fields in steel welding processes. A finite element method has been employed to study the residual stresses at high temperatures and during solid-liquid phase change. They compared the numerical results with the experimental results and good agreements have been obtained.

Ramamurti, et al. [110] investigated the residual stresses caused by welding. They estimated the residual stresses through a blend of experimental and theoretical approaches. They assumed that the residual strain is a plane strain. They estimate the residual stresses through the thickness by applying the first experimental value on the surface in the program data. They got a good agreement compared with other studies.

Tam, et al. [111] investigated the transient temperature distribution using finite element method. The results have been compared with those obtained using the commercial package PAFEC. The two sets of results were found to be in good agreement.

Argyris, et al. [112] applied the finite element method to study the heat flow mechanisms during arc welding of a rectangular steel plate.

As mentioned in the previous section, in the aspect of the determination of the residual stresses, different experimental methods have been established in the 1930s and they have been developed during the years to reach a very high level of adequateness and accuracy for carrying out this measurement. Mordfin [7] reviewed different methods of measuring residual stresses in manufactured articles and assembled structures. He referred in his paper to the programme of research and development to upgrade the reliability and reproducibility of residual stress measurement methods which has been carried out by the National Bureau of Standards (NBS). This study includes a discussion of details about residual stresses and about the different methods of measuring the residual stresses.

Rudd, et al. [34] applied three different residual stress measurement methods (hole-drilling method, x-ray diffraction method and Barkhausen method) to evaluate the residual stress on a mild steel bar. The results of this study showed that the hole-drilling method and x-ray diffraction method were in a good agreement. The absolute residual stress measurements by Barkhausen method were not possible due to the lack of a suitable zero-stress standard for this method, because of the effect of microstructure on the results.

Misra and Peterson [113] applied the sectioning technique for measuring residual stresses. In their paper they described the application and procedures of this method and they obtained the metal constant to calculate the residual stress value. They recommended this method as an accurate method for measuring residual stress in the different types of mechanical components.

In 1961 and 1962 Crites [114] published four papers about the stress analysis technique. In these paper he concentrated on the equipment and the application of the strain gauges. He went through the principle of the strain gauge and gave details about different kinds of connection circuit. The principal equations to calculate the uniaxial and biaxial strains have been derived.

In other paper [115], Crites demonstrated the different types of strain gauges and their application. The different basic techniques and materials which are needed to attach the strain gauges on the component have been demonstrated.

Wenski [116] did an experimental study to develop and calibrate a small strain gauge which can be used to measure the strain in very small and tiny area.

Lorentzen [40] has studied the neutron diffraction method for evaluating residual stresses in different types of component. He explained this method and gave a detailed discussion about its theoretical background.

Cheong and Marcus [117] reviewed different residual stress measurement methods which can be applied to measure the residual stress in composite materials. Their studies concluded that at the present time the x-ray diffraction method could be one of the most effective and reliable techniques for the residual stress measurement in composite materials.

Kashiwaya, et al. [49] reviewed the magnetic method for measuring the residual stress. They explained the magnetic anisotropy sensor (MAS) which is used in this method, some experimental results have been demonstrated which show that the magnetic sensor method might be a good and promise method. The major problems in this method are: first, the magneto stress susceptibility varies with the quality of material, and second, the biaxial tensile stress is not able to be measured.

In reference [42] the author gave full detailed discussion about neutron diffraction method. This method could be a very effective method for measuring the residual stresses especially in the depth of the objects.

Dowling, et al. [35] used a compact and portable x-ray stress analysis system equipped with a position sensitive proportional counter (PSPC) for measuring residual stress in notched fatigue test specimen for two types of metals (Aluminum and Titanium).

Eignmann, et al. [36] reviewed the application of x-ray diffraction method for the determination of residual stresses in ceramics and ceramic-metal composites.

Peck [37] studied the different variables in measuring residual stress by x-ray diffraction method. The results of this study can be concluded in that the measurement of surface residual stress by x-ray diffraction method is a proper technique to meet the needs of speed and precision. He presented the method of calculation, selection of set up equipments and choice of materials constants.

Titto [51] studied the Barkhausen method for measuring the residual stress. His paper includes detailed discussion about this method. Also he demonstrated some example to evaluate the residual stress in different types of components.

Karjalainen, et al. [50] investigated the application of Barkhausen noise measurement for evaluating the residual stresses in welded component. Their studies pointed out that the determination of absolute stress magnitudes seems difficult to achieve by this method.

1.6.4 THE DEVELOPMENT OF THE HOLE-DRILLING METHOD

The hole-drilling method was first proposed by Mathar [12]. He designed a special

mechanical equipment to apply this method, the hole was drilled in the area where the residual stress existed and the residual stresses were computed after measuring the distance change of some points around the hole by using an extensometer. A special calibration has been done to reach the proper value of the expecting residual stress. He applied this process on different type of structures which have residual stresses. This method has been recommended by Mathar to measure the residual stress as a new measurement method.

Soete [13] applied the hole-drilling method which had been proposed by Mathar. He developed this method by using the strain gauges instead of the extensometer for measuring the residual stresses. Different experimental testings have been carried out by using this procedure. He proposed different investigations to be done to develop and improve this method.

Many investigations have been carried out to develop this method. Rendler and Vigness [15] carried out experimental work to determine the material coefficients relevant to the principal residual stresses and their directions. They measured the residual stress in elastic materials, and were able to determine the magnitudes and principal directions of residual stresses at the hole location of the measuring point.

Lake, et al. [118] investigated the application of the hole-drilling method for measuring the residual stresses in orthotropic materials such as Fibreglass. They found that this technique can successfully be used for the hole depth to diameter ratio of up to unity.

Gupta [16] modified the equation to calculate the correct angle of the principal residual stresses. He applied this calculation in the determination of the directions of the resultant bearing loads in a crankshaft.

Bush and Kromer [18] investigated the accuracy of the hole-drilling stress measurements without performing prior calibration tests. They simulated residual stresses which were introduced by applying known stresses to steel and aluminum bars. These known stresses were

then compared with those measured using hole-drilling method. They used both the conventional drilling technique and the abrasive jet machining. The results show that without doing the calibration for the new specimen the results would be very acceptable by using the abrasive jet machining.

Nawwar, et al. [17] did some modification for the hole-drilling technique for determining residual stresses in thin plates. They applied this technique to measure the residual stresses in 1.27 and 3.17 mm thickness of Aluminum alloy specimen. It has been found that the accuracy of this technique for thin plates is in the range of $\pm 5\%$ or better.

Sandifer and Bowie [119] investigated the accuracy of the hole-drilling method using hand drilling. They found that the accuracy will be in the range of ± 4 microstrain. Also they found that the off centre hole can be calculated. Also this study pointed out that there are many factors which might effect the results such as gauge application, coating techniques, material and machining.

Schajer [120] has used finite element program to determine the materials constants. It seems possible to calculate these constants for different materials. He compared these analytical results with other experimental results carried out by other investigator. The results of the analytical and experimental results were in a good agreement with a difference of 5% in some cases.

Bynum [25] studied a number of factors (drilling procedure, the hole size and shape) which can have an influence on the accuracy and reliability of the hole-drilling technique. Also, he demonstrated the different equations to calculate the principal stresses and their directions.

An investigation was carried out by Flaman [21] to measure induced drilling stresses in the centre hole method of residual stress measurement. He studied the effect of the drilling speed

on the measurements. A comparison between the low speed end mill and ultra high speed drill was made. The results show that the ultra high speed drill would be much superior to the conventional low speed end mill in the measurement of the residual stress by the centre hole method.

Procter and Beaney [19] discussed in their paper the developments of hole-drilling method. They studied the effect of different factors (hole diameter and depth and the constant factors) on the accuracy of this method. They also studied the effect of these factors on different types of metals. The results point out that this method is a very accurate method for the residual stress measurement with accuracy of $\pm 1.5\%$.

Redner and Perry 1982, [121] studied the different factors which affect the accuracy of residual stress measurements using the blind-hole drilling method. Their investigation concludes that the hole-drilling method is now a mature, well-documented procedure, capable of producing consistently reliable results, and careful measurements have to be followed according to ASTM recommendations.

Ajovalasit [122] studied the effect of misalignment between the hole and rosette centres, which influence the strain values. An experimental determination for the calculation constants has been carried out.

Kabiri [26] investigated the hole drilling method, he proposed the use of rosette strain gauge with five elements to increase the accuracy. The formulas which are needed to calculate the principal stresses and their directions have been presented. Kabiri [27] also studied the influences of transverse sensitivity of the gauges on relieved strain coefficients, in the determination of residual stresses by the hole drilling methods. The results show that the transverse sensitivity of the gauges can be ignored.

Flaman and Manning [23] discussed in their paper a finite element procedure, which was applied to determine the constants of residual stress variation with the depth to be routinely performed by the hole-drilling method.

Chow and Cundiff [20] have studied the effect of drilling speed, milling cutter wear, drilling mode and applied drilling force on residual stress measurements in a light truck wheel using the milling guide of RS-200 hole drilling equipment. The results of this investigation revealed that the accuracy in the residual stress measurement for the wheel material SAE 1010 steel using the hole drilling technique can be improved by: using a new milling cutter, intermittent milling and by applying a minimum force during the milling. The maximum residual stress developed in the light truck wheel was found to be about 72 MPa in compression.

Other investigations [22] have been carried out to study the distribution of the residual stresses that vary with the depth. A finite element method was used to calculate the calibration factors for the hole drilling method. The experimental results show that the variation of surface strain of each layer is not only due to the removal of material but is also dependent on the geometry of the hole. Different types of steel and aluminum have been tested which have been subjected to shot-peening treatments. X-ray diffraction method and bending deflection methods also have been used to measure the residual stresses. These measurements show a very good agreement with the measurement results of the hole drilling method.

Boag, et al. [123] investigated the effect of hole-drilling technique and the hole shape on the accuracy and the reliability of hole-drilling method. They found that the high speed drill gave the most accurate results and produced the best hole shape. They applied these different techniques on seven different materials. They also applied FEM to predict the residual stress distribution for thick welded component, a good agreement between the analytical and the experimental results has been found.

Schajer [124] investigated the integral method for calculating non-uniform residual stress fields using strain relaxation data from the incremental hole-drilling method. A finite element method was used to evaluate the calibration coefficients which are required for the practical application of the method.

Wang [28] suggested a simple solution to measure the residual stress by hole-drilling method. This solution can be available for the centre and off-centre for the hole-drilling method to determine the principal residual stresses and their directions.

In reference [29] Wang presented a rigorous and analytical criterion for determining the direction of maximum residual stress. In this study the order of gauge number has been considered in addition to the reference coordinate to determine the direction of maximum residual stress.

Flaman and Boag [24] have compared the variation of residual stress with depth analysis techniques for the hole-drilling method. The comparison was between different analysis techniques e.g. conventional data analysis techniques which are described in ASTM standard E 837-85, equal weight solution method and finite element method (using three dimensional MSC/NASTRAN program). The results show that all data analysis techniques pointed out an excellent agreement for the uniaxial stress with the depth.

1.7 PRESENT WORK AND ITS OBJECTIVES

The objective of this project is to determine the optimum condition for Post Weld Heat Treatment which could give residual stress free welded components with good mechanical properties, for two types of steels, AISI 410 and AISI 1020.

To achieve this objective twelve different schemes of heat treatments have been applied for each of these type of components. These different schemes were varied in the heating rates, soaking temperatures, time durations and cooling rates. Then further schemes of heat treatments were applied to achieve the optimum conditions of heat treatments.

Finite element method was also applied to study the concentrated stress around the heat affected zone for these types of welded components. Chapter 2 describes the principle and theory of the hole-drilling method. The procedures for the metallurgical and mechanical tests are described in Chapter 3. Chapter 4 gives the results of the microstructure, mechanical properties and residual stresses for the different schemes of heat treatments.

Chapter 5 gives the Finite Element Model to study the effect of welding and residual stress on the welded component. Chapter 6 contains discussions of these results. Finally, Chapter 7 outlines the conclusion of this study and some recommendations for further work.

CHAPTER TWO

PRINCIPLE AND THEORY OF THE HOLE-DRILLING METHOD

2.1 INTRODUCTION

The hole-drilling method is one of the most widely used modern techniques for measuring residual stress by drilling a hole in the centre of the strain gauge rosettes.

The procedures of this method have been standardized in ASTM standard test method E 837-85. The method is very versatile, and can be performed in either laboratory or the field work and on horizontal, vertical and overhead surfaces, on a very wide range of different size and shape.

This method is also referred to as a semi-destructive technique, since the small hole will not be significant, causing little damage to the test piece. The hole is typically 1.5 to 3 mm in both diameter and depth.

2.2 PRINCIPLE AND DEVELOPMENT

The principle of this method is based on that when a small circular hole is drilled in a plate containing residual stresses, residual strain in areas outside the hole is partially relaxed. Residual stresses that existed in the drilled area are determined by measuring the amount of strain relaxation that takes place in the area surrounding the drilled hole.

As mentioned in Chapter one, the hole-drilling method was first proposed by Mathar [12] in 1934, and developed by Soete 1949 [13] and Suppiger 1951 [14], by introducing the strain gauge to this method. Many investigations have been carried out to develop this method, Rendler and Vigness [15], Gupta [16], Bush and Kromer [18], Nawwar et. al. [17], Schajer [120] and Flaman and Manning [23] carried out a series of investigations to calculate the material constants and to develop the equations for calculating the residual stresses and their directions.

Meanwhile, other investigations were carried out to study the effect of different parameters on the accuracy of this method. Scandifer and Bowie [119], Bynum [25], Protecter and Beaney [19], Chow and Cundiff [20] and Boag et.al. [123] studied the effect of different parameters such as, the drilling speed, drilling force, the drilling techniques and the drilling shape and geometry on the accuracy of this method. The aim of all these above investigations was to reach the best procedures for the application of this method.

2.3 THEORY OF THE HOLE-DRILLING METHOD

In most practical applications of this method, the drilled hole is blind, with a depth which is about equal to the diameter and small compared to the thickness of the test object.

The blind hole geometry is complex because there is no direct calculation of the residual stresses from the measured strains. The solution can be obtained by introducing the material empirical coefficients.

However, for a simpler case of a hole drilled completely through a thin plate in which the residual stress is uniformly distributed through the plate thickness. The following theory description will first be for the through-hole geometry, and it will be extended for the application of the blind holes.

2.3.1 THEORY OF THROUGH-HOLE DRILLING

When a local area within a thin plate is subjected to a uniform uniaxial residual stress, σ_x (as illustrated in Figure 2.1), the initial stress state at any point (R,α) can be expressed in polar coordinates by:

$$\sigma'_r = \frac{\sigma_x}{2}(1+cos2\alpha) \qquad \textbf{2.1(a)}$$

$$\sigma'_\theta = \frac{\sigma_x}{2}(1-cos2\alpha) \qquad \textbf{2.1(b)}$$

$$\tau'_{r_\theta} = -\frac{\sigma_x}{2}sin2\alpha \qquad \textbf{2.1(c)}$$

Figure 2.2 shows the same area of the plate after a small hole has been drilled through it. The stresses in the vicinity of the hole are now quite different, since σ_x and $\tau_{r\theta}$ must be zero everywhere on the surface. A solution for this case was obtained by Kirsch [125]. In this case the stresses at the point P(R,α) expressed as:

$$\sigma''_r = \frac{\sigma_x}{2}(1-\frac{1}{r^2}) + \frac{\sigma_x}{2}(1+\frac{3}{r^4}-\frac{4}{r^2})cos2\alpha \qquad \textbf{2.2(a)}$$

$$\sigma''_{\theta}=\frac{\sigma_x}{2}(1+\frac{1}{r^2})-\frac{\sigma_x}{2}(1+\frac{3}{r^4})cos2\alpha \qquad \textbf{2.2(b)}$$

$$\tau''_{r_\theta}=-\frac{\sigma_x}{2}(1-\frac{3}{r^4}+\frac{2}{r^2})sin2\alpha \qquad \textbf{2.2(c)}$$

where: $r = R/R_0 \qquad (R \geq R_0)$

Substrating the initial stresses from the final stresses (before and after drilling) gives the stress relaxation at this point. The following equations express this change:

$$\Delta\sigma_r=\sigma''_r-\sigma'_r \qquad \textbf{2.3(a)}$$

$$\Delta\sigma_\theta=\sigma''_\theta-\sigma'_\theta \qquad \textbf{2.3(b)}$$

$$\Delta\tau_{r_\theta}=\tau''_{r_\theta}-\tau'_{r_\theta} \qquad \textbf{2.3(c)}$$

Substituting equations 2.1 and 2.2 into equations 2.3 gives full expressions for the relieved stresses. If the material of the plate is homogeneous and isotropic in its mechanical properties, and linear-elastic in its stress/strain behaviour, these equations can be substituted into the biaxial Hooke's law [126] to give the relieved normal strains at the point P(R,α). Then, the resulting expressions are as follows:

$$\epsilon_r = -\frac{\sigma_x(1+\nu)}{2E}\left[\frac{1}{r^2} - \frac{3}{r^4}\cos 2\alpha + \frac{4}{r^2(1+\nu)}\cos 2\alpha\right] \qquad \textbf{2.4(a)}$$

$$\epsilon_\theta = -\frac{\sigma_x(1+\nu)}{2E}\left[-\frac{1}{r^2} + \frac{3}{r^4}\cos 2\alpha - \frac{4\nu}{r^2(1+\nu)}\cos 2\alpha\right] \qquad \textbf{2.4(b)}$$

The previous equations can be written in a simpler form, demonstrating that along a circle at any radios R ($R \geq R_0$) the relieved radial and tangential strains vary in a sinusoidal manner:

$$\epsilon_r = \sigma_x(A + B\cos 2\alpha) \qquad \textbf{2.5(a)}$$

$$\epsilon_\theta = \sigma_x(-A + C\cos 2\alpha) \qquad \textbf{2.5(b)}$$

Comparison of equations 2.4 and 2.5 demonstrates the coefficients A,B and C which have the following definitions:

$$A = -\frac{1+\nu}{2E}\left(\frac{1}{r^2}\right) \qquad \textbf{2.6(a)}$$

$$B = -\frac{1+\nu}{2E}\left[\left(\frac{4}{1+\nu}\right)\frac{1}{r^2} - \frac{3}{r^4}\right] \qquad \textbf{2.6(b)}$$

$$C=-\frac{1+\nu}{2E}\left[-\left(\frac{4\nu}{1+\nu}\right)\frac{1}{r^2}+\frac{3}{r^4}\right] \qquad \textbf{2.6(c)}$$

The relieved strains also vary with the distance from the hole surface. This variation is illustrated in Figure 2.3 where the strains are plotted along the principal axes, at $\alpha=0°$ and $\alpha=90°$. As illustrated by the Figure, the relieved strains decrease as distance from the hole increases. So, it is desirable to measure the strains close to the edge of the hole in order to get higher strain output signal. On the other hand, parasitic effects also increase in the immediate vicinity of the hole. A compromising in selecting the strain gage is needed to select the optimum radius (R) for the gage location, as specified by ASTM E 837-85 $r=R/R_0$ should be in the range of 2.5 to 3.4.

It can be noticed from Figure 2.3 that for $\alpha=0°$ (along the axis of the major principal stress) the relieved radial strain, ϵ_r, is considerably greater than the tangential strain, ϵ_θ, in the specified measurement area. The commercial strain gauge rosettes are designed with radially oriented grids to measure the relieved radial strain ϵ_r. This being the case, only equation 2.5(a) is directly relevant for further consideration. It is also evident from the Figure that the relieved radial strain along the major principal axis is opposite in sign to the initial residual stress. This occurs because the coefficients A and B in equation 2.5(a) are always negative.

The above discussion considered only the simplest case, uniaxial residual stress. In practice, residual stresses are more often biaxial, with two non-zero principal stresses. This condition can readily be incorporated in the analysis by employing the superposition principle which is applicable to linear-elastic material behaviour. From Figure 2.2, it is apparent that had the uniaxial residual stress been along only the Y axis instead of the X axis, equations 2.1 and 2.2 would still apply, with $\cos2\alpha$ replaced by $\cos2(\alpha+90°)$ or by the equivalent, $-\cos2\alpha$. Thus, the relieved residual strain at the point $P(R,\alpha)$ due to uniaxial residual stress in only the Y

direction can be written as :

$$\epsilon_r^y = \sigma_y(A - B\cos 2\alpha) \qquad 2.7$$

and employing the corresponding notation, equation 2.5(a) becomes:

$$\epsilon_r^x = \sigma_x(A + B\cos 2\alpha) \qquad 2.8$$

When both residual stresses are present simultaneously, the superposition principle permits algebraic addition for equations 2.7 and 2.8, so that the general expression for the relieved radial strain due to a plane biaxial residual stress state is:

$$\epsilon_r = \sigma_x(A + B\cos 2\alpha) + \sigma_y(A - B\cos 2\alpha) \qquad 2.9$$

or it can be written as:

$$\epsilon_r = A(\sigma_x + \sigma_y) + B(\sigma_x - \sigma_y)\cos 2\alpha \qquad 2.10$$

This equation represent the basic relation underlying the hole-drilling method of residual stress analysis.

Since there are three unknown quantities, three independent measurements of the radial strain are required for the complete solution. Using the strain gauge rosettes, where the three strain gauge elements located with their centre at the radius R from the hole centre, Figure 2.4

shows a schematic drawing for the strain gauge rosettes. The angle between the elements are known which are, 0, 45 and 90°. Equation 2.10 can be written three times, one for each gauge in the rosette,

$$\epsilon_1 = A(\sigma_x + \sigma_y) + B(\sigma_x - \sigma_y)cos2\alpha \qquad \textbf{2.11(a)}$$

$$\epsilon_2 = A(\sigma_x + \sigma_y) + B(\sigma_x - \sigma_y)cos2(\alpha + 45°) \qquad \textbf{2.11(b)}$$

$$\epsilon_3 = A(\sigma_x + \sigma_y) + B(\sigma_x - \sigma_y)cos2(\alpha + 90°) \qquad \textbf{2.11(c)}$$

When equations 2.11 are solved simultaneously for the principal stresses and their directions, the results can be expressed as:

$$\sigma_{max} = \frac{\epsilon_1 + \epsilon_3}{4A} - \frac{\sqrt{2}}{4B}\sqrt{(\epsilon_1 - \epsilon_2)^2 + (\epsilon_2 - \epsilon_3)^2} \qquad \textbf{2.12(a)}$$

$$\sigma_{min} = \frac{\epsilon_1 + \epsilon_3}{4A} + \frac{\sqrt{2}}{4B}\sqrt{(\epsilon_1 - \epsilon_2)^2 + (\epsilon_2 - \epsilon_3)^2} \qquad \textbf{2.12(b)}$$

$$tan2\alpha = \frac{\epsilon_1 - 2\epsilon_2 + \epsilon_3}{\epsilon_3 - \epsilon_1} \qquad \textbf{2.12(c)}$$

where α in equation 2.12(c) is the angle from gauge 1 to the nearer principal axis. The following rules have to be considered in determining which principal stress is referred to gauge number 1:

$$\epsilon_3 > \epsilon_1 : \alpha \text{ refers to } \sigma_{max}$$
$$\epsilon_3 < \epsilon_1 : \alpha \text{ refers to } \sigma_{min}$$
$$\epsilon_3 = \epsilon_1 : \alpha = \pm 45°$$
$$\epsilon_2 < \epsilon_1 : \sigma_{max} \text{ at } + 45°$$
$$\epsilon_2 > \epsilon_1 : \sigma_{max} \text{ at } - 45°$$

Also, consideration must be taken in determining the appropriate values for coefficients A and B, as defined algebraically in equations 2.6. This solution gives the stress distribution at points around a circular hole through a thin, wide plate subjected to uniform plane stress. However, the output of each gauge tends to represent the average strain over the element grid area. Moreover, because the strain gauge element grids are usually composed of parallel lines, those lines which are not directly on the centreline of a radially oriented grid are not radial. Therefore, the gauges are slightly sensitive to the tangential strain, as well as the radial strain. As a result, more accurate values for the coefficients can be obtained by integrating equations 2.4 over the areas of the respective gauge grids. The coefficients thus determined, which account for finite strain gage area, are designated here by A and B to distinguish them from the values at a point as defined by equations 2.6.

An experimental calibration can be carried out to determine the coefficients A and B. This calibration has been described by the Measurements Group [127]. Many investigators have carried out experimental and analytical studies to determine these coefficients. Next section have more details about the results of those studies.

2.3.2 THEORY OF THE BLIND-HOLE

Since most machine parts and structural members which requires residual stress analysis, could be of any size and shape, a blind hole is used in most applications of the hole drilling method.

Introducing a blind hole into a field of plane stress produces a complex local stress case, where there is no exact solution from the theory of elasticity. However, Rendler and Vigness [13] found that this case closely parallels the through hole condition in the general nature of the stress distribution. Thus, the relieved strains due to drilling the blind hole still vary sinusoidally along a circle concentric with the hole, in the manner described by equations 2.10. That means, that these equations, as well as equations 2.12 are equally applicable to the blind-hole implementation of the method, by employing appropriate blind-hole coefficients A and B. Since these coefficients can not be calculated directly from theoretical considerations, they must be obtained by experimental calibration or numerical analysis.

In the blind-hole analysis one additional variable is involved, the dimensionless hole depth, Z/D_0. Thus, in generalized functional form, The coefficients A and B can be expressed as:

$$A=\oint_A(E,\nu,r,Z/D_0) \qquad 2.13\ (a)$$

$$B=\oint_B(E,\nu,r,Z/D_0) \qquad 2.13(b)$$

Many investigators [17, 19, 20 and 22] studied the effect of the depth/diameter value. These studies show that the strain have been normalized in each case 100% at $Z/D_0 = 1.0$.

An important contribution is reference [13] which demonstrate that, for any given set of material properties E and ν, coefficients A and B are geometric functions, and thus constants for all geometrically similar cases. This means that once the coefficients have been determined for a particular rosette configuration, the rosette size can be scaled upward or downward and the same coefficients will still apply when the hole diameter and depth are similarly scaled. Other studies have been done to remove the material dependency from A and B, leaving only the geometric dependence. Schajer [122] introduced two new coefficients, denoted here as a and b, and defined as:

$$a=\frac{2EA}{1+\nu} \qquad 2.14(a)$$

$$b=2EB \qquad 2.14(b)$$

By comparing with equations 3.6, it can be seen that for the through-hole, at least , a is material independent, and b, depends only weakly on Poisson's ratio. Schajar has determined from finite element calculations that for the blind holes, a and b vary by less than 2% for the range of Poisson's ratio from 0.25 to 0.35.

2.3.3 THE COEFFICIENTS DETERMINATION

In the residual stress analysis application by through-hole or blind-hole drilling, the coefficients A and B or (a and b) must be determined to calculate the stresses from the relieved strains. In the case of the through-hole, reasonably accurate values of the coefficients can be obtained for any particular case by analytical means. This is done by integrating, over the area of the gauge grid, the component of strain parallel to the primary strain sensing axis of the gauge. Given the details of the stain gauge element grid geometry, slightly greater accuracy may

be obtained by integrating along the individual strain gauge element grid lines. This method cannot be applied to blind-hole analysis because closed - form expressions relating the relieved strains to the residual stress, in terms of hole depth, are not available.

These coefficients for either through-hole or blind-hole analysis can be determined by experimental and numerical analysis. These two coefficients depend only on the geometry of the hole and the elements grid and location. Micro-Measurements supplies special strain gauge rosettes for residual stress analysis in three different types (as illustrated in Figure 3.9). These rosettes are designed incorporate centring patterns for positioning the drilling tool precisely at the centre of the gauge circle. Three major types of strain gauges are supplied RE, RK and UM, where RE and RK have similar grid configuration. With the gauge-circle diameter equal to 3.25 times the active gauge length. The 062RE rosette, for example, has a gauge circle diameter of 5.13 mm. Because of this similitude, the same material independent coefficients a and b apply to all sizes of the RE rosette and to the RK rosette for similar geometric holes, for the same $D\backslash D_o$ and $Z\backslash D_o$ ratios. The 062UM rosette configuration has the same ratio of gauge circle to grid length, but the grid are narrower to permit their close grouping on one side of the hole. As a result, the sensitivity of the gauge to the relieved strains is slightly greater, and coefficients specific to the 062UM are required.

The a and b coefficients for Micro-Measurements residual stress rosettes are provided graphically in Figure 2.5, where the solid lines apply for full depth blind-holes and the dashed lines to through-holes assuming that in both cases the initial residual stress is uniform with depth. Through-hole coefficients for RE and RK rosettes were obtained by numerically integrated the expressions for the relieved longitudinal strains along the individual grid lines. Because blind-hole coefficients cannot be calculated in the same manner, these have been determined for the RE and RK rosettes by both experimental calibration and finite element analysis [13, 118 and 119]. Although results typically differ slightly from one investigator to the next, the curves plotted in Figure 2.5a are considered representative of the subject rosettes, and

suitable and accurate data to use in this method. Coefficients for the 062UM rosette, calculated by experimental from the RE\RK data, are given in Figure 2.5b.

In the present work, these coefficients were chosen from Figure 2.5, where $D/D_o = 3.2$. For the strain gauge rosette type UM, the coefficient a and b were 0.132 and 0.358 respectively. Then the coefficients A and B were calculated from the previous equations, the calculated values for A and B were 0.288×10^{-8} and 0.606×10^{-8} Psi^{-1} respectively. While, for strain gauges types RE and RK, the coefficients a and b were 0.124 and 0.302 respectively. Then the coefficients A and B were calculated, the values of A and B were 0.271×10^{-8} and 0.511×10^{-8} Psi^{-1} respectively.

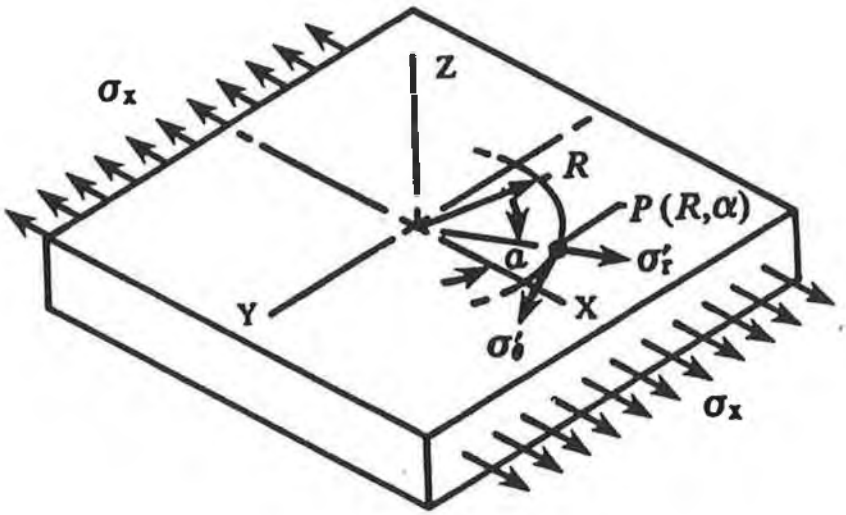

FIGURE 2.1 THE INITIAL STRESS AT POINT P(R,α) BEFORE DRILLING.

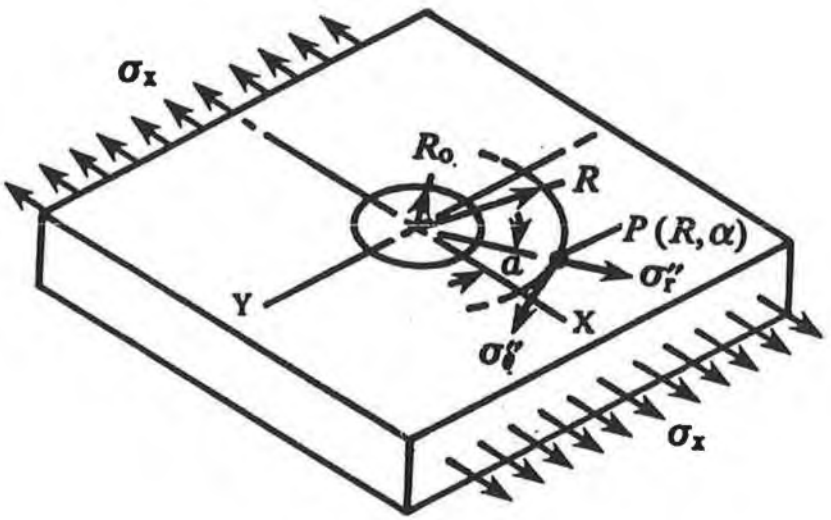

FIGURE 2.2 THE INITIAL STRESS AT POINT P(R,α) AFTER DRILLING.

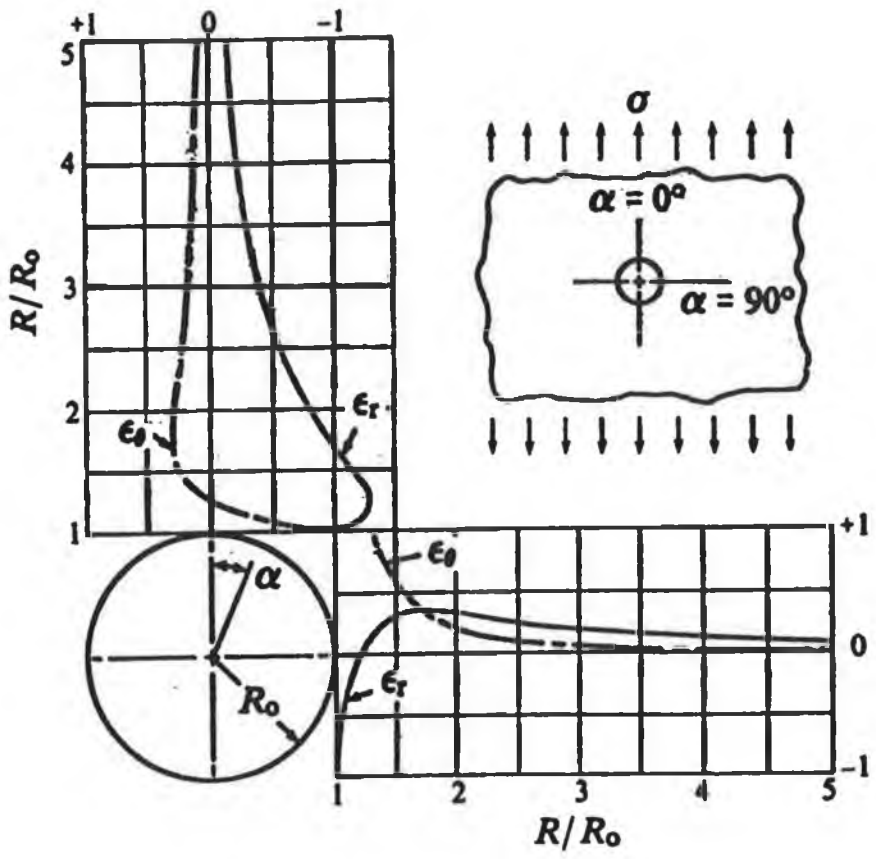

FIGURE 2.3 VARIATION OF RELIVED RADIAL AND TANGENTIAL STRAINS WITH DISTANCE FROM THE CENTRE OF THE DRILLED HOLE.

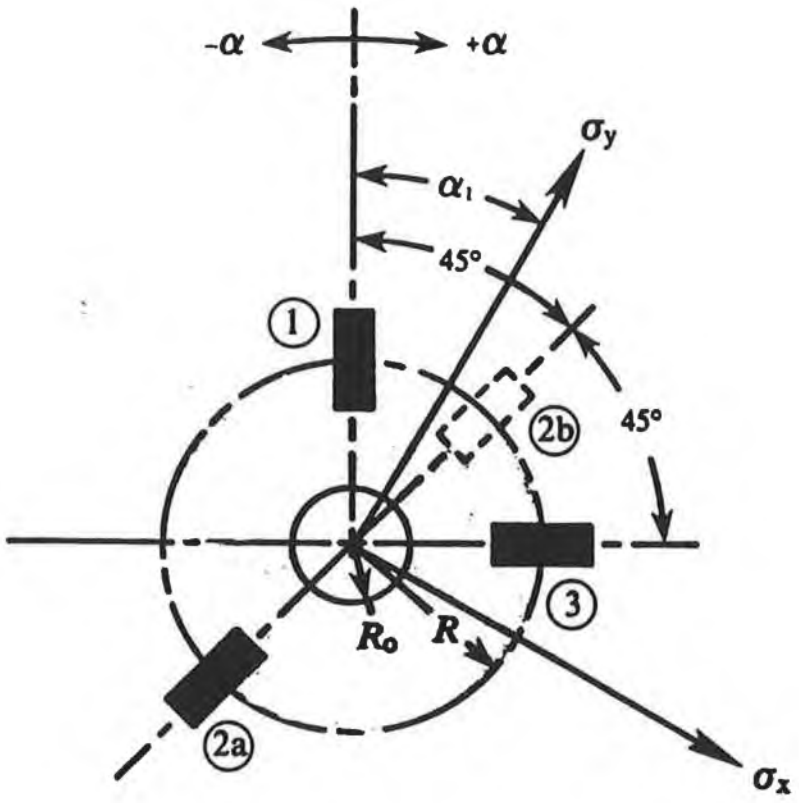

FIGURE 2.4 TYPICAL STRAIN GAUGE ROSETTE.

(b) UM ROSETTE

(a) RE & RK ROSETTES

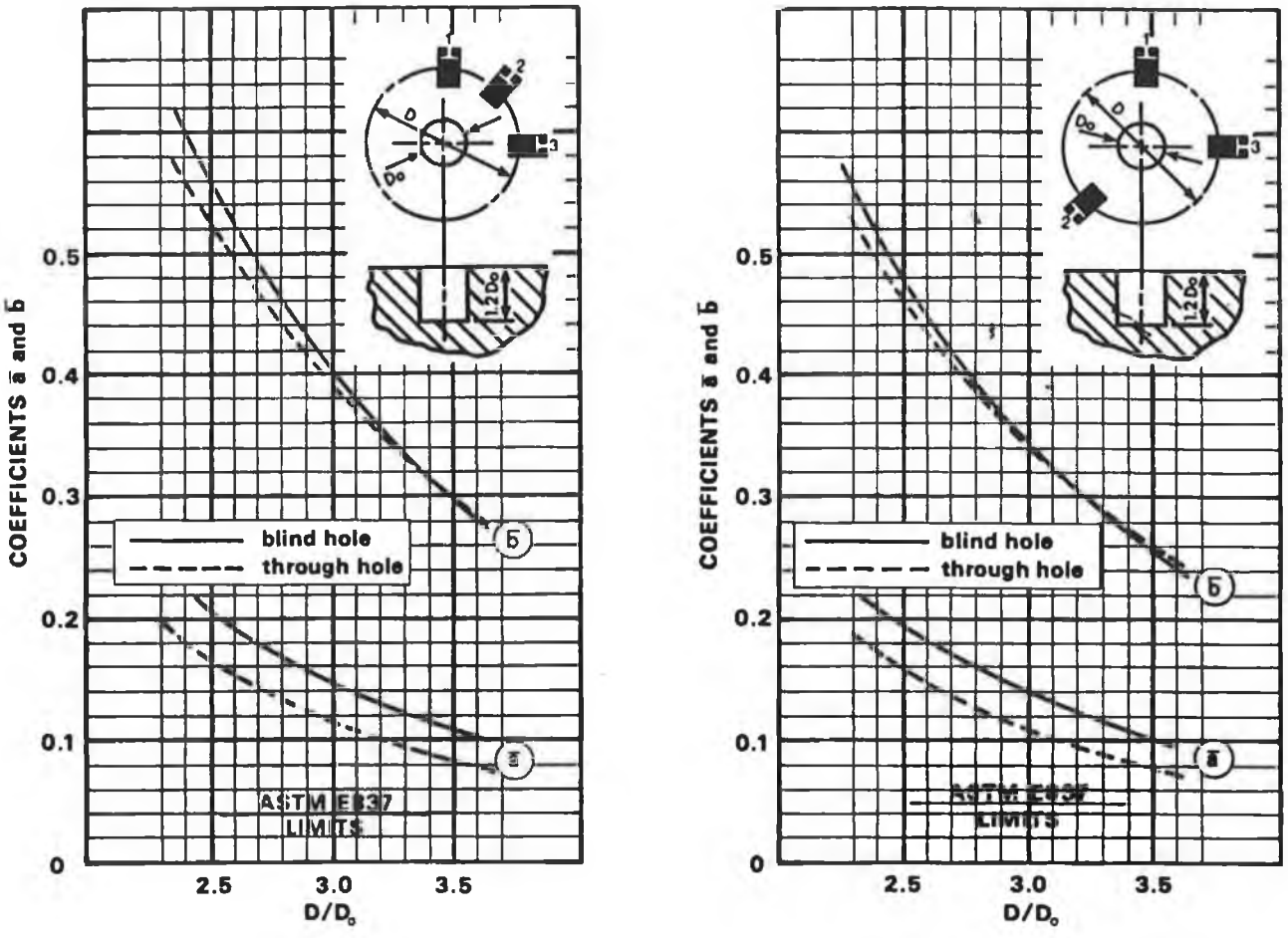

FIGURE 2.5 MATERIAL COEFFICIENTS a AND b.

CHAPTER THREE

EXPERIMENTAL EQUIPMENTS & TEST PIECE PREPARATION

3.1 TOOLS AND MATERIALS

3.1.1 METAL COMPOSITION

Two different types of steel were used in this work. High chromium steel AISI 410, the chemical composition of this steel being(wt%): 0.15% C, 1.00% Mn, 0.040% P, 0.030% S, 1.00% Si and 12.5% Cr.

Also low carbon steel AISI 1020 was used, the chemical composition of this steel being(wt%): 0.141% C, 0.246% Si, 0.82% Mn, 0.008% P, 0.025% S, 0.075% Cr, 0.083% Ni, 0.019% Mo, 0.269% Cu, 0.003% Al and 0.001% Ti.

3.2 SPECIMEN PREPARATION

Two main types of specimens were used. The first type was the stainless steel specimen AISI 410. The second type was the low carbon steel AISI 1020.

3.2.1 THE STAINLESS STEEL SPECIMEN

Double-V butt welded components were prepared for the carrying out of this work. In preparing the specimens, two rectangular metal pieces of 24 mm thickness were ground and machined to provide the double-V shape. Then, the welding was carried out using the TIG welding process. Four welding passes were made alternately on each face using filler metal which has the same chemical composition as the parent metal, and the component was firmly held together during welding by fixture. Figure 3.1 is a drawing of the stainless-steel welded component.

3.2.2 THE LOW CARBON STRUCTURE STEEL SPECIMEN

The initial test was carried out on the I-beam box-section specimen. This welded component consists of two I-beams welded together to produce box shape. MIG welding process has been used to do the welding, and a filler metal which has the same chemical composition as the parent metal was used. Figure 3.2 shows the cross-section of the box welded component.

After carrying out the initial testing, double-V butt welded components were also prepared. These specimens consist of two rectangular metal pieces of 10 mm thickness.The welding was carried out by using the MIG welding process. One welding pass was made on each face using filler metal which has also the same chemical composition of the parent metal, and the component was firmly held together during welding. Figure 3.3 is a drawing of this welded component.

3.2.3 STRAIN GAUGE PREPARATION

In order to obtain the best results from a strain gauge, it is important to prepare the

gauge and the surface of the specimen to which the gauge is to be attached.

To prepare the specimen surface, an area larger than the installation was smoothed with fine grade emery paper to provide a sound bonding surface. Then the area was degreased with a solvent cleaner; for this purpose a PCB solvent cleaner was used. Finally the specimen surface was neutralised with a weak detergent solution MN5-1 M-Prep Neutralizer 5. Tissues were used for this operation. The final cleaning was immediately prior to the installation of the gauge.

After preparing the specimen surface a desired location for the strain gauge was determined. After that a short length of adhesive tape was placed over about half of the gauge tabs. Then the gauge backing and the specimen surface were coated with a thin layer of M-Bond 200 adhesive. Then the strain gauge was placed in its desired location and reasonable pressure was applied for about 1 minute to ensure that the assembly was firmly in place. Finally, the connecting wires were soldered to each strain gauge element, and a gauge installation tester Model 1300 was used to ensure that there was no fault in the strain gauge installation. Figure 3.4 shows the different stages of strain gauge preparation.

3.3 TESTING PROCEDURES

3.3.1 METAL PROPERTIES TESTING PROCEDURES

To evaluate the hardness variation of these welded components before and after the application of PWHTs, slices of 10 mm width were cut, then the perpendicular faces of the surface were ground and polished. Then, the LEITZ MINILOAD 2 microhardness tester was used to carry out this test with a load of 100 g.

For determining the impact energy of these welded components standard shaped notched

impact specimens (10 X 10 X 55 and 7.5 X 10 X 55) were machined by following the guideline according to German Standard (DIN-50121). Plate 3.1 shows a photograph of the notched impact specimen.

For determining the tensile strength, standard tensile specimens were machined following the guideline according to German standard (DIN-50120). Plate 3.2 shows a photograph of the tensile specimen.

3.3.2 POST WELD HEAT TREATMENT PROCEDURE

The initial post weld heat treatment (PWHT) was applied on the steel with I-beam box-section component. In this heat treatment the welded component was kept in the furnace for 18 hours at soaking temperature of 580 °C and left to cool in the furnace.

Then, twelve types of post weld heat treatments (PWHTs) were applied for each type of the steel. These heat treatments were varied in the soaking temperatures, heating rates, cooling rates or soaking time durations. Tables 3.1 and 3.2 give the conditions for these different types of PWHTs. These will be referred in the following chapters as PWHT(1,2,.....,12) for AISI 410 stainless-steel and PWHT(a,b,.....,l) for AISI 1020 low carbon steel as noted in Tables 3.1 and 3.2.

3.3.3 RESIDUAL STRESS TESTING PROCEDURE

To evaluate the magnitude and distribution of the residual stress before and after the application of PWHTs, the RS-200 hole-drilling technique was employed. Different preparations were made in assessing the residual stress, after bonding the strain gauge to the test part at points where the residual stresses were to be determined. Each rosette grid element was

connected to a strain indicator P-3500 and 'zero' readings were recorded. Then the RS-200 milling guide was positioned over the centre of the gauge and securely attached to the test part by using a special kind of cement which was supplied with the instrument. The precise position over the centre of the rosette strain gauge was obtained by using the special purpose microscope and adjusting the accurate position by the four X-Y screws. After alignment was achieved, the microscope was removed from the guide, and the milling bar inserted with the tungsten carbide cutter of 1.6 mm diameter for drilling the hole. After drilling for the depth of 1.6 mm, the drilling bar was removed and the strain readings were taken from the strain indicator. Finally, the principal residual stresses and their directions were computed by using appropriate equations (see Chapter 3).

3.3.4 MICROSTRUCTURE TESTING PROCEDURE

To study the microstructure of these specimens, slices of about 5 mm width were cut from the middle of the specimen. Then the perpendicular face of the surface was ground. After that a metallurgy lab was used to polish this face. At first, however, before polishing this face, the specimen was surrounded by conductive BAKELITE by using the thermoplastic instrument. After that, different grades of polishing were employed. Then the surface of this specimen was treated with acid. Finally it was washed and dried. At this stage the microstructure testing got started.

As described above, an optical microscope was used to carry out the microstructure test. In the mean time, X-ray diffraction method was used to identify the structure of these different components. A number of specimens were prepared to carry out this work.In preparing these specimens, slices of 20 X 20 X 4 mm from the original metals (AISI-410 and AISI-1020) were machined and ground. Then, the preceding heat treatment schemes were applied for these specimens. After that, one face of the specimen was polished. After this stage the X-ray diffraction testing was carried out. From the diffraction pattern, different microstructure such

as martensite and different levels of tempered martensite can be identified. Figs. 3.5 to 3.8 show the diffraction pattern for Pre- and PWHT with different soaking temperatures for AISI-410.

After the identification of the microstructure of these different specimens, previously described procedures of preparing the microstructure specimens were followed. At this stage the standard specimen was ready to be compared with the prepared welded specimens.

3.4 EQUIPMENT

3.4.1 ELECTRIC FURNACE

In this work a Lenton Laboratory Electric Chamber Furnace, series ECF12/10, was used. The working temperature is up to 1200°C. It is operated from a 13 amp, 230 - 250 volt, single phase A.C. power supply.

The chamber size is 127 mm high, 178 mm wide, 406 mm deep. Maximum power rating is 2.5 kW. A controller 902 has been installed in this furnace to control the operation cycle. Plate 3.3 shows a photograph of this electric furnace.

3.4.2 TENSILE TESTING MACHINE

The tensile testing machine was an Instron Universal Testing instrument model 4204, which consists of a loading frame and a control console as separate assemblies. The frame hasa load capacity of up to 50 kN and is designed for testing materials in either tension or compression.

The basic operation of the instrument consists of selecting a load cell for a particular

testing application, mounting the load cell in the moving cross head within the loading frame, then setting the specimen in position so that an applied load can be measured. The specimen is held by grips for tension testing, or is table - mounted for compression testing. plate 3.4 shows a photograph of the machine and its accessories.

During a test, results are displayed as tracked values of load, extension and strain or, after a test, as stored break and peak values of these parameters. The action of the moving cross head during a test (stop, return, cycle) may be controlled manually by push button switches or automatically by the functions provided by the limits panel. These functions may be based on the applied load extension or strain, or to a specimen break detection.

3.4.3 HARDNESS TESTER

A micro hardness tester was used to measure the hardness of the specimens. This tester is capable of measuring three kinds of hardness - vickers, knoop and scratch hardness - by changing the diamond indenter.

However, for this project only vickers hardness method was employed. The tester is accompanied by a hardness test plate for calibration and a set of loads varying from 5g to 300g. These loads are chosen according to the thickness of the test piece; the tester type LEITZ MINILOAD 2. In this project 100g load was used.Plate 3.5 shows a photograph of the hardness tester.

3.4.4 OPTICAL MICROSCOPE

An entirely new metallograph Reichert MeF3 was used, which had the following facilities. It has a convenient position of binocular body with inclination angle of 32 and viewing

height of 420 mm. It provides 6 nosepieces to make it suitable for all types of objectives. There are four step magnification changers. It has reticule insert. The MeF3 has low coaxial coarse and fine controls which are easily accessible and a rotatable mechanical stage with coaxial controls.

A 4x5 Camera is built into the MeF3 Microscope and an additional 35 mm camera with automatic film transport is also provided. The Microscope is also supplied with an automatic control system for changing from one camera to the other with display of exposure time. The MeF3 is provided with an illuminated frame projection for focusing purposes using the binocular tube with automatic brightness regulator. It is supplied with a Rotoscope projection device with a high resolution screen. A 100 Watt Halogen lamp and mirror house for use with high power lamps of up to 450 Watt are built into it. A Macrodual zoom system for large specimen size (22 to 175 mm) imaging for both visual observation and photography is provided. It is also supplied with a Varicode projection system for luminous measuring bars with numbers or reticules for both visual observation and photography. A photograph of this device can be found on plate 3.6.

3.4.5 MIG AND TIG WELDING MACHINES

A FILARC TIG 350 was used to execute all stainless steel welded components needed in this work. A FILARC MIG 350 was used to execute all low carbon steel welded components. The current for these two machines ranges from 4-350 A. These machines have water hoses for providing proper cooling for the welding torch. The FILARC MIG and TIG welding machines are also supplied with a gas cable to provide the protective inert gas environment.

These welding machines are fitted to carry the gas bottle and optional water cooler, comprising plastic tank with a pump, well able to cool a torch employed at high welding temperatures. Water cooling lines pass under the power source, away from any circuitry.

In this work the current range was about 65 to 75 A for the TIG machine. The current range was about 110 to 115 A for the MIG machine. In both machines, Argon gas was employed to protect the welding.

3.4.6 DIGITAL STRAIN INDICATOR

Digital Strain Indicator P-3500 was used in this work. The P-3500 Digital Strain Indicator is designed primarily for use with resistive strain gauges or transducers. The P-3500 is a portable, battery-powered precision instrument, it accepts full, half or quarter bridge inputs, and the required bridge completion components for 120-ohm and 350-ohm bridges are provided.

The P-3500 accepts gauge factors of 0.500 to 9.900 with accuracy of $\pm 0.05\%$ reading or $\pm 3\mu\epsilon$ for gauge factor less than 1.00 and $\pm 0.5\%$ reading or $\pm\mu\epsilon$ for gauge factor bigger than 1.00. This instrument is capable of measuring ± 199990 microstrain in two ranges ± 19999 and ± 199990.

The SB-10 switch and balance unit was used. The SB-10 is designed to provide the output reading of ten channels of strain gauge information on a single strain indicator. Each channel can be initially balanced to zero output to greatly simplify data interpretation and reduction.

The P-3500 provides a direct reading for each channel, by switching the channel's key, direct reading will be appeared on the strain indicator panel. Plate 3.7 shows a photograph of the digital strain indicator P-3500 and the switch balance unit SB-10.

3.4.7 STRAIN GAUGES

EA-XX-062RE-120, TEA-XX-062RK-120 and CEA-XX-062UM-120 rosettes strain gauges were used to determine the residual stresses in this work. These three types of strain gauges have the same pattern geometry with centre hole diameter of 1.6 mm. These gauges have a resistance of 120 Ohms, and gauge factor of 2.04 $\pm$ 1.0%. The RK and UM are fully encapsulated, with copper terminals for ease of soldering. Figure 3.9 shows these different types of strain gauges.

3.4.8 THE HOLE-DRILLING EQUIPMENT

The RS-200 milling guide was used to carry out the drilling in the centre hole of the rosette strain gauge. The Rs-200 is a precision fixture for the accurate positioning and drilling of a hole through the centre of the strain gauge rosette. The milling guide is supported by three levelling screws which are footed with swivel mounting pads to facilitate attachment to curved surfaces.

The RS-200 is provided with a special purpose microscope which can be inserted into the guide centre, for positioning the guide precisely over the centre of the rosette strain gauge by means of four X-Y adjusting screws.

Two drilling techniques could be used by the RS-200, conventional and ultra-high speed drilling techniques. The ultra-high speed drilling was employed in this work which is in general, the most convenient and practical method for introducing the hole in the test materials. Tungsten carbide-tipped cutters of 0.8 and 1.6 mm diameter were supplied with this technique, but only carbide-tipped cutters of 1.6 mm were used in this work. A foot pedal control was included for operating the air turbine. Plate 3.8 shows a photograph of the RS-200 guide drilling equipment.

HEAT TREATMENT CYCLE	HEATING RATE °C/H	SOAKING TEMPERATURE °C	DURATION TIME H	COOLING RATE °C/H
PWHT (1)	400	550	2	40
PWHT (2)	400	650	2	40
PWHT (3)	400	750	2	40
PWHT (4)	50	550	2	40
PWHT (5)	100	550	2	40
PWHT (6)	400	550	2	40
PWHT (7)	400	550	0.5	40
PWHT (8)	400	550	2	40
PWHT (9)	400	550	10	40
PWHT (10)	400	550	2	10
PWHT (11)	400	550	2	40
PWHT (12)	400	550	2	125

Table 3.1 the different PWHTs procedures for AISI 410.

HEAT TREATMENT CYCLE	HEATING RATE °C/H	SOAKING TEMPERATURE °C	DURATION TIME H	COOLING RATE °C/H
PWHT (a)	400	450	2	40
PWHT (b)	400	550	2	40
PWHT (c)	400	650	2	40
PWHT (d)	50	450	2	40
PWHT (e)	100	450	2	40
PWHT (f)	400	450	2	40
PWHT (g)	400	450	0.5	40
PWHT (h)	400	450	2	40
PWHT (i)	400	450	10	40
PWHT (j)	400	450	2	10
PWHT (k)	400	450	2	40
PWHT (l)	400	450	2	125

Table 3.2 the different PWHTs procedures for AISI 1020.

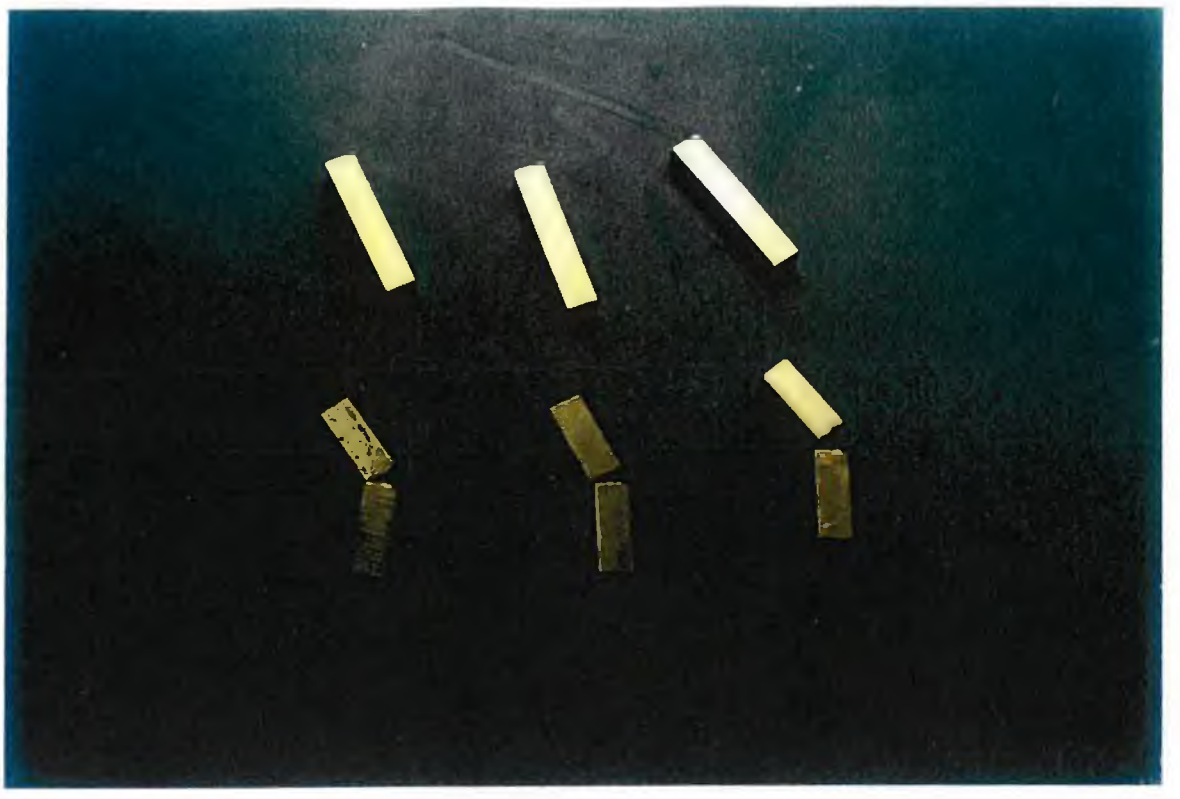

PLATE 3.1 THE NOTCHED-IMPACT SPECIMEN.

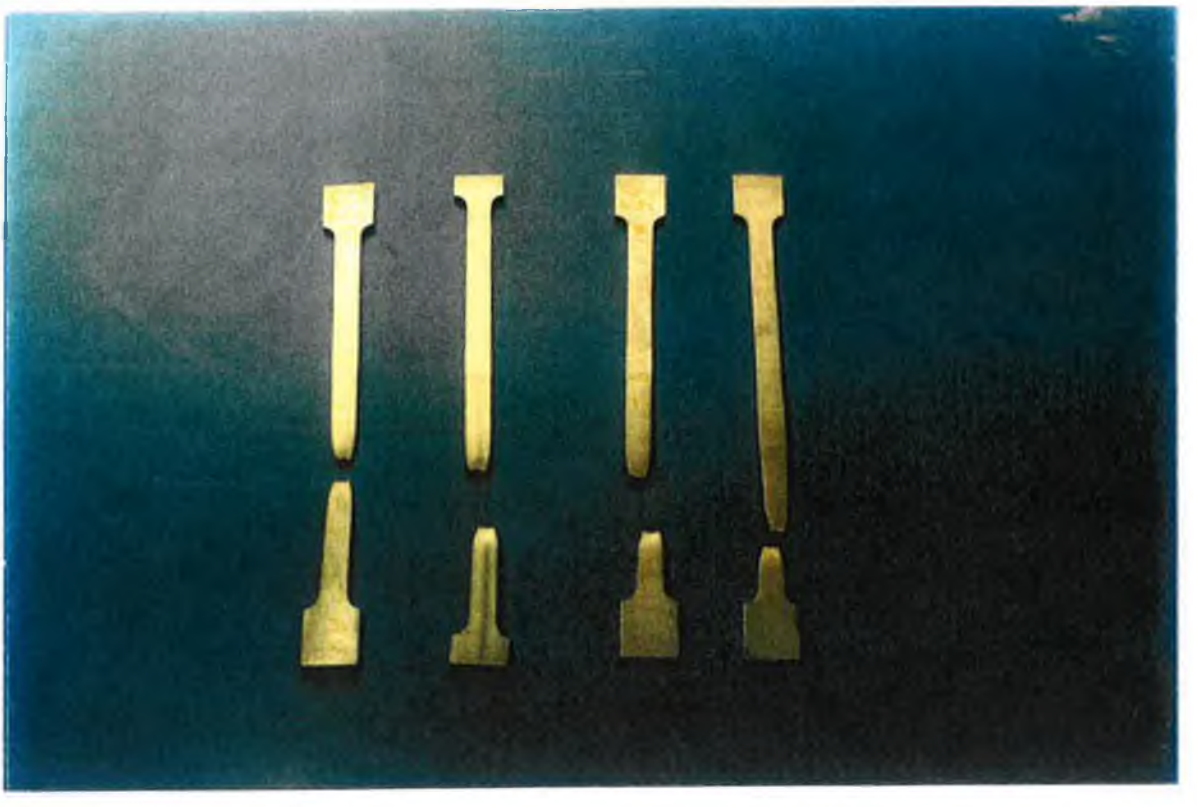

PLATE 3.2 THE TENSILE SPECIMEN.

PLATE 3.3 THE ELECTRIC FURNACE.

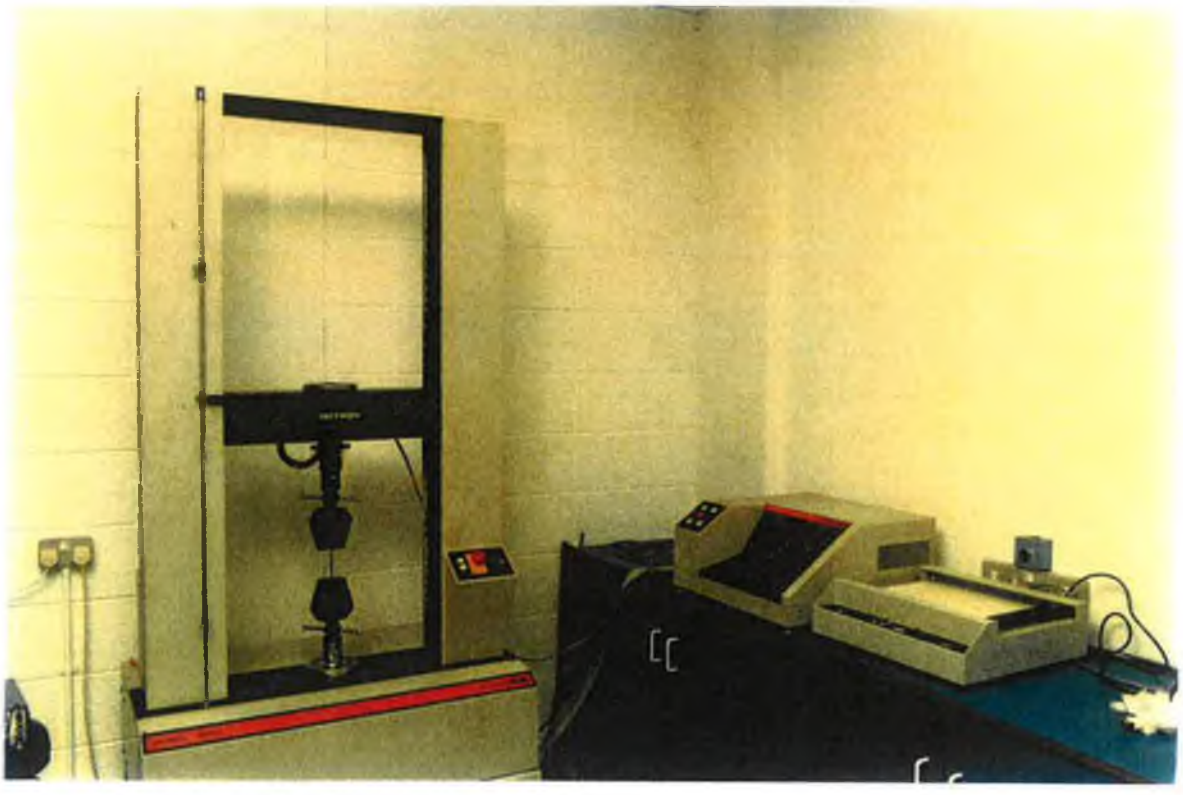

PLATE 3.4 THE TENSILE MACHINE.

PLATE 3.5 THE HARDNESS TESTER.

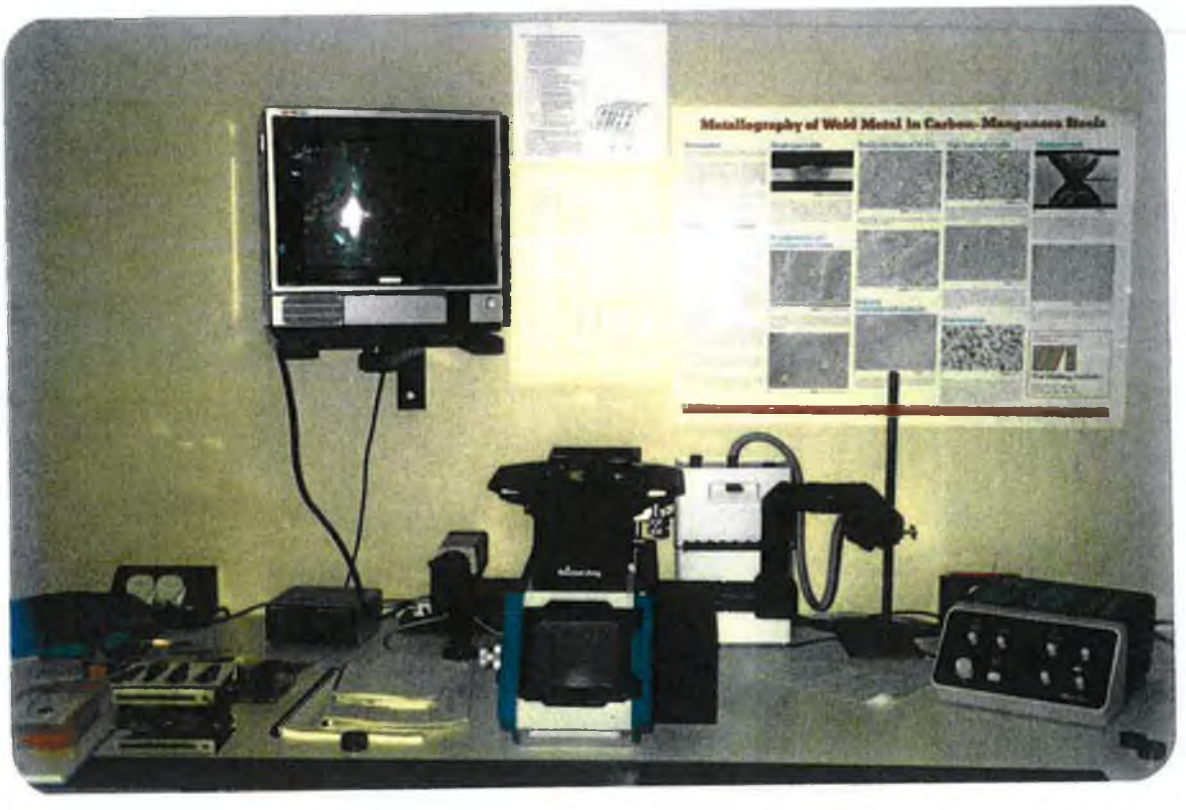

PLATE 3.6 THE OPTICAL MICROSCOPE.

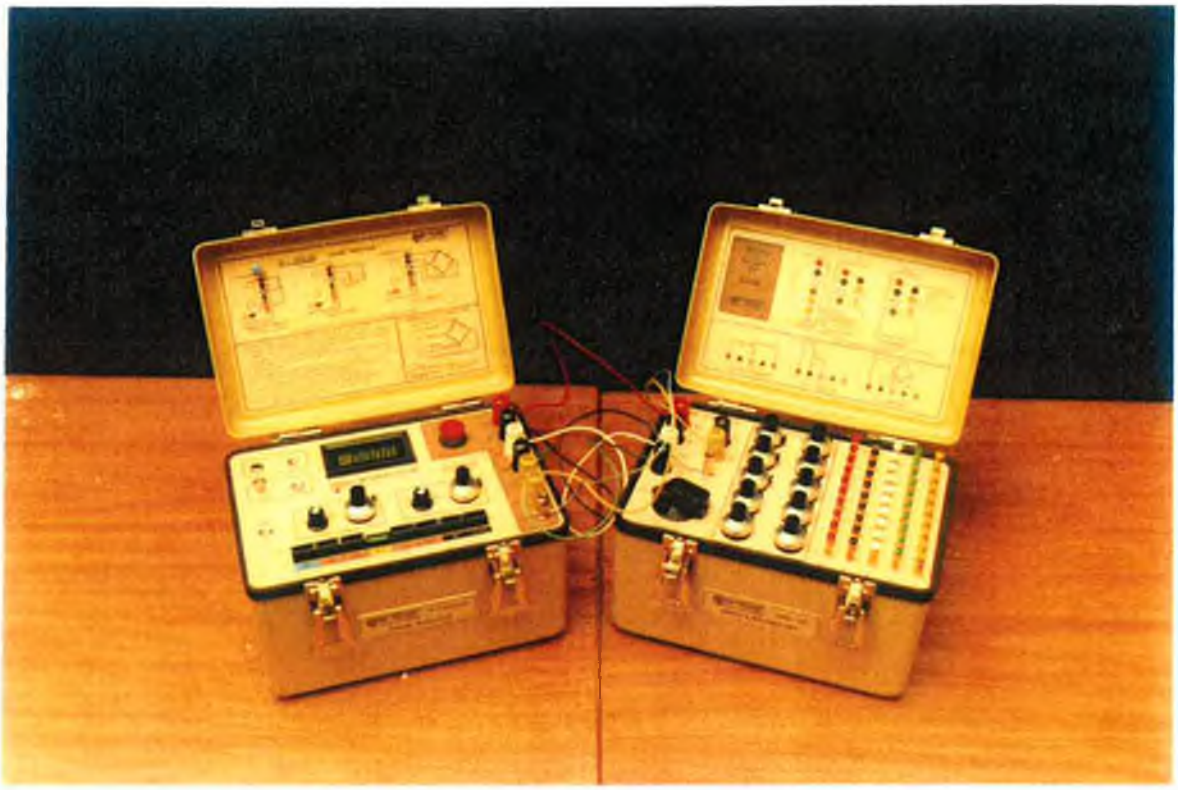

PLATE 3.7 THE DIGITAL INDICATOR P-3500 & THE SWITCH BALANCE SB-10.

PLATE 3.8 THE RS-200 GUIDE-DRILLING EQUIPMENT.

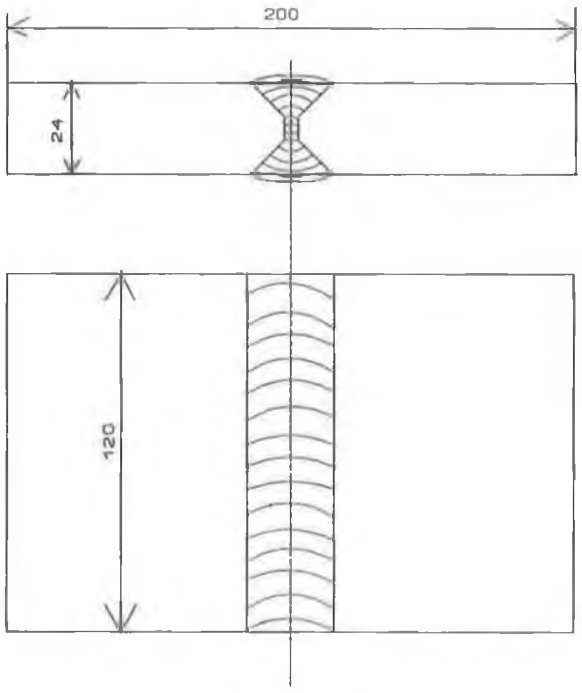

FIGURE 3.1 DRAWING OF THE STAINLESS-STEEL WELDED COMPONENT.

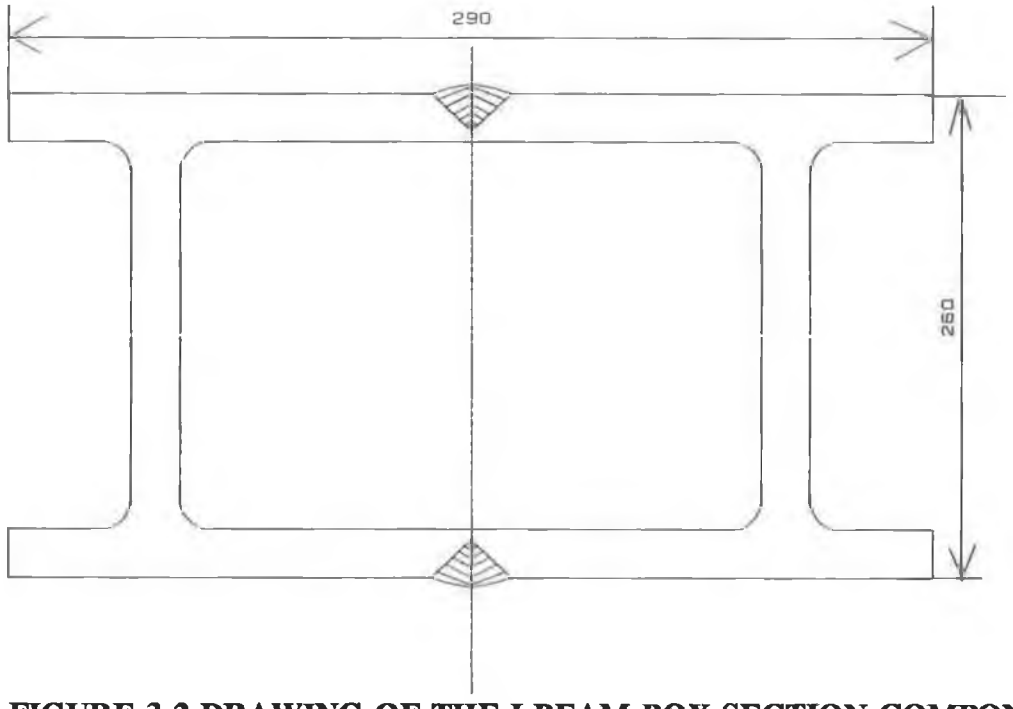

FIGURE 3.2 DRAWING OF THE I-BEAM BOX-SECTION COMPONENT.

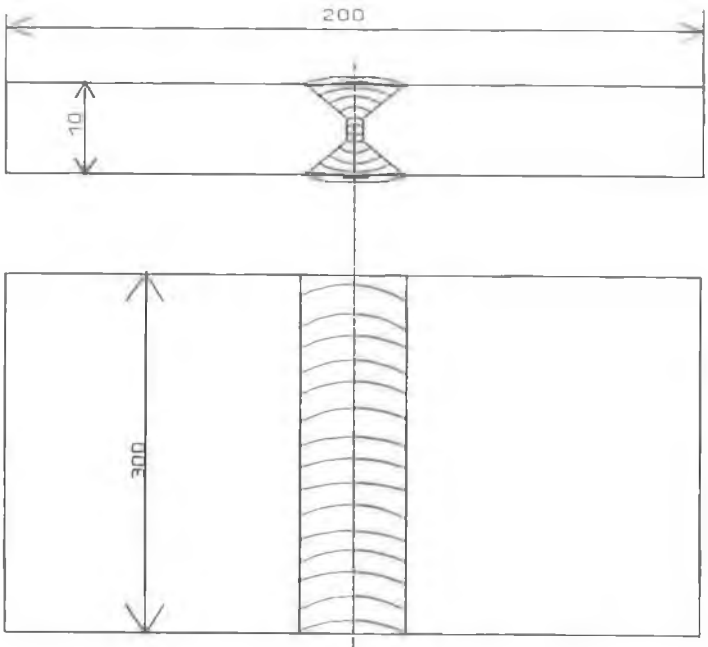

FIGURE 3.3 DRAWING OF THE DOUBLE-V CARBON STEEL COMPONENT.

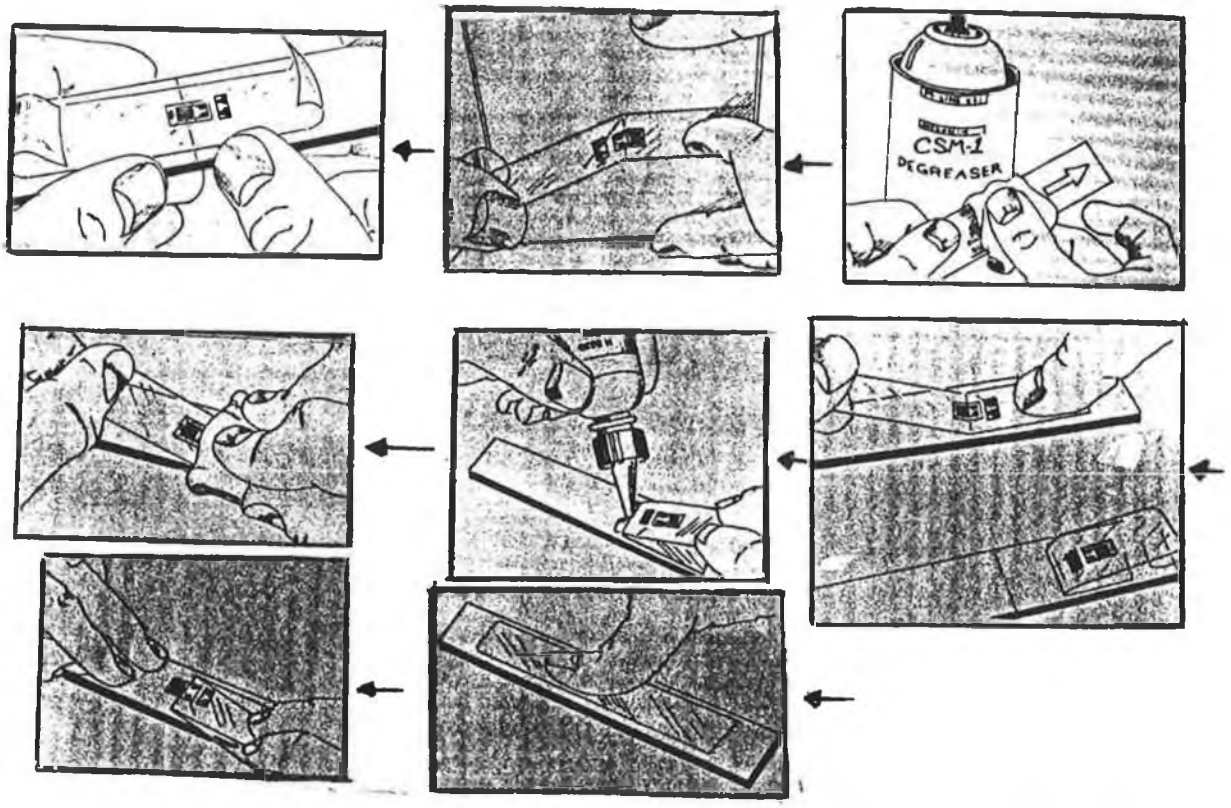

FIGURE 3.4 THE DIFFERENT STEPS OF STRAIN GAUGE PREPARATION.

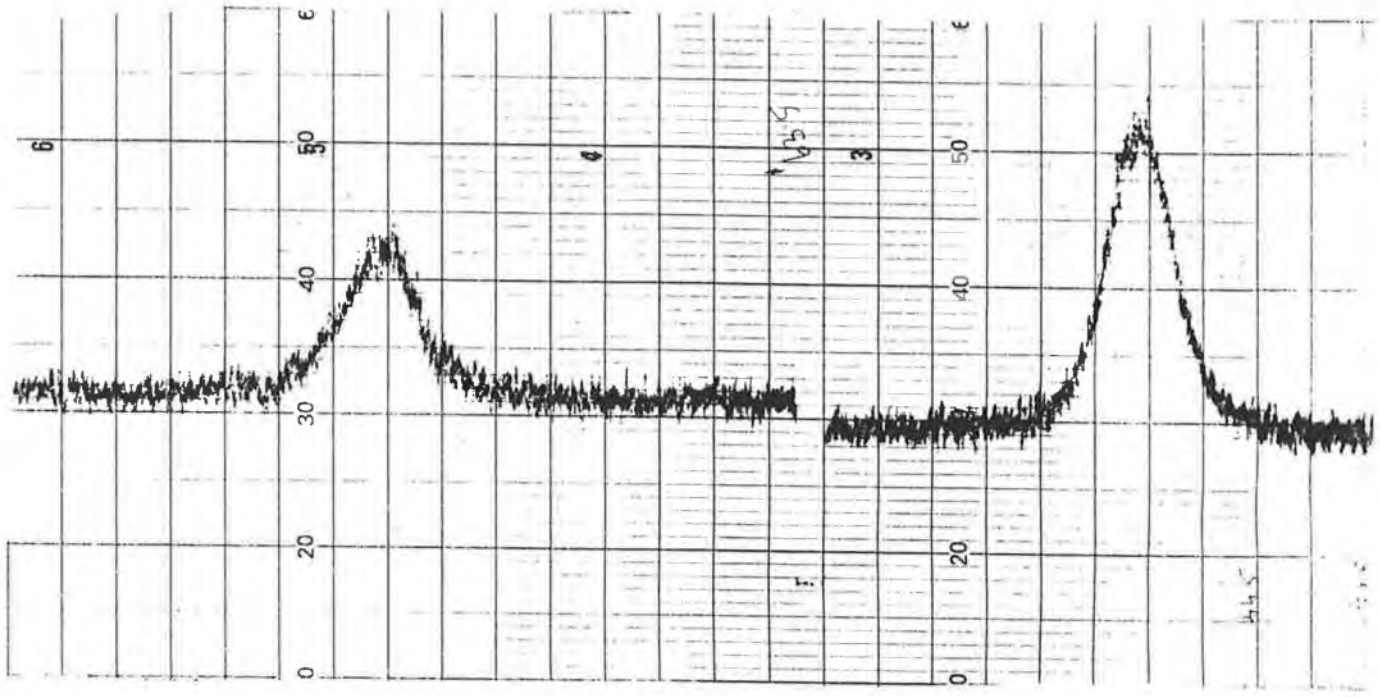

FIGURE 3.5 THE X-RAY DIFFRACTION PATTERN BEFORE PWHT FOR AISI-410.

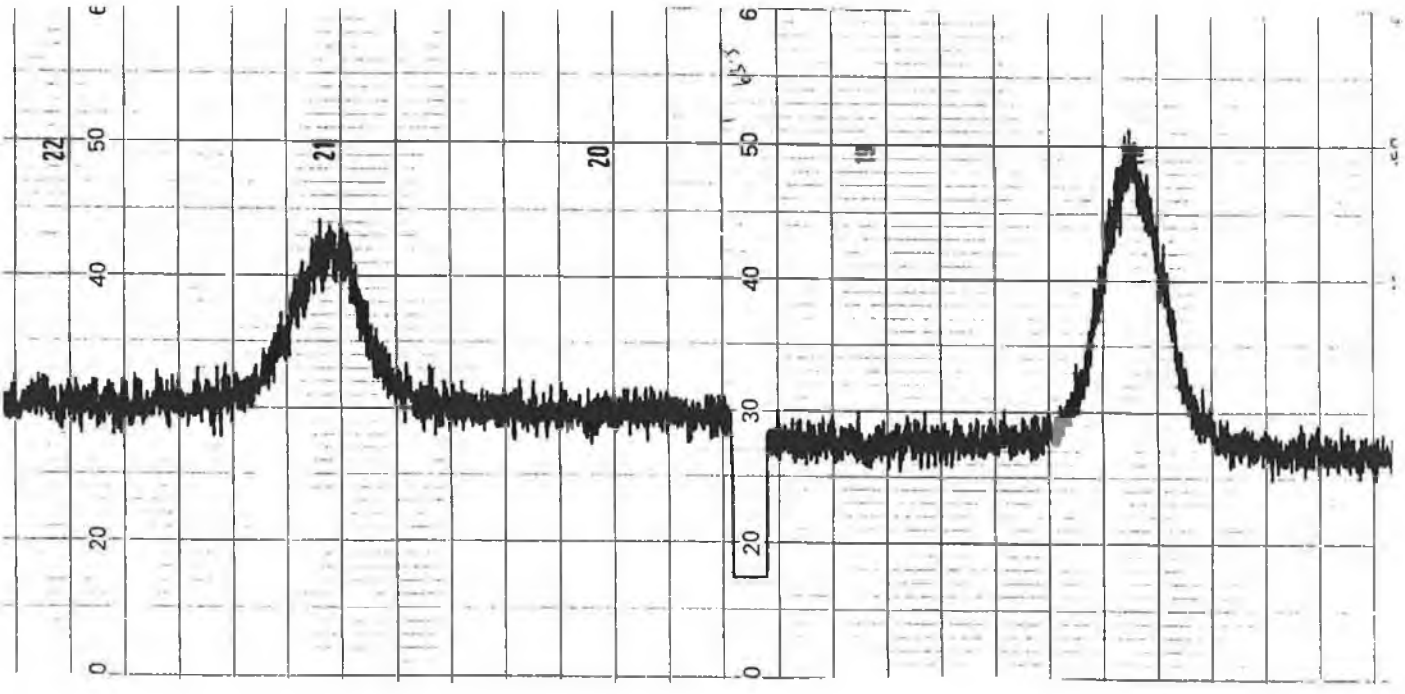

FIGURE 3.6 THE X-RAY DIFFRACTION PATTERN AFTER PWHT WITH SOAKING TEMPERATURE OF 550°C FOR AISI-410.

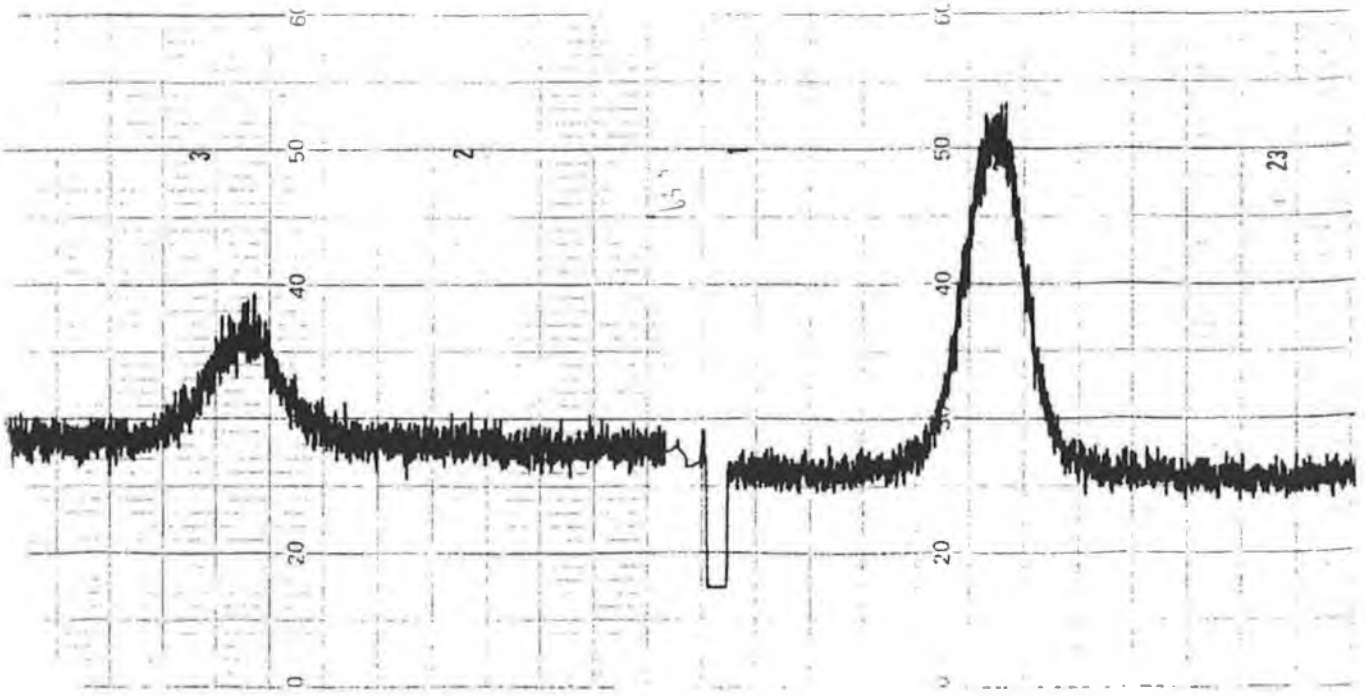

FIGURE 3.7 THE X-RAY DIFFRACTION PATTERN AFTER PWHT WITH SOAKING TEMPERATURE OF 650°C FOR AISI-410.

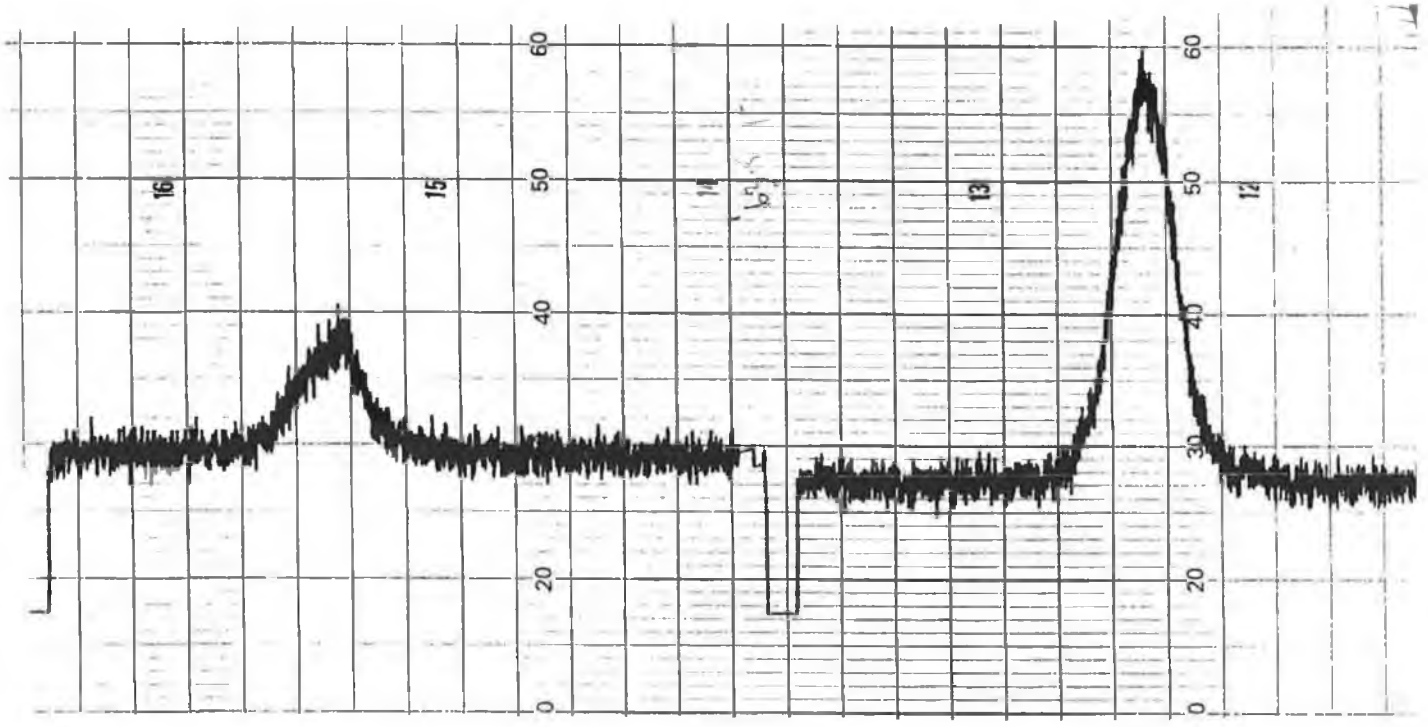

FIGURE 3.8 THE X-RAY DIFFRACTION PATTERN AFTER PWHT WITH SOAKING TEMPERATURE OF 750°C FOR AISI-410.

TEA-XX-062RK-120

CEA-XX-062UM-120

EA-XX-062RE-120

FIGURE 3.9 DIFFERENT TYPES OF STRAIN GAUGES.

CHAPTER FOUR

RESULTS

4.1 MICROSTRUCTURE AND MECHANICAL PROPERTIES RESULTS

4.1.1 INTRODUCTION

In order to study the effect of PWHT on microstructure and mechanical properties a number of testings were applied to these different types of welded specimens before and after the application of these different schemes of heat treatments.

Microstructure, microhardness, tensile and notch impact testings were carried out on all of these described conditions in Chapter 3. The following sections will demonstrate the results of these tests.

4.1.2 I-BEAM BOX-SECTION COMPONENT

4.1.2.1 HARDNESS TESTING RESULTS

As mentioned before, the initial tests for the low carbon steel AISI-1020 were applied on the I-beam box-section component before and after the application of PWHT (580°C for 18 hours). The hardness variation was determined across the specimen thickness at three different depths 1, 5 and 10 mm from the specimen surface and also in the depth along the specimen axis.

Figure 4.1 shows these different lines where the readings have been taken.

The results show that before the application of PWHT the hardness at a depth of 1 mm is about 260 HV in the HAZ and it gradually reduced to about 220 HV outside this zone. At a depth of 5 mm the hardness is reduced to about 245 HV in the HAZ and then gradually decreased to about 215 HV outside the HAZ. At a depth of 10 mm the hardness variation becomes higher in the HAZ with a value of 225 HV and about 215 HV outside this zone. Figure 4.2 shows these different results before the application of PWHT.

After the application of PWHT the hardness at a depth of 1 mm from the specimen surface is reduced to between 230 to 235 HV in the HAZ and to about 210 HV outside this zone. At a depth of 5 mm, the hardness is decreased to about 220 HV in the HAZ and also to about 210 HV in the base metal. Whilst, at a depth of 10 mm the HAZ is almost eliminated and the hardness value was just about 215 HV in the HAZ and about 205-210 HV outside this zone. Figure 4.3 shows the hardness variation after the application of PWHT.

Figure 4.4 compares the hardness variations along the specimen axis. These results point out that there is a gradual reduction of about 35 HV between the top and the bottom of the specimen for both conditions (before and after PWHT). There is also about 30 HV reduction in the hardness value after the application of PWHT.

Figures 4.5 compares the hardness before and after PWHT at a depth of 1 mm from the specimen surface. It can be seen from this Figure that the hardness value is reduced by about 30 HV in the HAZ and about 10 HV in the base metal, but the width of the HAZ becomes slightly smaller after the application of this scheme of heat treatment.

4.1.2.2 TENSILE STRENGTH RESULTS

The tensile test was carried out as part of investigating the metal toughness of this welded component. To carry out this investigation, a number of tensile specimens were prepared for both as-welded and after PWHT conditions.

The results of this test show that the tensile strength is 425 N/mm² for as welded condition before applying PWHT, and it becomes 453 N/mm² after applying PWHT. It is evident from these results that the tensile strength is improved by about 28 N/mm² after the application of PWHT.

4.1.2.3 IMPACT ENERGY RESULTS

The notched-impact energy test was carried out in order to determine the metal toughness. A number of specimens were prepared for both as-welded condition and after PWHT to ensure accurate result of this test.

The results obtained reveal that the metal toughness is 55 J before the application of PWHT and it increases to 75 J after the application of PWHT. This result shows that there is a good improvement in the metal toughness after applying this type of heat treatment.

4.1.3 DOUBLE-V LOW CARBON STEEL AISI-1020 COMPONENT

After the initial tests on the I-beam box-section component, many double-V butt-welded components were prepared and different types of PWHTs were applied. These heat treatments were applied by varying the heating rate, soaking temperature, time duration and cooling rate with the objective of assessing the effect of these heat treatment stages, to reach the optimum heat treatment procedures which could reduce or eliminate the residual stress without

compromising the mechanical properties.

4.1.3.1 MICROSTRUCTURE RESULTS

As mentioned before, microstructure inspection was carried out to evaluate the effect of heat treatment on the metal microstructure. An optical microscope was used to carry out this work. In the mean time, an X-ray diffraction test was carried out to identify the structure of these different types of welded components for both before and after the application of PWHTs.

The results show that before the application of PWHT the microstructure of the welding zone consists of bainite and small percentage of ferrite. It can be seen from this inspection that there is no noticeable difference in the structure of the HAZ. Plate 4.1 shows a photograph of the microstructure of the welding zone for as-welded condition. The structure outside this zone consists of ferrite and perlite. Plate 4.2 shows a photograph of the microstructure of the base metal.

It was found that after the application of PWHTs which have different soaking temperatures, the microstructure of the welding zone is tempered and the structure consists of tempered bainite, ferrite and a very small percentage of precipitated carbide. Moreover, the percentage of ferrite was slightly increased as the soaking temperature increased. Plates 4.3, 4.4 and 4.5 show photographs for the microstructure of the welding zone after the application of PWHTs with soaking temperatures 450, 550 and 650°C respectively. Meanwhile, the structure of the base metal (outside the welding zone) is still the same consisting of ferrite and pearlite.

The results show that after the application of PWHT with different heating rates, time durations and cooling rates with soaking temperatures of 450°C, there is no significant difference in the metal microstructure after the application of these different schemes and the

metal microstructure consists of tempered bainite, ferrite and a very low percentage of precipitated carbide. Plate 4.6 shows the microstructure of the welding zone after PWHT 7 (time duration of 10 h).

4.1.3.2 HARDNESS TEST RESULTS

As described before, different PWHT schemes were applied to the welded components. To evaluate the hardness variation on these welded components, a large number of readings were taken to determine the hardness variation across the specimen thickness at different depths from the specimen surface.

The initial results show that there is no difference in the hardness values at the same depth from either the top or the bottom surface. Then, the measurements were taken at two depths 1 and 5 mm from the specimen surface (lines L1 and L2) and along the axis in the specimen's depth (line L3). Figure 4.6 shows these different lines for the hardness measurements.

The results obtained reveal that before the application of PWHT the hardness value at 1 mm depth increases to about 280 HV in the HAZ and is about 230 HV outside this zone. However, at a depth of 5 mm the hardness is about 260 HV in the HAZ and is about 225 HV outside this zone. Figure 4.7 shows the hardness variation results before the application of PWHT.

However, after the application of PWHTs the hardness values decreased in the HAZ to different levels depending on the heat treatment procedures. Figures 4.8 to 4.24 show the hardness variation for each type of these heat treatments at two different depths 1 and 5 mm. Comparison diagrams were plotted to compare these different heat treatment schemes which

differ in the soaking temperatures, heating rates, time durations or cooling rates. These comparisons were carried out for both in the depth of the thickness across the welding axis (line L3) and along the specimen axis at the depth of 1 mm from the specimen surface (line L1).

After the application of PWHT a (soaking temperature = 450 °C), the hardness value at a depth of 1 mm from the specimen surface is decreased to about 260 HV in the HAZ and to a range of 210-215 HV outside this zone. The hardness value at a depth of 5 mm is reduced to about 240 HV in the HAZ and again to the same range between 210 and 215 HV outside this zone. It can be noticed that the width of the HAZ becomes smaller at a depth of 5 mm from the surface. Fig. 4.8 shows the hardness variation after the application of this scheme of PWHT.

Figure 4.9 shows the hardness variation after PWHT b (soaking temperature = 550 °C). After the application of this scheme of PWHT, the hardness value at a depth of 1 mm is reduced to about 240 HV in the HAZ and to about 210 HV outside this zone. The hardness value at a depth of 5 mm is reduced to about 225 HV in the HAZ and to about 210 HV outside this zone.

Figure 4.10 shows the hardness variation after PWHT c (soaking temperature = 650 °C). These results reveal that the hardness value at a depth of 1 mm is reduced to about 220 HV in the HAZ and to about 200 HV outside this zone. The hardness at a depth of 5 mm decreases to about 210 HV in the HAZ and to about 200 HV outside this zone.

Figure 4.11 shows a comparison diagram between the hardness variation at a depth of 1 mm, for as-welded condition and after the application of these heat treatment schemes, a, b and c which have different soaking temperature 450, 550 and 650 °C respectively. These results show that with increasing the heat treatment soaking temperature the hardness values have been reduced.

Figure 4.12 compares the hardness variation in the depth of the thickness (line L3) for these four above described conditions, before and after PWHT with different soaking temperatures. It can be seen from this Figure that the hardness value for as-welded condition is reduced from about 280 HV near the specimen surface to about 260 HV in the middle of the thickness. After PWHT-a the hardness value is about 260 HV near the specimen surface and it decreases to about 240 HV in the middle of the specimen thickness. After the application of PWHT-b the hardness is reduced to about 240 HV near the surface and to about 225 HV in the middle of the thickness. Finally, after PWHT-c the hardness is reduced to about 220 HV near the specimen surface and about 210 HV in the middle of the thickness.

Post weld heat treatments with different heating rates 50, 100 and 400 °C/h were applied. The obtained results of these tests reveal that there is no significant difference after the application of these different schemes and the hardness value at a depth of 1 mm is in the range of 250-260 HV in the HAZ and between 210 and 215 HV outside this zone. The hardness value at the depth of 5 mm is reduced to about 240 HV in the HAZ and to about 210 HV outside this zone. These results are illustrated in Figures 4.13, 4.14 and 4.8 for PWHT with heating rates of 50, 100 and 400°C/h respectively.

Figure 4.15 shows a comparison diagram for the hardness variation at a depth of 1 mm for both as-welded condition and after the application of PWHT schemes, d, e and f which have the same heat treatment procedures with the only difference being in the heating rate. The results show that there is no significant change in the hardness variation by varying the heating rates.

Figure 4.16 shows the hardness variation across the specimen thickness for the same conditions described above. The results show that the hardness decreases in the middle of the specimen thickness by about 25 HV for as-welded condition and also it decreases after the application of PWHT schemes d, e and f by about 20 HV in the middle of the specimen

thickness.

In this investigation, PWHTs with different soaking time durations 0.5, 2 and 10 hours have been applied. The results show that the hardness value is decreased to different levels depending on the PWHT scheme.

Figure 4.17 shows the hardness variation after PWHT-g (time duration = 0.5 h). These results show that the hardness value at a depth of 1 mm is slightly decreased to about 275 HV in the HAZ and to about 220 HV outside this zone. At a depth of 5 mm the hardness is about 255 HV in the HAZ and also about 220 HV outside this zone. Figure 4.8 shows the hardness variation after PWHT h (time duration = 2 h) which has the same heat treatment procedures of PWHT-a.

Figure 4.18 shows the hardness variation after PWHT i (time duration = 10 h). These results show that the hardness at a depth of 1 mm is decreased to the range of 240-245 HV in the HAZ and to about 205 HV outside this zone. The hardness value at a depth of 5 mm is reduced to about 235 HV in the HAZ and gradually decreased to about 205 HV outside this zone.

Figure 4.19 shows a comparison diagram for the hardness variation at a depth of 1 mm, for as-welded condition and after the application of PWHT schemes, g, h and i with soaking time duration 0.5, 2 and 10 hours respectively. The results show that the hardness is decreased by increasing the soaking time duration of PWHT.

Figure 4.20 shows the hardness variation across the specimen thickness for the same conditions described above. The results obtained reveal that after the application of PWHT scheme g the hardness is reduced from about 275 HV near the specimen surface to about 255

HV in the middle of the specimen thickness. After PWHT h the hardness value also decreases from about 260 HV near the surface to about 240 HV in the middle of the thickness. Finally, after PWHT scheme i the hardness is decreased from about 245 HV near the surface to about 235 HV in the middle of the specimen thickness.

Finally, PWHTs with different cooling rates have been applied. The hardness variations were also measured across the specimen at the depths of 1 and 5 mm from the specimen surface. The results of this test are plotted in Figures 4.21, 4.22 and 4.8.

Figure 4.21 shows the hardness variation after PWHT-j (cooling rate = 10 °C/h). These results reveal that the hardness variation at a depth of 1 mm is in the range of 245-250 HV in the HAZ and about 210 HV outside this zone. Meanwhile, the hardness variation at a depth of 5 mm is in the range of 230-235 HV in the HAZ and about 210 HV outside this zone. Figure 4.8 shows the hardness variation after PWHT-k (cooling rate = 40 °C/h) which has the same heat treatment procedures of PWHT-a.

Figure 4.22 shows the hardness variation after PWHT-l (cooling rate = 125 °C/h). These results reveal that the hardness variation at a depth of 1 mm is reduced to the range of 270-275 HV in the HAZ and to about 220 HV outside this zone. At a depth of 5 mm, the hardness value is decreased to about 250 HV in the HAZ and is about 215 HV outside this zone.

Figure 4.23 shows a comparison diagram between the hardness variation at a depth of 1 mm, for as-welded condition and after PWHT schemes j, k, and l which have different cooling rates 10, 40 and 125 °C/h respectively. The results show that the hardness value is decreased by applying PWHT with slower cooling rate.

Figure 4.24 shows the hardness variation across the specimen thickness for the same

previous conditions. These results show that after PWHT j the hardness value is reduced from about 250 HV near the specimen surface to about 235 HV in the middle of the specimen thickness. The hardness value is reduced from about 260 HV near the surface to about 240 HV in the middle of the thickness after the application of PWHT k. Finally, after PWHT l the hardness is reduced from about 270 HV near the surface to about 250 HV in the middle of the specimen thickness.

4.1.3.3 TENSILE STRENGTH RESULTS

This test was made to determine the ultimate tensile strength for these different schemes of heat treatment. The results reveal that after the application of these different PWHT schemes, the tensile strength is improved for different levels and the maximum improvement can be obtained after the application of PWHT with soaking temperature of 650°C.

It is evident from these results that the tensile strength of these types of welded components will be increased by applying PWHTs with higher soaking temperature, longer time duration or slower cooling rate. It can also be noticed from these results that there is no significant change in the tensile strength by varying the heating rates.

The tensile strength for the HAZ has been investigated. The results show that the tensile strength of the HAZ is 485 N/mm² for as-welded condition. After the application of PWHT with soaking temperature of 650 °C the tensile strength improved by about 15%. These results are illustrated in Table 4.1.

Heat Treatment Schemes	Description	Tensile Strength [N/mm²]	Tensile Strength For The HAZ [N/mm²]
The Original metal		410	
Before PWHT		420	485
PWHT-a	S.T. = 450°C	432	
PWHT-b	S.T. = 550°C	445	
PWHT-c	S.T. = 650°C	458	560
PWHT-d	H.R. = 50°C/h	435	
PWHT-e	H.R. = 100°C/h	432	
PWHT-f	H.R. = 400°C/h	432	
PWHT-g	T.D. = 0.5 h	425	
PWHT-h	T.D. = 2 h	432	
PWHT-i	T.D. = 10 h	444	
PWHT-j	C.R. = 10°C/h	445	
PWHT-k	C.R. = 40°C/h	432	
PWHT-l	C.R. = 125°C/h	430	

S.T.: Soaking Temperature; H.R.: Heating Rate; T.D.: Time Duration; C.R.: Cooling Rate.

TABLE 4.1 THE RESULTS OF THE TENSILE TEST FOR THE CARBON STEEL WELDED COMPONENT.

4.1.3.4 IMPACT ENERGY RESULTS

As mentioned before, this test was carried out to determine the effect of PWHTs on the impact energy. Many specimens were prepared to carry out this test for all these different schemes of heat treatments.

These results reveal that the metal toughness is improved by about 20 to 35% after the application of these different schemes of PWHTs. These results show that the impact toughness was about 54 J for as-welded condition. It was ranging between 62 and 80 after the application of these schemes of heat treatments. It is evident from these results that the maximum improvement in the toughness is obtained after the application of PWHT with soaking temperature of 650°C. It can also be noticed that the PWHT with longer time duration and slower cooling rate has a good effect on improving the toughness of this welded component. Table 4.2 summarizes the results of this test.

Heat Treatment Schemes	Description	Impact Energy [J]
The Original Metal		60
Before PWHT		54
PWHT-a	S.T. = 450°C	70
PWHT-b	S.T. = 550°C	73
PWHT-c	S.T. = 650°C	80
PWHT-d	H.R. = 50°C/h	72
PWHT-e	H.R. = 100°C/h	70
PWHT-f	H.R. = 400°C/h	70
PWHT-g	T.D. = 0.5 h	62
PWHT-h	T.D. = 2 h	70
PWHT-i	T.D. = 10 h	72
PWHT-j	C.R. = 10°C/h	73
PWHT-k	C.R. = 40°C/h	70
PWHT-l	C.R. = 125°C/h	65

S.T.: Soaking Temperature; H.R.: Heating Rate; T.D.: Time Duration; C.R.: Cooling Rate.

TABLE 4.2 THE RESULTS OF THE IMPACT ENERGY TEST FOR THE CARBON STEEL WELDED COMPONENT.

4.1.4 DOUBLE-V STAINLESS-STEEL AISI-410 COMPONENT

4.1.4.1 MICROSTRUCTURE RESULTS

In this investigation, the metal microstructure was inspected for this type of welded component for both before and after the application of PWHTs. An optical microscope was also employed to carry out this work. An X-ray diffraction test was also carried out to identify the structure of these different types of welded components for as-welded condition and after the application of PWHTs.

This test was carried out in both the HAZ and the base metal. It was found that there is no noticeable difference in the structure of the HAZ across the specimen depth for both as-welded condition and after the application of PWHTs. The results show that the microstructure for as-welded condition in the welding zone is completely martensite. Plate 4.7 shows a photograph of the microstructure of the welding zone for as-welded condition. Meanwhile, the metal microstructure outside this zone consists of tempered martensite, low percentage of ferrite and a very low percentage of precipitated carbide.

It can be noticed that after the application of PWHT with different soaking temperature the metal microstructure of the welding zone is tempered and the structure consists of tempered martensite and low percentage of ferrite with a small amount of fine precipitated carbide. It can also be noticed that the percentages of the ferrite and the precipitated carbide were increased as the soaking temperature increased. Plate 4.8, 4.9 and 4.10 show photographs of the microstructure in the welding zone after the application of PWHT with soaking temperatures of 550, 650 and 750°C respectively.

The results show that after the application of PWHT with different heating rates, soaking

time durations and cooling rates with same soaking temperatures of 550°C, there is no significant difference in the metal microstructure of the welding zone after the application of these different schemes of PWHT and the metal microstructure consists of tempered martensite, ferrite and fine precipitated carbide. Plate 4.11 shows a photograph of the microstructure of the welding zone for PWHT 10 (as an example for these different schemes).

4.1.4.2 HARDNESS TEST RESULTS

This test was made across the specimen thickness at different depths from the specimen surface. The initial results show that there is no difference in the hardness values at the same depth from either the top or the bottom surface. Then, the hardness test was carried out at three different depths from the specimen surface (1, 5 and 12 mm) and across the welding line. Figure 4.25 shows these different lines of the hardness measurements.

Figure 4.26 shows the results of the hardness variation before the application of PWHT at these three different depths. The results obtained reveal that before the application of PWHTs the hardness value at a depth of 1 mm is increased to the range of 505-515 HV in the HAZ and is about 260 HV outside this zone. At a depth of 5 mm the hardness value decreases to about 475 HV in the HAZ and to about the same 260 HV in the base metal. However, at a depth of 12 mm the hardness decreases to about 460 HV in the HAZ and to the range of 255-260 HV in the base metal. It can be also seen that the width of the HAZ decreases as the distance from the surface increases.

Figures 4.27, 4.28 and 4.29 show the hardness variation after the application of PWHTs which have different soaking temperatures 550, 650 and 750 °C respectively. It can be seen from Figure 4.27 that after the application of PWHT-1 (soaking temperature of 550 °C) the hardness value at a depth of 1 mm is reduced to the range of 465-475 HV in the HAZ and to

about 260 HV outside this zone. At a depth of 5 mm the hardness is found to be about 460 HV in the HAZ which decreases to about 260 HV outside this zone. Finally, at a depth of 12 mm the hardness value is decreased to about 430 HV in the HAZ and again it reduced to about the same 260 HV in the base metal.

Figure 4.28 shows the hardness variation after PWHT-2 (soaking temperature of 650 °C). The results obtained reveal that after the application of this type of heat treatment the hardness value at a depth of 1 mm is dropped to about 345 HV in the HAZ and to about 255 HV outside this zone. The hardness value at a depth of 5 mm is decreased to about 325 HV in the HAZ and to about 255 HV outside this zone. Also the hardness at a depth of 12 mm is dropped to about 295 in the HAZ and gradually decreased to about 255 HV in the base metal.

Figure 4.29 shows the results of the hardness variation after the application of this scheme of heat treatment. After the application of PWHT-3 (soaking temperature of 750 °C) the results reveal that the hardness value at a depth of 1 mm is dropped to about 300 HV in the HAZ and to about 255 HV outside this zone. At a depth of 5 mm the hardness is reduced to about 280 HV in the HAZ and to the range of 245 to 255 HV in the base metal. Finally, at a depth of 12 mm the hardness is about 270 HV in the HAZ and to the range of 245 to 250 HV in the base metal.

Figure 4.30 reveals the results obtained of the hardness variation along the specimen axis (line L4). These results show that before the application of PWHT the hardness value is about 510 HV near the specimen surface and it reduces to about 460 HV in the middle of the thickness. After PWHT with soaking temperature of 550 °C the hardness decreased to about 475 HV near the surface and to about 430 HV in the middle of the specimen thickness. However, after PWHT with soaking temperature of 650 °C the hardness value is dropped to about 350 HV near the specimen surface and to about 300 HV in the middle of the specimen thickness.

Finally, after PWHT-3 the hardness variation is dropped to about 300 HV near the specimen surface and to about 270 HV in the middle of the specimen thickness. It is evident from these results that the hardness value decreases as the distance from the surface increases, due probably to the faster cooling rate near the surface.

A comparison diagram has been plotted to compare the hardness value across the specimen axis at the depth of 1 mm from the specimen surface for as-welded condition and after the application of different schemes of PWHT which varied in their soaking temperature 550, 650 and 750°C. It can be seen from this comparison (Figure 4.31) that the hardness is dropped by about 35 HV in the HAZ after PWHT-1 and by about 160 HV after PWHT-2 and by more than 200 HV after PWHT-3. Meanwhile, the hardness in the base metal is still about the same without any significant change.

To assess the effect of the heating rate on the hardness variation three different schemes of PWHTs with different heating rates were applied. The results show that after PWHT-4 (heating rate of 50 °C/h) the hardness value at a depth of 1 mm is reduced to about 470-475 HV in the HAZ and to about 260 HV in the base metal. At a depth of 5 mm, the hardness is decreased to about 455 HV but with smaller width and also to about 260 HV in the base metal. Meanwhile, at a depth of 12 mm the hardness value dropped to about 425 HV in the HAZ and to about the same 260 HV outside this zone. Figure 4.32 shows the hardness variation after the application of this type of heat treatment.

Figure 4.33 shows the results after the application of PWHT-5 (heating rate of 100 °C/h). These results show that the hardness value at a depth of 1 mm is ranging between 470-475 HV in the HAZ and it decreased to about 260 HV outside this zone. At a depth of 5 mm, the hardness value is around 455 and 460 HV in the HAZ, which is about 3 to 4 mm smaller than HAZ at the depth of 1mm. Meanwhile, the hardness value is decreased to about 260 HV

in the base metal. Finally, the hardness at a depth of 12 mm is in the range of 425-430 HV in the HAZ and decreased to about 260 HV in the base metal. Figure 4.27 reveal the results of PWHT-6 (heating rate of 400 °C/h) which has the same procedure of PWHT-1.

Figure 4.34 compares the hardness variation along the specimen axis in the depth of the thickness. The results obtained reveal that the hardness is decreased to about 470 to 475 HV near the surface for these three schemes of heat treatments and it gradually reduces to the range of 425 and 430 HV in the middle of the specimen's thickness after the application of these different heat treatments which have different heating rates. It can also be seen from these results that the hardness value decreases as the distance from the surface increases both before and after the application of these schemes of heat treatments.

Figure 4.35 compares the hardness variation at a depth of 1 mm for as-welded condition and after the applications of PWHTs with three different heating rates. The results obtained point out that the hardness value is dropped from about 510 HV in the HAZ for as-welded specimen to about 475 HV after the application of these three types of heat treatments. It can also be seen that there is no change in the hardness value in the base metal for these different conditions. It is evident from these results that there is no significant change in the hardness value of the HAZ after the application of these different schemes of PWHTs which varied in their heating rates.

In this investigation, the effect of time durations of heat treatment were studied. Three different schemes of PWHT were applied which varied in their time duration 0.5, 2 and 10 hours. Figure 4.36 shows the hardness variation after the application of this scheme of heat treatment. The results show that after the application of PWHT-7 (time duration of 0.5 h) the hardness value at a depth of 1 mm is in the range of 490 to 495 HV in the HAZ and about 260 HV outside this zone. At a depth of 5 mm the hardness is also reduced to about 480 HV in the HAZ and dropped to about 260 HV outside this zone. Finally, at a depth of 12 mm the hardness

value is about 445 HV in the HAZ and becomes again about 260 HV in the base metal. Figure 4.27 shows the results of PWHT-8 (time duration of 2 h) which has the same heat treatment procedures of PWHT-1.

Figure 4.37 shows the results obtained after the application of PWHT-9 (time duration of 10 h). It can be seen from this Figure that the hardness value at a depth of 1 mm is dropped to about 410 HV in the HAZ and to about 260 HV outside this zone. At a depth of 5 mm, the hardness value is reduced to about 380 HV in the HAZ and again to about 260 HV in the base metal. Finally, the hardness value at a depth of 12 mm is dropped to about 350 HV in the HAZ and to about 260 HV outside this zone.

The hardness variation has been measured in the depth along the specimen axis. Figure 4.38 shows a comparison diagram between these different conditions, as-welded and after PWHTs with different time durations. The obtained results reveal that after PWHT-7 (time duration = 0.5 h) the hardness is about 495 HV near the surface and about 450 HV in the middle of the specimen thickness. However, after PWHT-8 (time = 2 h) the hardness is dropped to about 475 HV near the surface and to about 430 HV in the middle of the thickness. Finally, after PWHT-9 (time duration = 10 h) the hardness is decreased to about 410 HV near the specimen surface and to about 350 HV in the middle of the thickness. These results show again that the hardness value decreases as the distance from the surface increases.

Figure 4.39 compares the hardness variation at the depth of 1 mm from the specimen surface before and after the application of PWHTs with different time duration 0.5, 2 and 10 hours. These results reveal that the hardness value in the HAZ is reduced by about 15 HV after the application of PWHT-7 (time duration = 0.5 h) and by about 35 HV after PWHT-8 (time duration = 2 h) and by about 100 HV after PWHT-9 (time duration = 10 h). Meanwhile, after the application of these schemes the hardness value outside the HAZ is still the same as before

the application of these heat treatment schemes.

Different PWHTs were applied to study the effect of the cooling rate on the hardness variation. These heat treatment schemes have the same heating rate, soaking temperature and time duration with the only difference being in the cooling rate.

It can be seen from Figure 4.40 that after PWHT-10 (cooling rate = 10 °C/h) the hardness at a depth of 1 mm from the specimen surface is dropped to about 435 HV in the HAZ and to about 260 HV outside this zone. At a depth of 5 mm the hardness value is reduced to the range of 400-410 HV in the HAZ and again to about 260 HV outside this zone. Finally, at a depth of 12 mm the hardness value is decreased to about 385 HV in the HAZ and again to about 260 HV in the base metal. Figure 4.27 shows the results of PWHT-11 (cooling rate of 40 °C/h) which has the same heat treatment procedures of PWHT-1.

Figure 4.41 shows the hardness variation after PWHT-12 (cooling rate of 125 °C/h). It can be seen from this Figure that the hardness value at a depth of 1 mm is in the range of 485-495 HV in the HAZ and is about 260 HV in the base metal. Meanwhile, the hardness value at a depth of 5 mm is decreased to about 470 HV in the HAZ and again to 260 HV in the base metal. Finally, the hardness value at a depth of 12 mm is reduced to about 445 HV in the HAZ and to about 260 HV outside this zone.

Figure 4.42 compares the hardness variation along the specimen axis for these previous schemes of heat treatments which have different cooling rates. These results reveal that after PWHT-10 the hardness is reduced from about 435 HV near the surface to about 385 HV in the middle of the specimen thickness. After PWHT-11 the hardness value is dropped from about 475 HV near the specimen surface to about 430 HV in the middle of the thickness. Finally, after PWHT-12 the hardness is dropped from about 485 HV near the specimen surface to about 445

HV in the middle of the specimen thickness. It is evident from these results that the hardness decreases as the distance from the surface increases.

Figure 4.43 compares the hardness variation at the depth of 1 mm for these heat treatment schemes which varied in their cooling rates. It can be seen from this Figure that after PWHT-10 the hardness value is dropped by about 75 HV in the HAZ. Meanwhile, the hardness value is also reduced in the HAZ by about 35 HV after the application of PWHT-11. Finally, the hardness value is reduced by about 25 HV after the application of PWHT-12. It can be also seen from these results that there is no reduction in the hardness value outside the HAZ before and after the application of these heat treatment schemes.

4.1.4.3 TENSILE STRENGTH RESULTS

An adequate number of specimens were prepared to carry out this test for this type of welding component. This test was made to evaluate the ultimate tensile strength for as-welded condition and after the application of these different schemes of PWHTs. Table 4.3 shows the results of the tensile test for the stainless-steel welding component. These results varied between a slight reduction and a good improvement in the tensile strength depending on the heat treatment scheme. These results show that the maximum improvement can be obtained after the application of PWHT with soaking temperature of 550°C.

It is evident from these results that the tensile strength is improved after the application of PWHT with lower soaking temperature. Meanwhile, the faster heating rate, the shorter time duration and the faster cooling rate have a slight effectiveness in improving the tensile strength.

It can be also noticed from this test that the fracture for these tensile specimens occurred outside the HAZ without any significant reduction in the HAZ area for all these different

conditions.

The tensile strength of the HAZ has been investigated the results show that the tensile strength of the HAZ for as-welded condition is 665 N/mm². After the application of PWHT with soaking temperature of 750 °C the tensile strength has improved by about 25 N/mm². These results are given in Table 4.3. It should be noted however, that the average elongation of the original metal is 18.3%. The elongation of the HAZ after welding is 14.7% which application of PWHT-3 (soaking temperature of 750 °C), changed to 17.5%. This is only marginally less than that of the original material.

Heat Treatment Scheme	Description	Tensile Strength [N/mm²]	Tensile Strength For The HAZ [N/mm²]
The Original Metal		510	
Before PWHT		515	665
PWHT-1	S.T. = 550°C	580	
PWHT-2	S.T. = 650°C	520	
PWHT-3	S.T. = 750°C	480	690
PWHT-4	H.R. = 50°C/h	565	
PWHT-5	H.R. = 100°C/h	570	
PWHT-6	H.R. = 400°C/h	580	
PWHT-7	T.D. = 0.5 h	588	
PWHT-8	T.D. = 2 h	580	
PWHT-9	T.D. = 10 h	560	
PWHT-10	C.R. = 10°C/h	566	
PWHT-11	C.R. = 40°C/h	580	
PWHT-12	C.R. = 125°C/h	585	

S.T.: Soaking Temperature; H.R.: Heating Rate; T.D.: Time Duration; C.R.: Cooling Rate.

TABLE 4.3 THE RESULTS OF THE TENSILE TEST FOR THE STAINLESS-STEEL WELDED COMPONENT.

4.1.4.4 IMPACT ENERGY RESULTS

The notched-impact energy test was carried out for as-welded condition and after the application of these different schemes of PWHTs. A large number of notched-impact specimens were prepared to carry out this test.

These results reveal that the metal toughness is improved after the application of these heat treatment schemes. These improvements were ranging between 1 and 14 J depending on the heat treatment scheme. The results reveal that the impact energy for as-welded condition is about 10 J. After the application of these different schemes of heat treatments the impact energy was ranging between 11 J and 24 J. It is evident from these results that the maximum improvement in the toughness is obtained after the application of PWHT with soaking temperature of 750 °C. It can also be noticed that the longer time duration and the slower cooling rate have improved the metal toughness. However, there is no significant effect on the toughness by varying the heating rate. Table 4.4 shows the result of the notched-impact test for the stainless-steel welded component.

Heat Treatment Schemes	Description	Impact Energy [J]
The Original metal		18
Before PWHT		10
PWHT-1	S.T. = 550°C	12
PWHT-2	S.T. = 650°C	20
PWHT-3	S.T. = 750°C	24
PWHT-4	H.R. = 50°C/h	14
PWHT-5	H.R. = 100°C/h	12
PWHT-6	H.R. = 400°C/h	12
PWHT-7	T.D. = 0.5 h	10
PWHT-8	T.D. = 2 h	12
PWHT-9	T.D. = 10 h	21
PWHT-10	C.R. = 10°C/h	20
PWHT-11	C.R. = 40°C/h	12
PWHT-12	C.R. = 125°C/h	11

S.T.: Soaking Temperature; H.R.: Heating Rate; T.D.: Time Duration; C.R.: Cooling Rate.

TABLE 4.4 THE IMPACT ENERGY RESULTS OF THE STAINLESS-STEEL WELDED COMPONENT.

4.2 RESIDUAL STRESS TESTING

4.2.1 Introduction

In order to determine the residual stresses in these different welded components, the hole-drilling method was used and the RS-200 drilling guide has been employed to carry out these measurements.

As mentioned in Chapter 2, different procedures have been carried out to ensure the best measurement conditions. The measurements were carried out at many points across the welding line, in the middle of the specimen, Plate 4.12 shows a photograph for the measurements line over one of these specimens. Three readings were taken from the strain indicator for each point. Following the measurement of these three strain values ($\epsilon 1$, $\epsilon 2$, $\epsilon 3$) the principal residual stresses and their directions were computed. This was done by substituting these three strain values in equations 2.12. The material coefficients a and b were chosen from diagram 2.5 depending on the rosette type. Then A and B calculated from equation 2.14. Figure 4.44 shows the strain gauge and its orientation on the specimen surface for these different types of welded components.

As described above, the residual stress measurements were carried out at different points across the welding line. Due to the difficulties of installing the strain gauge in the welding zone, the closest possible measurements were taken at a distance of 15 mm from the welding axis. Moreover, the residual stress along the welding line could be higher by 10-15% than the determined residual stress at the measured points near the welding line [8, 128].

Efforts were made to measure the residual stress in the welding zone. These measurements were carried out after machining a thin layer from the welding zone. The results

emphasize that the residual stress in the welding zone is about 10% higher than the residual stress at the point close to the welding line. The residual stresses were also measured at different points close to the welding line before and after executing this machining. These results show that there is a negligible difference in the residual stress value. All these preceding measurements were carried out for as-welded condition for both types of double-V welded components (AISI-410 and AISI-1020). Plate 4.13 shows a photograph of the welding specimen after machining the welding zone to measure the residual stress.

As described above, the principal residual stresses and their directions have been calculated. These results show that the directions of these stresses were varied for different levels and the angle α between the maximum residual stress and strain gauge Number 1 (see Figure 4.44) ranged between 10 and 30°. The principal residual stress values and their directions are illustrated in Appendix A for the different measured points and for the different heat treatment conditions for all types of the welded joints.

4.2.2 THE I-BEAM BOX-SECTION COMPONENT

In order to determine the residual stress in the I-beam box-section welded component, a number of strain gauge rosettes were used to measure the three strain values around the drilled hole. These measurements were repeated at different lines on the middle of the specimen, where the maximum value of the principal residual stresses were expected to be in the middle of the welded component [8, 129, 130].

It can be seen from Figure 4.45 that the maximum residual stresses at a distance of 15 mm from the welding line is about 330 N/mm² in tension and it decreases as the distance from the welding line increases. Meanwhile, the minimum residual stress reaches a value of 80 N/mm² at a distance of 15 mm from the welding line and it changes to a state of compression

at a distance more than 35 mm from the welding line.

Figure 4.46 shows the distribution of the principal residual stresses after the application of PWHT. After the application of PWHT (580 °C for 18 hours) the maximum residual stresses were decreased to about 90 N/mm² at a distance of 15 mm from the welding line and gradually decreases as the distance from the welding line increases. The minimum residual stresses showed a change of between 30 N/mm² in tension at a distance of 15 mm from the welding line to -20 N/mm² at a distance of 35 mm from the welding line and gradually the stress decreased to around zero at a distance of 80 mm from the welding line. .

Figure 4.47 compares the maximum residual stresses before and after PWHT. These results show that there is considerable reduction in the value of the maximum residual stress, which dropped from 330 N/mm² to 90 N/mm² after the application of this scheme of PWHT.

4.2.3 DOUBLE-V LOW CARBON STEEL AISI-1020 COMPONENT

The magnitude and distribution of the residual stress was determined for the double-v butt-welded low carbon steel component. The residual stress measurements were carried out across the middle of the specimen for as-welded and after the application of these different schemes of heat treatments. The initial measurements were carried out at the top and bottom surfaces of the welded component for the as-welded condition. The results show that there is a negligible difference between the magnitude of the maximum value of the residual stress at the top and the bottom surface. Then, the measurements were carried out only at the top surface for after PWHTs. The principal residual stresses have been determined for each condition. Figures 4.48 to 4.61 show the results of these tests.

It can be seen from Figure 4.48 that the maximum residual stress is about 365 N/mm²

at a distance of 15 mm from the welding axis and it reduces to about 165 N/mm² at a distance of 80 mm. Meanwhile, the minimum residual stress is about 85 N/mm² (tensile stress) near the welding axis and it becomes about 60 N/mm² in compression at a distance of about 60 mm, then it reduces to about 10 N/mm² in tension.

Figure 4.49 shows the principal residual stresses after the application of PWHT-a. After the application of PWHT-a (soaking temperature = 450 °C) the maximum residual stress reduced to about 200 N/mm² at a distance of 15 mm from the welding axis and continuously decreased to about 110 N/mm² at a distance of 80 mm. The minimum residual stress also decreased to about 55 N/mm² near the welding line and it reduced to about 40 N/mm² in compression at a distance of 80 mm.

Figure 4.50 shows the principal residual stresses after the application of PWHT-b (soaking temperature = 550 °C). It can be seen from this Figure that the maximum residual stress is decreased to about 95 N/mm² near the welding line and it decreased to about 35 N/mm² at a distance of 80 mm from the welding axis. Whilst, the minimum residual stress is decreased to about less than 20 N/mm² in tension near the welding line and changed to less than 20 N/mm² in compression at a distance of more than 50 mm from the welding axis.

Figure 4.51 shows the principal residual stresses after the application of PWHT-c. A tremendous stress relief was gained by applying PWHT scheme c (soaking temperature = 650 °C) where the maximum residual stress is ranging between 10 N/mm² near the welding line and -4 N/mm² at a distance of 60 mm from the welding axis. The minimum residual stress is ranging between 5 and -5 N/mm². These results show that this scheme of heat treatment can relieve the residual stresses for this type of welded component.

A comparison diagram for the maximum residual stress has been plotted for as-welded

condition and after the application of these three schemes of heat treatments. It can be seen from Figure 4.52 that the maximum residual stress near the welding line is decreased by about 160 N/mm² after the application of PWHT scheme a. Whilst, after the application of PWHT b the maximum residual stress is reduced by more than 250 N/mm². Finally, by the application of PWHT scheme c the residual stress is mostly relieved.

To distinguish the effect of the heating rate of PWHT on the residual stress, three PWHT schemes which have different heating rates were applied. Figures 4.49, 4.53 and 4.54 show the principal residual stresses for these three different schemes of heat treatments.

Figure 4.53 shows the principal residual stresses after the application of PWHT scheme d (heating rate = 50 °C/h). It can be seen from this Figure that the maximum residual stress is reduced to about 180 N/mm² at a distance of 15 mm from the welding line and to less than 120 N/mm² after a distance of about 35 mm from the welding axis. Meanwhile, the minimum residual stress is decreased to about 40 N/mm² near the welding line and to less than 20 N/mm² at a distance over than 35 mm.

Figure 4.54 shows the principal residual stresses after the application of PWHT-e. After the application of PWHT scheme e (heating rate = 100 °C/h) the maximum residual stress is reduced to about 190 N/mm² at the distance of 15 mm from the welding line and to the range of 85 to 100 N/mm² after the distance of about 35 mm. Whilst, the minimum residual stress is ranging between about 50 N/mm² near the welding line to about -50 N/mm² at the distance of 80 mm from the welding axis. Figure 4.49 shows the principal residual stresses after PWHT-f (heating rate = 400 °C/h), this scheme has the same heat treatment procedures of PWHT-a.

Figure 4.55 compares the maximum residual stresses for the above described heat treatments schemes. It can be seen from this Figure that the maximum value of the residual

stress is reduced by about 190 N/mm² after the application of PWHT d, and by about 180 N/mm² after heat treatment scheme e, and by about 165 N/mm² after the application of PWHT scheme f. These results show that the maximum value of the residual stresses has reduced to different levels after the application of these types of heat treatments, but there is a very slight reduction in the maximum value of the residual stresses by decreasing the heating rate of PWHT.

The principal residual stresses were determined after the application of PWHT with different time durations. Figure 4.56 shows the principal residual stresses after the application of PWHT scheme g (time duration = 0.5 h). These results reveal that the maximum residual stress was about 220 N/mm² at a distance of 15 mm from the welding axis and continuously decreased to about 100 N/mm² at a distance of 80 mm from the welding axis. Meanwhile, the minimum residual stress is decreased to about 65 N/mm² (tensile stress) near the welding line and it changes to a state of compression at a distance more than 30 mm from the welding line. Figure 4.49 shows the principal residual stresses after the application of PWHT scheme h (time duration = 2 h) which has the same heat treatment procedures of PWHT a.

Figure 4.57 shows the principal residual stresses after the application of PWHT-i. After the application of PWHT scheme i (time duration = 10 h) the maximum residual stress is dropped to about 110 N/mm² at a distance of 15 mm from the welding axis and continuously decreased to about 50 N/mm² at a distance of 80 mm. Whilst, the minimum residual stress is decreased to about 35 N/mm² near the welding line and to the range of -15 to 25 N/mm² at a distance more than 30 mm from the welding axis.

Figure 4.58 compares the maximum residual stress for these above schemes of heat treatment. It can be seen from this Figure that the maximum value of the residual stress is reduced by about 145 N/mm² after PWHT-g and by about 160 after PWHT-h and by about 250

N/mm^2 after PWHT-i. These results point out that there is a substantial effect on reducing the residual stress by applying PWHT with long time duration for this type of welded component.

To distinguish the effect of the cooling rate of PWHT on the residual stresses, three schemes of PWHT were applied which have different cooling rates. Figure 4.59 shows the principal residual stresses after the application of PWHT-j (cooling rate = 10 °C/h). It can be seen from this Figure that the maximum residual stress is reduced to about 170 N/mm^2 at a distance of 15 mm from the welding axis and continuously reduced to be less than 100 N/mm^2 at a distance of 80 mm. Meanwhile, the minimum residual stress is dropped to about 40 N/mm^2 near the welding line and to the range of -15 to 20 N/mm^2 at a distance of more than 30 mm. Figure 4.49 shows the principal residual stresses after PWHT scheme k (cooling rate = 40 °C/h) which has the same procedure of PWHT-a.

Figure 4.60 shows the principal residual stresses after PWHT-l (cooling rate = 125 °C/h). These results reveal that after the application of this scheme of heat treatment the maximum residual stress is reduced to about 215 N/mm^2 near the welding line and gradually decreased to less than 100 N/mm^2 at a distance of more than 50 mm from the welding axis. While, the minimum residual stress is reduced to about 65 N/mm^2 near the welding line and changed to compression stresses with a value of less than 80 N/mm^2 at a distance of 80 mm from the welding axis.

A comparison diagram (Figure 4.61) has been plotted to compare the maximum residual stress of these different preceding schemes of heat treatments. It can be seen from this Figure that the maximum value of the residual stress is reduced by about 200, 165 and 150 N/mm^2 after the application of PWHT scheme j, k and l respectively. These results show that higher stress relaxation can be achieved by the application of PWHT with slower cooling rate.

4.2.4 DOUBLE-V STAINLESS-STEEL AISI-410 COMPONENT

In order to study the effect of PWHT on the residual stress for the stainless-steel AISI 410 welded component, double-V welded components were prepared following the described procedures. The magnitude and distribution of residual stresses were measured before and after the application of these different types of PWHTs. These measurements were also carried out across the middle area of the specimen. The residual stresses were measured at the top and bottom of surfaces of the welded component for the as-welded condition. The results show that there is no significant difference between the magnitude of the residual stresses at both surfaces of the specimen and that the maximum value of the residual stress is about 220 N/mm^2. Then, only the residual stresses at the top surface were determined for after PWHTs.

Many diagrams have been plotted for the measured principal residual stresses for each condition. It can be seen from the results obtained that the maximum residual stress has noticeably higher magnitudes than the minimum residual stresses with more or less regular shape for the residual stress distribution across the specimen axis.

These results show that the maximum residual stress for as-welded condition (Figure 4.62) is about 220 N/mm^2 in tensile near the welding line and it decreases to about zero at a distance of about 35 mm from the welding axis and it changes to be a compression residual stress with value of less than 40 N/mm^2 at the distance over than 50 mm. However, the minimum residual stress ranges from about 40 N/mm^2 in tension near the specimen axis and changes to be in compression with a range of 50 to 80 N/mm^2 at a distance of more than 35 mm from the welding axis.

Figure 4.63 shows the results of the principal residual stresses after the application of PWHT-1. After PWHT-1 (soaking temperature = 550 °C) the maximum residual stress is

reduced to around 110 N/mm² at a distance of 15 mm from the welding axis and it is in the range of 25 to 30 N/mm² at a distance between 35 to 85 mm from the welding axis. In the mean time, the minimum residual stress changes from about 50 N/mm² at a distance of 15 mm to become zero at distance of about 30 mm and then changing to a negligible value in compression and it increases to less than 15 N/mm² at a distance of 85 mm from the welding axis.

Figure 4.64 reveals the results after the application of PWHT-2 (soaking temperature = 650 °C). The results obtained show that the maximum residual stress is decreased to about 60 N/mm² (tensile stress) at a distance of 15 mm from the welding axis and it decreases to be in compression with a value of less than 20 N/mm² at a distance more than 30 mm. However, the minimum residual stress is about 20 N/mm² in tension at a distance of 15 mm from the welding axis, then it decreases to be in compression at a distance more than 20 mm with value of less than 35 N/mm².

After the application of PWHT-3 (soaking temperature = 750 °C) the residual stresses is totally diminished. Figure 4.65 compares the maximum residual stress before and after PWHT 1, 2 and 3. It can be seen from this Figure that the maximum residual stress value has been reduced by about 50% after PWHT-1 and by about 70% after PWHT-2 and by 100% after PWHT-3.

Figures 4.63, 4.66 and 4.67 show the distribution of the principal residual stresses across the specimen surface after applying PWHTs with different heating rates. It can be seen from Figure 4.66 that after PWHT-4 (heating rate = 50 °C/h) the maximum residual stress value is around 100 N/mm² (tensile stress) at a distance of 15 mm from the welding axis and it changes to a state of compression stress with a value of less than 25 N/mm². The minimum residual stress is about 30 N/mm² at a distance of 15 mm from the welding axis, and changing to be in a compression with a value of less than 35 N/mm².

After PWHT-5 (heating rate = 100 °C/h) the maximum residual stress reduced to about 110 N/mm² at a distance of 15 mm from the welding axis and it reduces to about 30 N/mm² at a distance of 85 mm. The minimum residual stress is about 40 N/mm² at a distance of 15 mm from the welding axis and changing to a value of less than 25 N/mm² in compression at the distance of more than 30 mm from the welding axis. Figure 4.67 shows the principal residual stress after the application of this type of heat treatment. Figure 4.63 shows the principal residual stress after PWHT-6 (heating rate = 400 °C/h) which has the same heat treatment procedures of PWHT-1.

Figure 4.68 compares the distribution of the maximum residual stresses before and after PWHT-4, 5 and 6. This comparison shows that the maximum value of the residual stress is reduced by about 50 % but there is no significant change by employing PWHTs with different heating rates.

Figure 4.69 shows the distribution of the principal residual stress after PWHT-7 (time duration = 0.5 h). The maximum residual stress is reduced to about 120 N/mm² (tensile stress) at a distance of 15 mm from the welding axis and gradually decreases to about 45 N/mm² at a distance of 85 mm. However, the minimum residual stress ranges from about 50 N/mm² in tension near the welding line and to about -40 N/mm² at a distance of about 35 mm from the welding axis and again to less than 20 N/mm² in tension at a distance of 85 mm from the welding axis. Figure 4.63 shows the results of PWHT-8 (time duration = 2 h) which has the same heat treatment procedures of PWHT-1.

Figure 4.70 shows the distribution of the principal residual stress after the application of PWHT-9 (time duration = 10 h). The results reveal that the maximum residual stress is decreased to about 65 N/mm² at a distance of 15 mm from the welding axis and it reduces to the range of 25 to 35 N/mm² at a distance more than 35 mm. The minimum residual stress is

about 35 N/mm² near the welding line and is about 10 N/mm² at a distance of 85 mm from the welding axis.

Figure 4.71 compares the maximum residual stress for as-welded condition and after the application of PWHTs with different time duration. This comparison shows that the maximum value of the residual stress is reduced by about 110 N/mm² after PWHT-7 and by about 120 N/mm² after PWHT-8 and by about 155 N/mm² after PWHT-9. It is evident from these results that the maximum value of the residual stress decreases as the time duration of PWHT increases.

The effect of cooling rate on the residual stress has been investigated. Figure 4.72 shows the distribution of the principal residual stresses after PWHT-10. The results show that after PWHT-10 (cooling rate = 10 °C/h) the maximum residual stress is reduced to about 70 N/mm² at a distance of 15 mm from the welding axis and to a range of -20 to 10 N/mm² at a distance of more than 35 mm. Meanwhile, the minimum residual stress is about 30 N/mm² near the welding line and changing to be in compression with a value of about 20 N/mm² at a distance of 85 mm from the welding axis. Figure 4.63 shows the principal residual stresses after PWHT-11 (cooling rate = 40 °C/h) which has the same heat treatment procedures of PWHT-1.

Figure 4.73 shows the principal residual stresses after PWHT-12 (cooling rate of 125 °C/h). It can be seen from this Figure that the maximum residual stress is about 120 N/mm² (tensile stress) at a distance of 15 mm from the welding axis and it reduces to range between -20 and -35 N/mm² at a distance of about 35 mm and more. The minimum residual stress is about 50 N/mm² tensile near the welding line which changes to compressive at a distance of more than 20 mm from the welding axis.

Figure 4.74 shows a comparison diagrams between the maximum residual stress for the as-welded condition and after the application of these types of heat treatments (different cooling

rates) was made. These results reveal that there is about 145 N/mm² reduction in the maximum value of the residual stress after PWHT-10. Whilst, the reduction is about 110 and 100 N/mm² after PWHT-11 and 12 respectively.

4.3 OPTIMIZATION OF PWHT

It can be seen from the results obtained that after the application of PWHTs, the mechanical properties have been improved and the residual stresses reduced for different levels depending on the heat treatment parameters. There is clear evidence from these results that the soaking temperature has the maximum effect on reducing the residual stress and improving the mechanical properties of these two types of welded components, since it is evident that the residual stress can be eliminated by applying the higher soaking temperatures of 650 and 750°C for the low carbon steel and the stainless-steel welded components respectively. The following studies aim to optimize the heat treatment parameters which could lead to obtaining the best heat treatment procedure with shorter time and less cost (energy) for both types of welded components.

It can be seen from the previous results that there is no significant effect on the residual stress and the mechanical properties by varying the heating rate; for this reason the faster heating rate (400°C/h) will be used as an optimum heating rate in the following study. However, the soaking time duration and the cooling rate will be investigated to obtain the best heat treatment condition with shorter soaking time duration and faster cooling rate to eliminate the residual stress without compromising the mechanical properties of these welded components.

4.3.1 THE LOW CARBON STEEL COMPONENT

4.3.1.1 POST WELD HEAT TREATMENT PROCEDURES

To determine the shorter soaking time duration and the faster cooling rate different PWHT schemes were applied. The soaking temperature and the heating rate were chosen as 650°C and 400°C/h respectively. Whilst, different soaking time durations and cooling rates were applied. Some modification on the procedures (time duration and cooling rate) were made, depending on the results of the first heat treatment scheme and so on. Table 4.5 summarizes the different heat treatment schemes which have been applied in this study.

Heat Treatment Cycle	Heating Rate °C/h	Soaking Temperature °C	Duration Time h	Cooling Rate °C/h
PWHT A1	400	650	0.5	40
PWHT A2	400	650	1	40
PWHT A3	400	650	1	125
PWHT A4	400	650	1	100

TABLE 4.5 THE HEAT TREATMENT PROCEDURES FOR THE LOW-CARBON STEEL COMPONENT (OPTIMIZATION).

4.3.1.2 METALLURGICAL TESTING

To carry out the metallurgy test, transverse sections of the welded components were prepared following the same procedures described in Chapter two. This was to enable a study of the effect of the heat treatments on the microstructure to be made. An optical microscope was used to study the microstructure.

As described before, the results show that the microstructure of the welding zone before the application of PWHT consisted of ferrite and bainite as illustrated in Plate 4.1. After the application of different schemes of PWHTs the metal microstructure tests were carried out which reveal that there is no significant difference in the microstructure of the welding zone for these different schemes of PWHTs and it consists of tempered bainite, ferrite and precipitated carbide. Plate 4.14 shows a photograph of the microstructure of the welding zone after the application of PWHT A2 (as an example of these heat treatment schemes).

4.3.1.3 HARDNESS TESTING

This test was made across the specimen thickness at different depths from the specimen surface. As noticed in the previous results there is no difference in the hardness values at the same depth from either the top or the bottom surface. Therefore, the hardness test was carried out at two different depths from the specimen surface (1 and 5 mm) and across the welding line.

Figures 4.75 to 4.78 show the results of this test for these four different schemes of heat treatments. It can be seen from these results that the hardness value after the application of these different PWHTs at a depth of 1 mm from the specimen surface is reduced to between 220 HV and 235 HV in the HAZ and to about 200 HV outside this zone. The hardness value at a depth of 5 mm ranges between 210 and 220 HV in the HAZ and again to about 200 HV outside this

zone. It is evident from these results that the hardness value is reduced in the HAZ and the difference between the HAZ and the base metal is also decreased.

A comparison between the hardness variation across the specimen at the depth of 1 mm from the surface was made for these four heat treatment schemes and for as-welded condition. These diagrams are illustrated in Figure 4.79. It can be observed from this Figure that after the application of these heat treatment schemes the hardness value is reduced by about 50 to 60 HV in the HAZ and the base metal becomes softer by about 30 HV. Meanwhile, it can be seen from these results that there is no significant difference for the hardness value after the application of these different schemes of PWHTs.

Figure 4.80 compares the hardness variation for these different conditions along the specimen axis. It can be seen from this Figure that the hardness value after the application of these different schemes of PWHT is in the range of 220 to 235 HV near the specimen surface and is about 210 and 220 HV in the middle of the specimen thickness. It is evident from these results that the hardness decreases as the distance from the specimen surface increases, due to the faster cooling rate near the specimen surface.

4.3.1.4 TENSILE STRENGTH TEST

This test was made to determine the ultimate tensile strength for these different schemes of heat treatments. It is evident from these results (Table 4.6) that the tensile strength is improved by about 25 N/mm^2 after the application of these above schemes of heat treatments and there is no significant difference in the tensile strength due to the application of these heat treatment schemes. It is evident from these results that the difference in these heat treatment schemes would not have any major effect on the tensile strength. It was also found the tensile strength of the HAZ has improved by about 15% after the application of these PWHTs.

Specimen Condition	Before PWHT	PWHT A1	PWHT A2	PWHT A3	PWHT A4
Tensile Strength [N/mm²]	420	445	449	444	446

TABLE 4.6 THE RESULTS OF TENSILE STRENGTH TEST FOR AISI-1020 (OPTIMIZATION).

4.3.1.5 NOTCHED-IMPACT TEST

An adequate number of specimens were prepared to carry out this test. The results obtained reveal that the metal toughness is improved by about 20 to 25% after the application of these different schemes of PWHTs. The impact energy results ranged between 64 and 72 J after the application of these schemes of heat treatments. It can be noticed from these results that these different schemes have about similar effect on improving the impact energy. It is also clearly evident that there is a negligible difference in the impact energy after the application of these different heat treatment schemes. Table 4.7 shows these different results.

Specimen Condition	Before PWHT	PWHT A1	PWHT A2	PWHT A3	PWHT A4
Impact Energy [J]	54	64	72	66	66

TABLE 4.7 THE RESULTS OF NOTCHED-IMPACT TEST FOR AISI-1020 (OPTIMIZATION).

4.3.1.6 RESIDUAL STRESS TESTING RESULTS

The magnitude and distribution of the residual stresses were also determined by employing the hole drilling method, where three readings were taken from the strain indicator for each point. By measuring these three strain values (ϵ_1, ϵ_2, ϵ_3), the principal stresses and their directions were computed.

As reported in previous sections, the residual stresses were measured at the top and bottom sides of the welded component for as welded condition and the results showed that there is no difference between the magnitude of the residual stresses at the two surfaces of the specimen. The magnitude and distribution of the residual stresses were determined at the top surface only for all of the above conditions of PWHTs. Figures 4.81 to 4.84 show the distribution of the principal residual stresses across the weld line. It can be seen from these results that the maximum value of the residual stress is reduced to be about 30 to 35 N/mm^2 after the application of PWHT A1 and A3. Whilst, it is reduced to be less than 10 N/mm^{2}after the application of PWHT A2 and A4.

Figures 4.85 and 4.86 show a comparison diagram between the maximum residual stress after the application of these heat treatment schemes and for as-welded condition (Figure 4.85) and only after the application of these heat treatment schemes (Figure 4.86). It is evident from these results that the residual stresses have been reduced to very low levels after the application of these above different schemes of heat treatments. It can also be noticed from Figure 4.86 that the residual stresses are virtually eliminated after the application of PWHT A2 and A4. These results point out that after the application of PWHT A4, the residual stress was virtually eliminated without compromising the mechanical properties. It can also be noticed that this heat treatment scheme has a shorter time to be completed compared to other schemes.

4.3.2 THE STAINLESS-STEEL WELDED COMPONENT

4.3.2.1 POST WELD HEAT TREATMENT PROCEDURES

Different heat treatment schemes were applied to optimize the heat treatments procedures, with the objective of eliminating the residual stress and obtaining good mechanical properties for this type of welded component. In this study, the soaking temperature of 750°C is chosen to be applied in these PWHT schemes, due to the effectiveness of this temperature in eliminating the residual stresses and giving good mechanical properties. It was found from the previous results that there is no significant difference in the residual stress and mechanical properties by varying the heating rate of PWHT; according to those previous results a heating rate of 400 °C/h is chosen. However, the soaking time duration and the cooling rate have to be determined. These heat treatment schemes were modified by increasing or decreasing the soaking time durations and the cooling rates depend on the residual stress and mechanical test results of the first scheme and so on. Table 4.8 shows these heat treatment schemes.

Heat Treatment Cycle	Heating Rate °C/h	Soaking Temperature °C	Duration Time h	Cooling Rate °C/h
PWHT B1	400	750	0.5	40
PWHT B2	400	750	1	40
PWHT B3	400	750	1	100
PWHT B4	400	750	1	70

TABLE 4.8 THE HEAT TREATMENT PROCEDURES FOR STAINLESS-STEEL COMPONENT.

4.3.2.2 METALLURGICAL TESTING

To carry on the metallurgy test, special specimens were prepared following the procedures described in Chapter two. After these preparations, an optical microscope was used to carry out this test.

As described before, X-ray diffraction method was used to identify the obtained structure after the application of these above heat treatment schemes. These results reveal that after the application of these heat treatment schemes the microstructure of the welding zone consists of tempered martensite, ferrite and a low percentage of precipitated carbide. It can be seen from these results that the welding zone has about the same structure after the application of these above schemes of PWHT. Plate 4.15 shows a photograph for the welding zone after the application of one of the above heat treatment schemes.

4.3.2.3 HARDNESS TESTING

This test was carried out across the specimen thickness at different depths from the specimen surface (1, 5 and 12 mm lines L1, L2 and L3 respectively) and across the weld line (line L4).

It can be seen from these results (Figures 4.87 to 4.90) that after the application of the above described schemes of heat treatments the hardness value in the HAZ at the depth of 1 mm from the surface is reduced to a range of 305 and 335 HV. While, the hardness value in the parent metal is about 250 HV. At a depth of 5 mm from the specimen surface the hardness value ranges between 290 and 310 HV in the HAZ and about 250 HV outside this zone. Finally, at a depth of 12 mm the hardness value is decreased to about 275 and 285 HV in the HAZ and again about 250 HV outside this zone.

It is evident from these results that after the application of these heat treatment schemes the hardness value in the HAZ is reduced by about 180 to 200 HV. Figure 4.91 shows comparison diagrams for the hardness variation for as-welded condition and after the application of the above schemes of PWHTs across the specimen at a depth of 1 mm from the surface. It can be noticed from this Figure that the sharp difference in the hardness between the HAZ and the parent metal for as-welded condition is reduced from about 250 HV for as-welded condition to about 55 to 85 HV after the application of these heat treatment schemes. In the meantime, it can be noticed that there no significant difference in the hardness value after the application of these different heat treatment schemes.

Figure 4.92 shows a comparison diagram for the hardness variation in the depth of the specimen. It can be seen from these results that the hardness value ranges between 305 and 335 HV near the specimen surface and it is reduced to be about 275 to 285 HV in the middle of the specimen thickness.

4.3.2.4 TENSILE STRENGTH TEST

In order to determine the tensile strength for these different schemes of heat treatments, special tensile specimens were prepared to carry out this test following the procedures described in Chapter two.

The results (Table 4.9) show that after the application of these different types of PWHTs the tensile strength is slightly reduced by up to 15 N/mm^2 after the application of these heat treatment schemes. It can be noticed from these results that there is negligible difference in the hardness value after the application of these different heat treatment schemes. The tensile strength of the HAZ has been investigated. The results show that the tensile strength is slightly improved by 15 to 20 N/mm^2 after the application of these PWHTs.

Specimen Condition	Before PWHT	PWHT B1	PWHT B2	PWHT B3	PWHT B4
Tensile Strength [N/mm²]	515	515	503	508	500

TABLE 4.9 THE RESULTS OF TENSILE STRENGTH FOR AISI-410 (OPTIMIZATION).

4.3.2.5 NOTCHED-IMPACT TEST

A number of specimens were prepared to carry out this test, following the procedures described in Chapter two. These results show that there is a good improvement in the impact energy after the application of the above schemes of PWHTs.

It can be seen from these results that the metal toughness is improved from about 10 J for as-welded condition to about 20 to 23 J after the application of these heat treatment schemes. These results are illustrated in Table 4.10.

Specimen Condition	Before PWHT	PWHT B1	PWHT B2	PWHT B3	PWHT B4
Impact Energy [J]	10	20	23	22	22

TABLE 4.10 THE RESULTS OF NOTCHED-IMPACT TEST FOR AISI-410 (OPTIMIZATION).

4.3.2.6 RESIDUAL STRESS TESTING RESULTS

The magnitude and distribution of the residual stresses were determined by employing the hole-drilling method. The principal residual stresses were determined for each measured point.

The results (Figures 4.93 to 4.96) show that the residual stress is virtually eliminated after the application of PWHT with time duration of 1 h and cooling rate of 40 °C/h. After the application of the same scheme but with time duration of 0.5 h the maximum residual stress is about 30 N/mm² near the welding zone and it is reduced to about 5 N/mm² at a distance of 80 mm from the welding line. After the application of PWHT with time duration of 1 h and cooling rate of 100 °C/h the maximum residual stress is reduced to about 25 N/mm² near the welding line and around 5 N/mm² at a distance of 80 mm. Meanwhile, the residual stress is eliminated again after the application of the previous heat treatment scheme with reducing the cooling rate to 70 °C/h.

Figure 4.97 shows a comparison diagram for the distribution of the maximum residual stress for both as-welded condition and after the application of the above schemes of PWHTs. It can be seen from this Figure that after the application of PWHT B2 and B4 the residual stress is virtually eliminated. Nevertheless, after the application of PWHT B1 and B3 the residual stress also reduced to a very low level. Figure 4.98 shows comparison diagrams for the maximum residual stress after the application of these heat treatment schemes only.

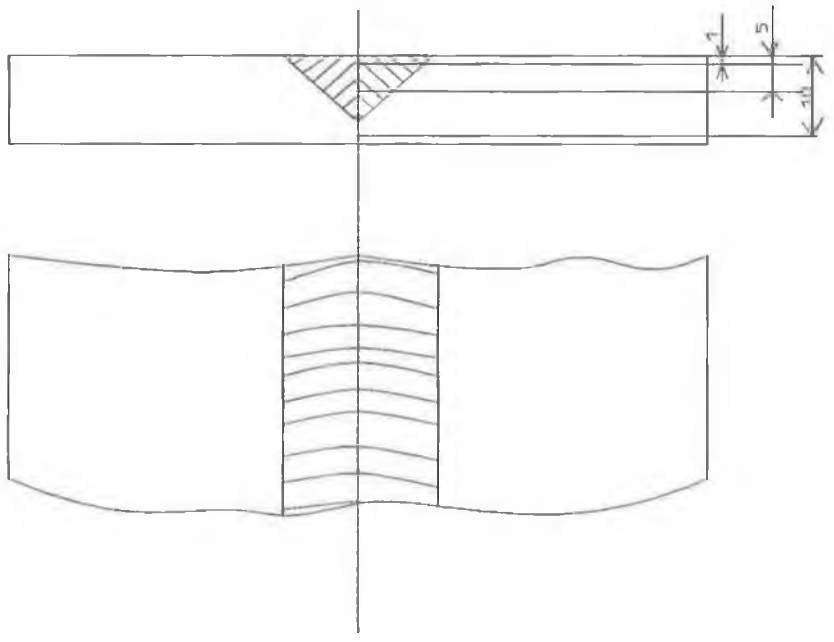

FIGURE 4.1 DIFFERENT AXIS OF THE HARDNESS MEASUREMENTS FOR I-BEAM BOX-SECTION COMPONENT.

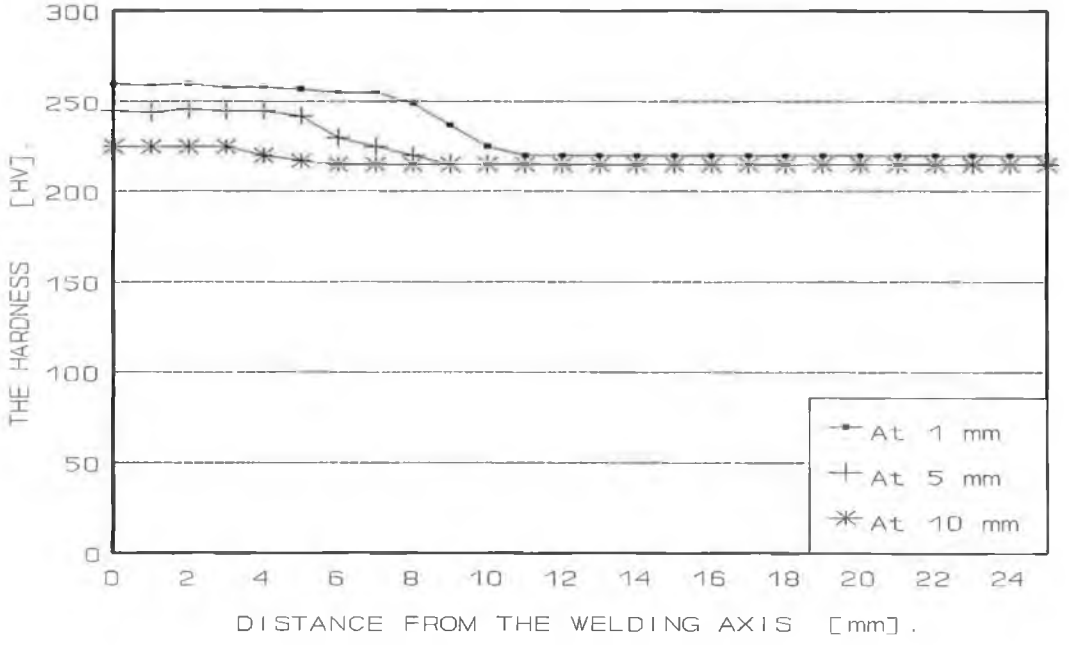

FIGURE 4.2 HARDNESS VARIATION BEFORE THE APPLICATION OF PWHT FOR I-BEAM BOX-SECTION COMPONENT.

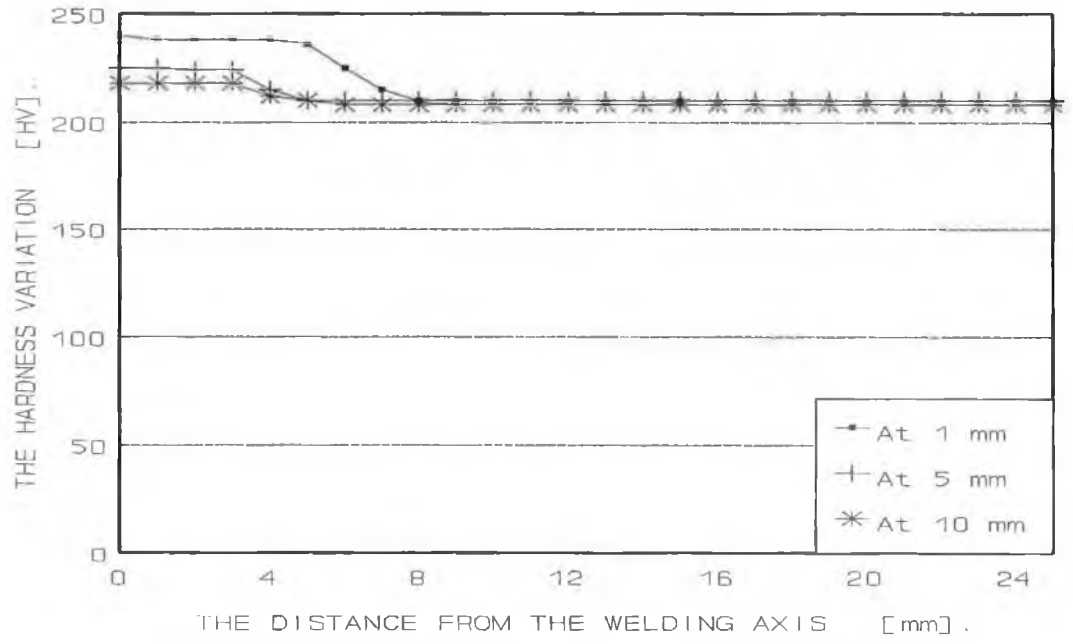

FIGURE 4.3 HARDNESS VARIATION AFTER THE APPLICATION OF PWHT FOR I-BEAM BOX-SECTION COMPONENT.

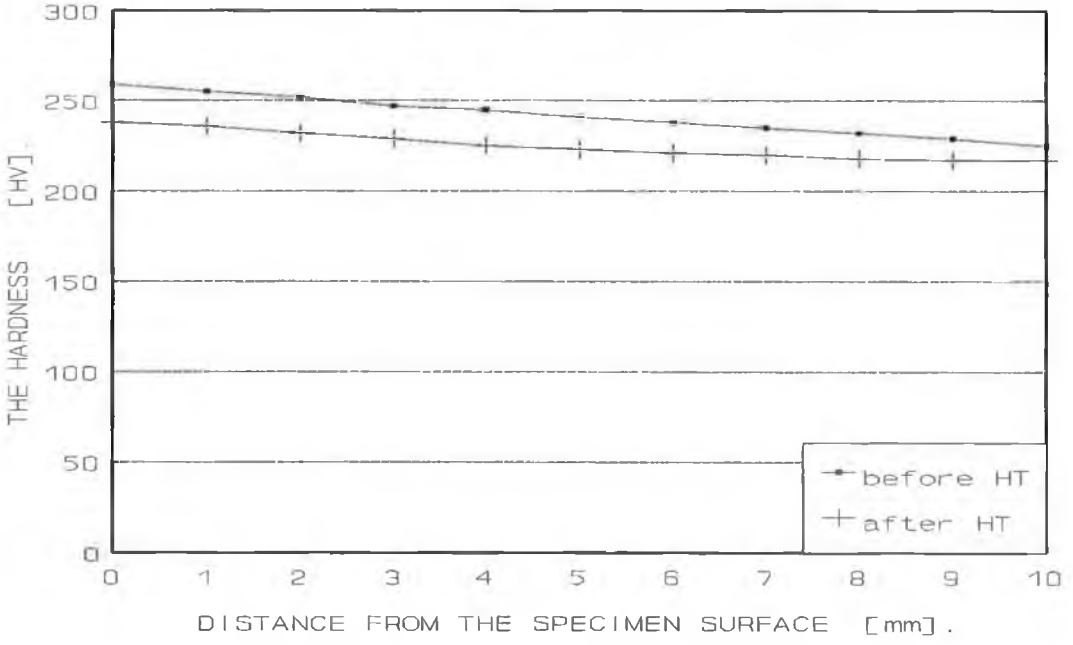

FIGURE 4.4 HARDNESS VARIATION ALONG THE SPECIMEN AXIS FOR I-BEAM BOX-SECTION COMPONENT.

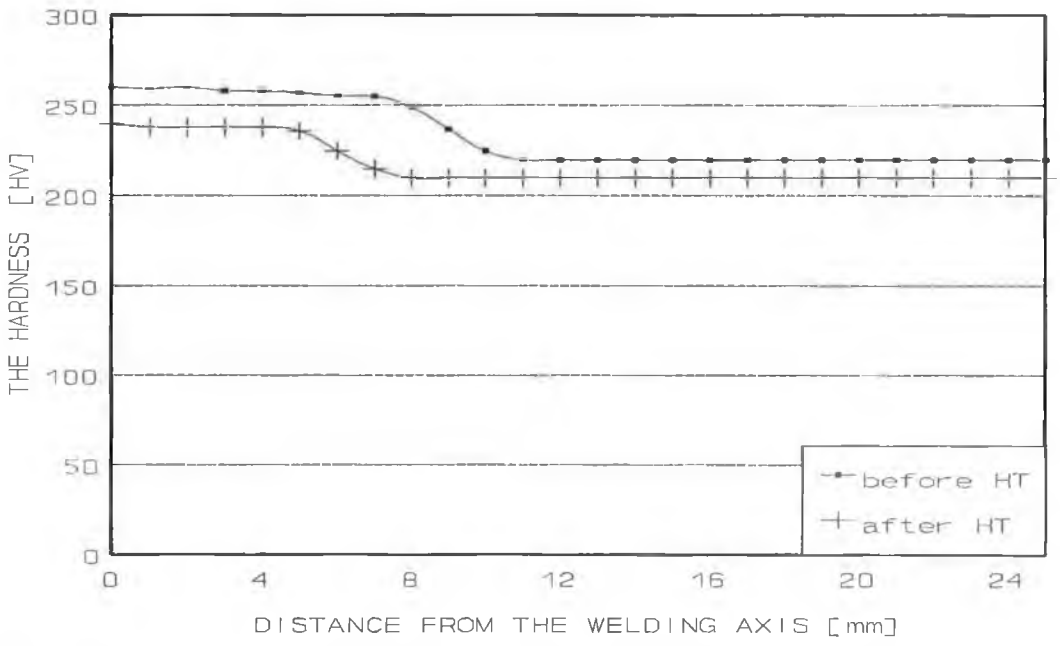

FIGURE 4.5 HARDNESS VARIATION AT THE DEPTH OF 1 mm FROM THE SPECIMEN SURFACE FOR I-BEAM BOX-SECTION COMPONENT.

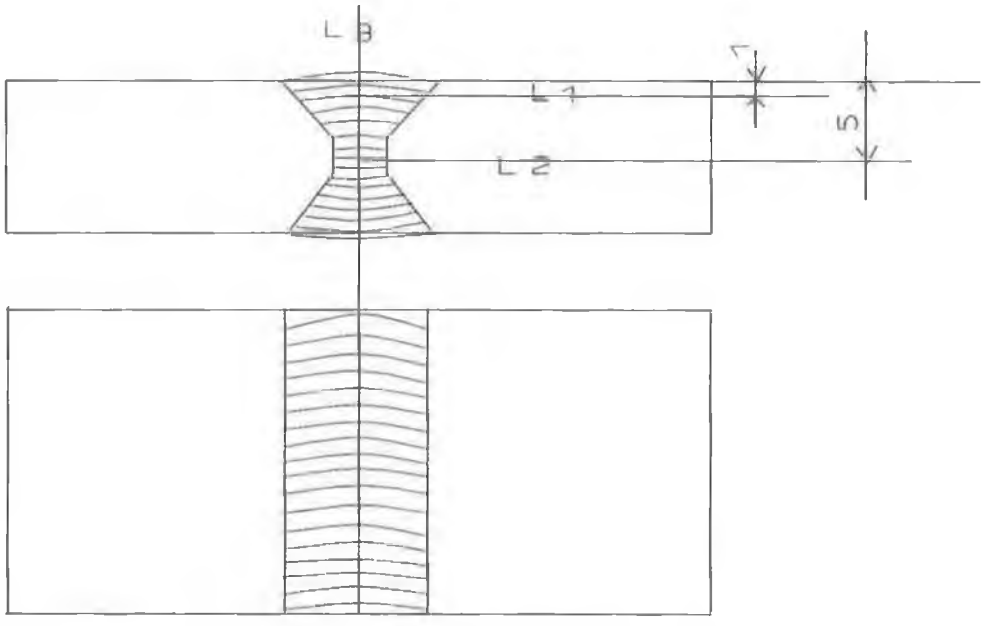

FIGURE 4.6 DIFFERENT LINES OF THE HARDNESS MEASUREMENTS FOR THE CARBON STEEL COMPONENT.

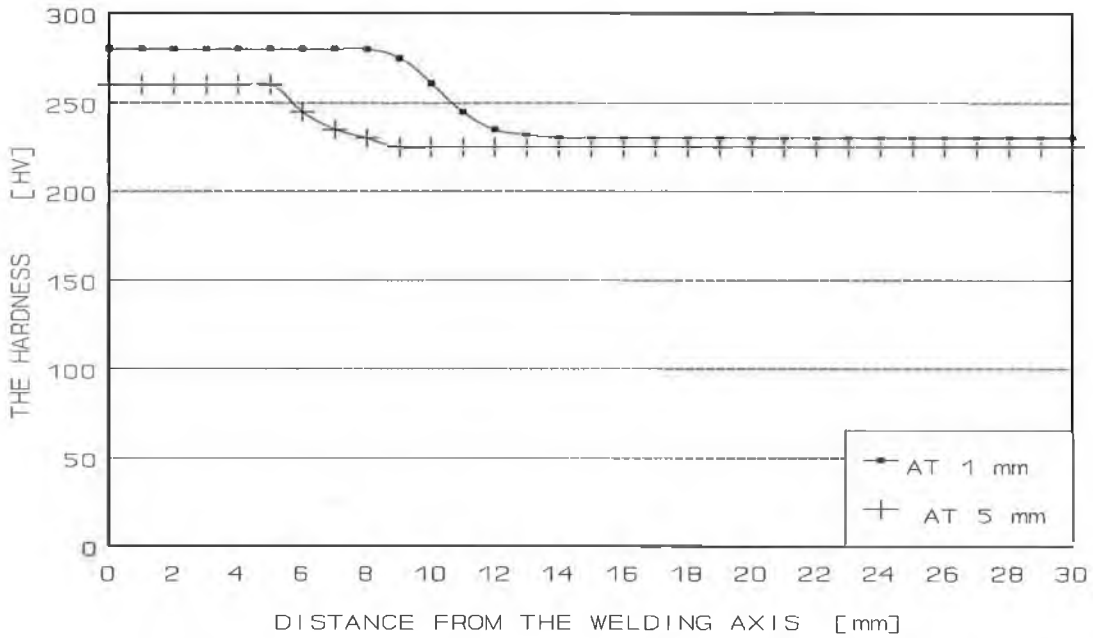

FIGURE 4.7 HARDNESS VARIATION BEFORE PWHT FOR AISI-1020 WELDED COMPONENT.

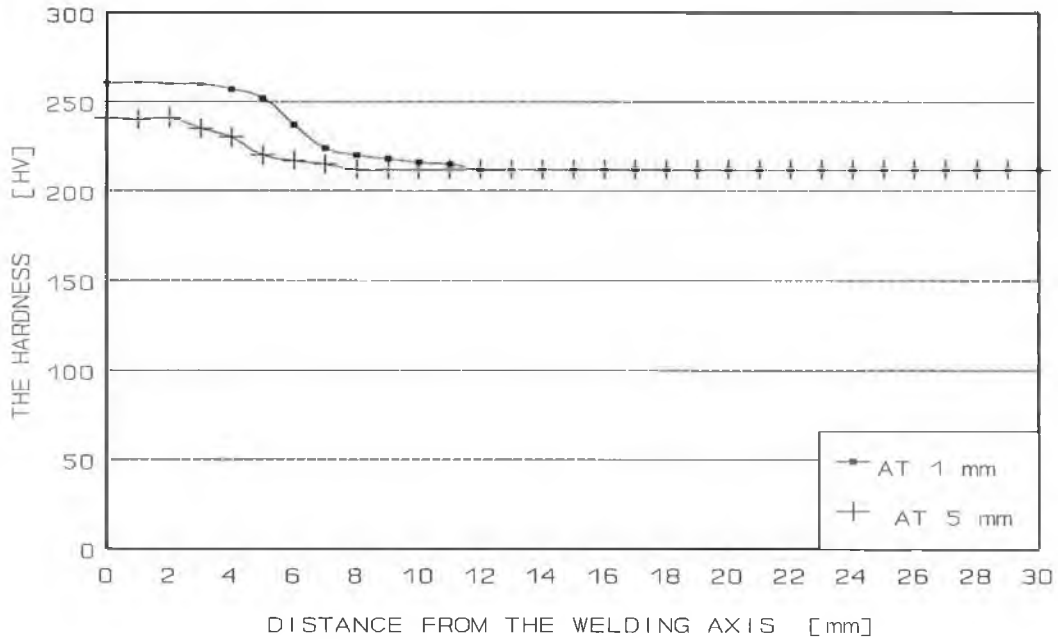

FIGURE 4.8 HARDNESS VARIATION AFTER PWHT a (SOAKING TEMPERATURE = 450°C) FOR AISI-1020 WELDED COMPONENT.

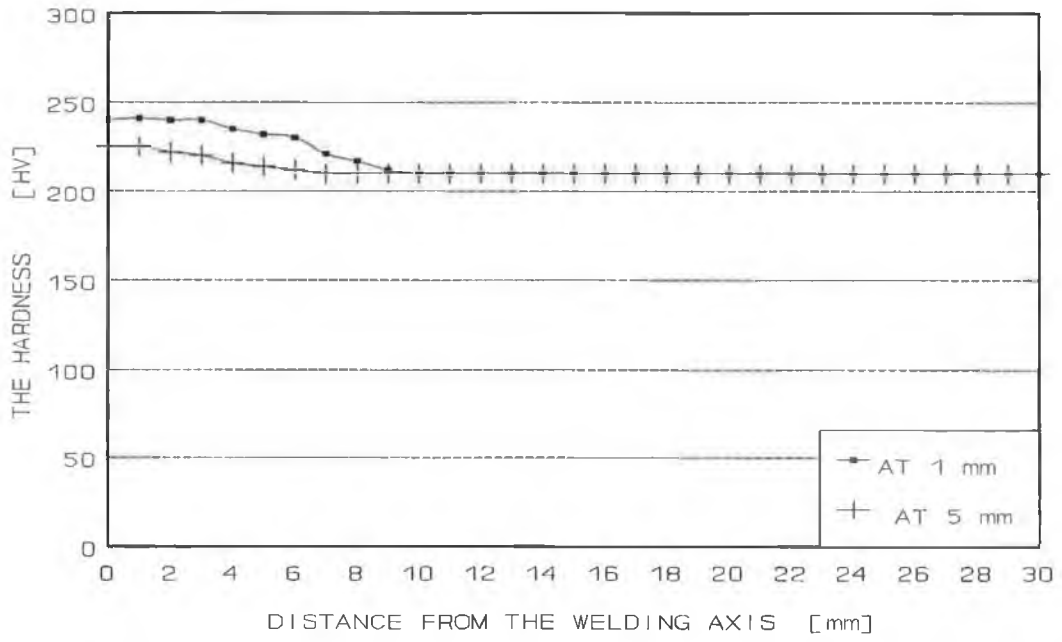

FIGURE 4.9 HARDNESS VARIATION AFTER PWHT b (SOAKING TEMPERATURE = 550°C) FOR AISI-1020 WELDED COMPONENT.

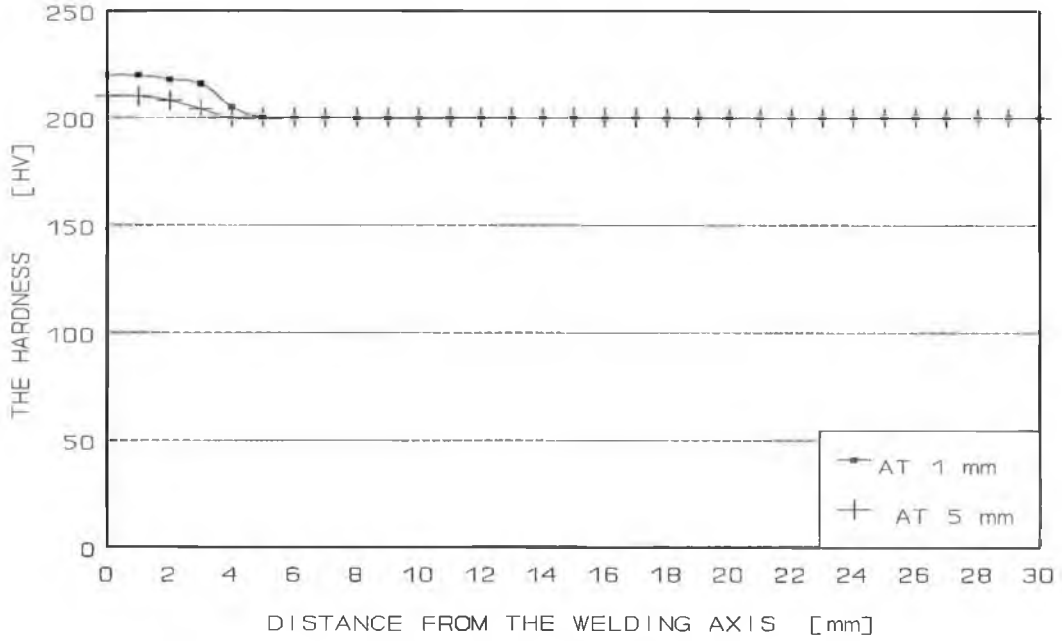

FIGURE 4.10 HARDNESS VARIATION AFTER PWHT c (SOAKING TEMPERATURE = 650°C) FOR AISI-1020 WELDED COMPONENT.

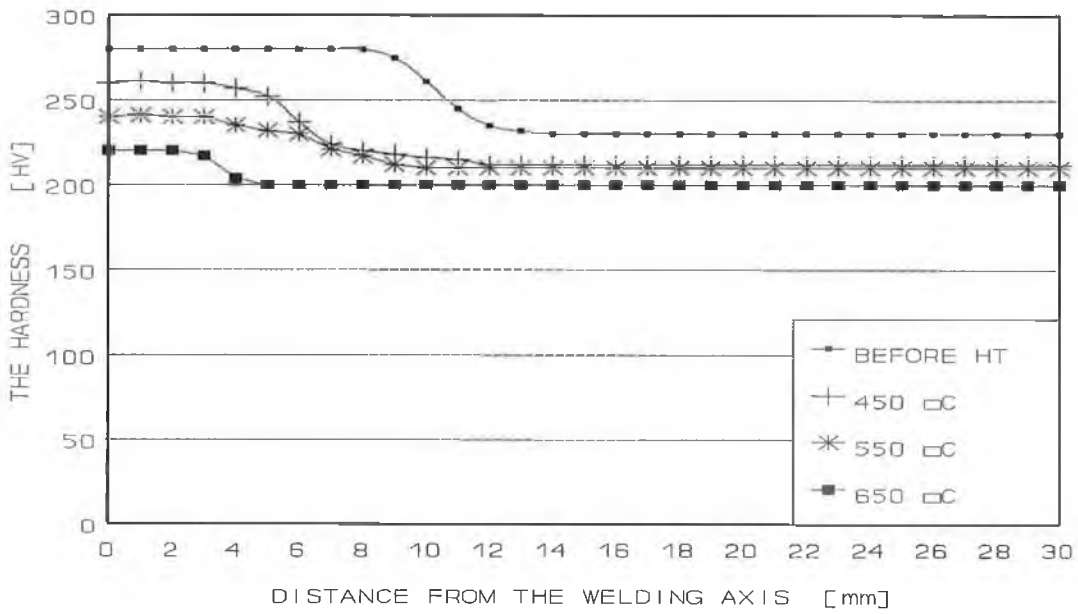

FIGURE 4.11 HARDNESS VARIATION AT THE DEPTH OF 1 mm FROM THE SPECIMEN SURFACE WITH DIFFERENT SOAKING TEMPERATURE FOR AISI-1020 WELDED COMPONENT.

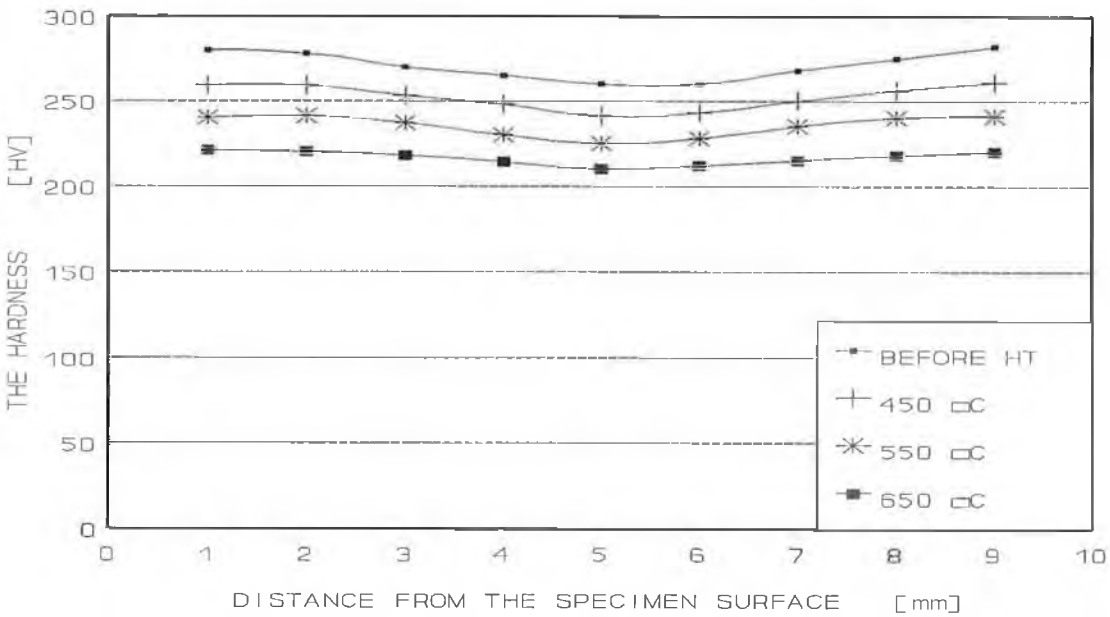

FIGURE 4.12 HARDNESS VARIATION IN THE DEPTH, WITH DIFFERENT SOAKING TEMPERATURE FOR AISI-1020 WELDED COMPONENT.

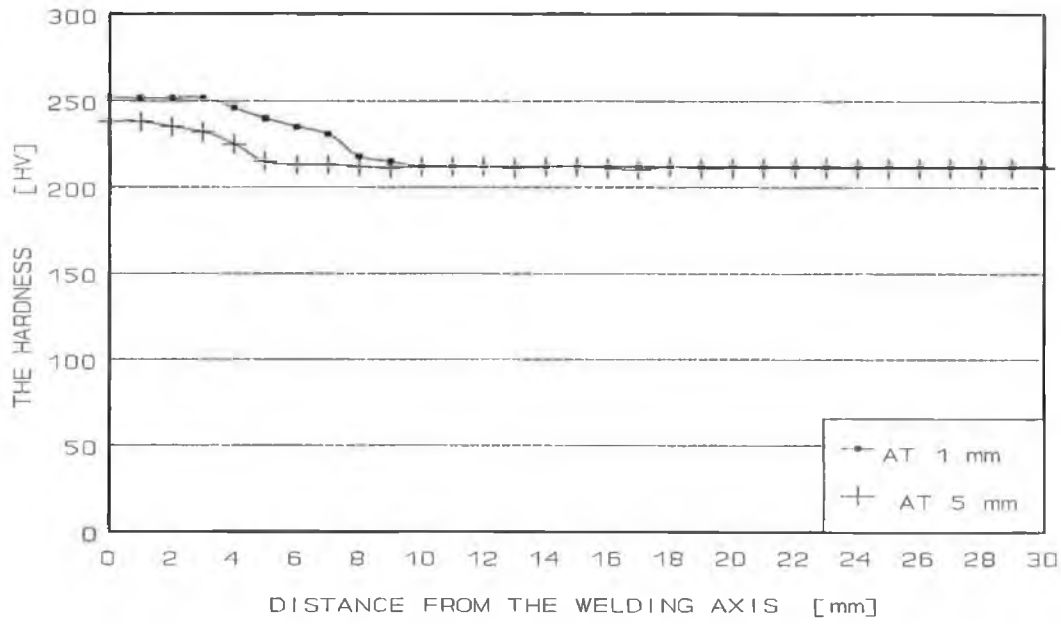

FIGURE 4.13 HARDNESS VARIATION AFTER PWHT d (HEATING RATE = 50°C/h) FOR AISI-1020 WELDED COMPONENT.

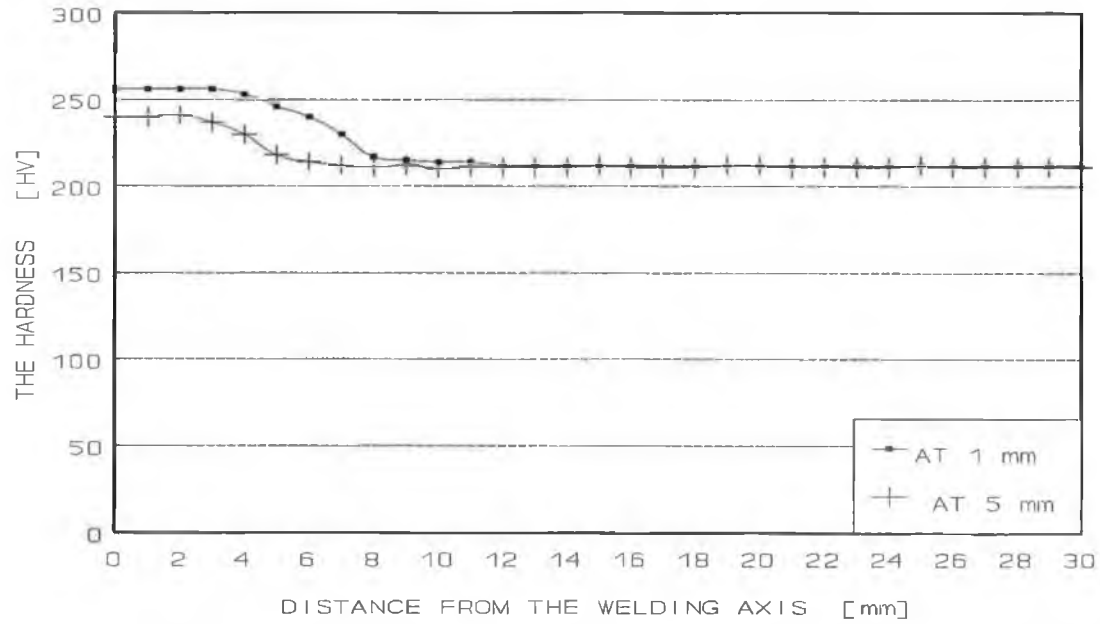

FIGURE 4.14 HARDNESS VARIATION AFTER PWHT e (HEATING RATE = 100°C/h) FOR AISI-1020 WELDED COMPONENT.

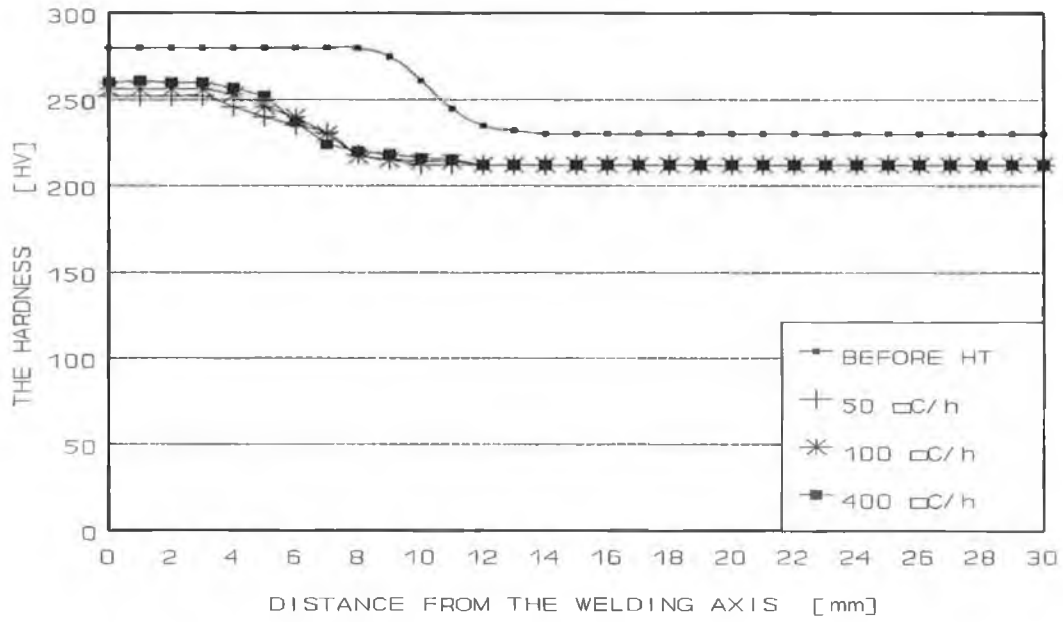

FIGURE 4.15 HARDNESS VARIATION AFTER PWHT AT THE DEPTH OF 1 mm, WITH DIFFERENT HEATING RATES, FOR AISI-1020 WELDED COMPONENT.

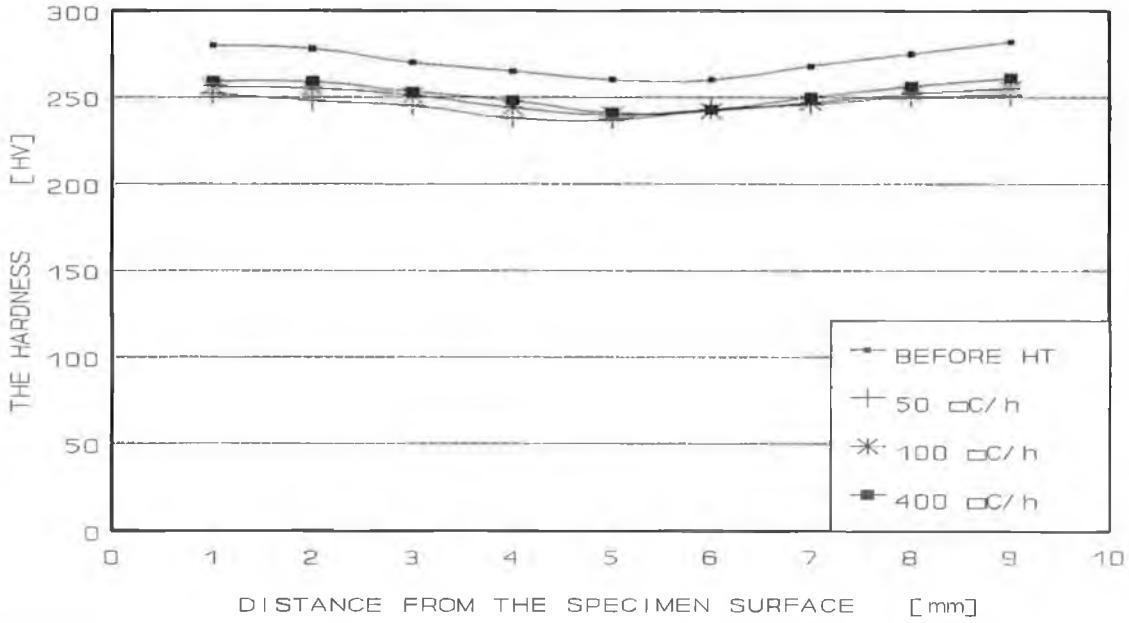

FIGURE 4.16 HARDNESS VARIATION IN THE SPECIMEN'S DEPTH, FOR DIFFERENT HEATING RATES FOR AISI-1020 WELDED COMPONENT.

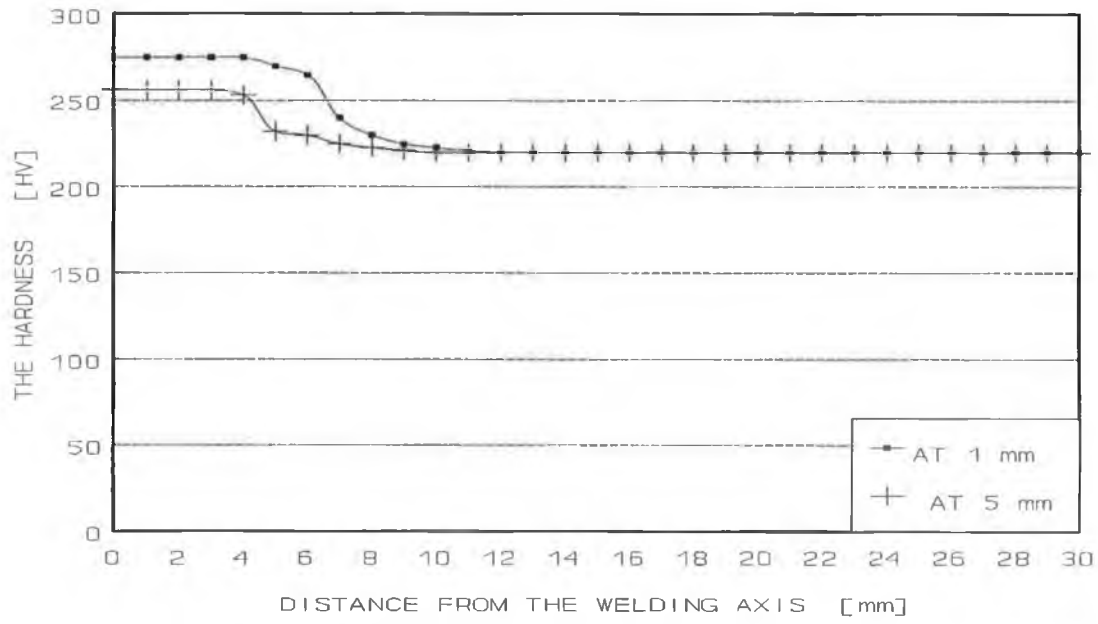

FIGURE 4.17 HARDNESS VARIATION AFTER PWHT g (TIME DURATION = 0.5 h) FOR AISI-1020 WELDED COMPONENT.

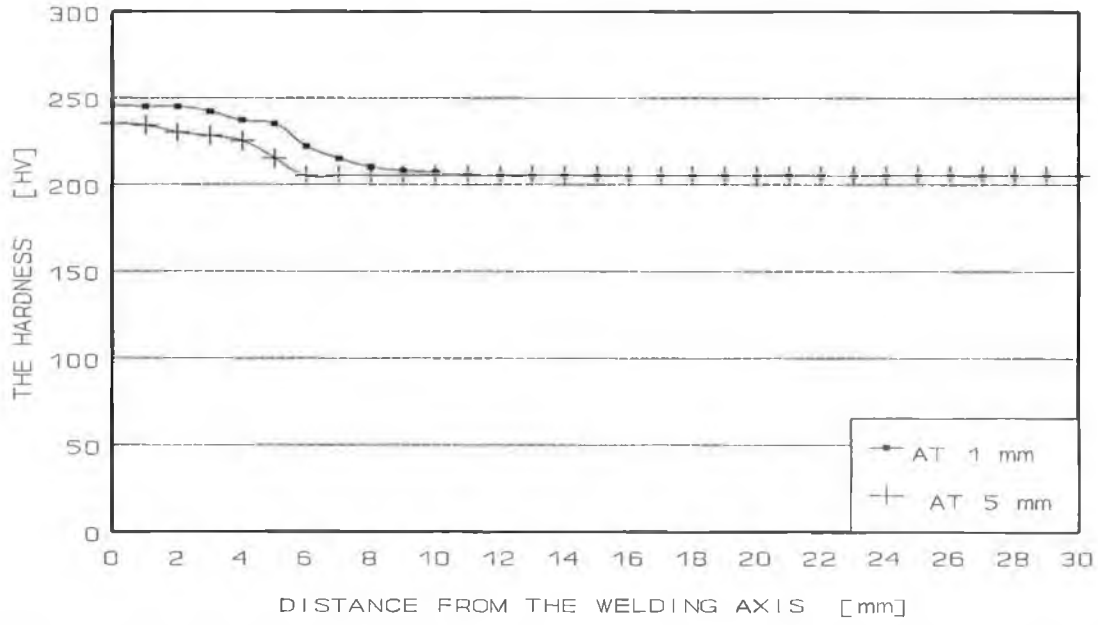

FIGURE 4.18 HARDNESS VARIATION AFTER PWHT i (TIME DURATION = 10 h) FOR AISI-1020 WELDED COMPONENT.

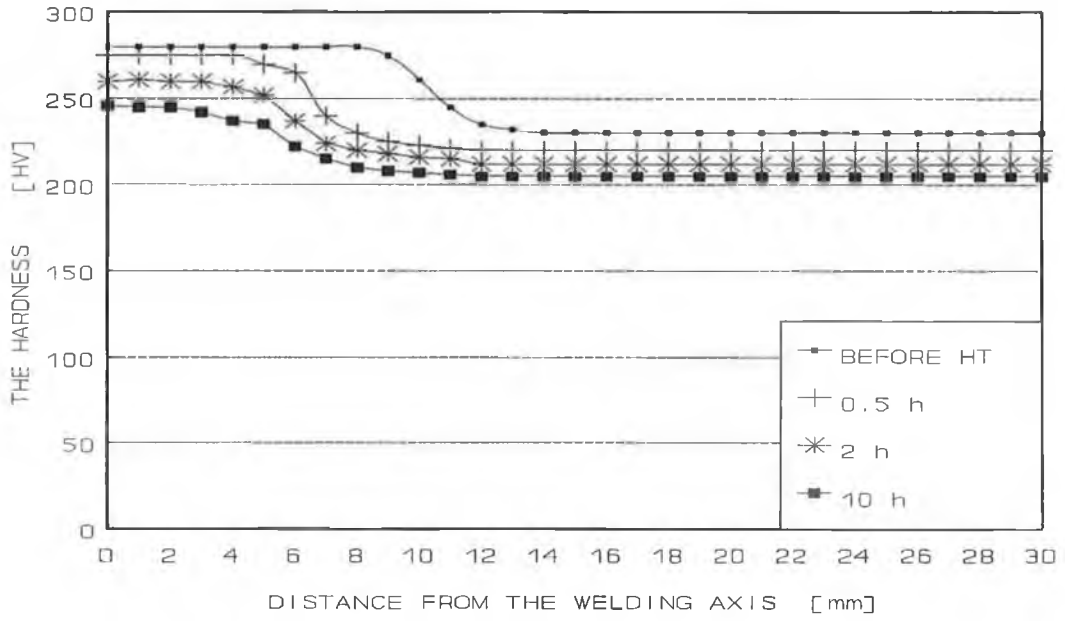

FIGURE 4.19 HARDNESS VARIATION AT THE DEPTH OF 1 mm, AFTER PWHT WITH DIFFERENT TIME DURATIONS FOR AISI-1020 WELDED COMPONENT.

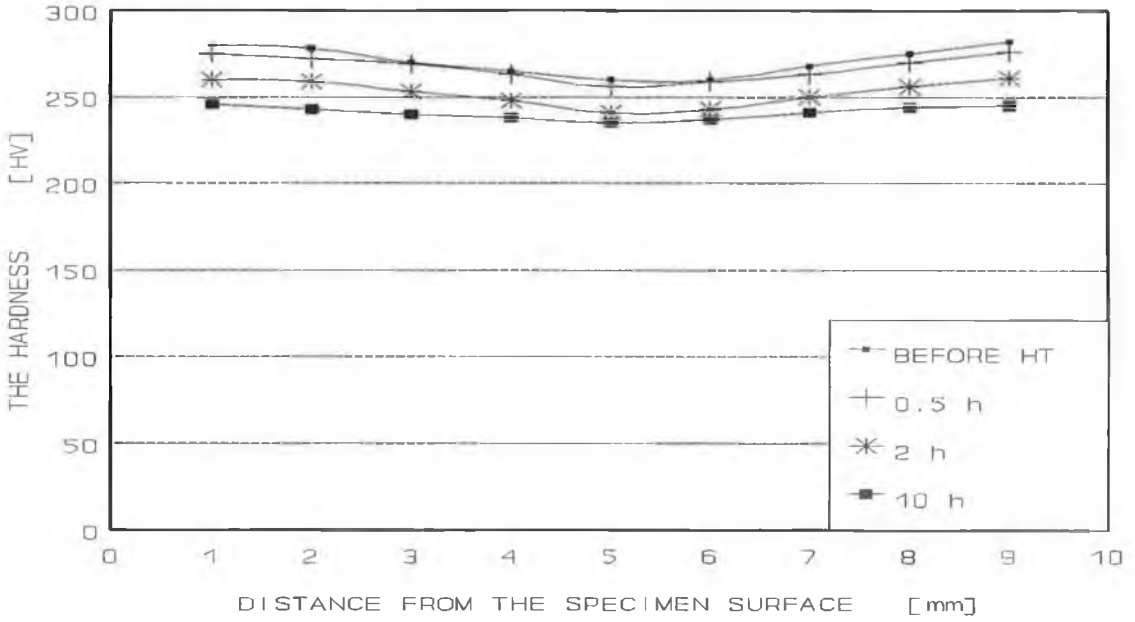

FIGURE 4.20 HARDNESS VARIATION IN THE SPECIMEN'S DEPTH, AFTER PWHT WITH DIFFERENT TIME DURATIONS FOR AISI-1020 WELDED COMPONENT.

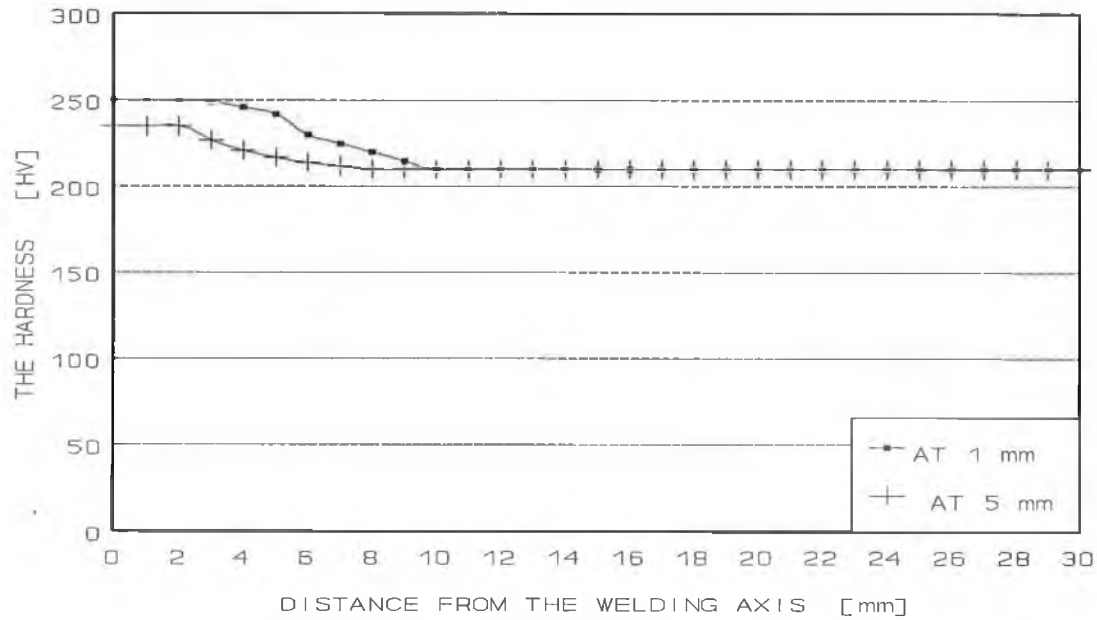

FIGURE 4.21 HARDNESS VARIATION AFTER PWHT j (COOLING RATE = 10°C/h) FOR AISI-1020 WELDED COMPONENT.

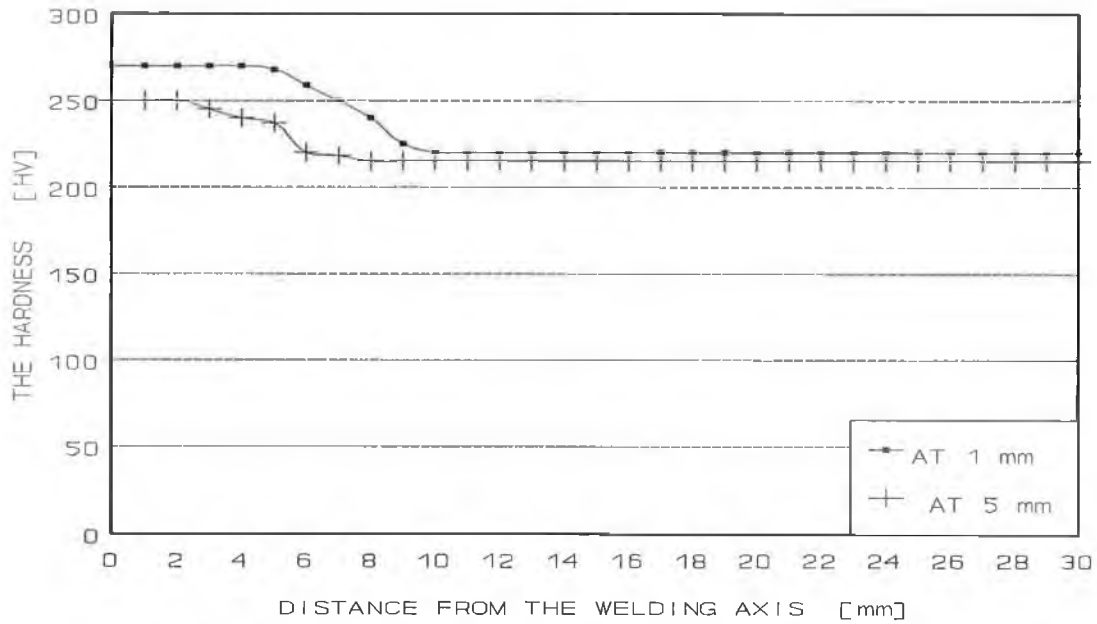

FIGURE 4.22 HARDNESS VARIATION AFTER PWHT l (COOLING RATE = 125°C/h) FOR AISI-1020 WELDED COMPONENT.

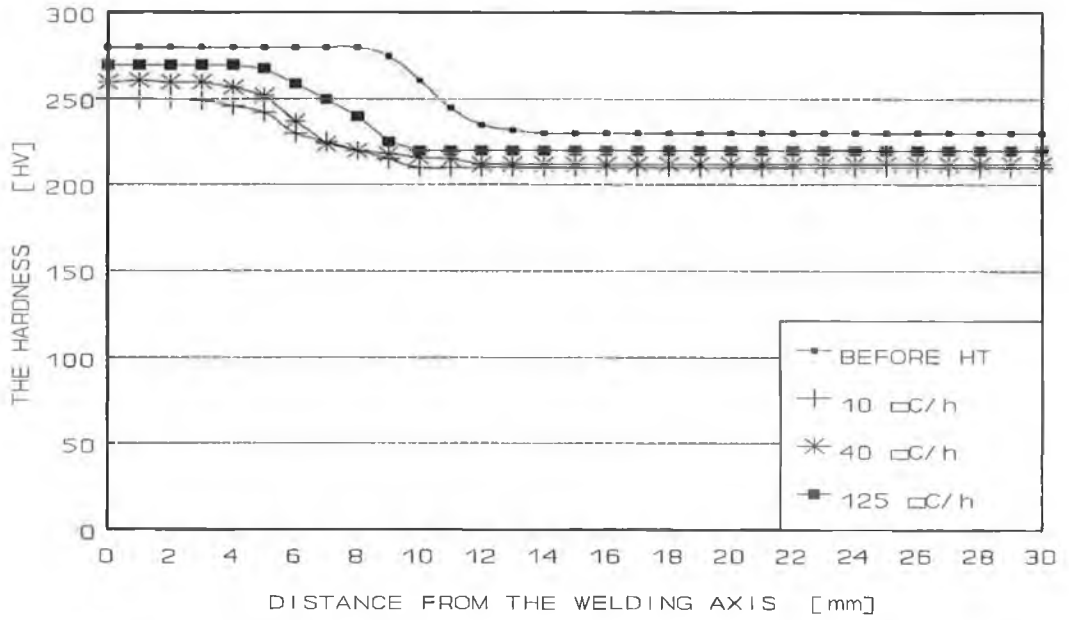

FIGURE 4.23 HARDNESS VARIATION AT THE DEPTH OF 1 mm AFTER PWHT WITH DIFFERENT COOLING RATES FOR AISI-1020 WELDED COMPONENT.

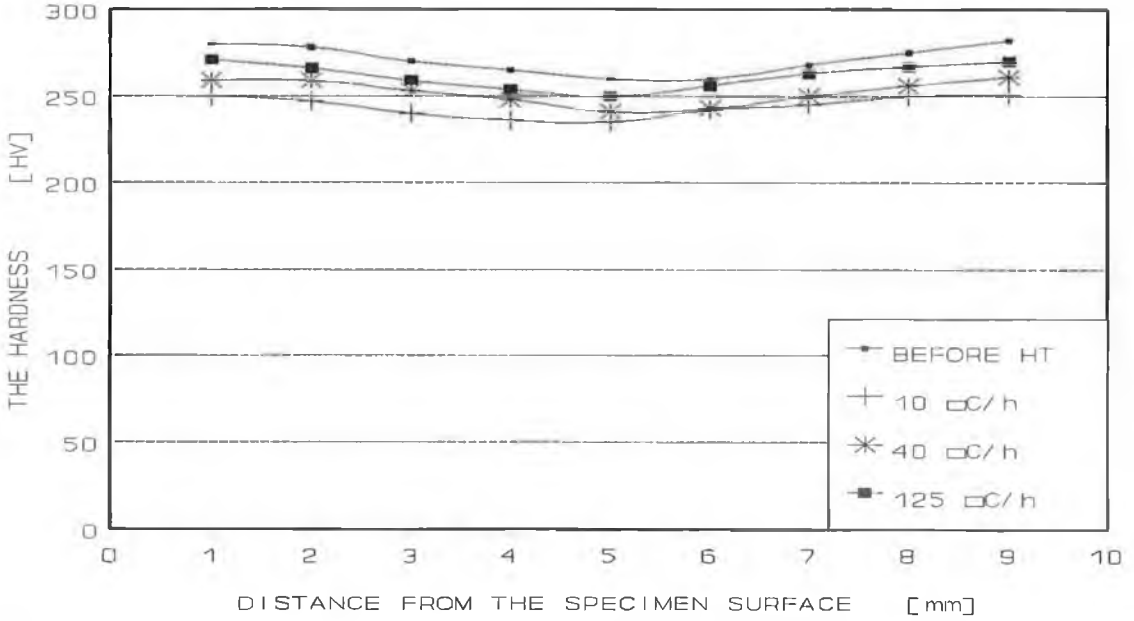

FIGURE 4.24 HARDNESS VARIATION IN THE SPECIMEN'S DEPTH AFTER PWHT WITH DIFFERENT COOLING RATES FOR AISI-1020 WELDED COMPONENT.

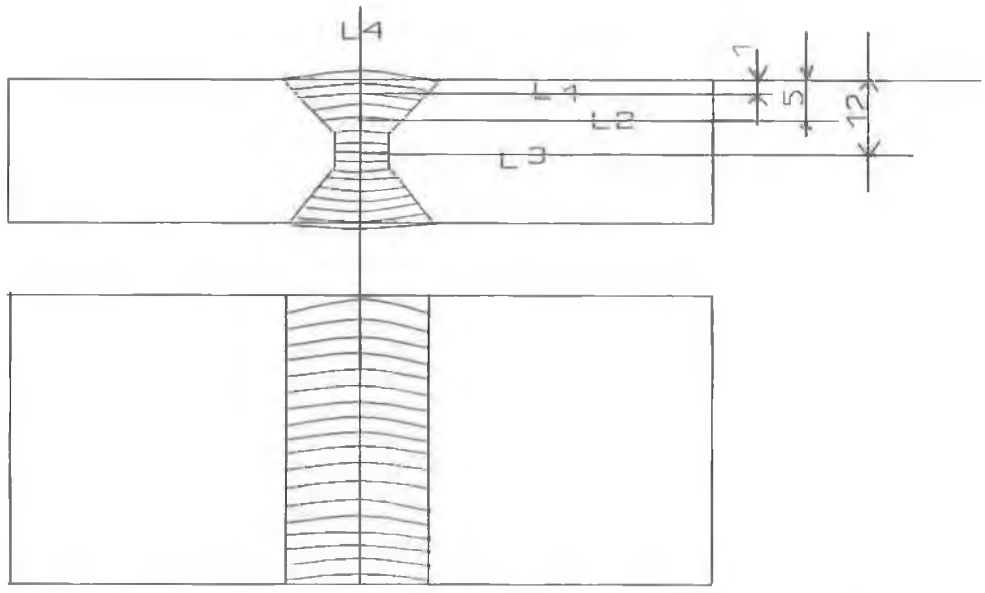

FIGURE 4.25 DIFFERENT LINES OF THE HARDNESS MEASUREMENTS FOR THE STAINLESS-STEEL COMPONENT.

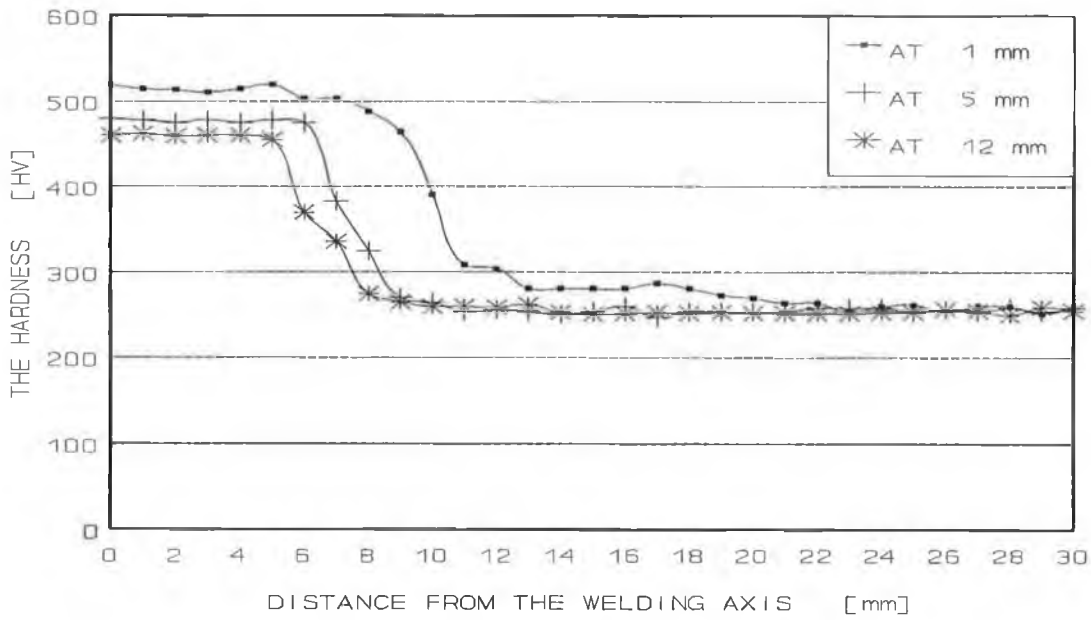

FIGURE 4.26 HARDNESS VARIATION BEFORE PWHT FOR AISI-410 WELDED COMPONENT.

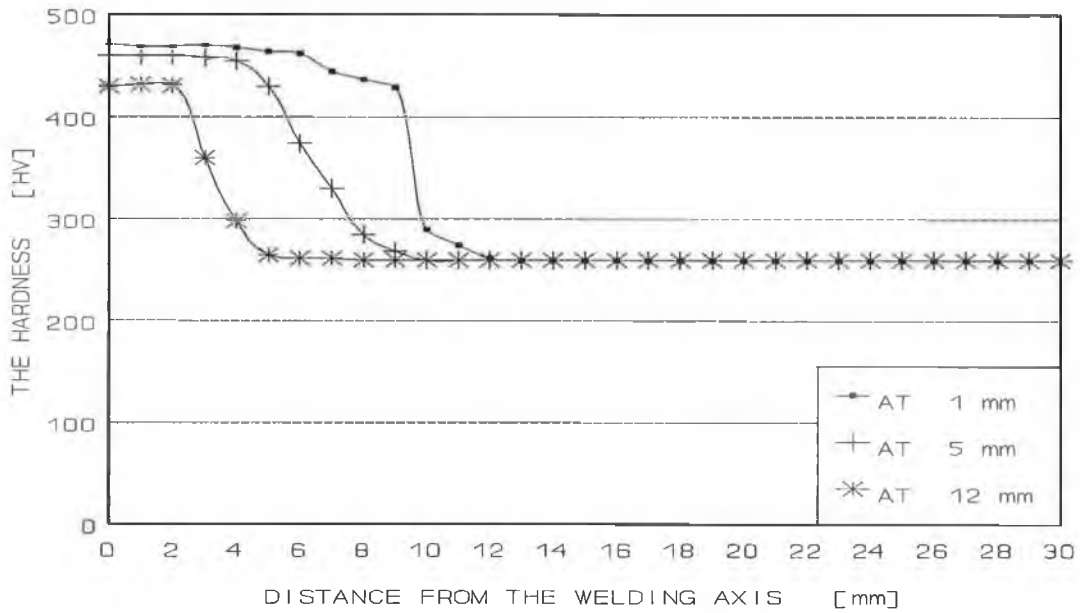

FIGURE 4.27 HARDNESS VARIATION ACROSS THE SPECIMEN AXIS AFTER PWHT WITH SOAKING TEMPERATURE OF 550°C FOR AISI-410 WELDED COMPONENT.

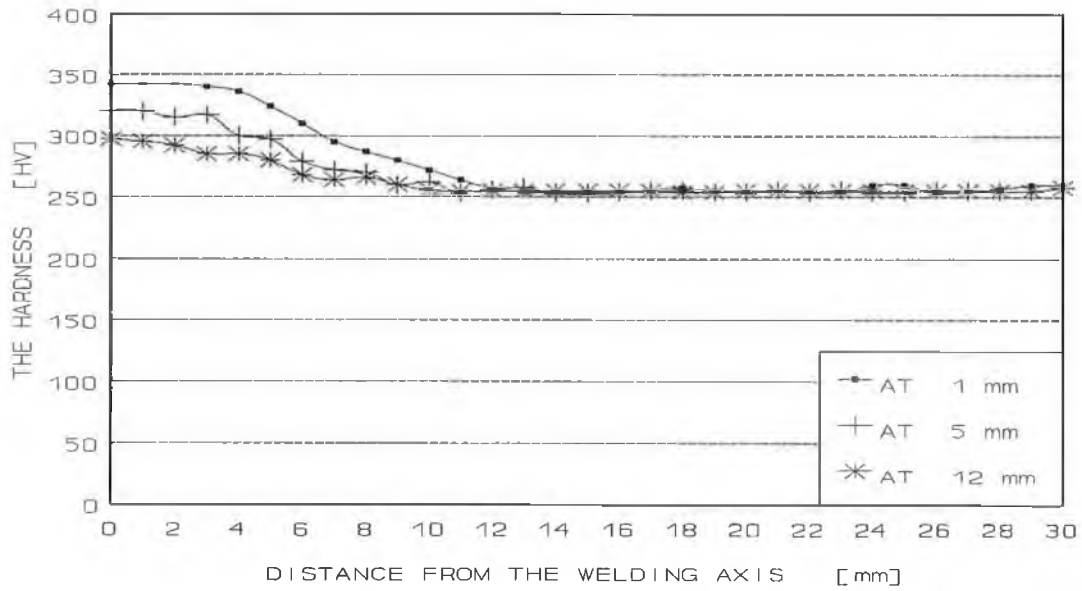

FIGURE 4.28 HARDNESS VARIATION ACROSS THE SPECIMEN AXIS AFTER PWHT WITH SOAKING TEMPERATURE OF 650°C FOR AISI-410 COMPONENT.

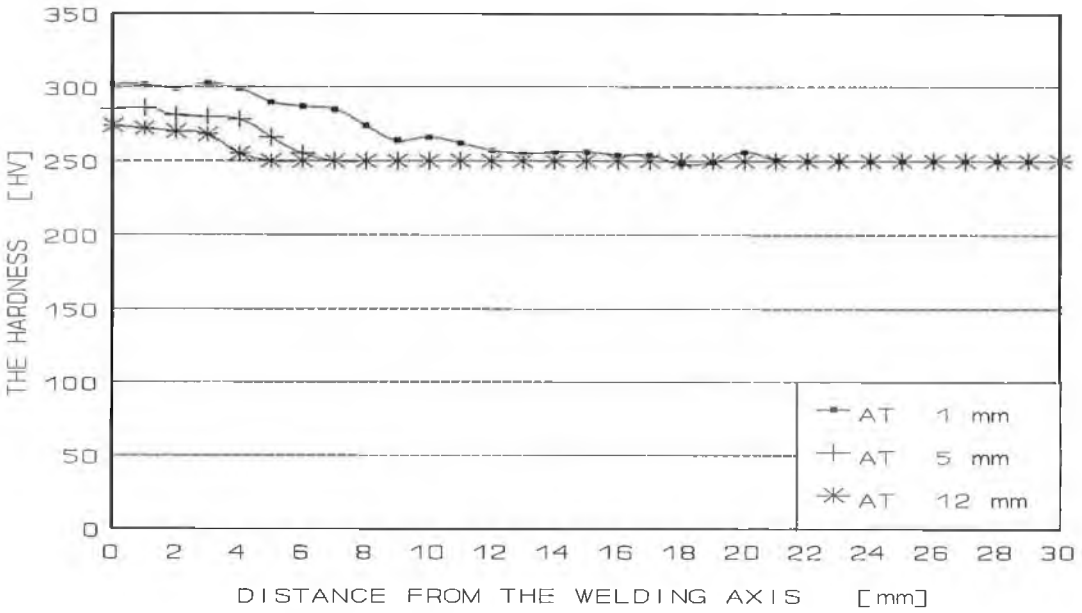

FIGURE 4.29 HARDNESS VARIATION ACROSS THE SPECIMEN AXIS AFTER PWHT WITH SOAKING TEMPERATURE OF 750°C FOR AISI-410 COMPONENT.

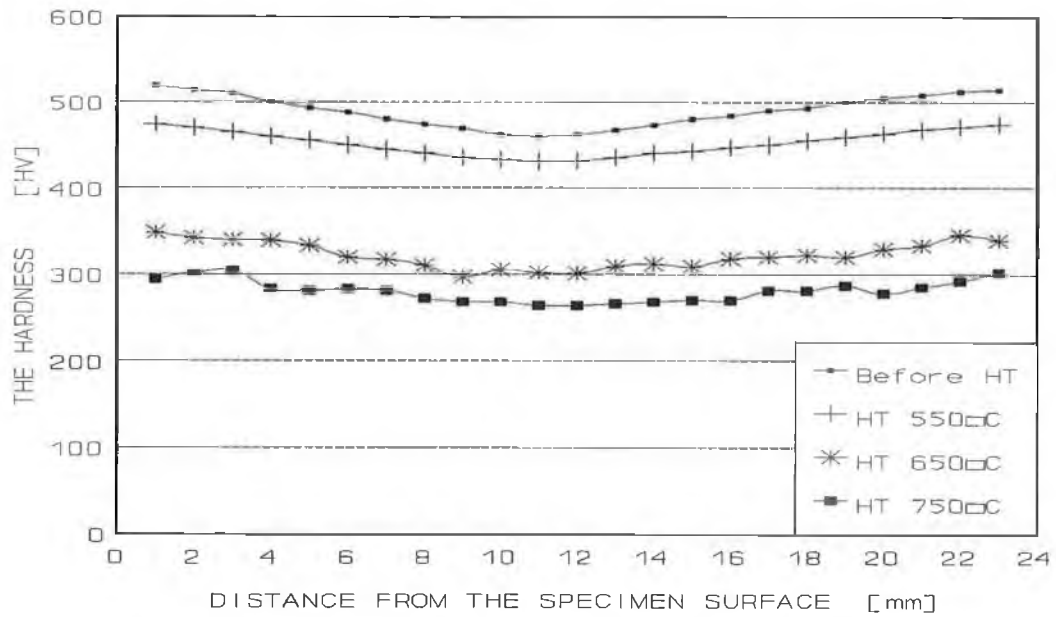

FIGURE 4.30 HARDNESS VARIATION IN THE SPECIMEN'S DEPTH FOR AISI-410 WELDED COMPONENT.

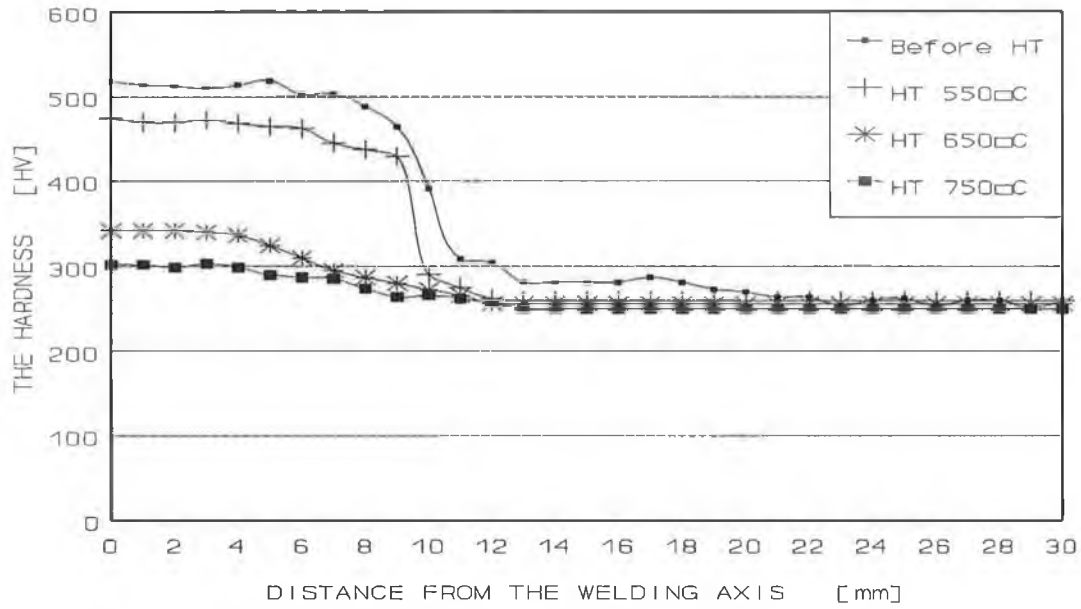

FIGURE 4.31 HARDNESS VARIATION AT THE DEPTH OF 1 MM BEFORE AND AFTER PWHT WITH DIFFERENT SOAKING TEMPERATURE FOR AISI-410 COMPONENT.

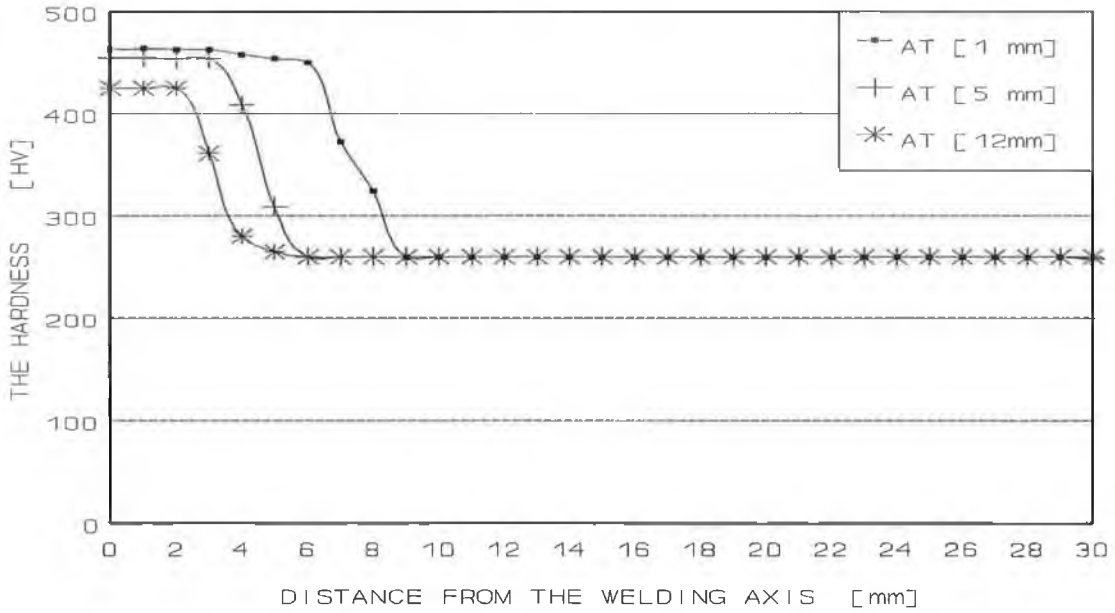

FIGURE 4.32 HARDNESS VARIATION AFTER PWHT WITH HEATING RATE OF 50°C/h FOR AISI-410 WELDED COMPONENT.

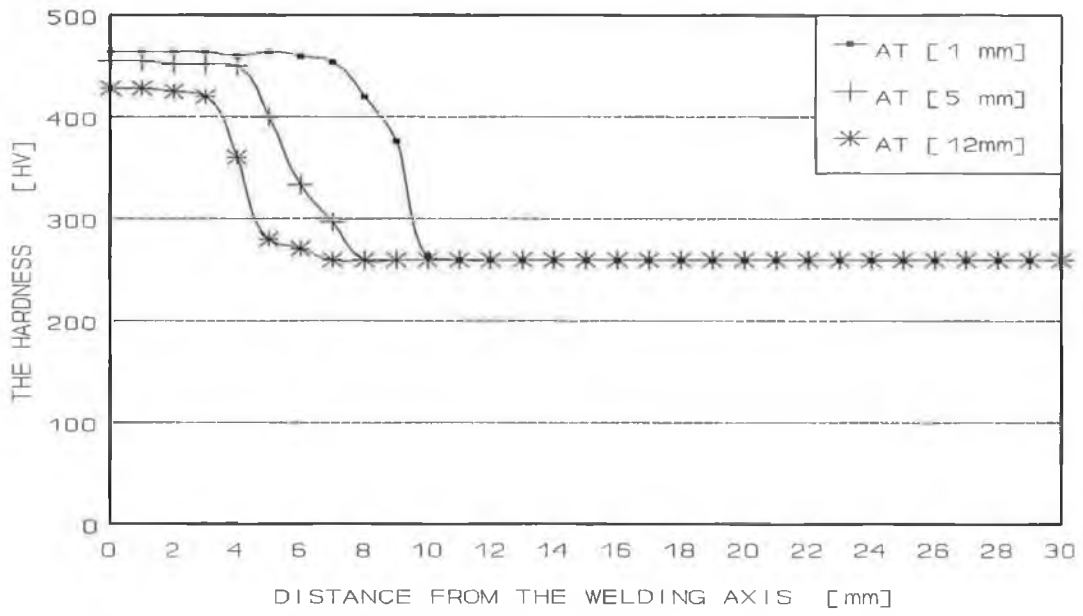

FIGURE 4.33 HARDNESS VARIATION AFTER PWHT WITH HEATING RATE OF 100°C/h FOR AISI-410 WELDED COMPONENT.

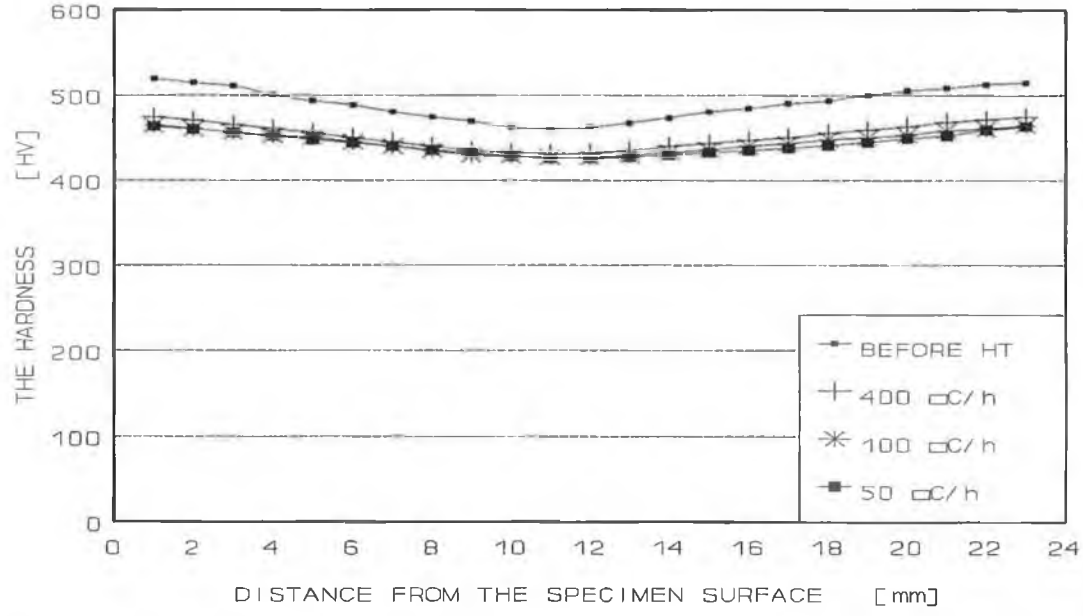

FIGURE 4.34 HARDNESS VARIATION IN THE SPECIMEN'S DEPTH BEFORE AND AFTER PWHT WITH DIFFERENT HEATING RATES FOR AISI-410 WELDED COMPONENT.

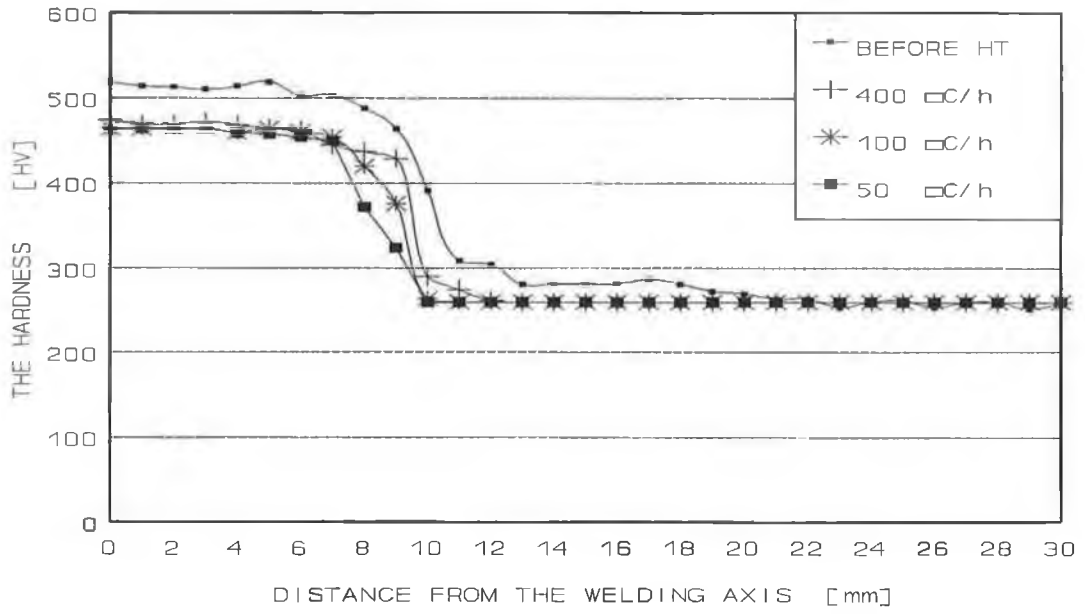

FIGURE 4.35 HARDNESS VARIATION AT THE DEPTH OF 1 mm BEFORE AND AFTER PWHT WITH DIFFERENT HEATING RATES FOR AISI-410 COMPONENT.

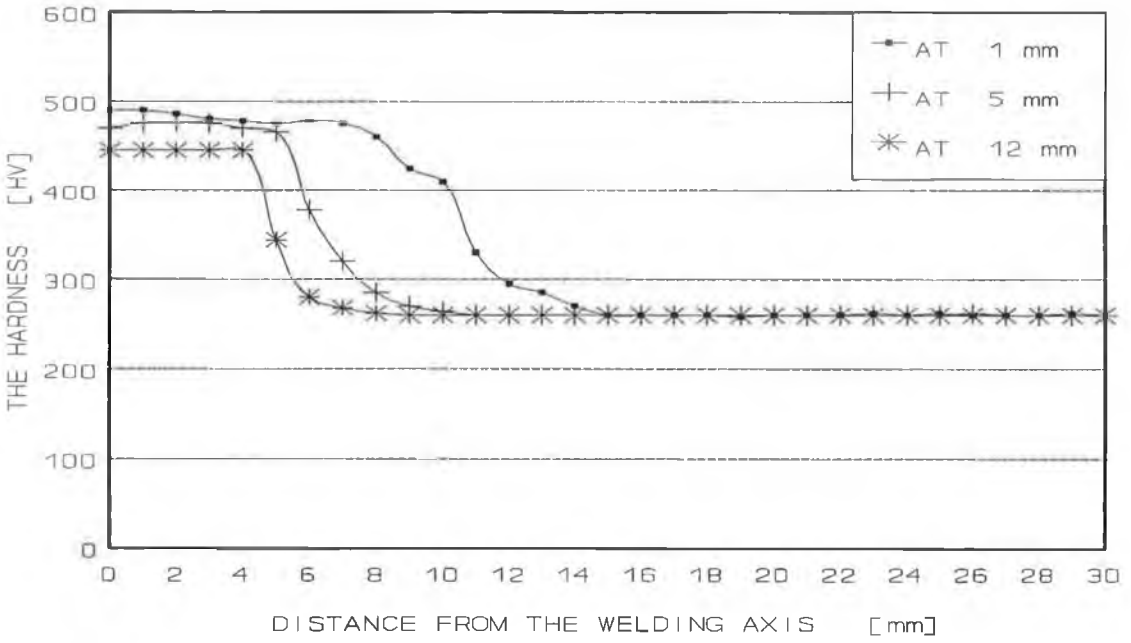

FIGURE 4.36 HARDNESS VARIATION AFTER PWHT WITH TIME DURATION OF 0.5 h FOR AISI-410 WELDED COMPONENT.

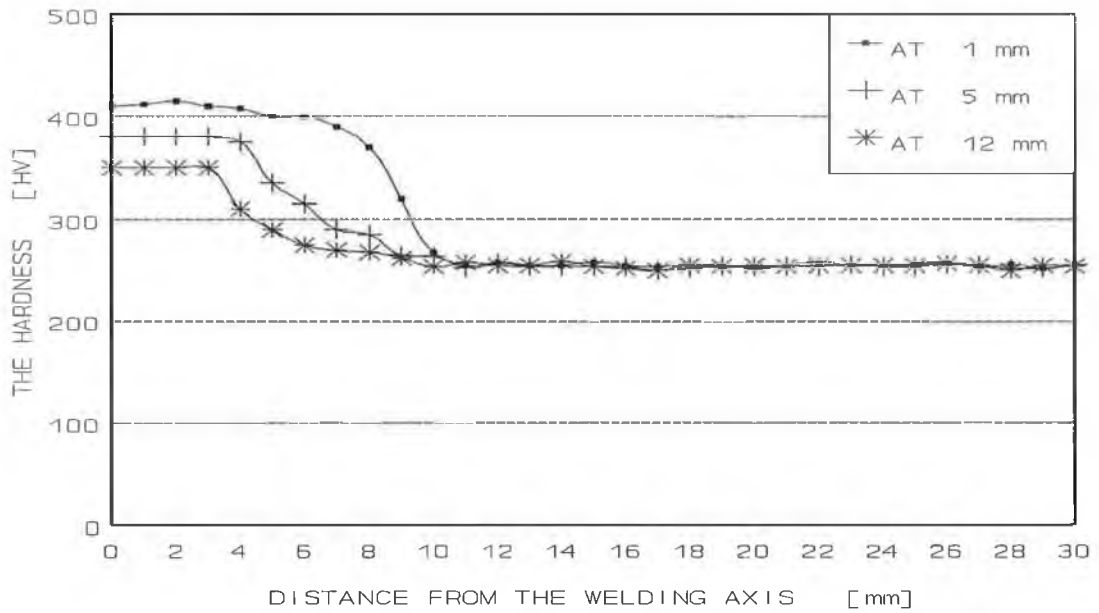

FIGURE 4.37 HARDNESS VARIATION ACROSS THE SPECIMEN AXIS AFTER PWHT WITH TIME DURATION OF 10 hRS FOR AISI-410 COMPONENT.

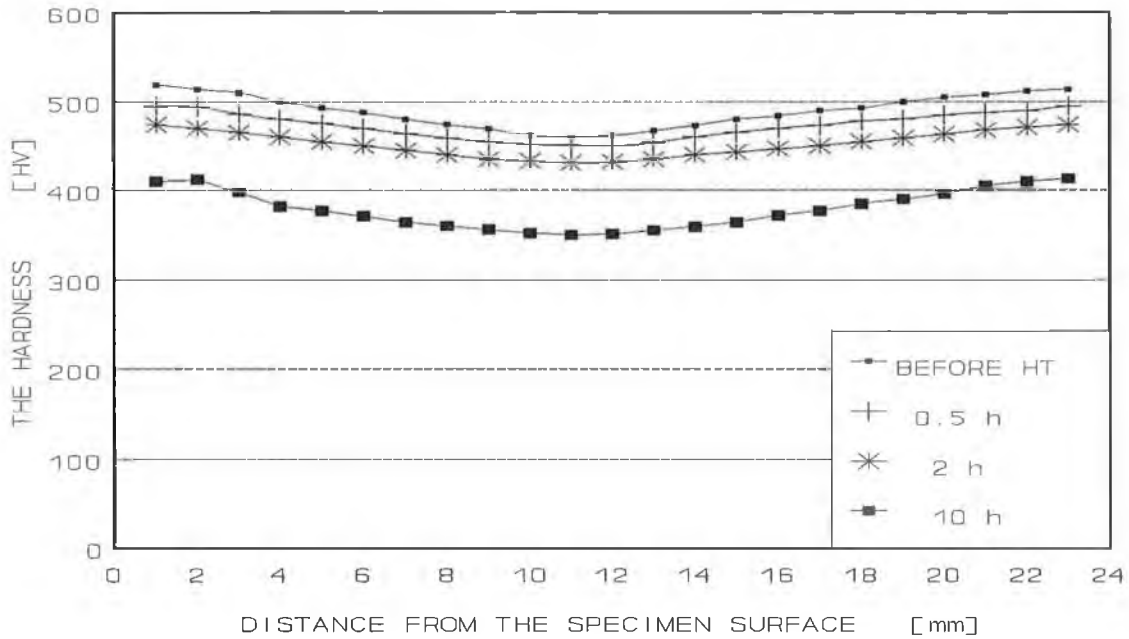

FIGURE 4.38 HARDNESS VARIATION IN THE SPECIMEN'S DEPTH AFTER PWHT WITH DIFFERENT TIME DURATIONS FOR AISI-410 WELDED COMPONENT.

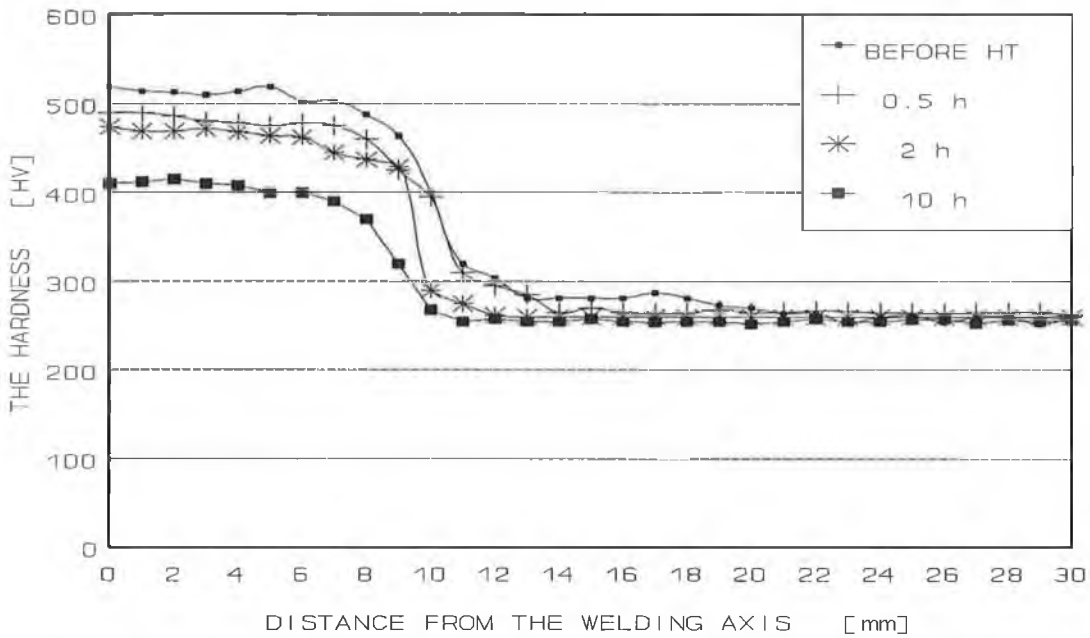

FIGURE 4.39 HARDNESS VARIATION AT THE DEPTH OF 1 mm BEFORE AND AFTER PWHT FOR DIFFERENT TIME DURATIONS FOR AISI-410 WELDED COMPONENT.

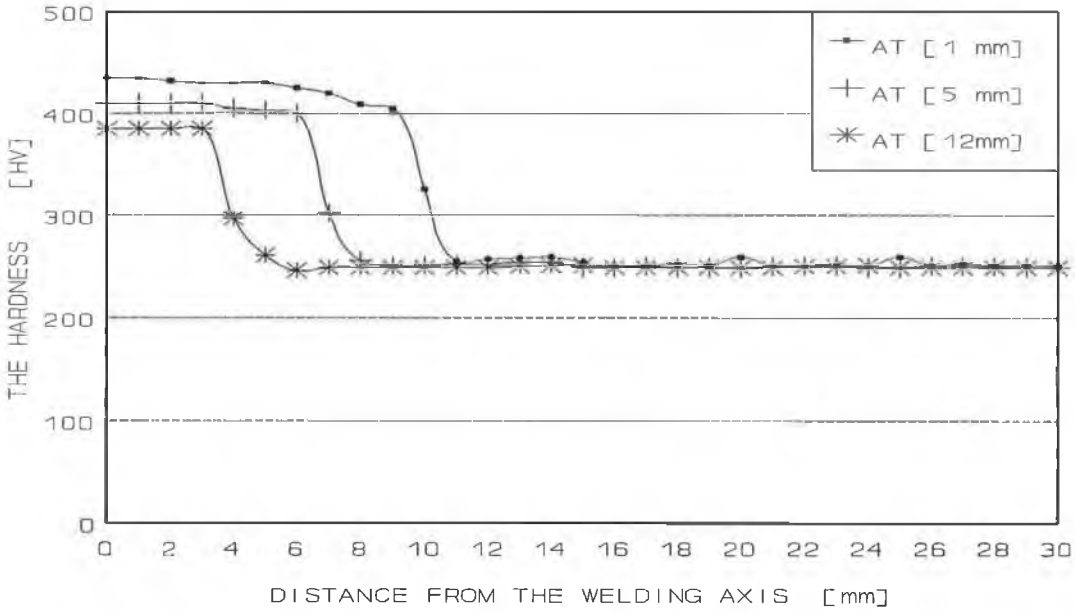

FIGURE 4.40 HARDNESS VARIATION AFTER PWHT WITH COOLING RATE OF 10°C/h FOR AISI-410 WELDED COMPONENT.

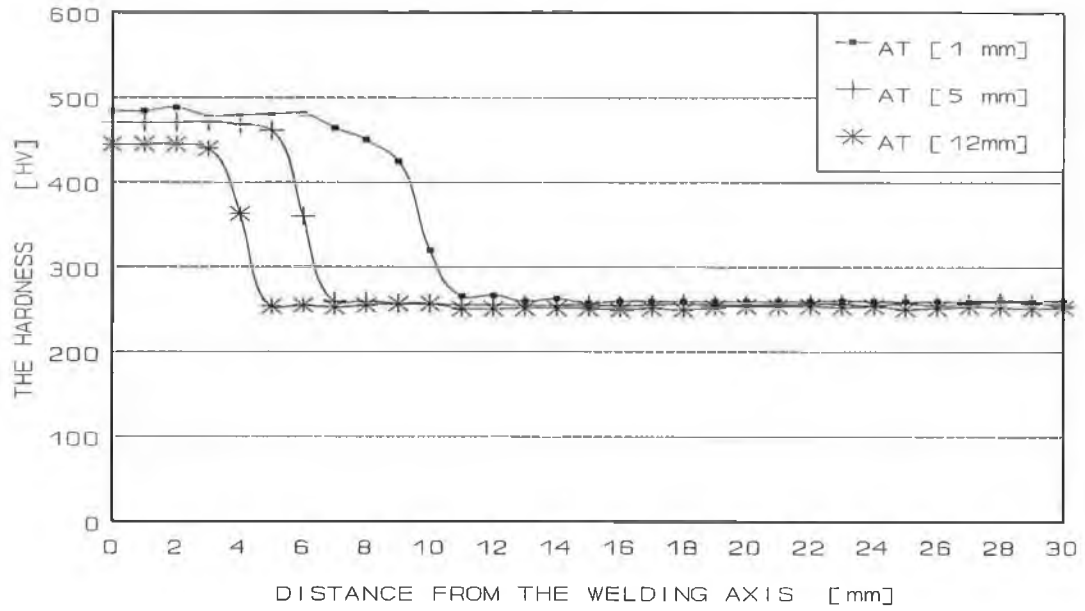

FIGURE 4.41 HARDNESS VARIATION ACROSS THE SPECIMEN AXIS AFTER PWHT WITH COOLING RATE OF 125°/h FOR AISI-410 COMPONENT.

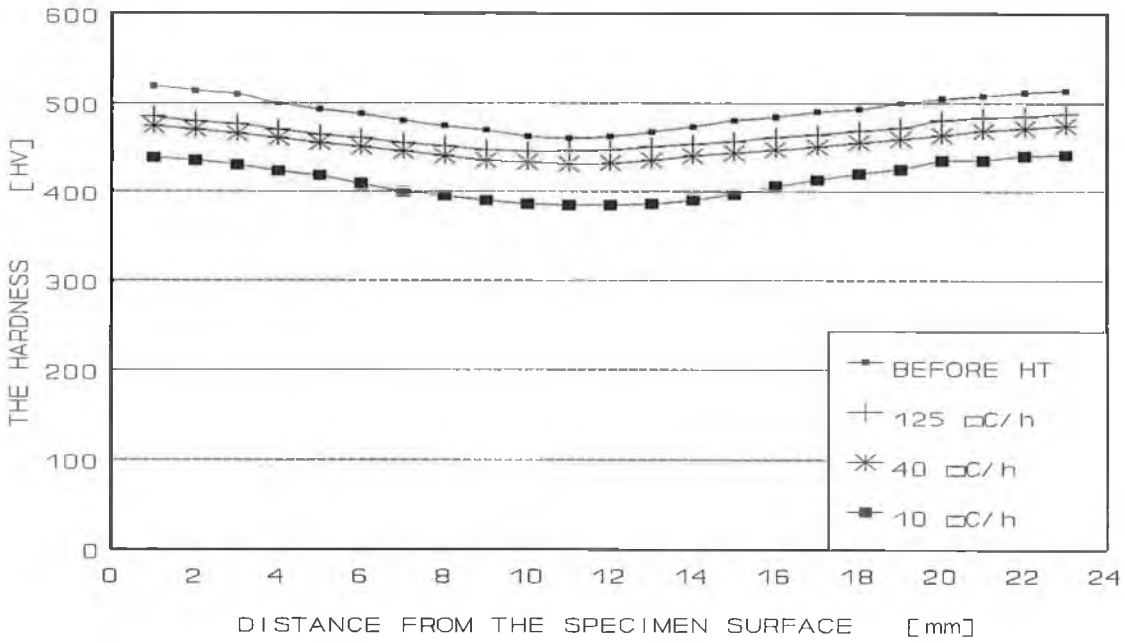

FIGURE 4.42 HARDNESS VARIATION IN THE SPECIMEN'S DEPTH AFTER PWHT WITH DIFFERENT COOLING RATES FOR AISI-410 WELDED COMPONENT.

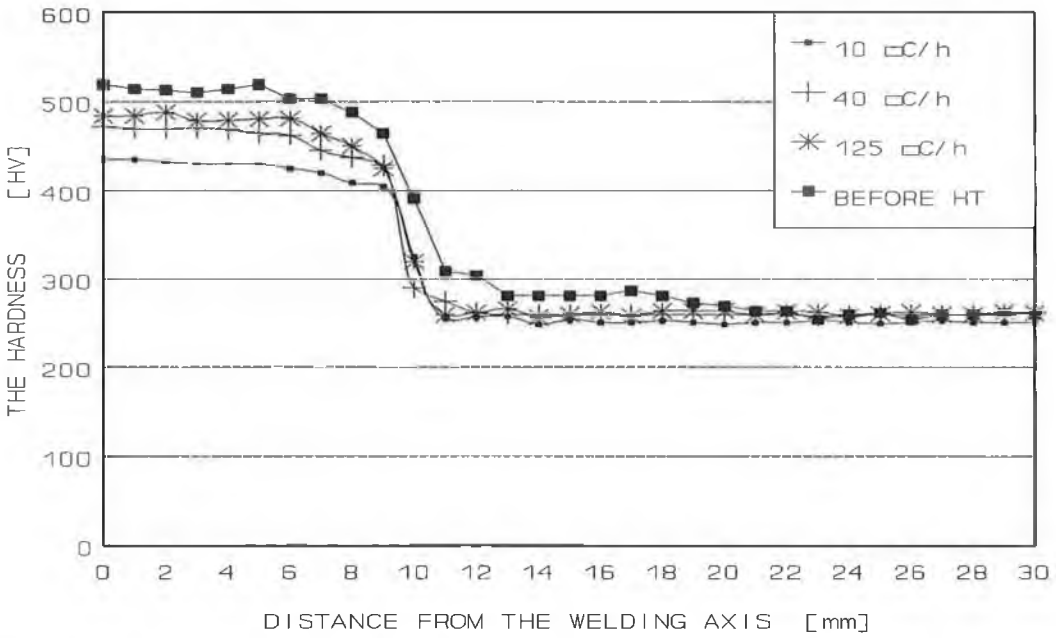

FIGURE 4.43 HARDNESS VARIATION AT THE DEPTH OF 1 mm BEFORE AND AFTER PWHT WITH DIFFERENT COOLING RATES FOR AISI-410 COMPONENT.

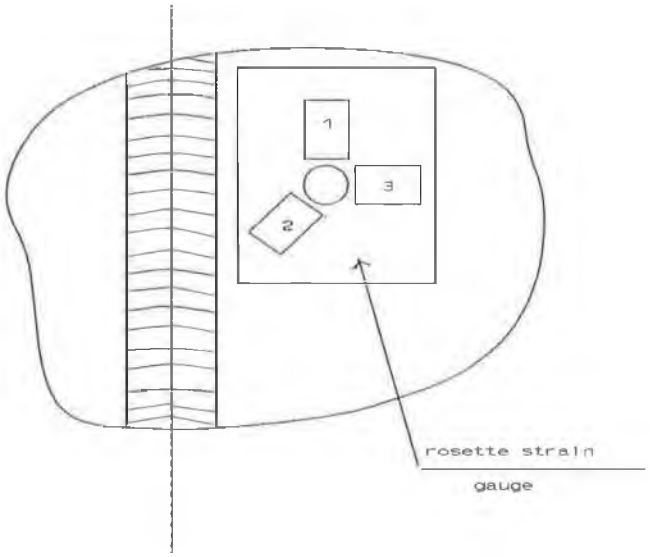

FIGURE 4.44 STRAIN GAUGE ORIENTATION ON THE SPECIMEN.

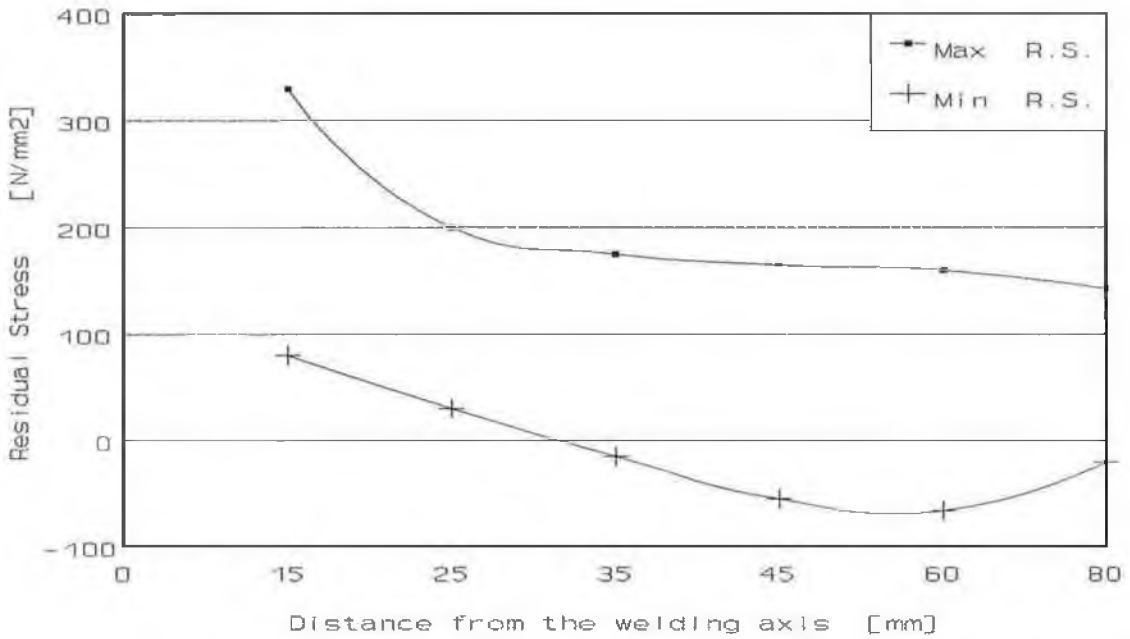

Figure 4.45 PRINCIPAL RESIDUAL STRESSES BEFORE PWHT FOR THE I-BEAM BOX-SECTION COMPONENT.

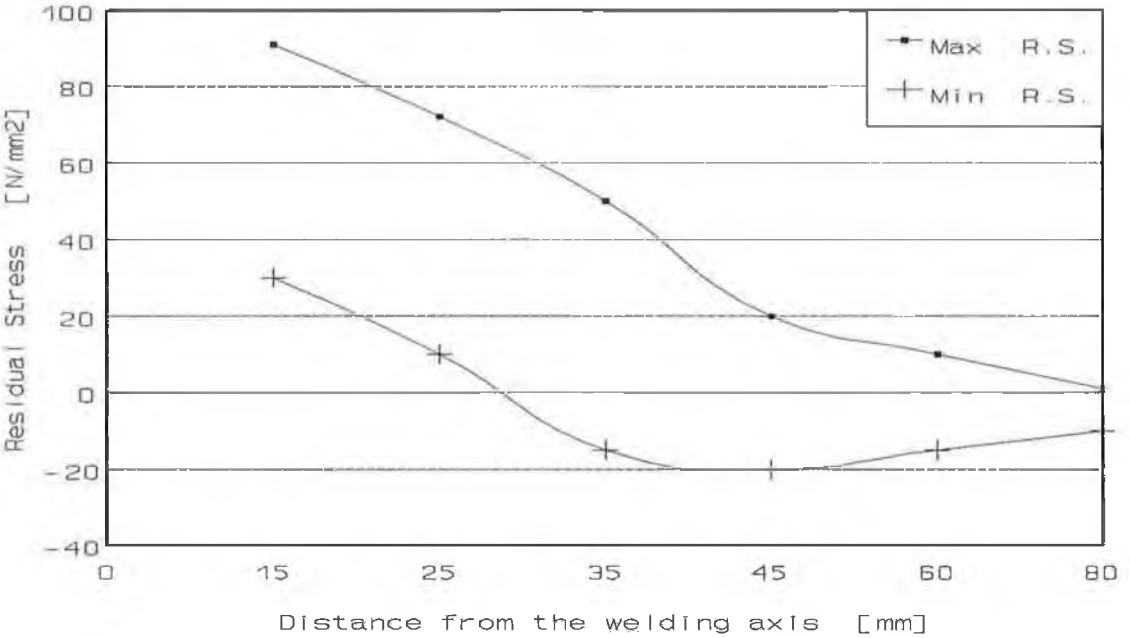

FIGURE 4.46 PRINCIPAL RESIDUAL STRESSES AFTER PWHT FOR I-BEAM BOX-SECTION COMPONENT.

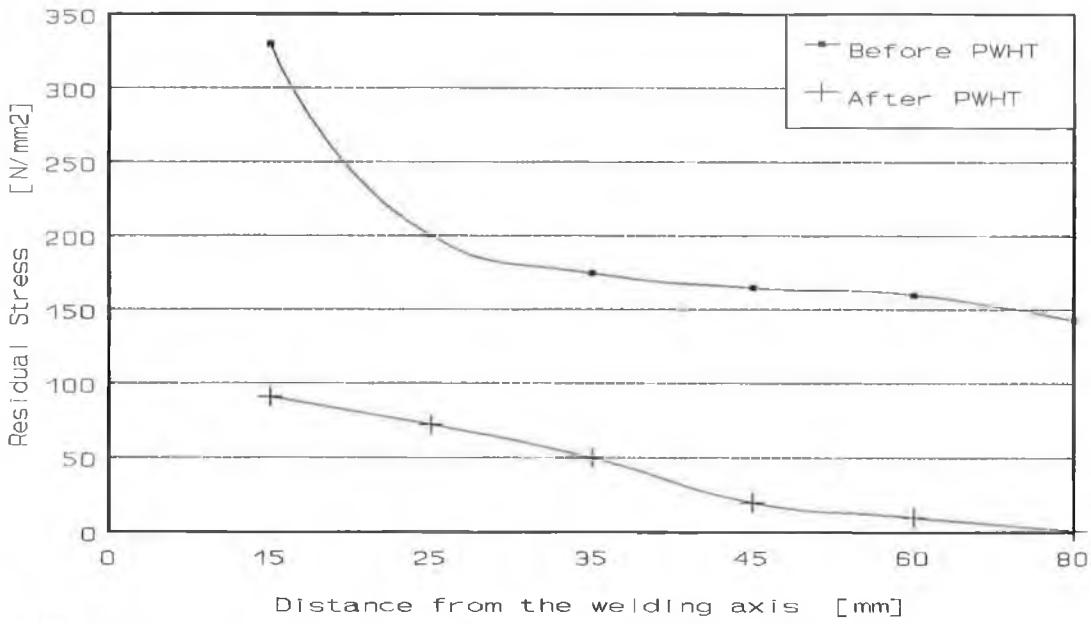

FIGURE 4.47 MAXIMUM RESIDUAL STRESSES BEFORE AND AFTER PWHT FOR I-BEAM BOX-SECTION COMPONENT.

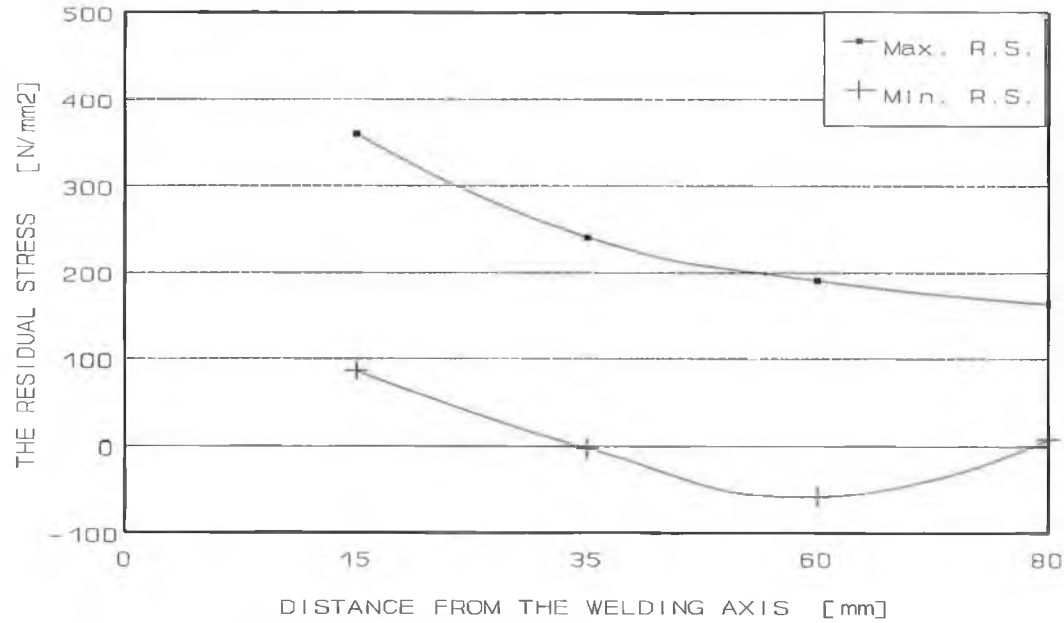

FIGURE 4.48 PRINCIPAL RESIDUAL STRESSES BEFORE PWHT FOR THE CARBON STEEL COMPONENT.

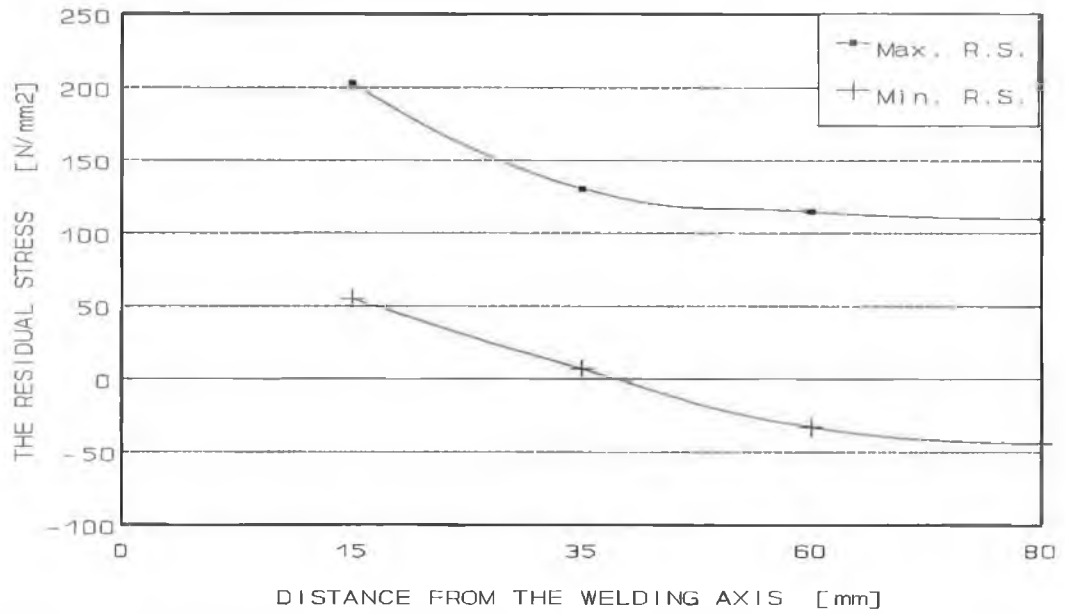

FIGURE 4.49 PRINCIPAL RESIDUAL STRESSES AFTER PWHT WITH SOAKING TEMPERATURE OF 450°C FOR AISI-1020 COMPONENT.

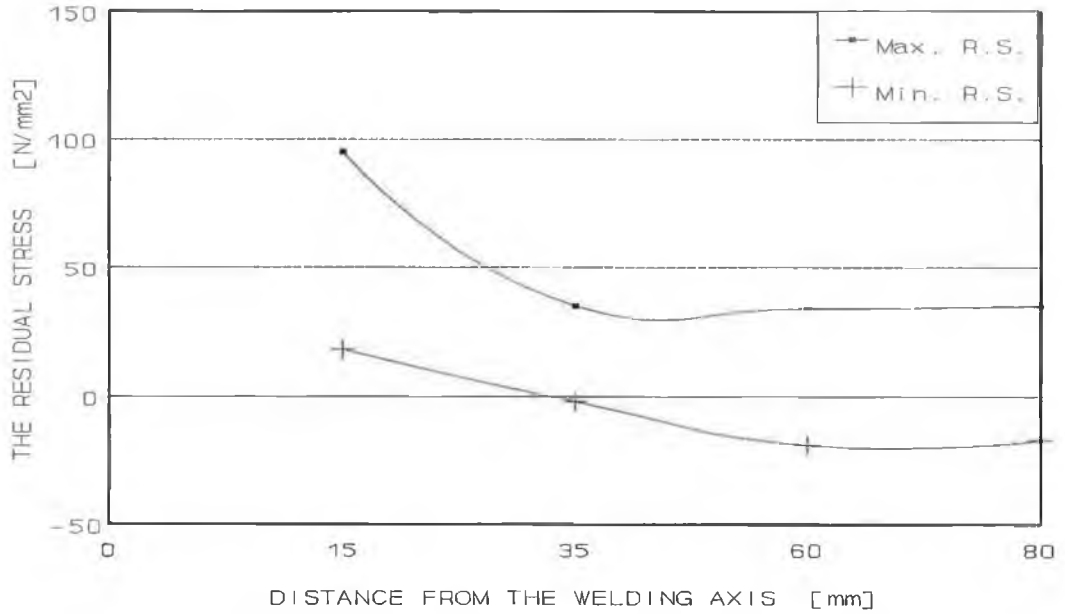

FIGURE 4.50 PRINCIPAL RESIDUAL STRESSES AFTER PWHT WITH SOAKING TEMPERATURE OF 550°C FOR AISI-1020 COMPONENT.

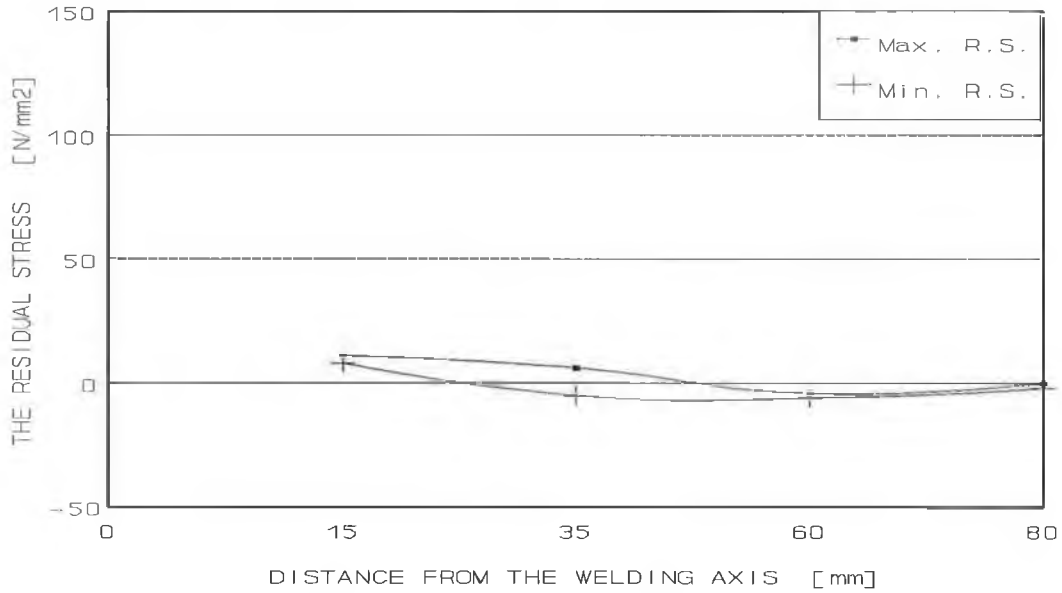

FIGURE 4.51 MAXIMUM RESIDUAL STRESSES AFTER PWHT WITH SOAKING TEMPERATURE OF 650°C FOR AISI-1020 COMPONENT.

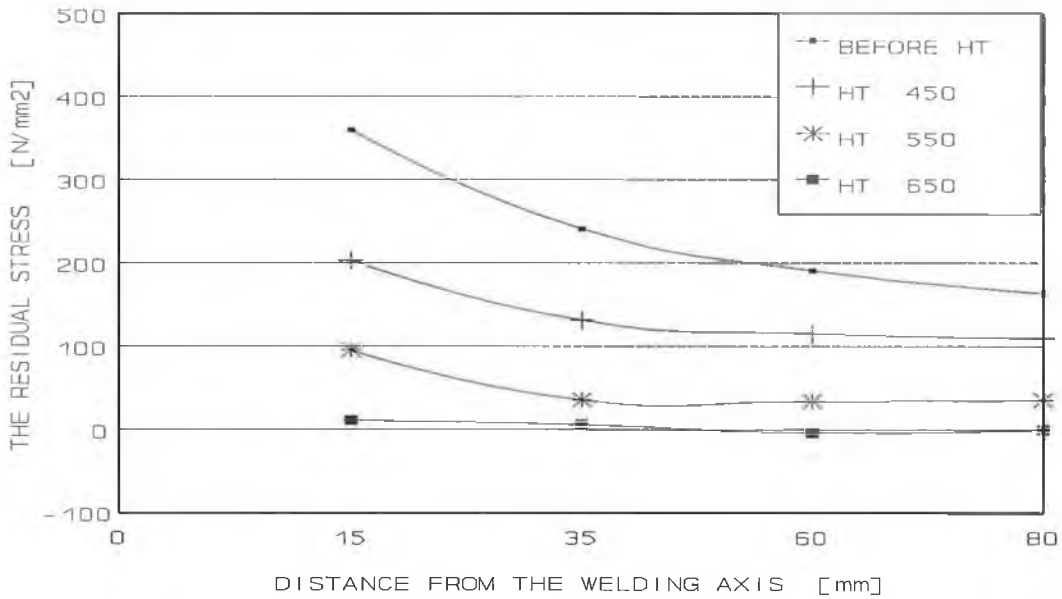

FIGURE 4.52 MAXIMUM RESIDUAL STRESSES BEFORE & AFTER PWHT WITH DIFFERENT SOAKING TEMPERATURES FOR AISI-1020 COMPONENT.

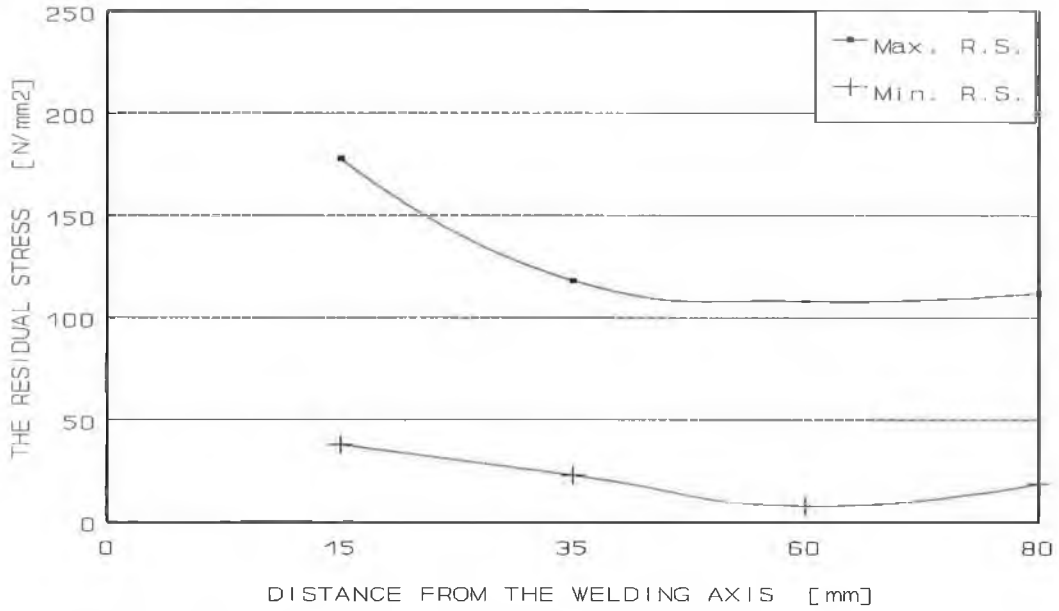

FIGURE 4.53 PRINCIPAL RESIDUAL STRESSES AFTER PWHT WITH HEATING RATE OF 50°C/h FOR AISI-1020 COMPONENT.

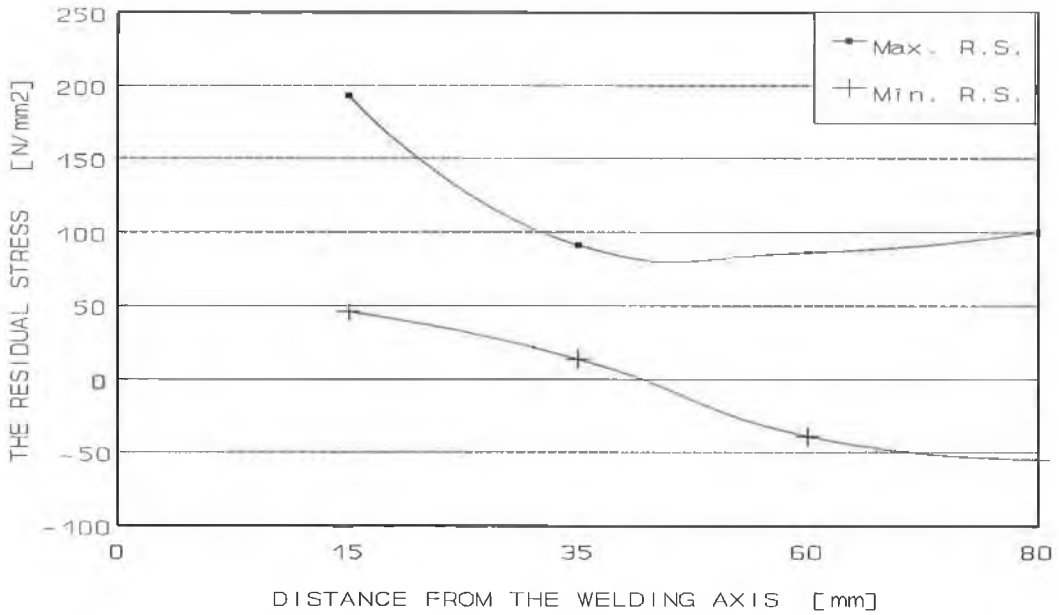

FIGURE 4.54 PRINCIPAL RESIDUAL STRESSES AFTER PWHT WITH HEATING RATE OF 100°C/h FOR AISI-1020 COMPONENT.

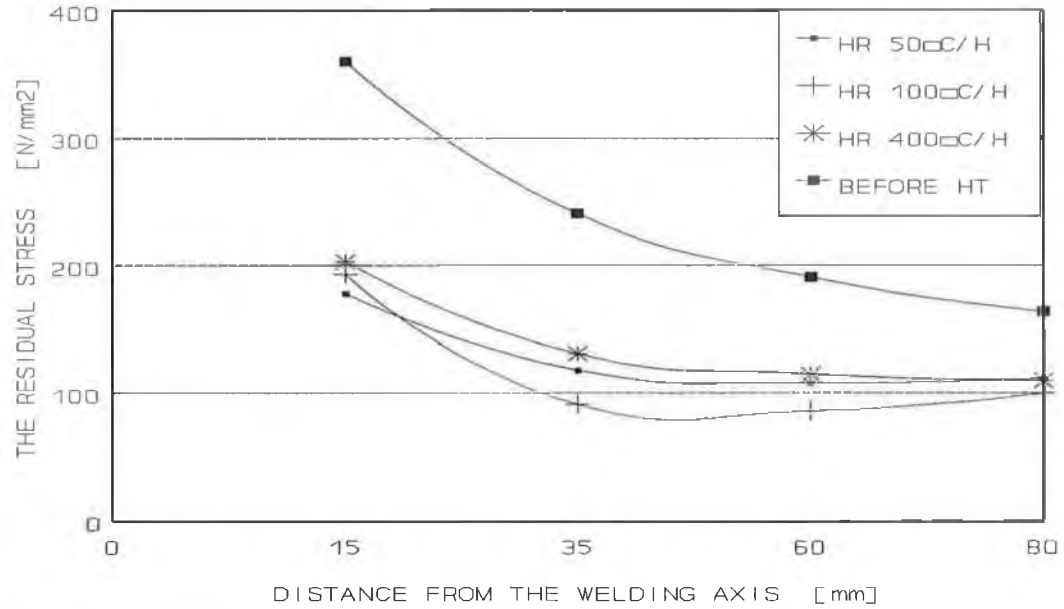

FIGURE 4.55 MAXIMUM RESIDUAL STRESSES BEFORE & AFTER PWHT WITH DIFFERENT HEATING RATES FOR AISI-1020 COMPONENT.

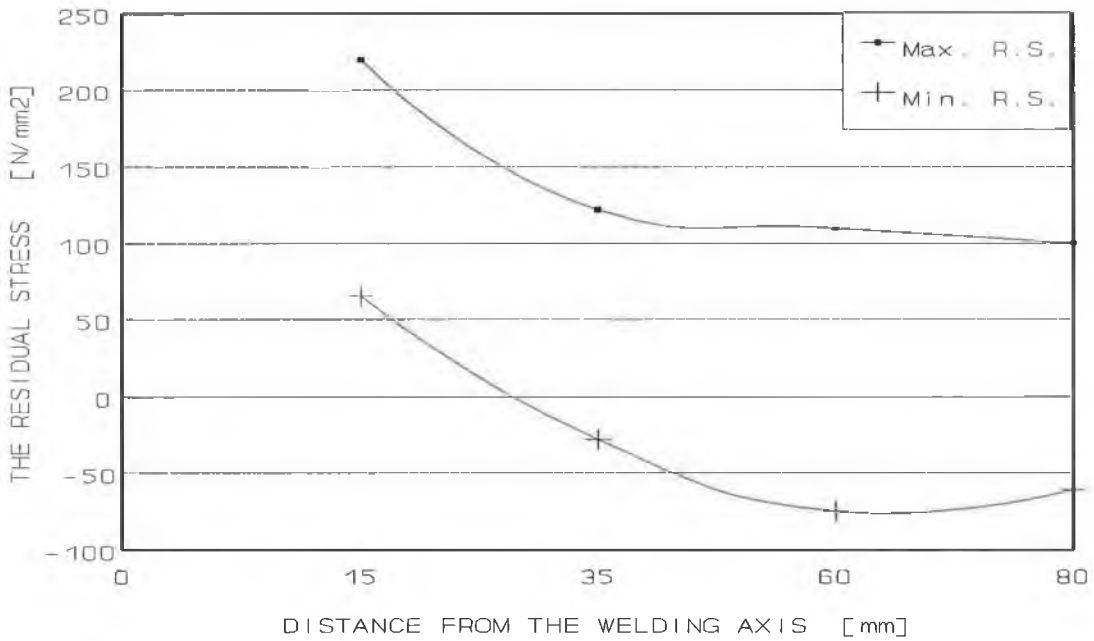

FIGURE 4.56 PRINCIPAL RESIDUAL STRESSES AFTER PWHT WITH TIME DURATION OF 0.5 h FOR AISI-1020 COMPONENT.

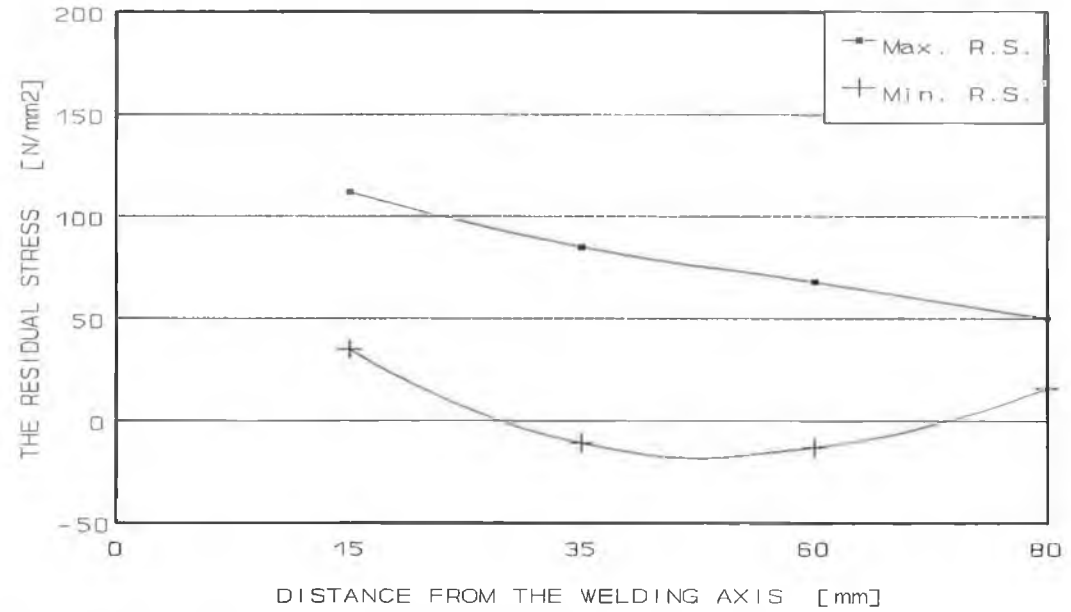

FIGURE 4.57 PRINCIPAL RESIDUAL STRESSES AFTER PWHT WITH TIME DURATION OF 10 hrs FOR AISI-1020 COMPONENT.

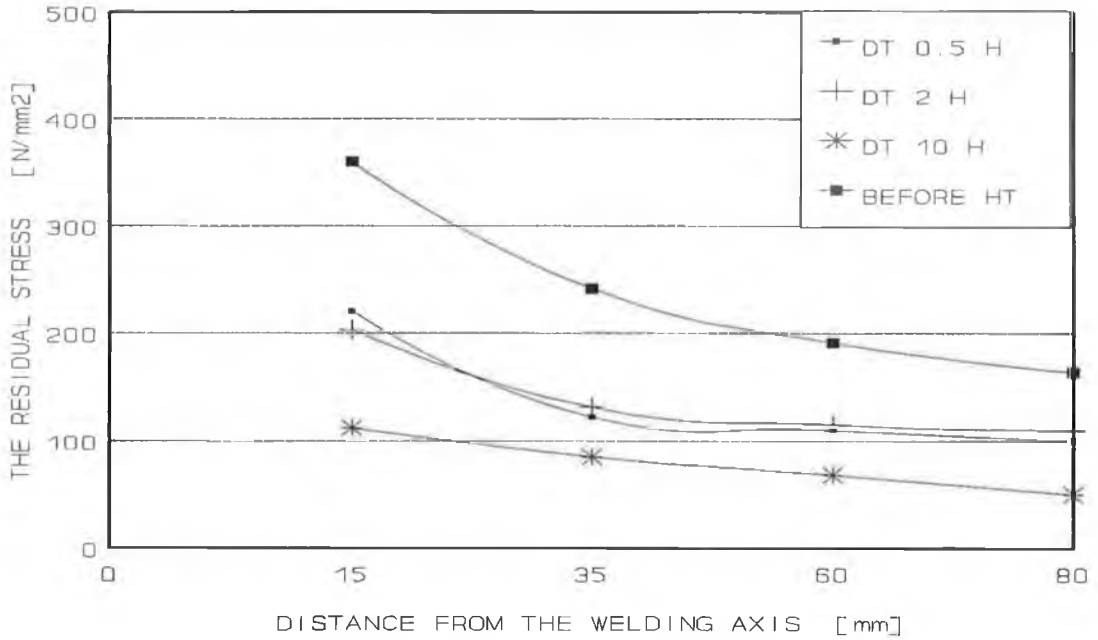

FIGURE 4.58 MAXIMUM RESIDUAL STRESSES BEFORE & AFTER PWHT WITH DIFFERENT DURATIONS FOR AISI-1020 COMPONENT.

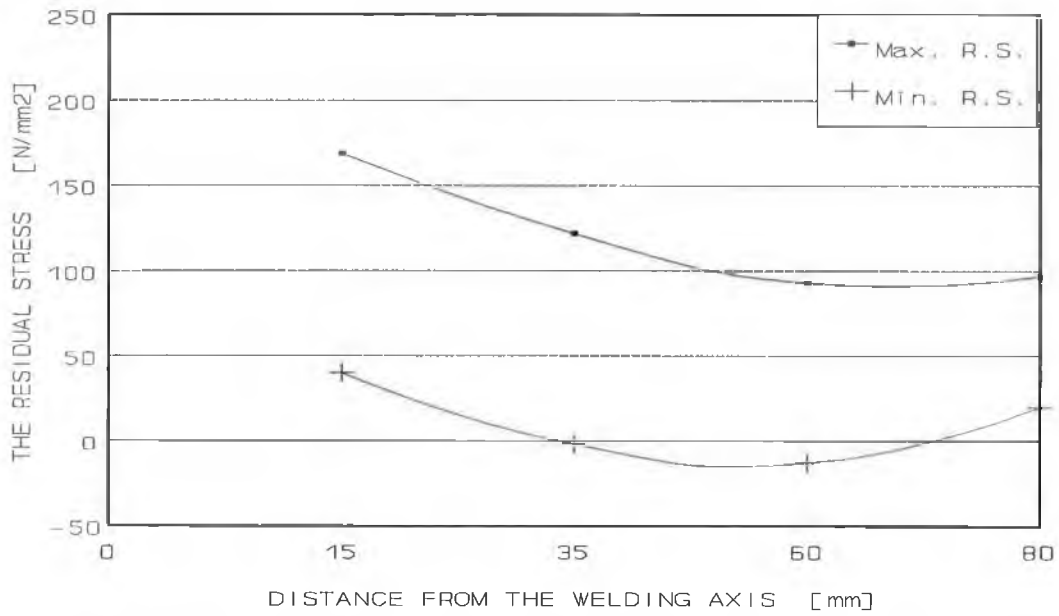

FIGURE 4.59 PRINCIPAL RESIDUAL STRESSES AFTER PWHT WITH COOLING RATE OF 10°C/h FOR AISI-1020 COMPONENT.

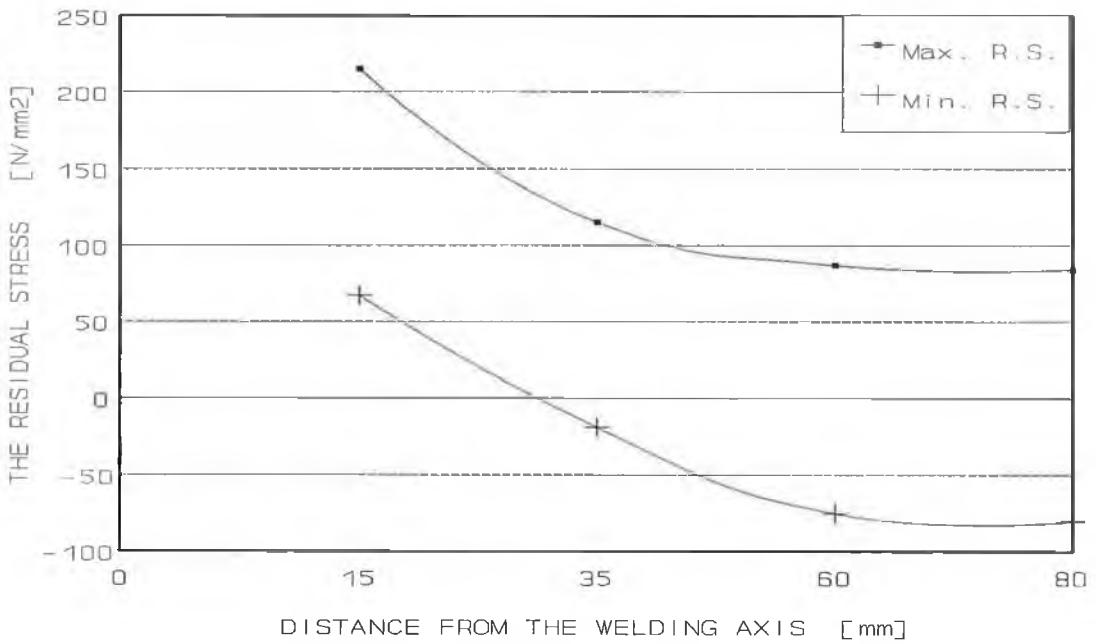

FIGURE 4.60 PRINCIPAL RESIDUAL STRESSES AFTER PWHT WITH TIME DURATION OF 125°C/h FOR AISI-1020 COMPONENT.

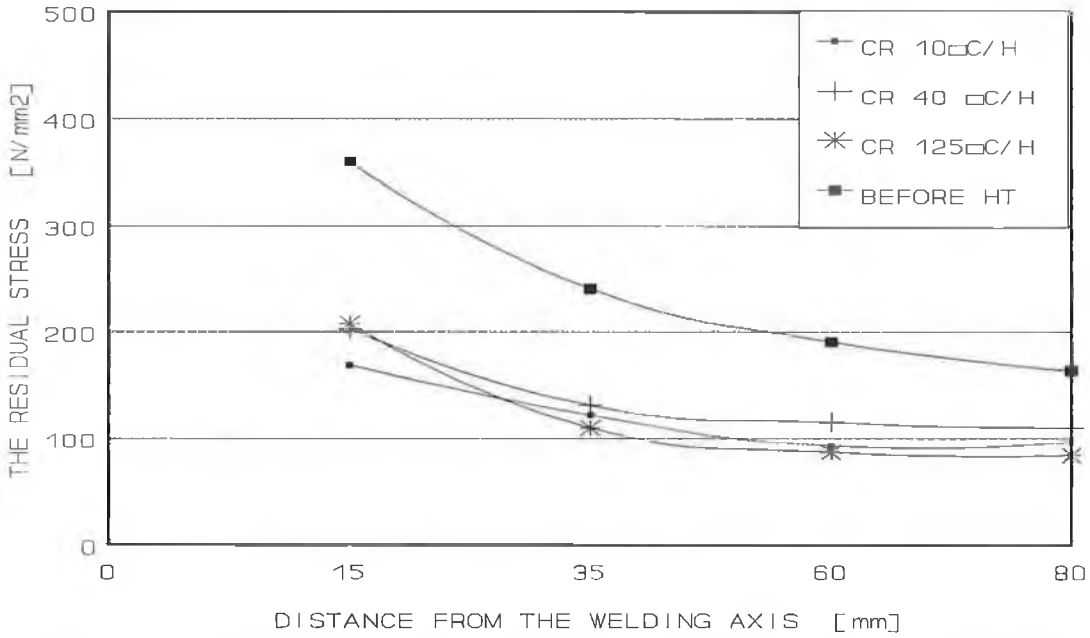

FIGURE 4.61 MAXIMUM RESIDUAL STRESSES BEFORE & AFTER PWHT WITH DIFFERENT COOLING RATES FOR AISI-1020 COMPONENT.

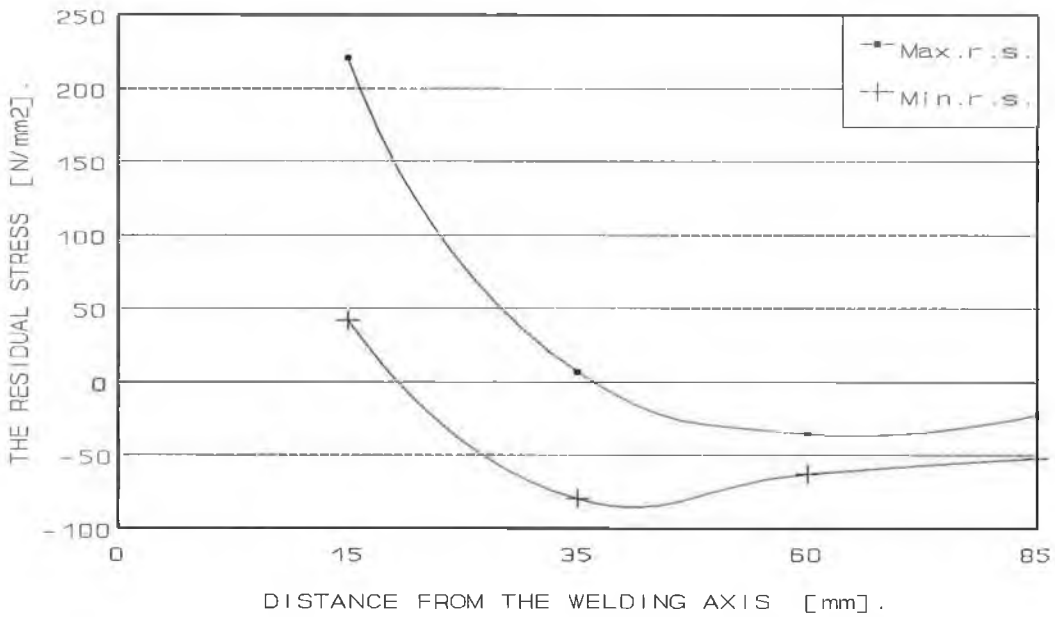

FIGURE 4.62 PRINCIPAL RESIDUAL STRESSES BEFORE PWHT AT THE TOP SURFACE FOR AISI-410 COMPONENT.

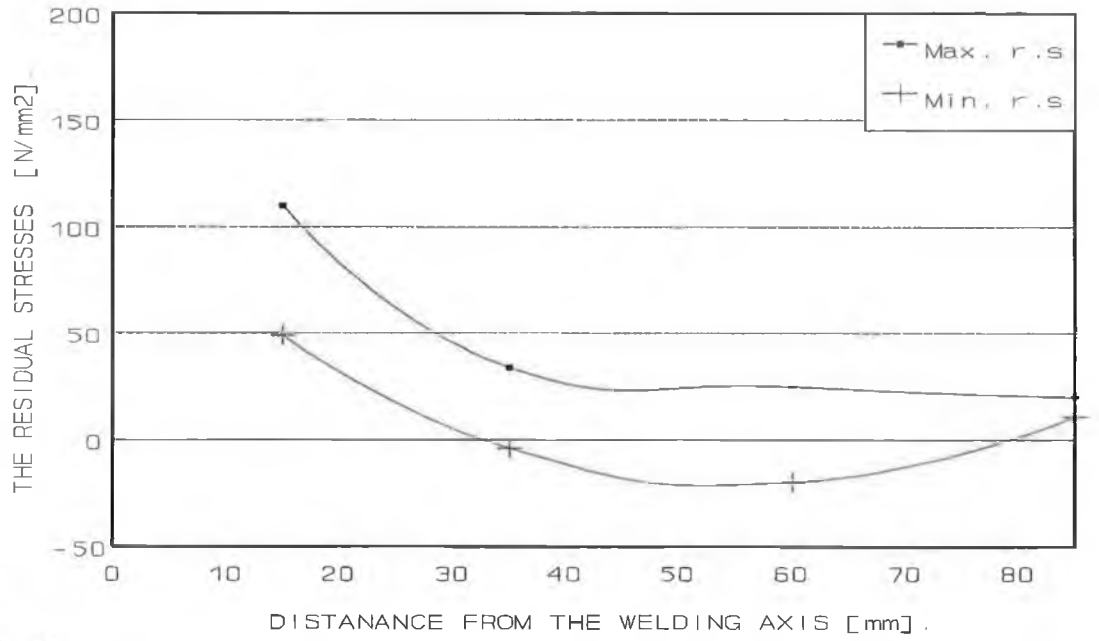

FIGURE 4.63 PRINCIPAL RESIDUAL STRESSES AFTER PWHT WITH SOAKING TEMPERATURE OF 550°C FOR AISI-410 WELDED COMPONENT.

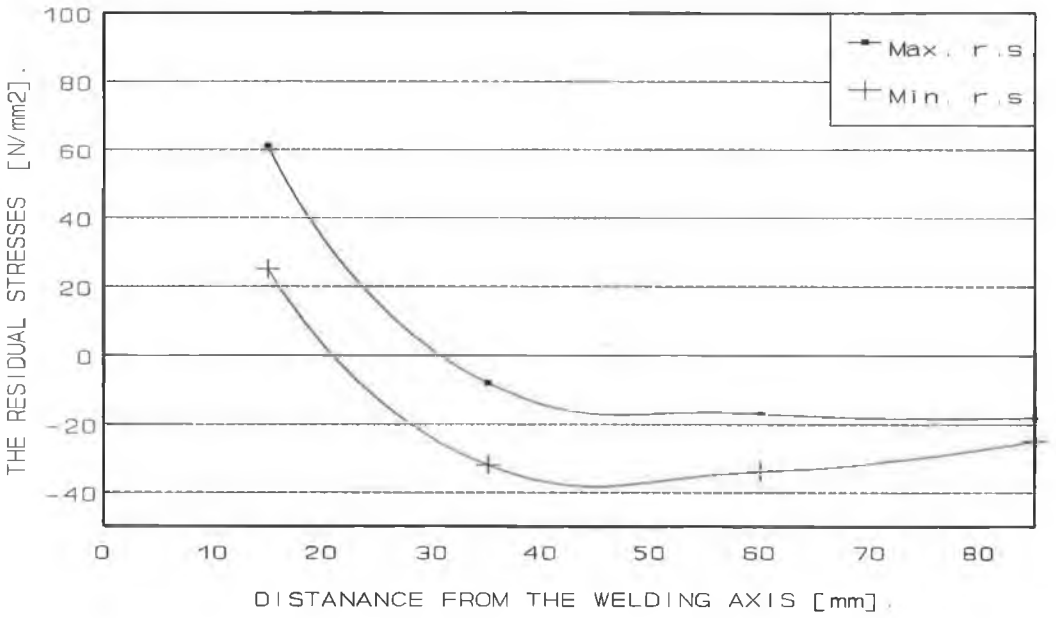

FIGURE 4.64 PRINCIPAL RESIDUAL STRESSES AFTER PWHT WITH SOAKING TEMPERATURE OF 650°C FOR AISI-410 COMPONENT.

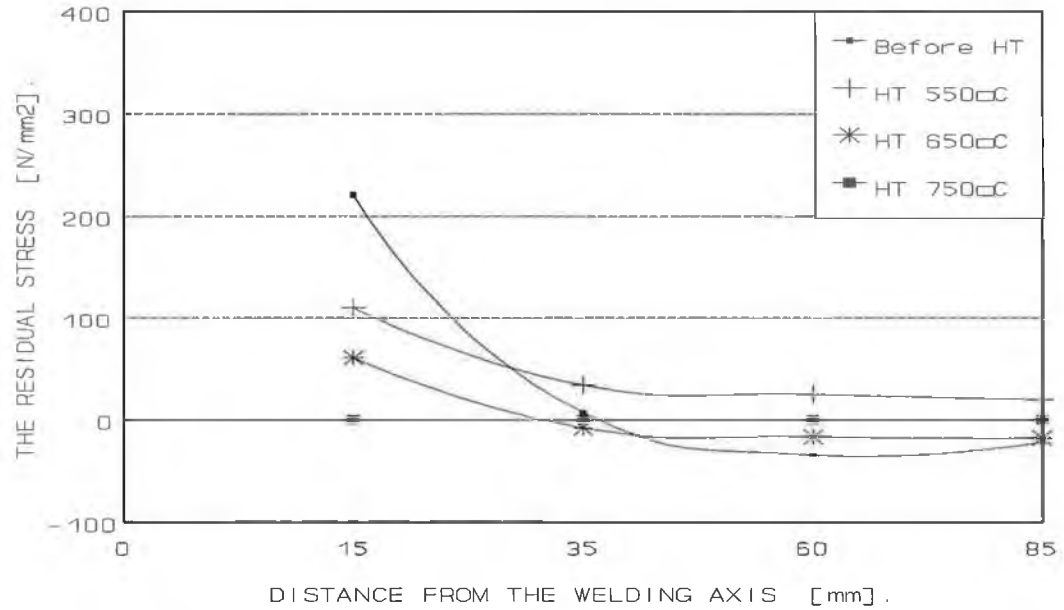

FIGURE 4.65 MAXIMUM RESIDUAL STRESSES BEFORE & AFTER PWHT WITH DIFFERENT TEMPERATURES FOR AISI-410 COMPONENT.

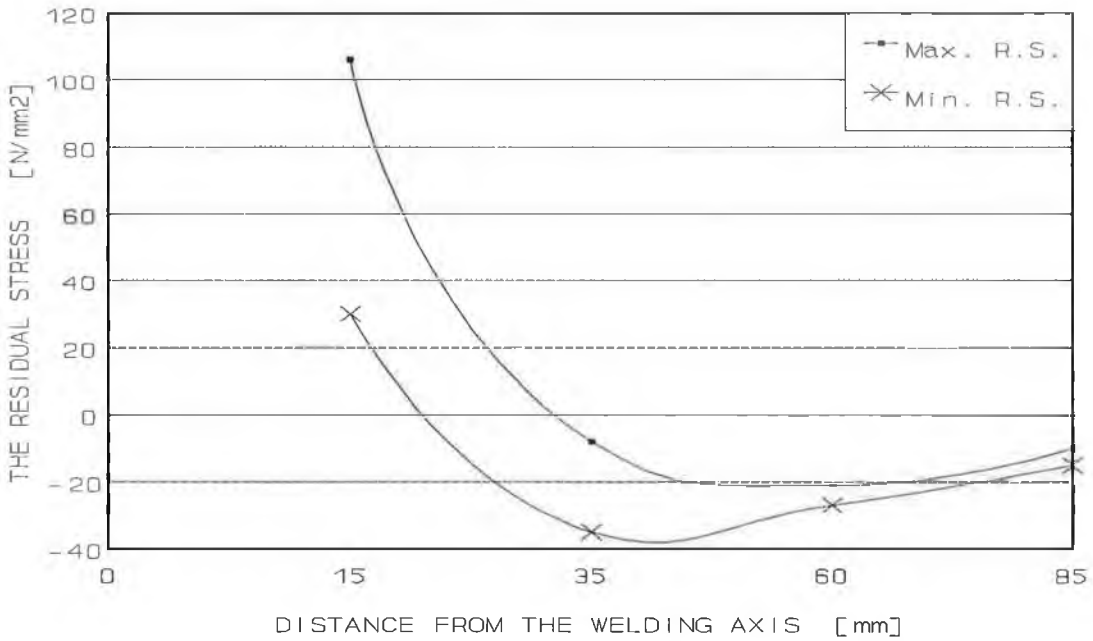

FIGURE 4.66 PRINCIPAL RESIDUAL STRESSES AFTER PWHT WITH HEATING RATE OF 50°C/h FOR AISI-410 COMPONENT.

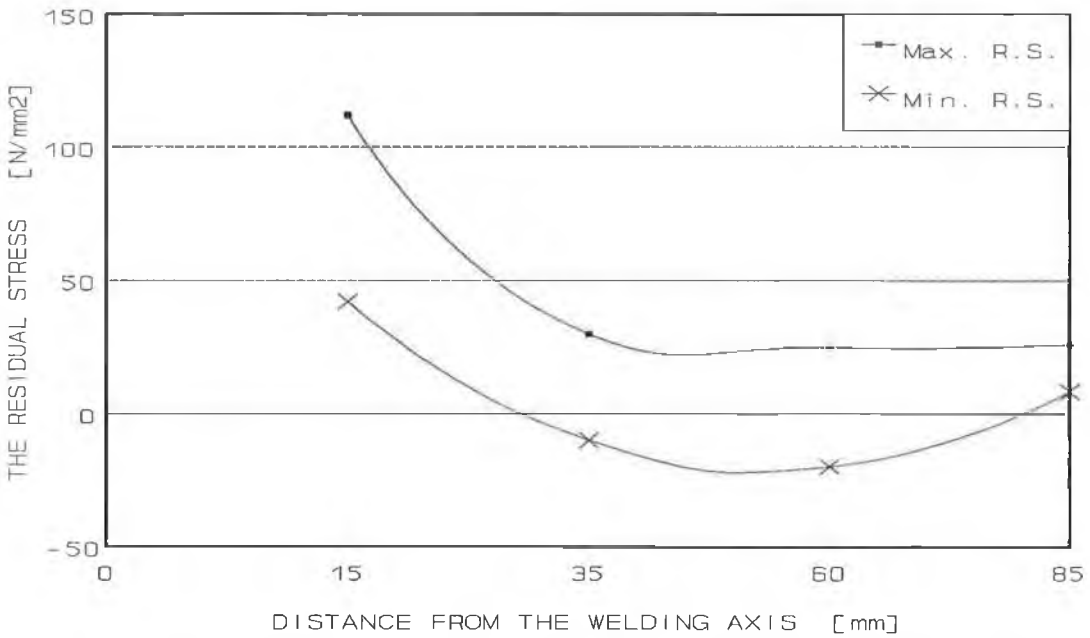

FIGURE 4.67 PRINCIPAL RESIDUAL STRESSES AFTER PWHT WITH HEATING RATE OF 100°C/h FOR AISI-410 COMPONENT.

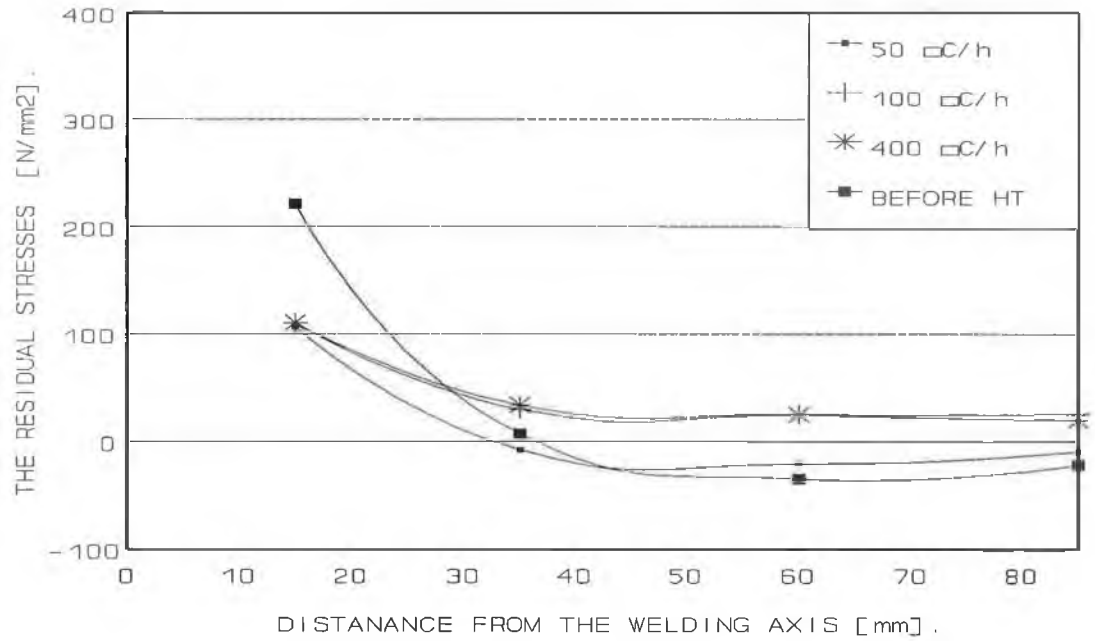

FIGURE 4.68 MAXIMUM RESIDUAL STRESSES BEFORE & AFTER PWHT WITH DIFFERENT HEATING RATES FOR AISI-410 COMPONENT.

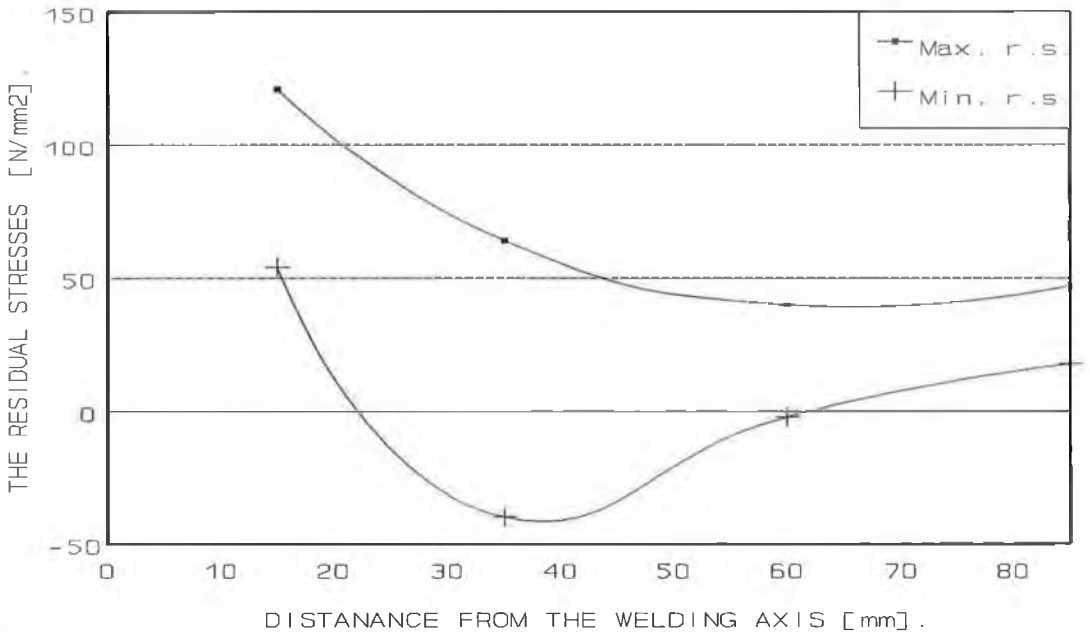

FIGURE 4.69 PRINCIPAL RESIDUAL STRESSES AFTER PWHT WITH TIME DURATION OF 0.5 h FOR AISI-410 COMPONENT.

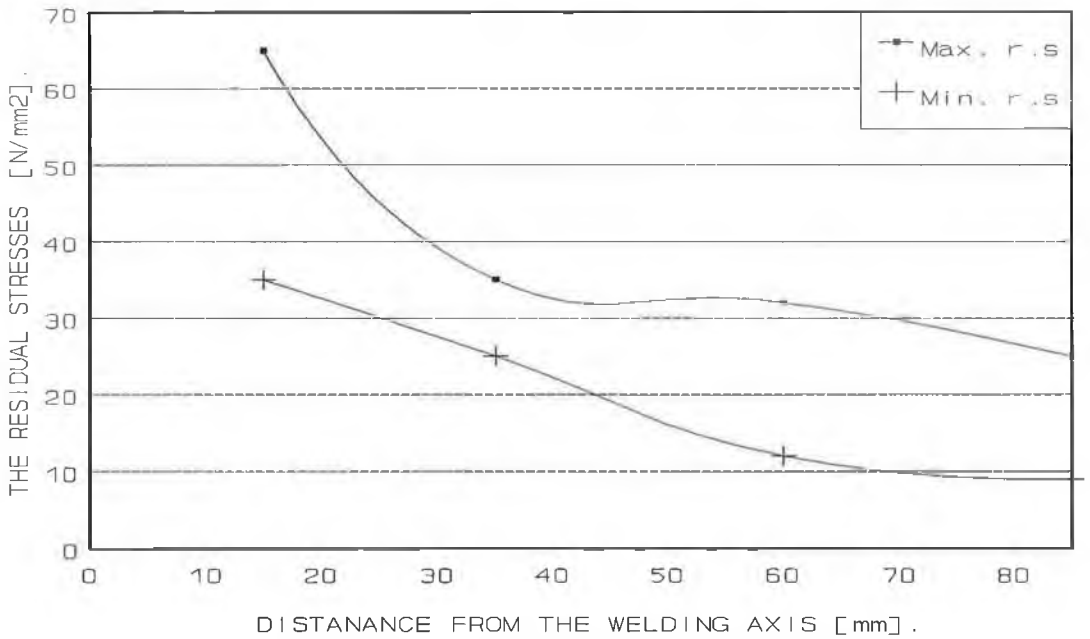

FIGURE 4.70 PRINCIPAL RESIDUAL STRESSES AFTER PWHT WITH TIME DURATION OF 10 hrs FOR AISI-410 COMPONENT.

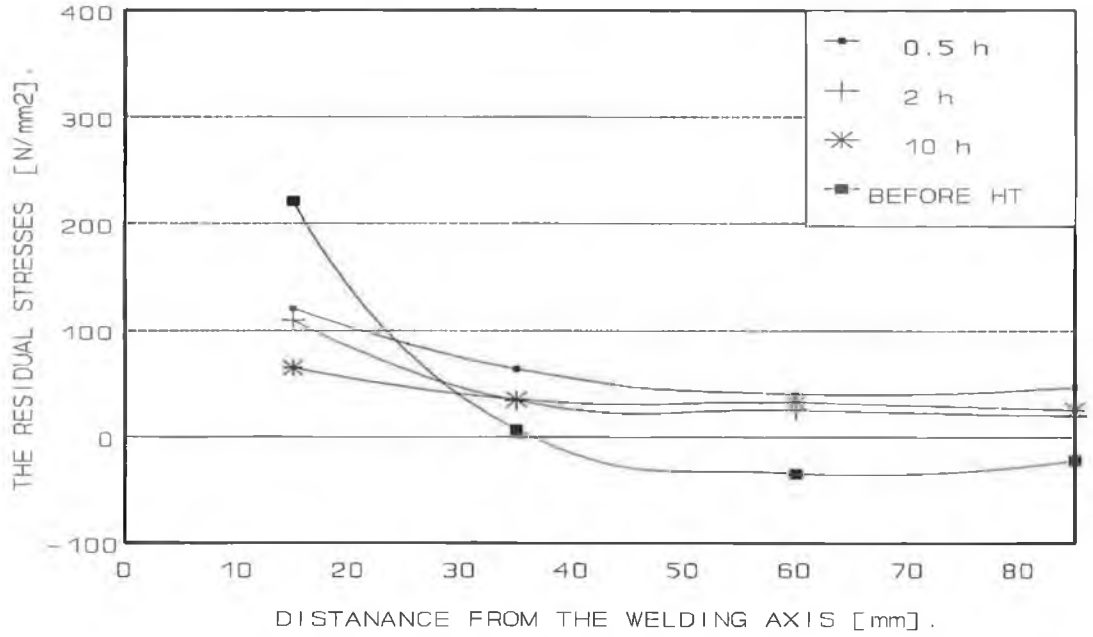

FIGURE 4.71 MAXIMUM RESIDUAL STRESSES BEFORE & AFTER PWHT WITH DIFFERENT TIME DURATIONS FOR AISI-410 COMPONENT.

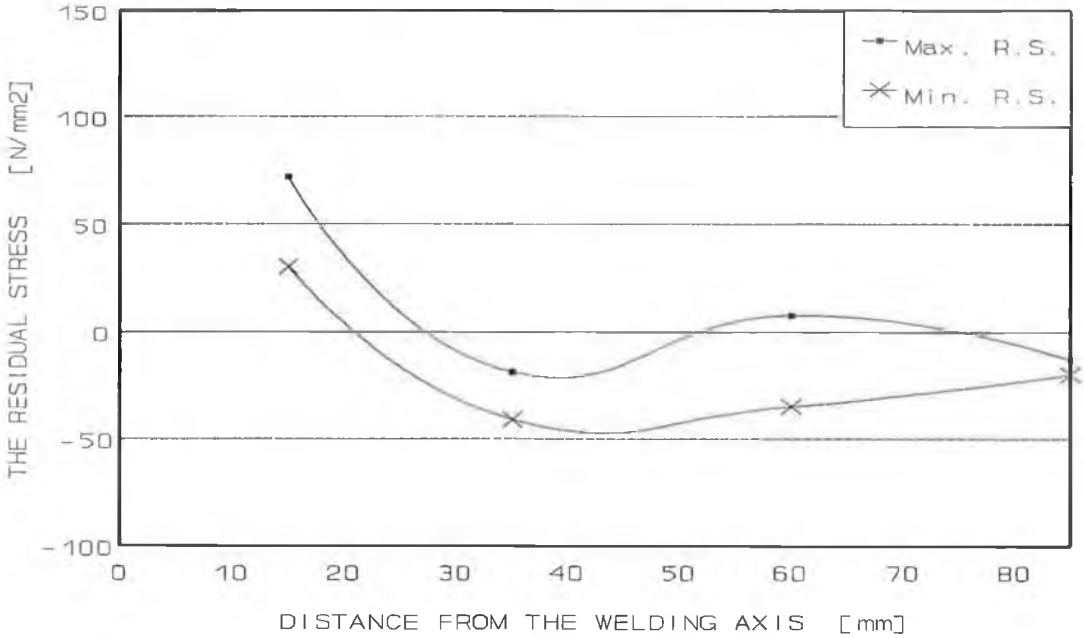

FIGURE 4.72 PRINCIPAL RESIDUAL STRESSES AFTER PWHT WITH COOLING RATE OF 10°C/h FOR AISI-410 COMPONENT.

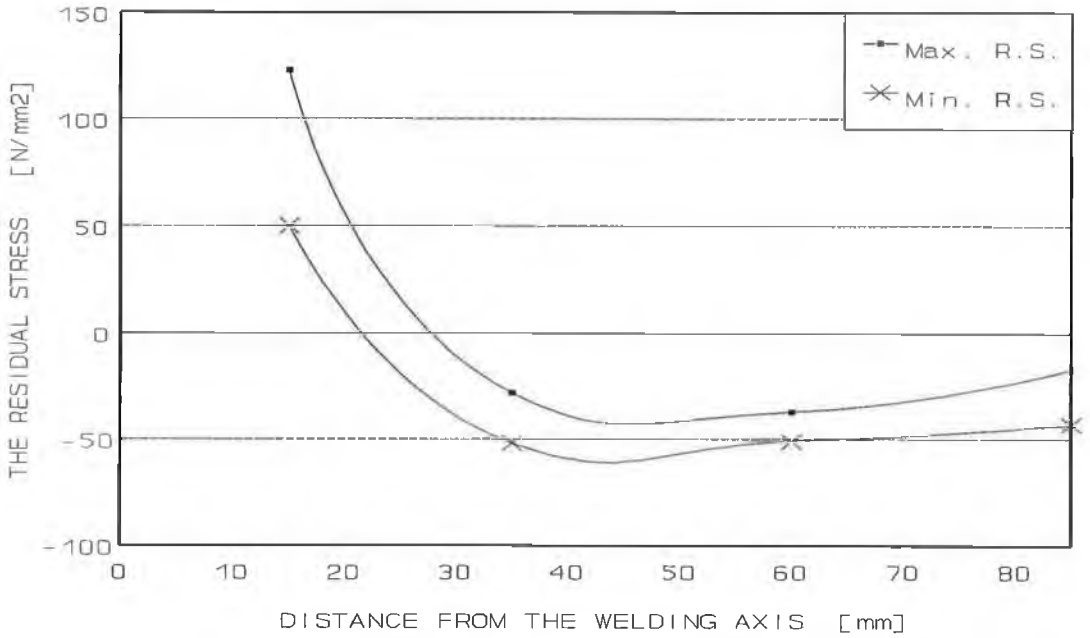

FIGURE 4.73 PRINCIPAL RESIDUAL STRESSES AFTER PWHT WITH COOLING RATE OF 125°C/h FOR AISI-410 COMPONENT.

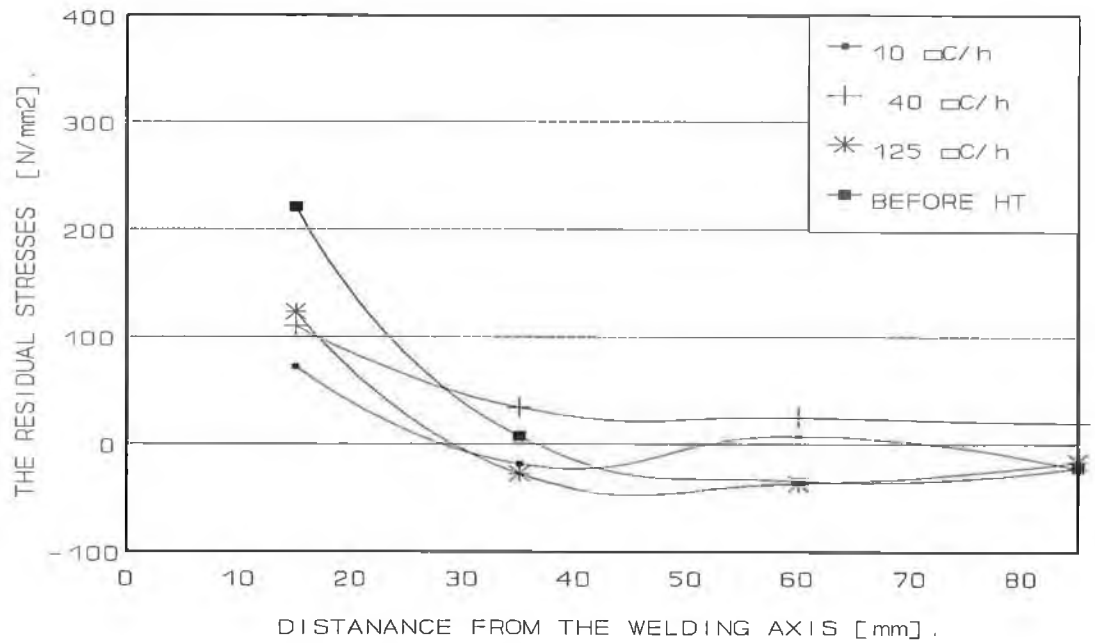

FIGURE 4.74 MAXIMUM RESIDUAL STRESSES BEFORE & AFTER PWHT WITH DIFFERENT COOLING RATES FOR AISI-410 COMPONENT.

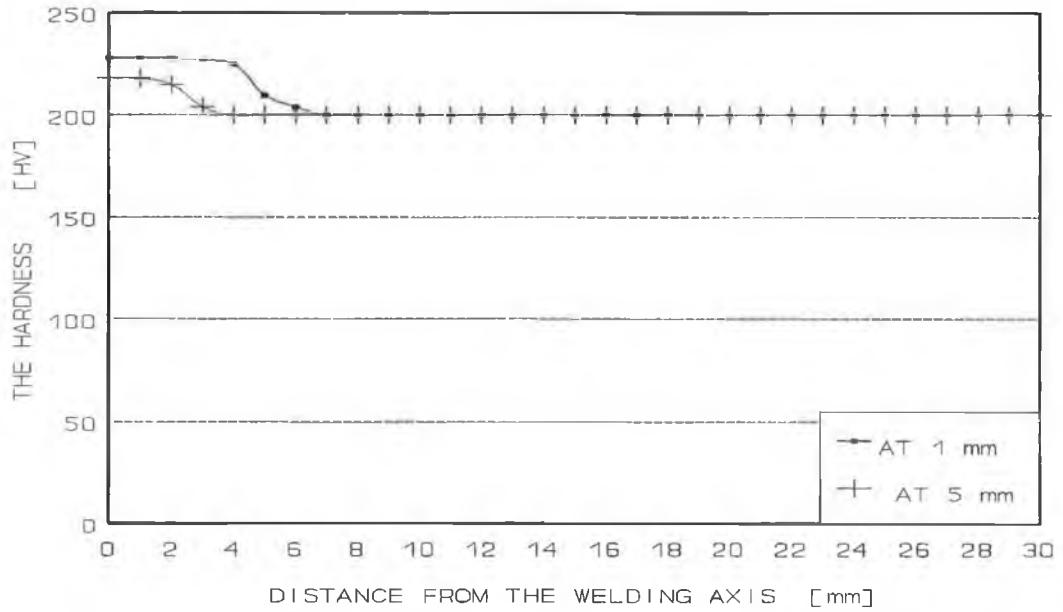

FIGURE 4.75 HARDNESS VARIATION AFTER PWHT A1 (OPTIMIZATION) FOR AISI-1020 WELDED COMPONENT.

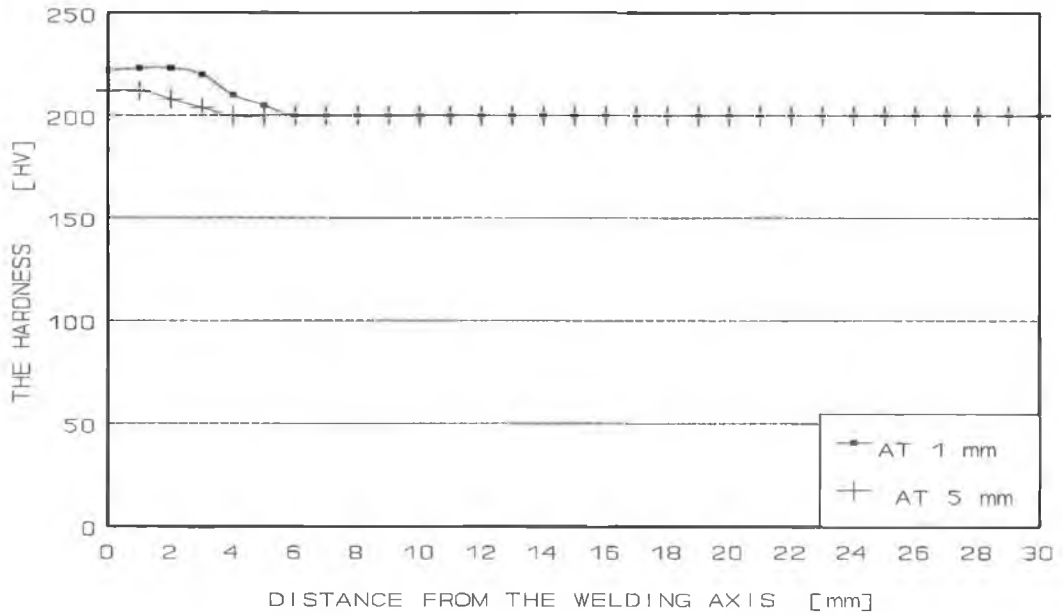

FIGURE 4.76 HARDNESS VARIATION AFTER PWHT A2 (OPTIMIZATION) FOR AISI-1020 WELDED COMPONENT.

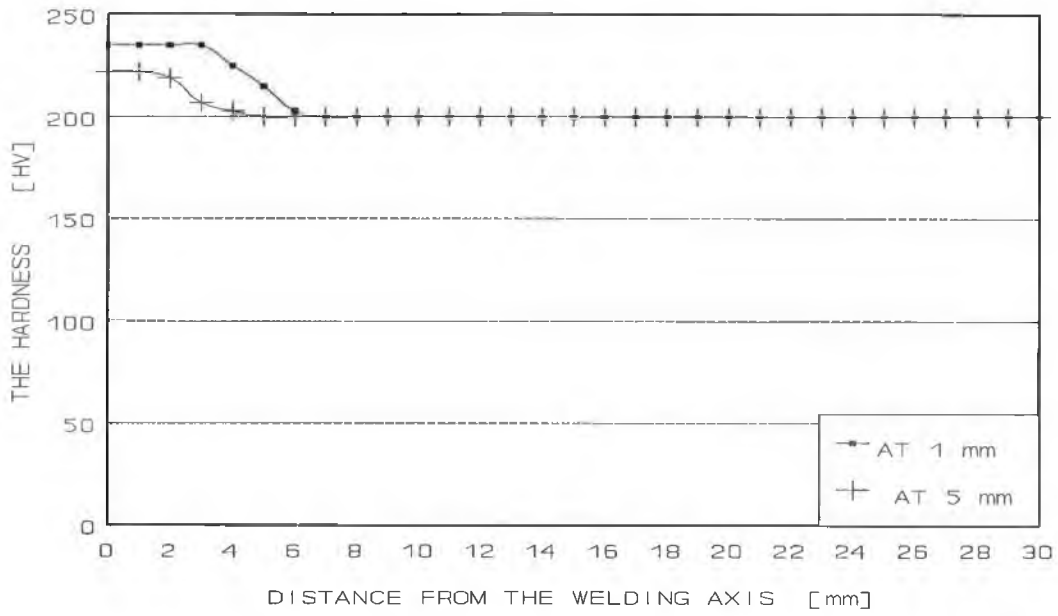

FIGURE 4.77 HARDNESS VARIATION AFTER PWHT A3 (OPTIMIZATION) FOR AISI-1020 WELDED COMPONENT.

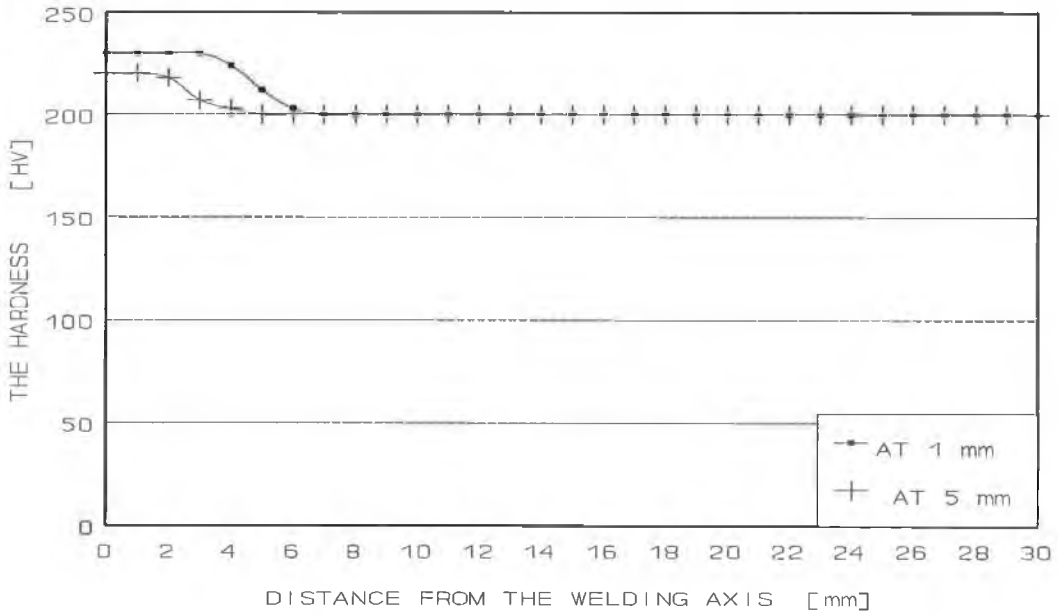

FIGURE 4.78 HARDNESS VARIATION AFTER PWHT A4 (OPTIMIZATION) FOR AISI-1020 WELDED COMPONENT.

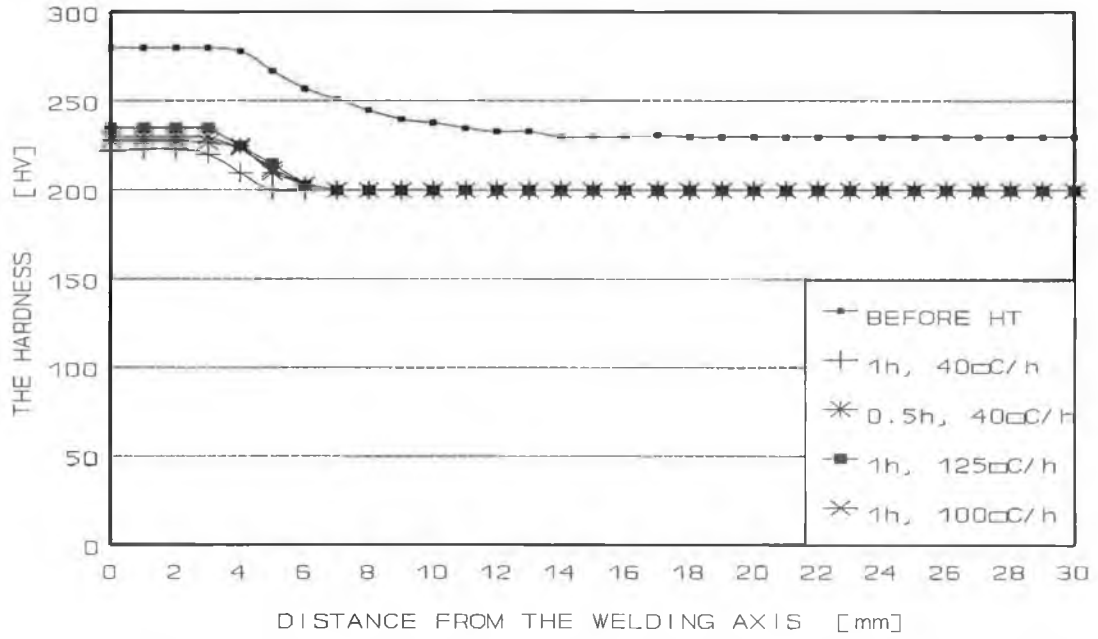

FIGURE 4.79 HARDNESS VARIATION AT THE DEPTH OF 1 mm, (OPTIMIZATION) FOR AISI-1020 WELDED COMPONENT.

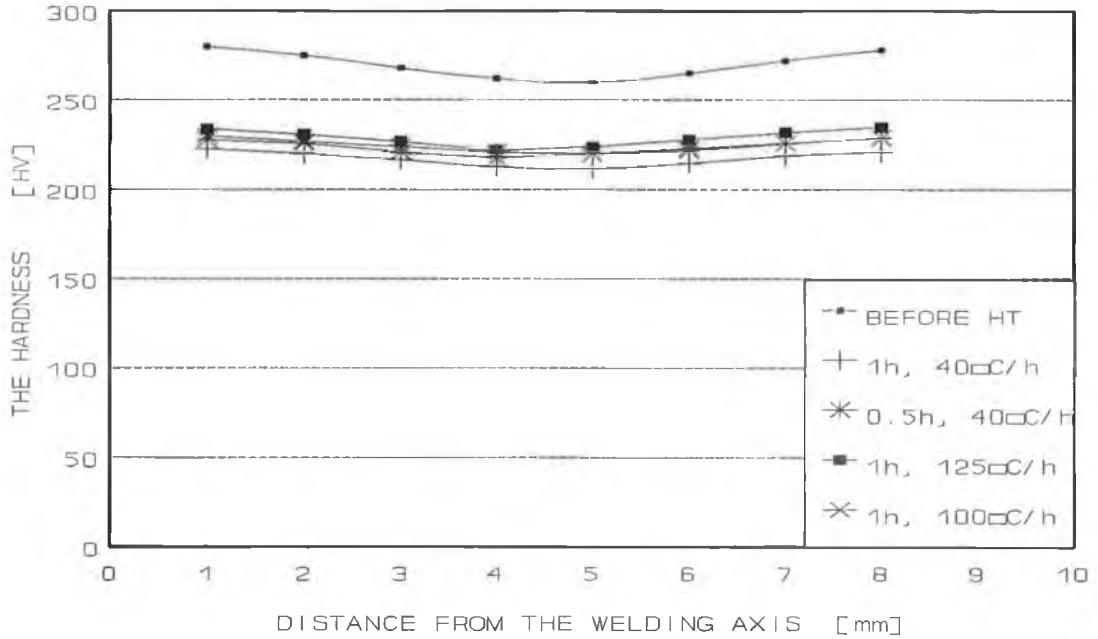

FIGURE 4.80 HARDNESS VARIATION IN THE DEPTH, (OPTIMIZATION) FOR AISI-1020 WELDED COMPONENT.

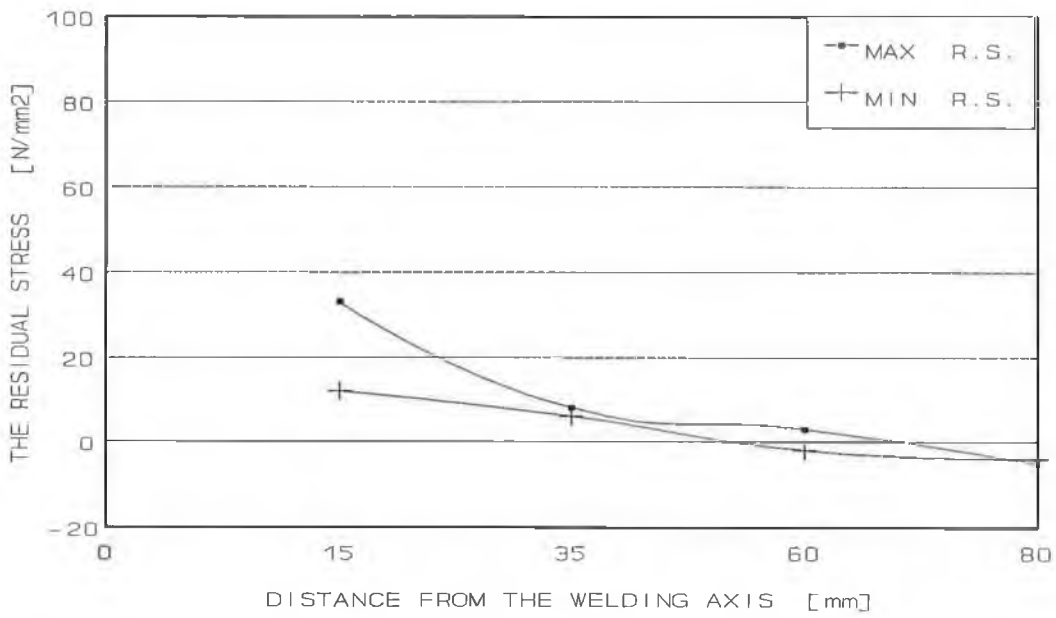

FIGURE 4.81 PRINCIPAL RESIDUAL STRESS AFTER PWHT A1 (OPTIMIZATION) FOR AISI-1020 WELDED COMPONENT.

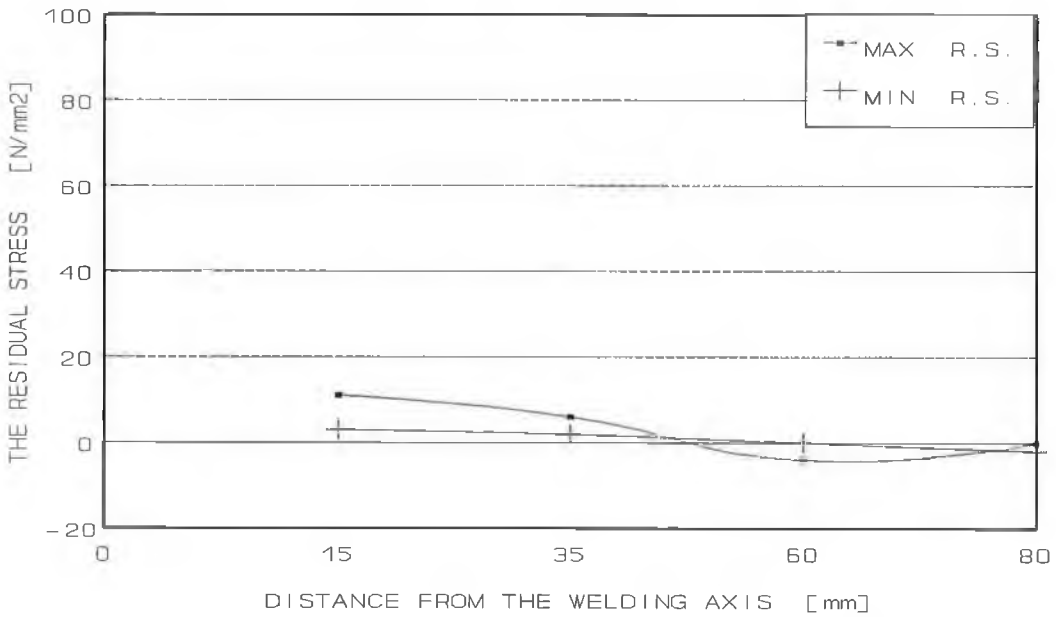

FIGURE 4.82 PRINCIPAL RESIDUAL STRESS AFTER PWHT A2 (OPTIMIZATION) FOR AISI-1020 WELDED COMPONENT.

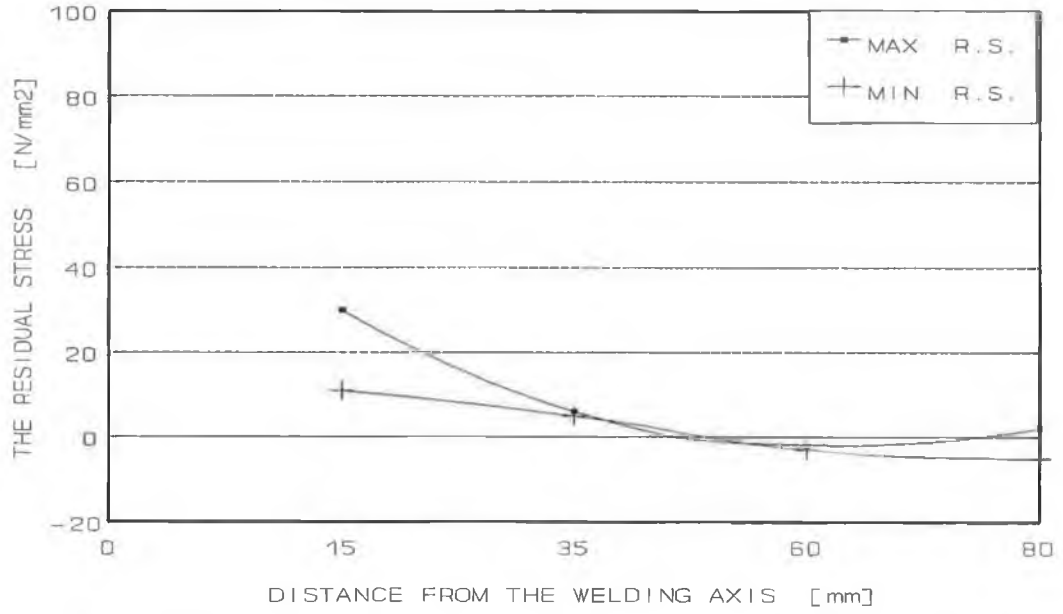

FIGURE 4.83 PRINCIPAL RESIDUAL STRESS AFTER PWHT A3 (OPTIMIZATION) FOR AISI-1020 WELDED COMPONENT.

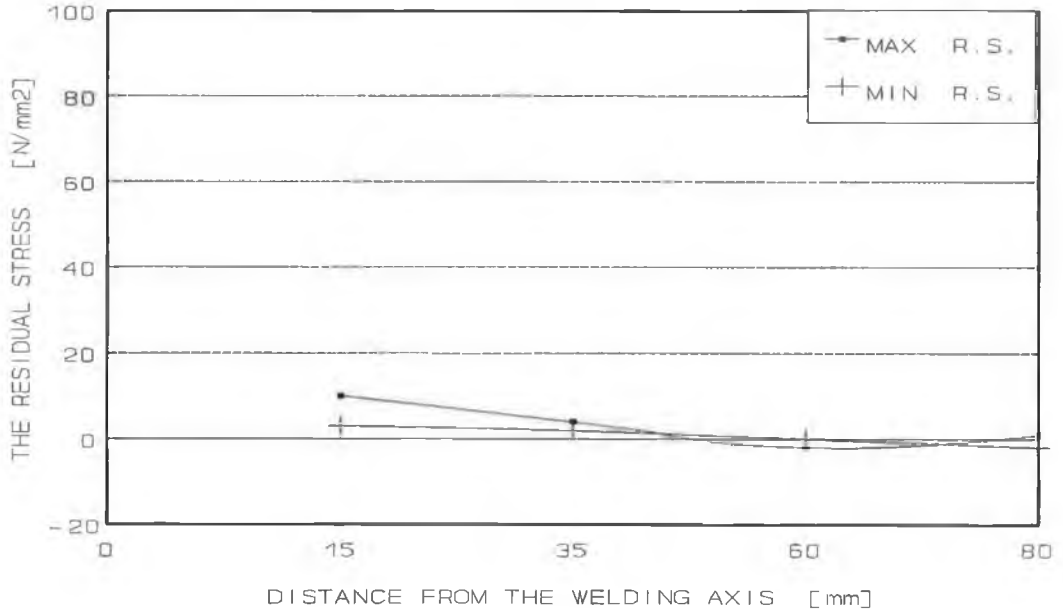

FIGURE 4.84 PRINCIPAL RESIDUAL STRESS AFTER PWHT A4 (OPTIMIZATION) FOR AISI-1020 WELDED COMPONENT.

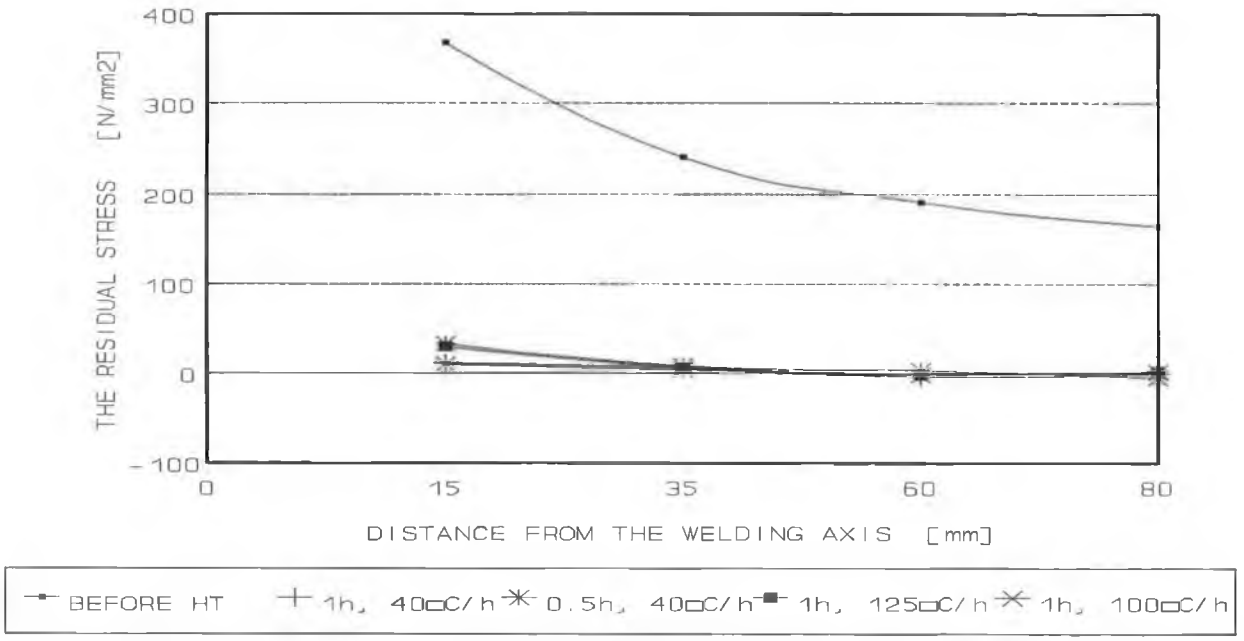

FIGURE 4.85 MAXIMUM RESIDUAL STRESS BEFORE AND AFTER PWHTS (OPTIMIZATION) FOR AISI-1020 WELDED COMPONENT.

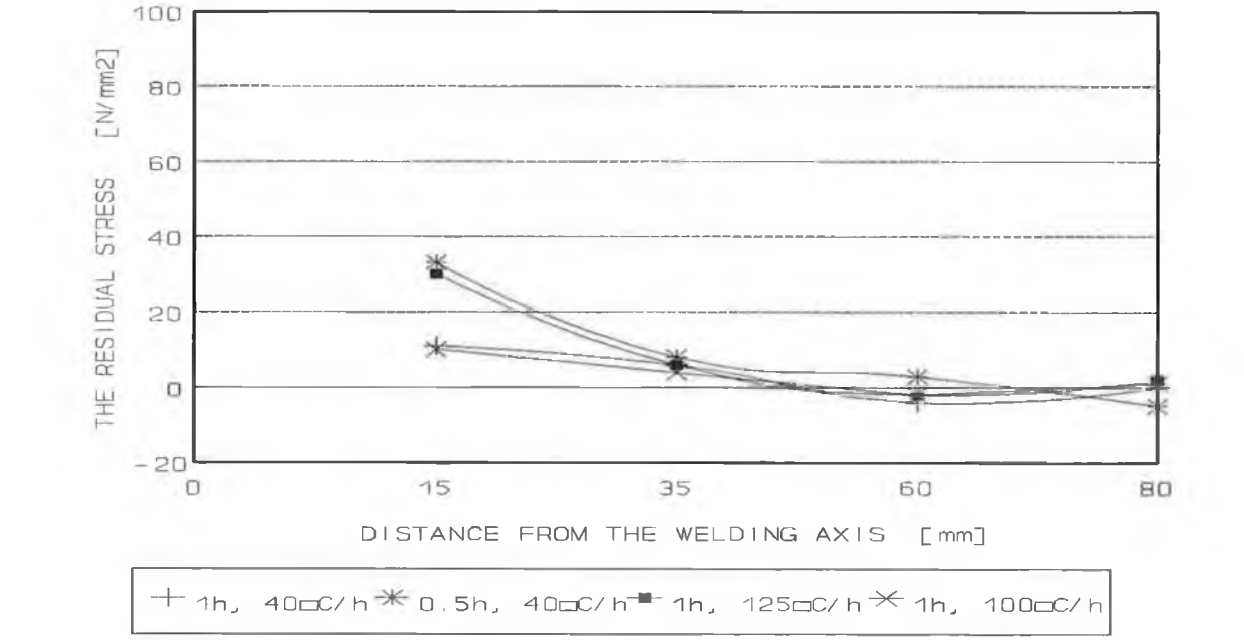

FIGURE 4.86 MAXIMUM RESIDUAL STRESS AFTER PWHTS (OPTIMIZATION) FOR AISI-1020 WELDED COMPONENT.

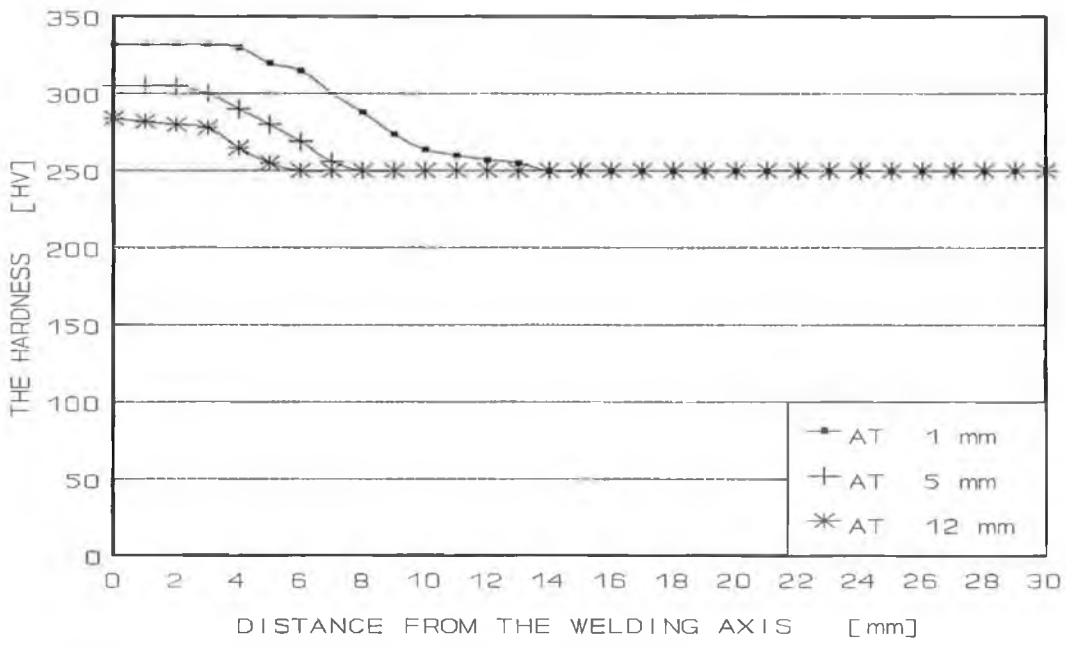

FIGURE 4.87 HARDNESS VARIATION AFTER PWHT B1 (OPTIMIZATION) FOR AISI-410 WELDED COMPONENT.

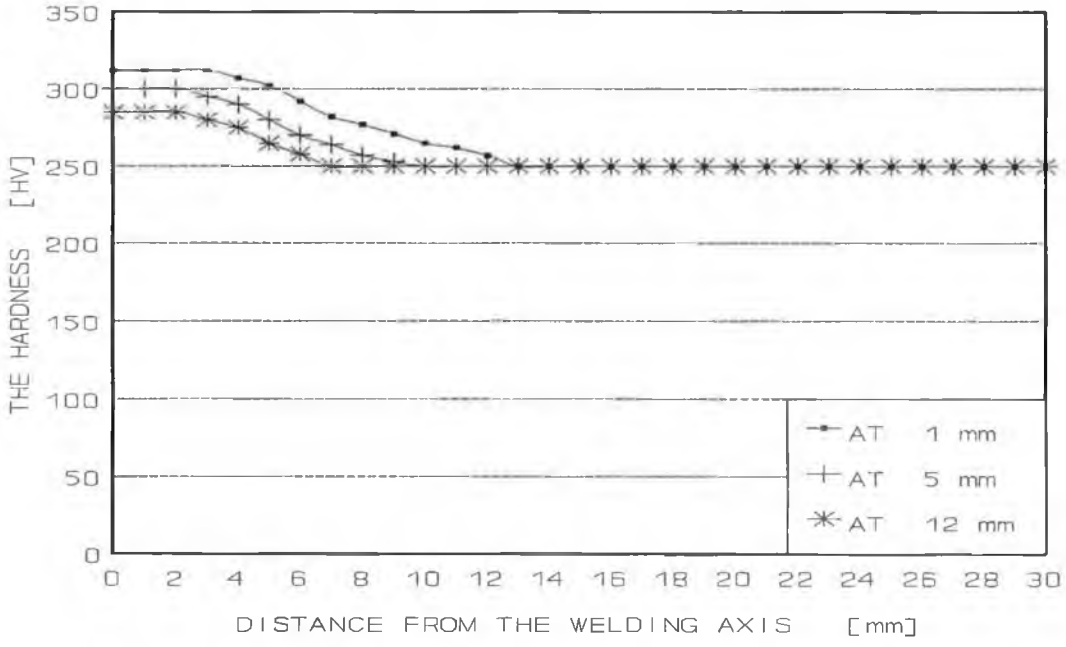

FIGURE 4.88 HARDNESS VARIATION AFTER PWHT B2 (OPTIMIZATION) FOR AISI-410 WELDED COMPONENT.

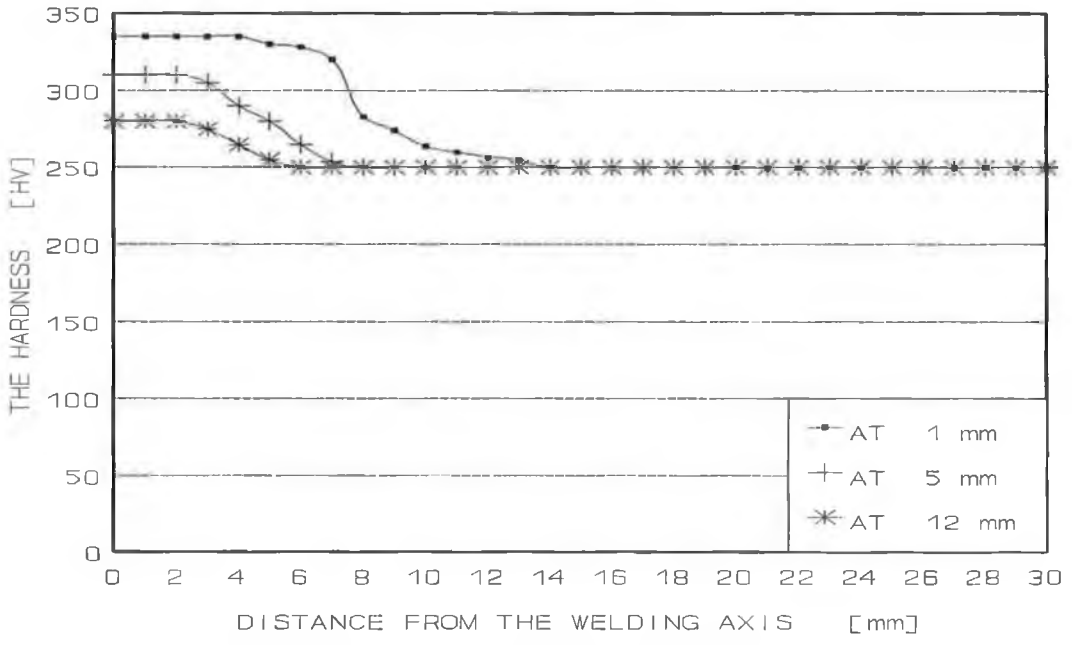

FIGURE 4.89 HARDNESS VARIATION AFTER PWHT B3 (OPTIMIZATION) FOR AISI-410 WELDED COMPONENT.

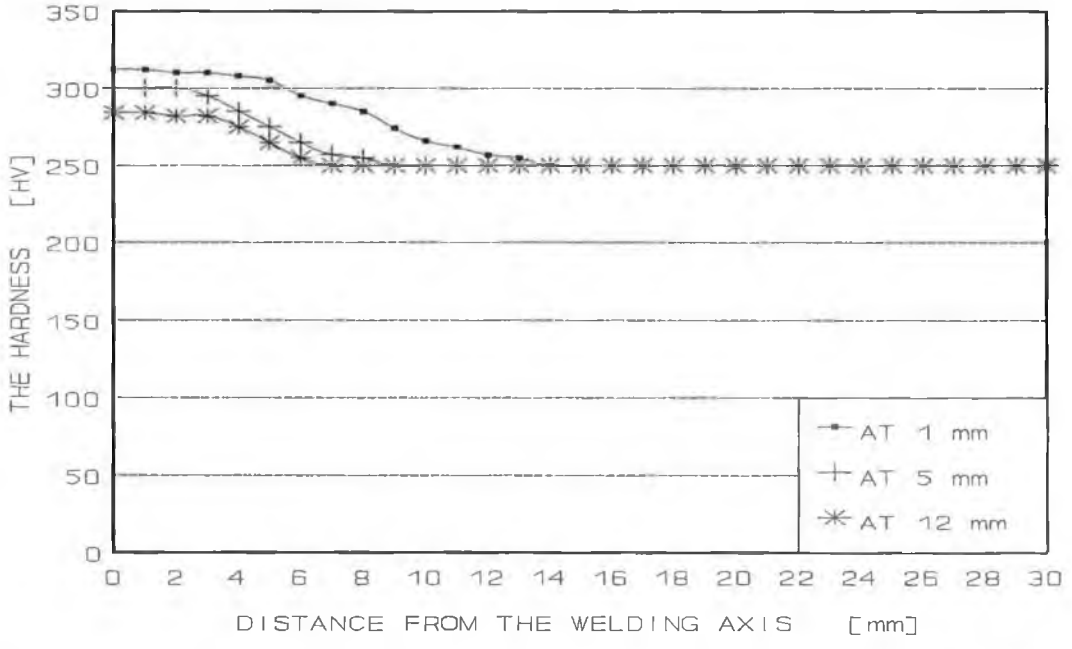

FIGURE 4.90 HARDNESS VARIATION AFTER PWHT B4 (OPTIMIZATION) FOR AISI-410 WELDED COMPONENT.

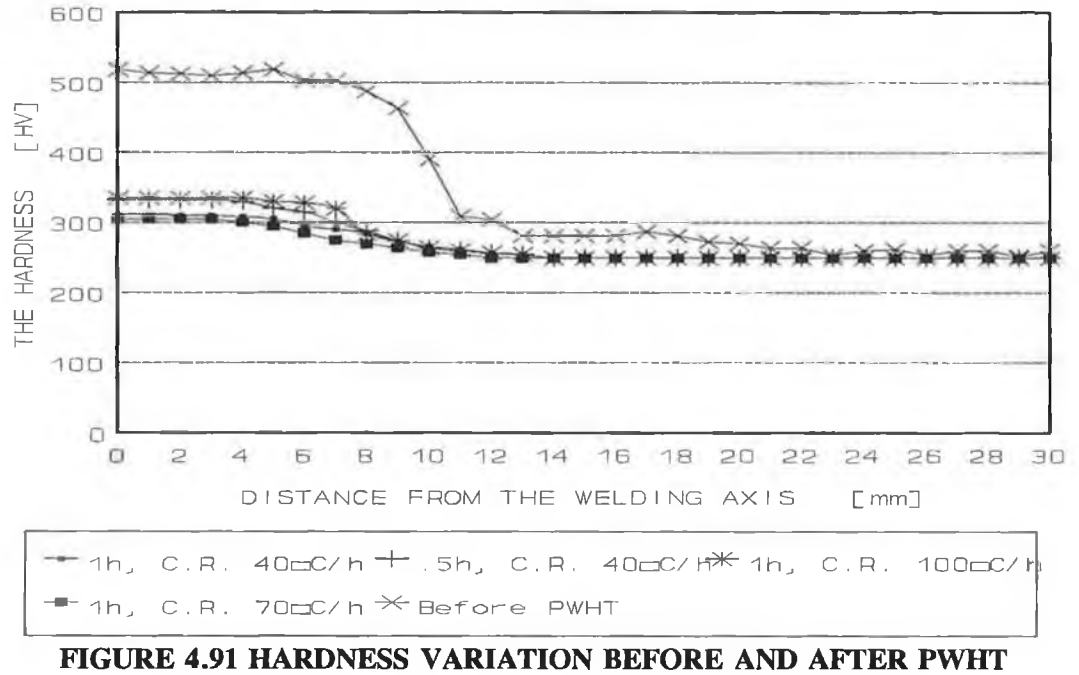

FIGURE 4.91 HARDNESS VARIATION BEFORE AND AFTER PWHT (OPTIMIZATION)FOR AISI-410 WELDED COMPONENT.

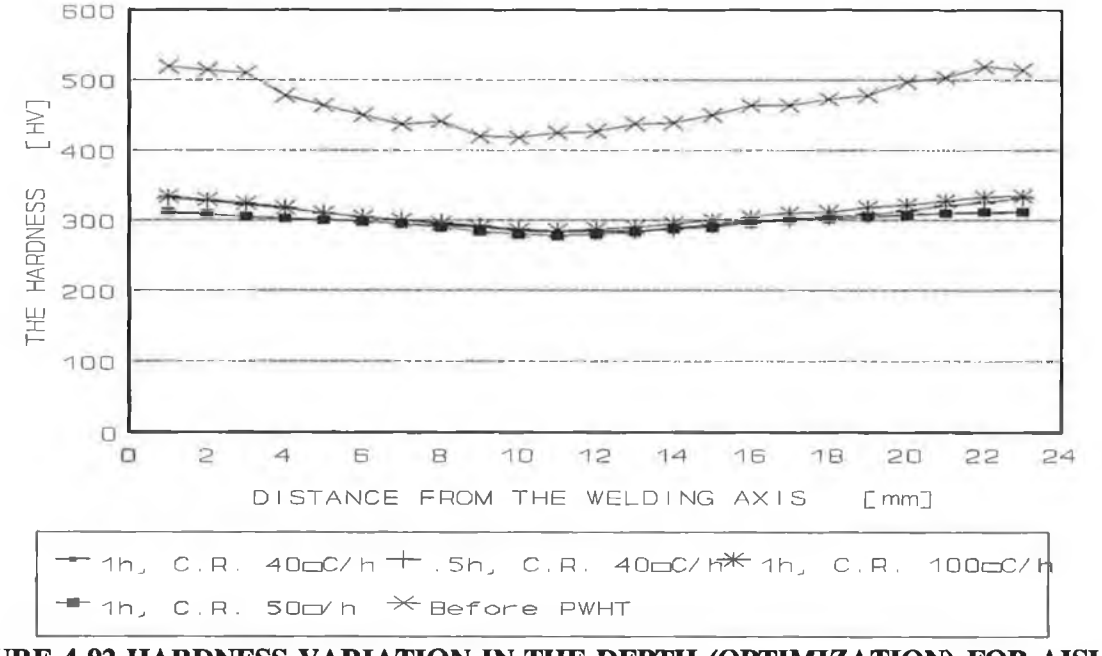

FIGURE 4.92 HARDNESS VARIATION IN THE DEPTH (OPTIMIZATION) FOR AISI-410 WELDED COMPONENT.

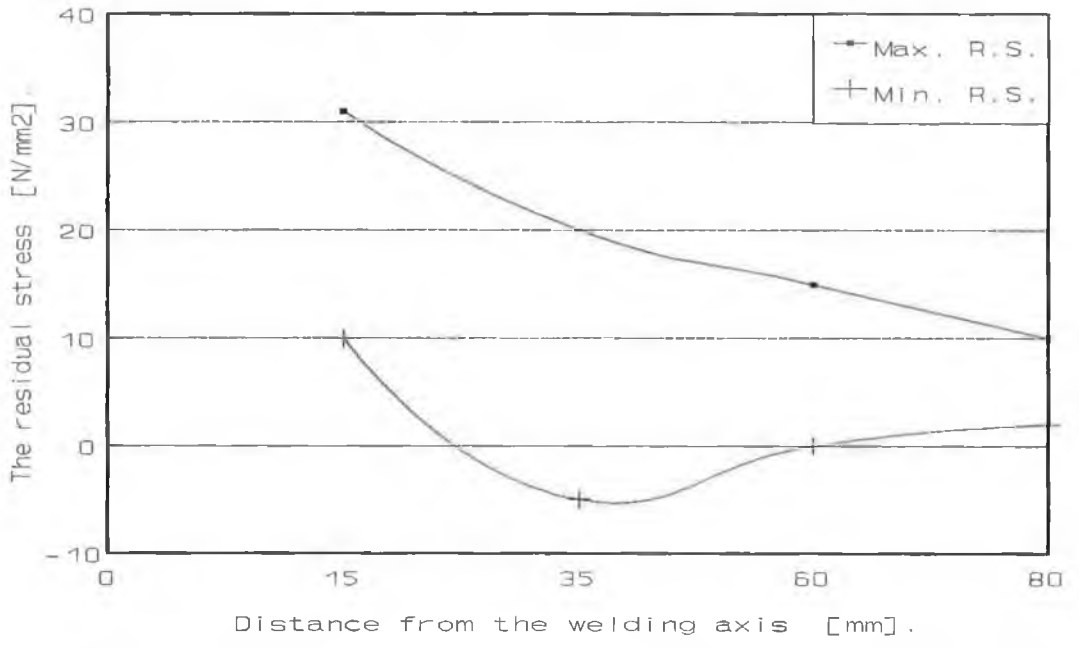

FIGURE 4.93 PRINCIPAL RESIDUAL STRESS AFTER PWHT B1 (OPTIMIZATION) FOR AISI-410 WELDED COMPONENT.

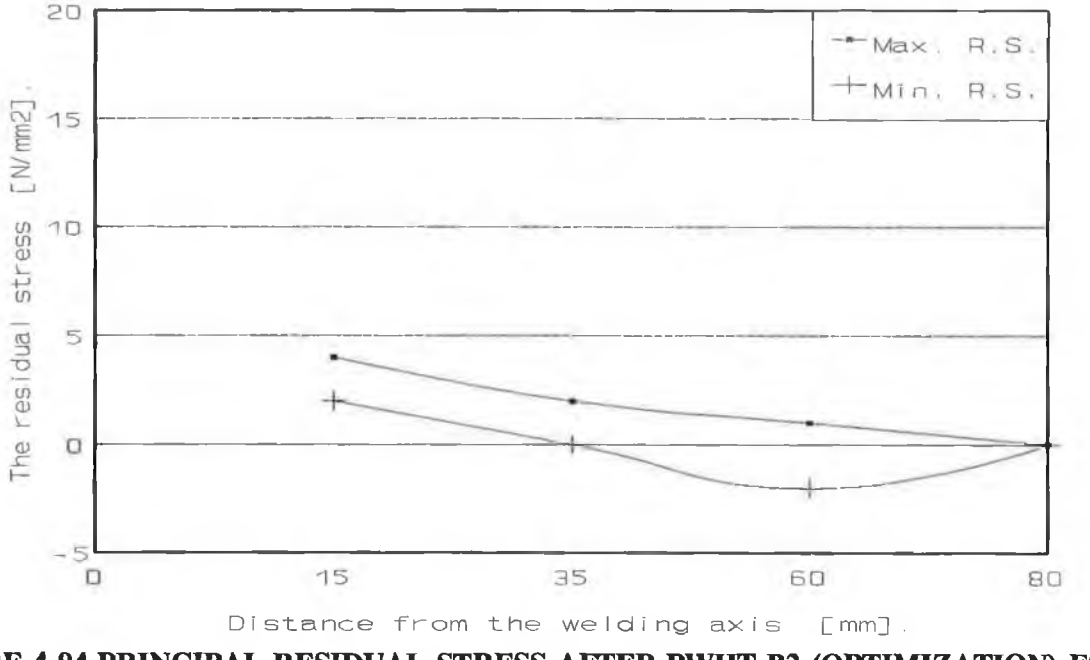

FIGURE 4.94 PRINCIPAL RESIDUAL STRESS AFTER PWHT B2 (OPTIMIZATION) FOR AISI-410 WELDED COMPONENT.

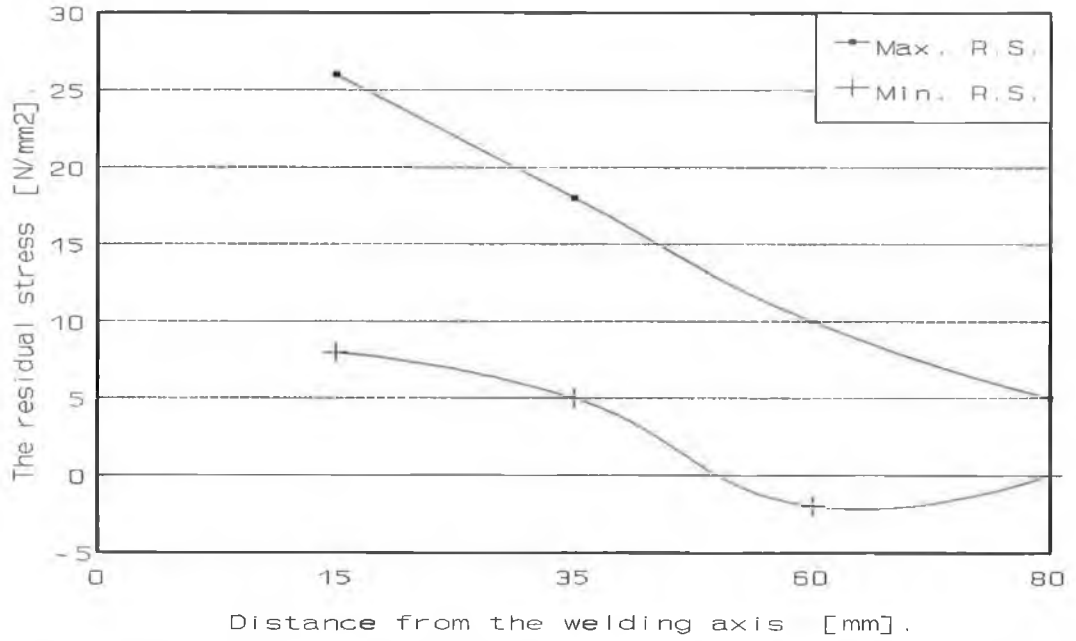

FIGURE 4.95 PRINCIPAL RESIDUAL STRESS AFTER PWHT B3 (OPTIMIZATION) FOR AISI-410 WELDED COMPONENT.

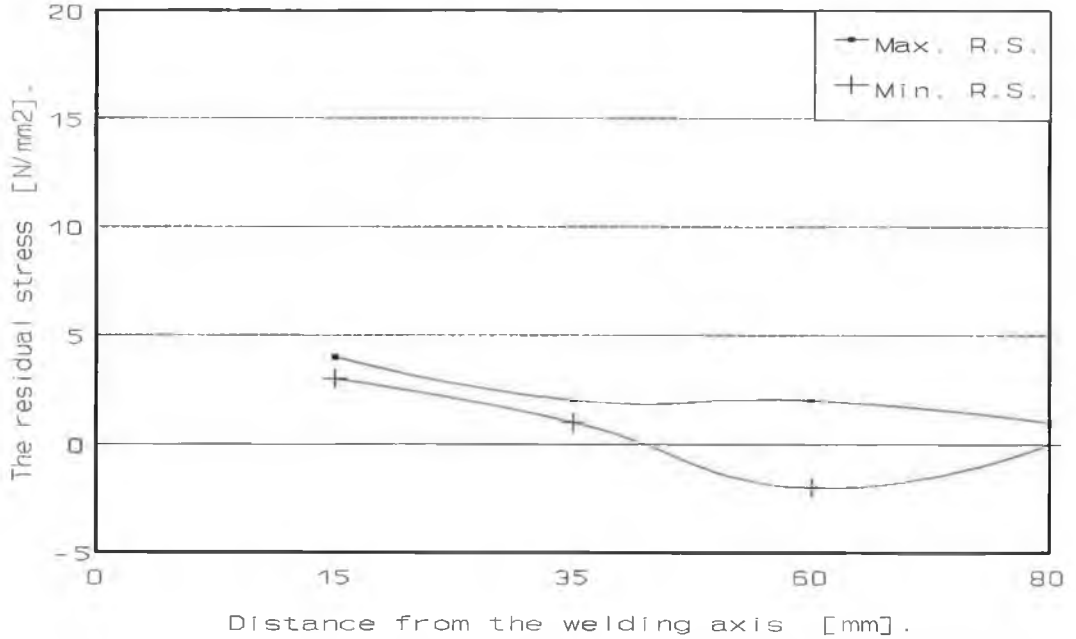

FIGURE 4.96 PRINCIPAL RESIDUAL STRESS AFTER PWHT B4 (OPTIMIZATION) FOR AISI-410 WELDED COMPONENT.

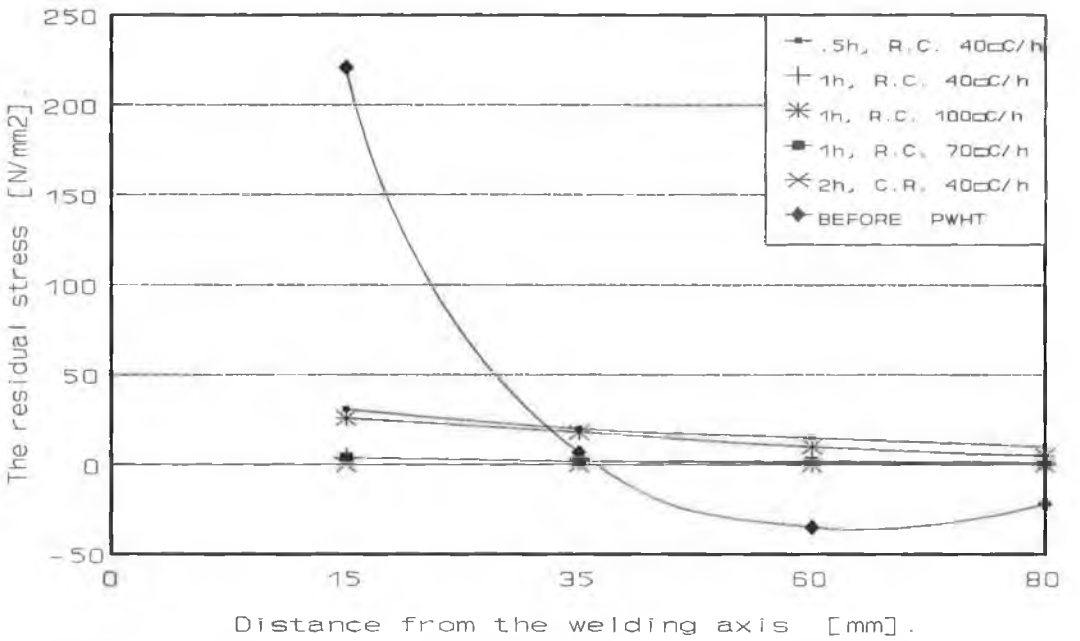

FIGURE 4.97 MAXIMUM RESIDUAL STRESS BEFORE AND AFTER PWHT (OPTIMIZATION) FOR AISI-410 WELDED COMPONENT.

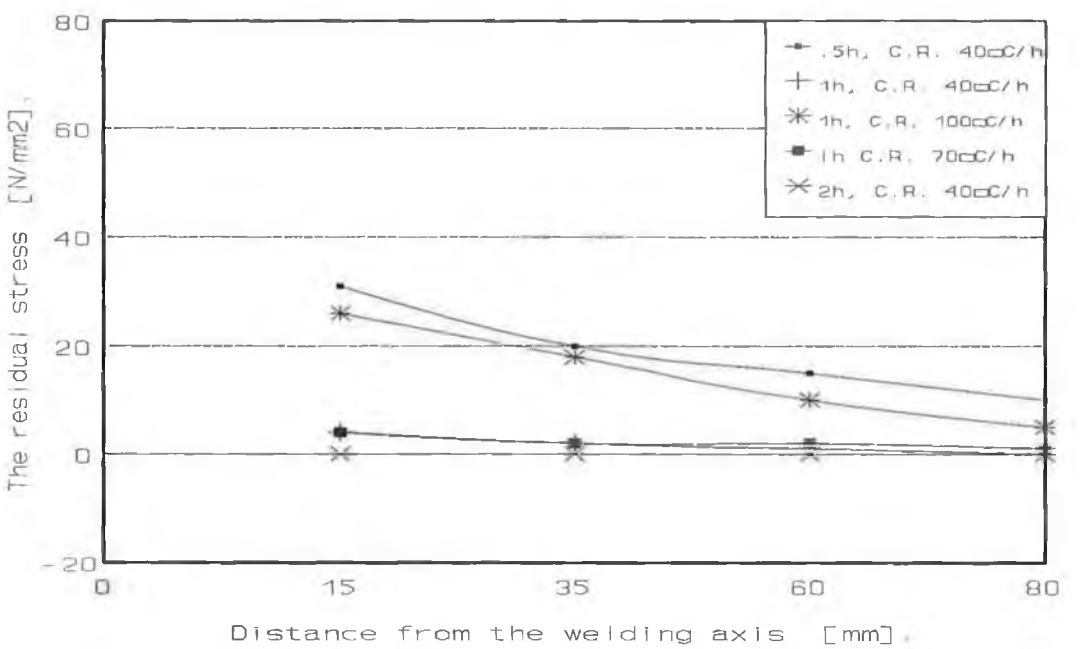

FIGURE 4.98 MAXIMUM RESIDUAL STRESS AFTER PWHTS (OPTIMIZATION) FOR AISI-410 WELDED COMPONENT.

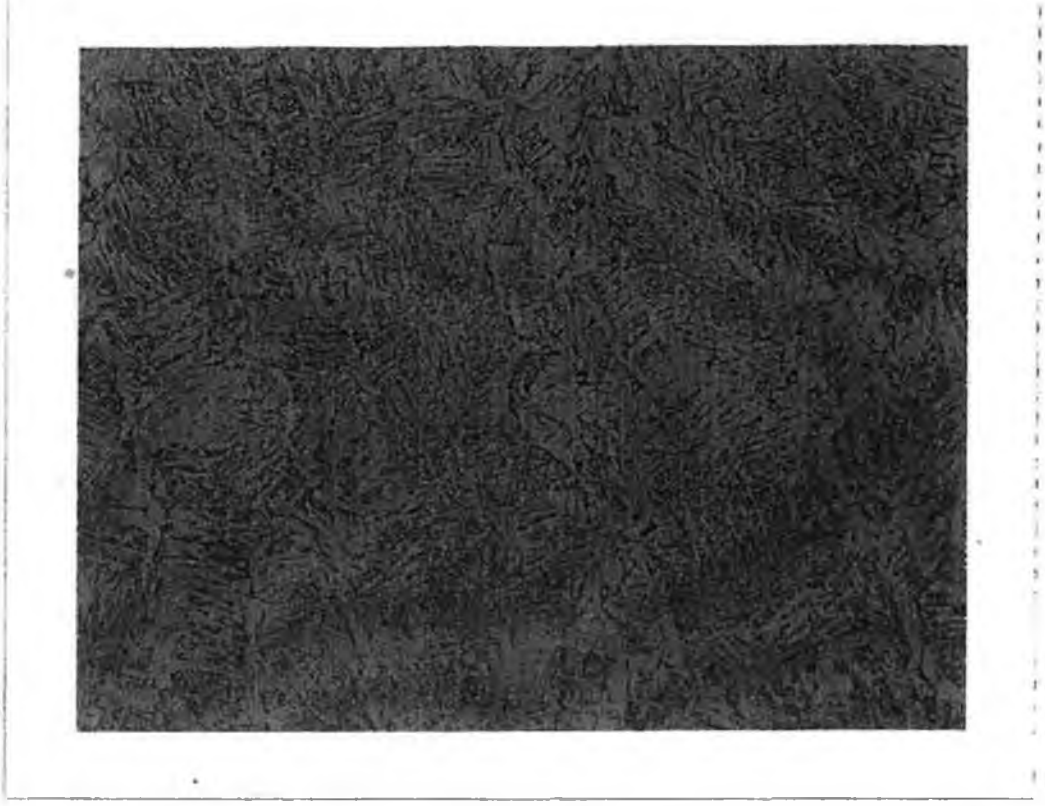

PLATE 4.1 THE MICROSTRUCTURE OF THE WELDING ZONE BEFORE PWHT FOR AISI-1020 WELDED COMPONENT, X500.

PLATE 4.2 THE MICROSTRUCTURE OF THE BASE METAL BEFORE PWHT FOR AISI-1020 WELDED COMPONENT, X500.

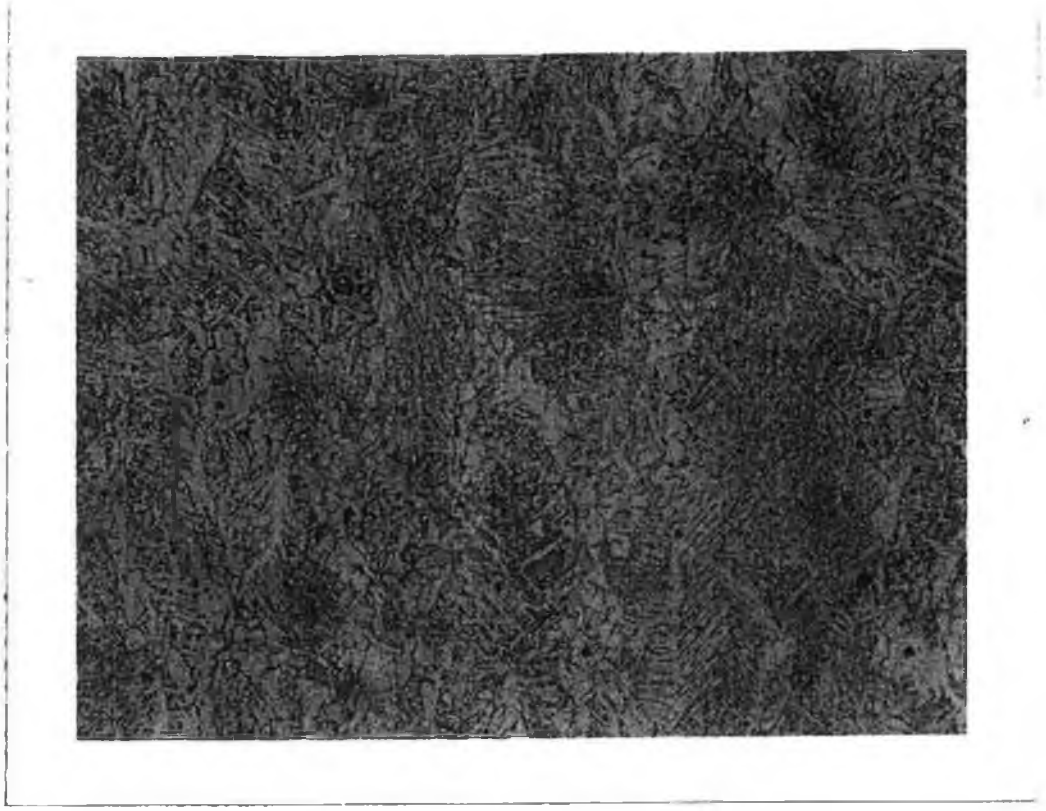

PLATE 4.3 THE MICROSTRUCTURE OF THE WELDING ZONE AFTER PWHT, SOAKING TEMP. OF 450°C FOR AISI-1020 WELDED COMPONENT, X500.

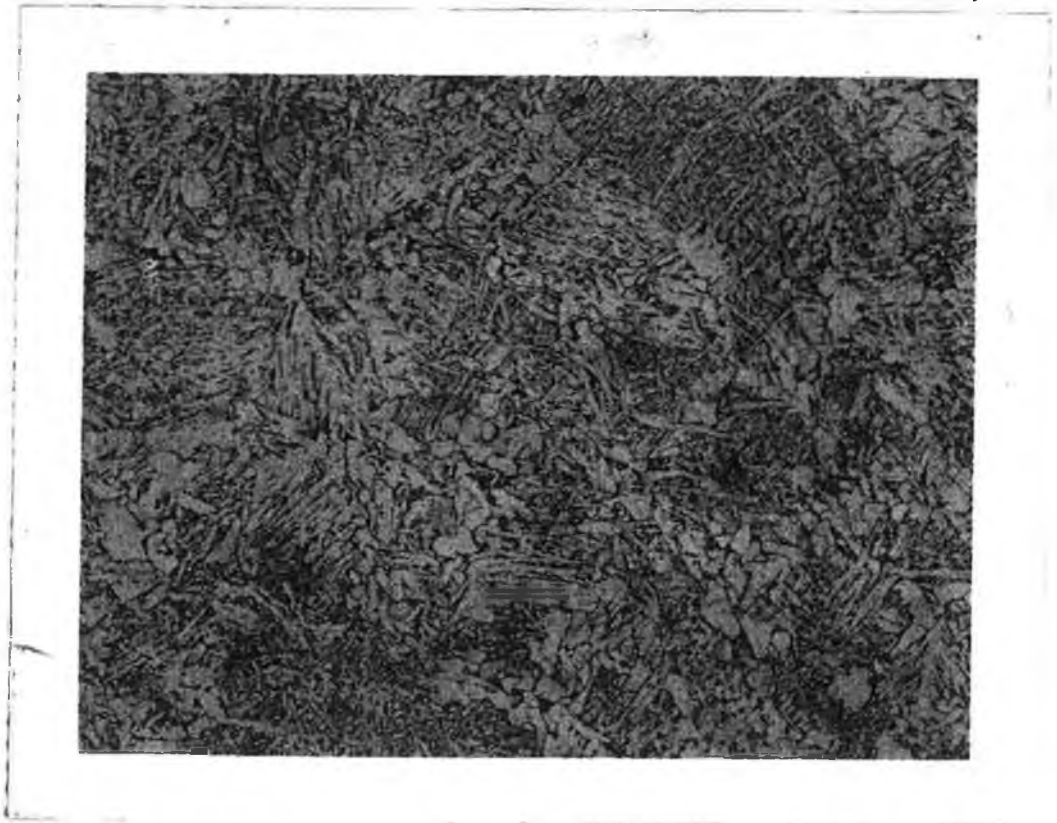

PLATE 4.4 THE MICROSTRUCTURE OF THE WELDING ZONE AFTER PWHT, SOAKING TEMP. OF 550°C FOR AISI-1020 WELDED COMPONENT, X500.

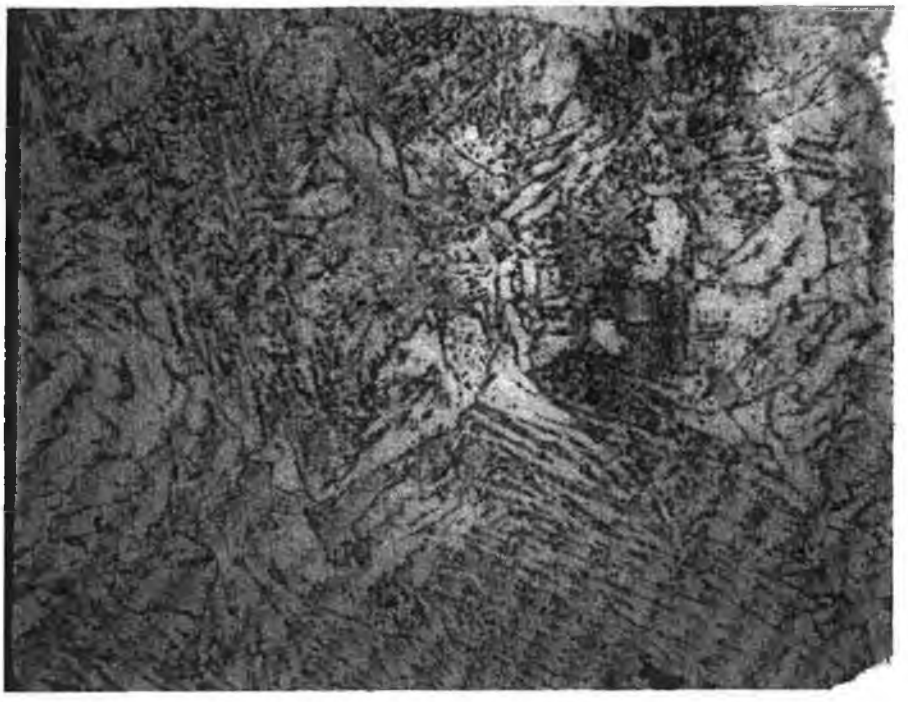

PLATE 4.5 THE MICROSTRUCTURE OF THE WELDING ZONE AFTER PWHT, SOAKING TEMP. OF 650°C FOR AISI-1020 WELDED COMPONENT, X500.

PLATE 4.6 THE MICROSTRUCTURE OF THE WELDING ZONE AFTER PWHT (TIME DURATION OF 10 h) FOR AISI-1020 WELDED COMPONENT, X500.

PLATE 4.7 THE MICROSTRUCTURE OF THE WELDING ZONE BEFORE PWHT FOR AISI-410 WELDED COMPONENT, X500.

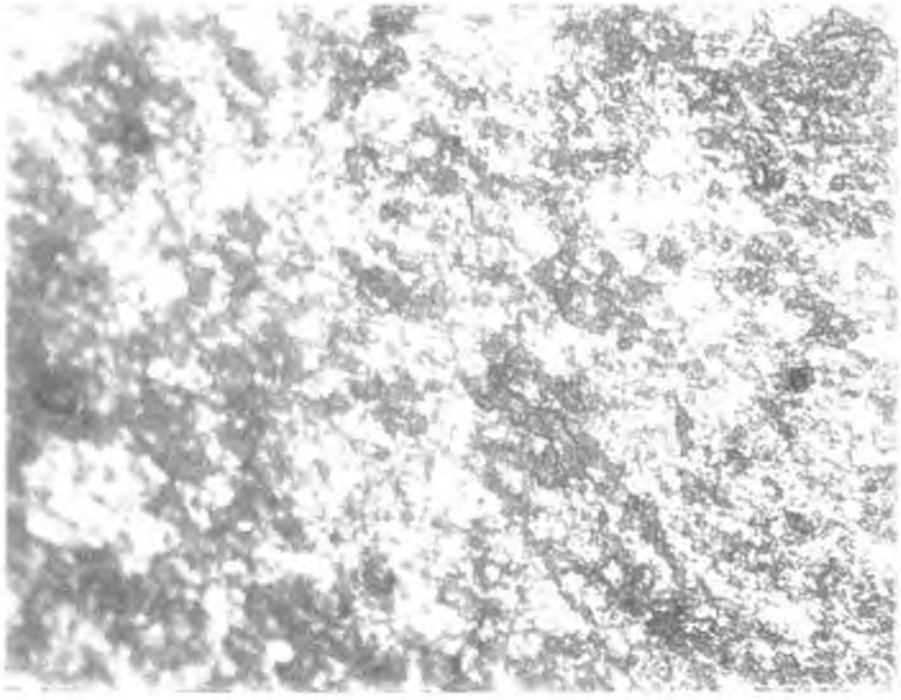

PLATE 4.8 THE MICROSTRUCTURE OF THE WELDING ZONE AFTER PWHT, SOAKING TEMP. OF 550°C FOR AISI-410 WELDED COMPONENT, X500.

PLATE 4.9 THE MICROSTRUCTURE OF THE WELDING ZONE AFTER PWHT, SOAKING TEMP. OF 650°C FOR AISI-410 WELDED COMPONENT, X500.

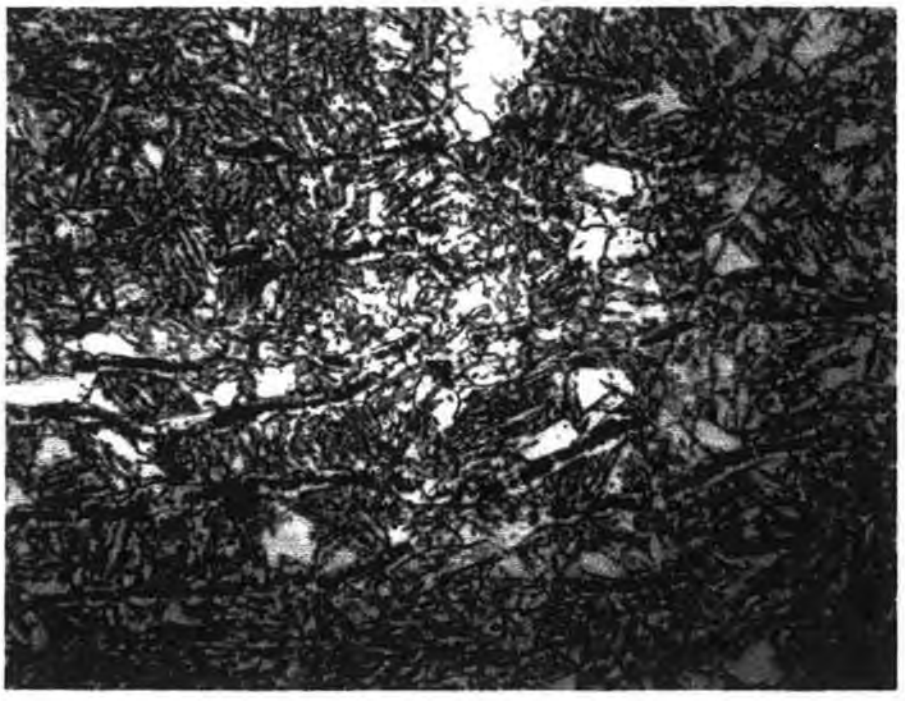

PLATE 4.10 THE MICROSTRUCTURE OF THE WELDING ZONE AFTER PWHT, SOAKING TEMP. OF 750°C FOR AISI-410 WELDED COMPONENT, X500.

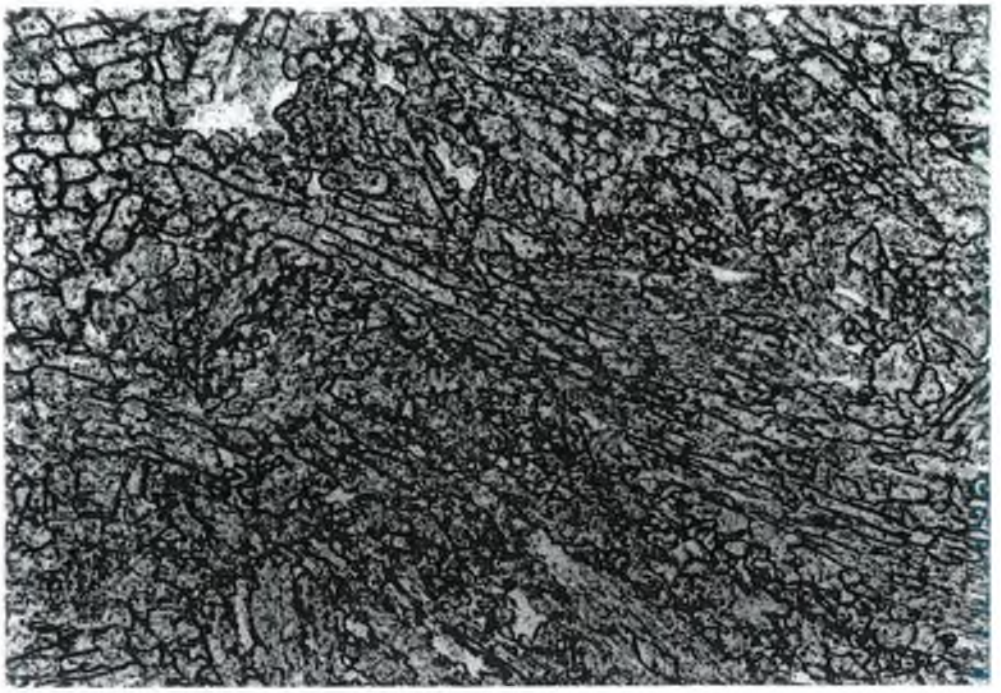

PLATE 4.11 THE MICROSTRUCTURE OF THE WELDING ZONE AFTER PWHT (COOLING RATE OF 10 °C/h) FOR AISI-410 WELDED COMPONENT, X500.

PLATE 4.12 THE RESIDUAL STRESSES MEASUREMENT POINTS ON THE WELDED COMPONENT.

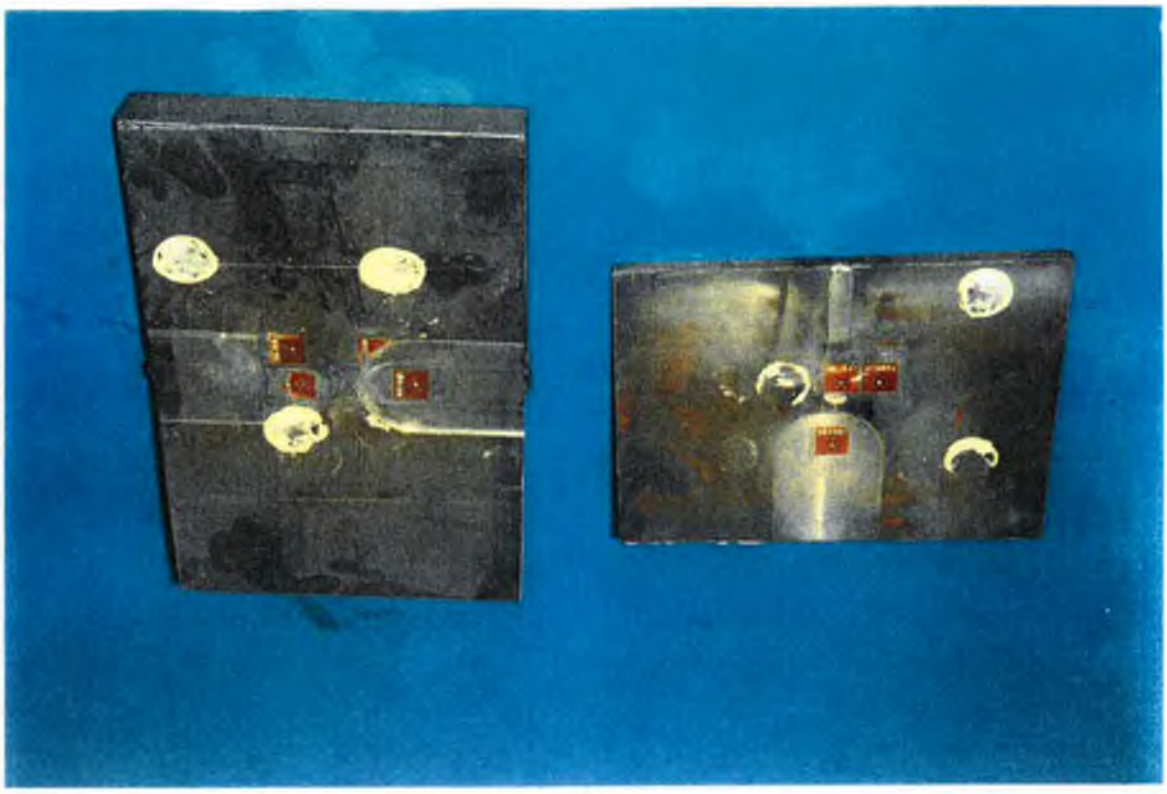

PLATE 4.13 THE WELDING SPECIMEN AFTER MACHINING THE WELDING ZONE TO MEASURE THE RESIDUAL STRESSES.

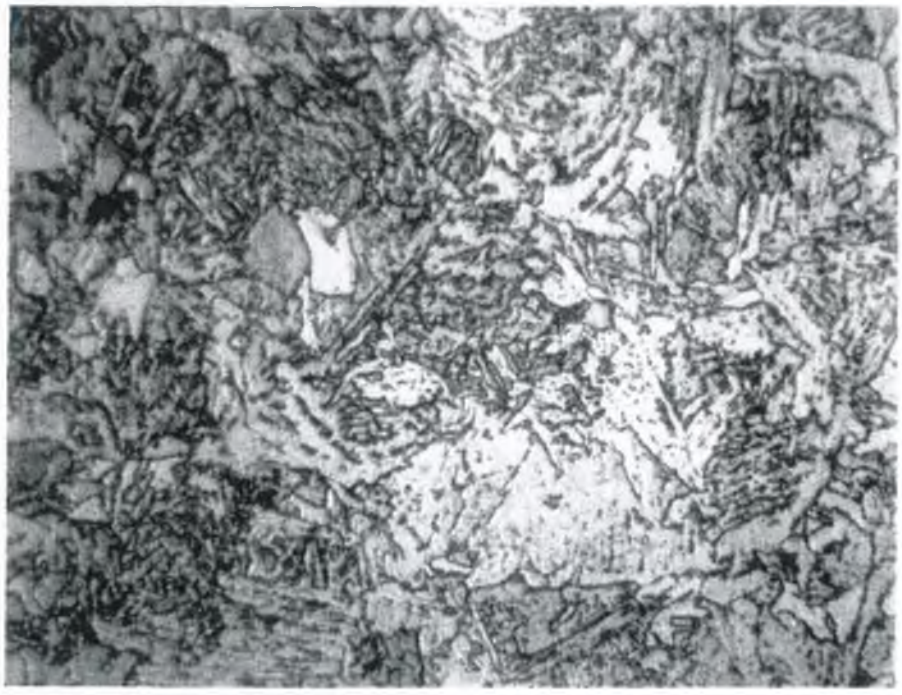

PLATE 4.14 THE MICROSTRUCTURE OF THE WELDING ZONE AFTER PWHT A2 (OPTIMIZATION) FOR AISI-1020 WELDED COMPONENT, X500.

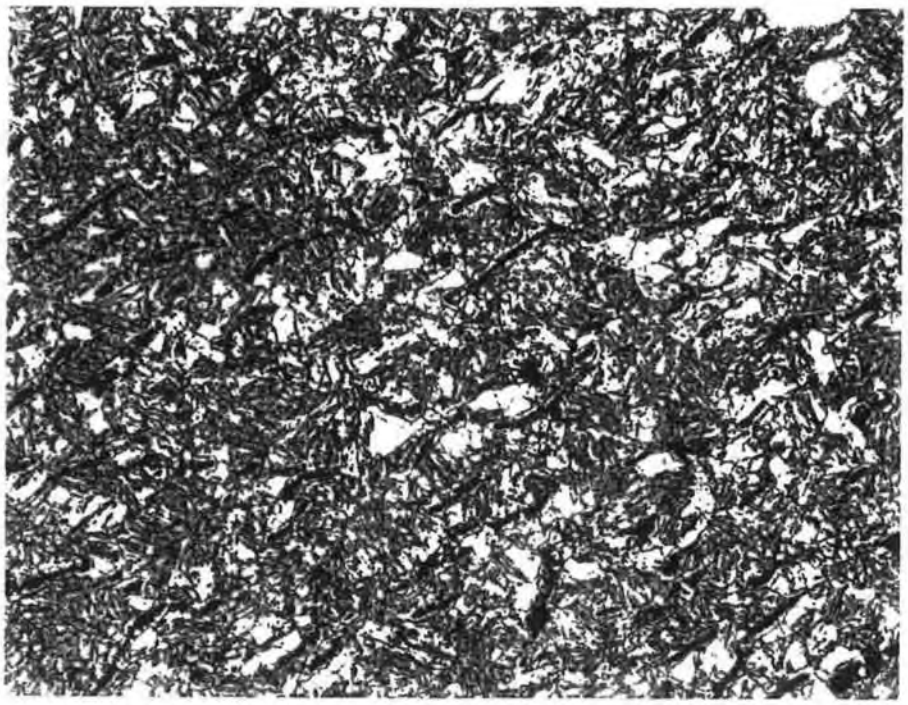

PLATE 4.15 THE MICROSTRUCTURE OF THE WELDING ZONE AFTER PWHT B2 (OPTIMIZATION) FOR AISI-410 WELDED COMPONENT, X500.

CHAPTER FIVE

FINITE ELEMENT MODELLING FOR AISI-410 COMPONENT

5.1 INTRODUCTION

It is evident from the previously described results that a sharp difference in the microstructure has resulted in the stainless steel welded component due to the welding process and the composition of this steel. It can also be noticed that a considerable difference between the HAZ and the base metal has existed in the structure of this welded component. The structure of this joint has been totally varied, between martensite in the HAZ and tempered martensite, ferrite and precipitate carbide in the base metal. It is also evident from the hardness test results that there is a substantial difference in the hardness value between these two zones (the HAZ and the base metal). This substantial difference in the microstructure and mechanical properties would generate a stress concentration around the HAZ [134] which could have a major defect during the service for this type of welded joint.

In this study the welded joint has been modeled to study the effect of the variation in the microstructure and the mechanical properties on the service life of this component for both before and after the application of PWHT (soaking temperature of 750 °C; heating rate of 400 °C/h; soaking duration of 1 hour and cooling rate of 70 °C/h). A number of assumptions have been made to apply the FEM on this current case. The material of this joint is considered as two different metals:

1) the HAZ.
2) the base metal.

Which have different mechanical properties.

5.2 FINITE ELEMENT METHOD

The finite element method is a numerical technique for the solution of partial derivative equations. This it does by computing the answers at discrete points in the domain (nodes) and from the set of values the solution at any point in the domain may be derived by the means of suitable interpolation functions. The nodes lie on a mesh and it is crucial that the mesh be well adapted to the physical properties of the problem. With proper meshing for the engineering structure we can get better solution for the engineering problems.

The finite element method has become a powerful tool for the numerical solution of a wide range of engineering problems. Applications range from deformation and stress analysis of automotive, aircraft, building, and bridge structures to field analysis of heat flux, fluid flow, seepage, and other flow problems. With the advances in computer technology, complex problems can be modeled with relative ease. Several alternative configurations can be tried out on a computer before the first prototype is built. In this method of analysis, a complex region defining a continuum is discretized into simple geometric shapes called finite elements. The material properties and the governing relationships are considered over these elements and expressed in terms of unknown values at element corners. An assembly process, duly considering the loading and constraints, results in a set of equations. Solution of these equations gives us the approximate behaviour of the continuum. A large number of books have been published about the theory and the application of this method, references [135-138] give a good idea about the theory of this method.

The art of finite element analysis lies in the development of a suitable model idealisation. The element discretization, or, the mesh must be neither too fine, making the preparation of data execution computer time, and interpretation of results excessively expensive, nor too coarse, rendering the accuracy of the results unacceptable. The problem is thus one of balance. To develop a suitable idealisation, some knowledge of the likely distribution of stresses or their field

equivalent is generally required. In this work, fine meshing has been generated in and around the HAZ and a coarse mesh has been generated in the base metal.

5.3 FINITE ELEMENT PACKAGE LUSAS 10.3

The finite element software used in this study is a package from Finite Element Analysis UK Limited, named LUSAS [139]. LUSAS is a general purpose finite element analysis software code which incorporates facilities for linear and non-linear static and dynamic analysis, natural frequency analysis, buckling analysis, spectral response analysis, harmonic response analysis, Fourier analysis, steady state field analysis, transient field analysis and coupled thermo-mechanical analysis. A range of linear and non-linear constitutive models are available, covering most commonly used engineering materials. The constitutive models included linear isotropic, linear orthotropic/anisotropic elasto-plastic with strain hardening, nonlinear concrete with strain softening, etc.

The LUSAS element library contains over 100 element types, enabling a wide range of engineering applications to be efficiently modelled. The element types include bar, beam, 2-D continuum, 3-D continuum, plate and shell element, etc.

Boundary conditions may be applied to the finite element model as restrained or prescribed values, springs, slidelines, etc. In addition, a variety of loading conditions may be simply applied. The loading types include the prescribed displacements, concentrated loads, element loads, initial values and field loading.

Data is input via a LUSAS data file, and is based on a series of self descriptive data sections. The data input is flexible, completely free-format, and is suitable for input from a terminal. Powerful data generation facilities are available, which have been designed to reduce the time spent preparing data to a minimum. Alternatively, preprocessing may be carried out

using the graphical interactive system MYSTRO [140], which is also used in the present study.

The method of solving the equilibrium equations in LUSAS is the frontal technique [141], which is generally regarded as the most efficient method for the solution of large systems of simultaneous equations, as commonly encountered in finite element analysis.

The basic information needed to define a problem in LUSAS includes the element topology, nodal coordinates, geometrical properties, material properties, support conditions and loading.

The program can output a variety of values and a graphical output which can be analyzed using the accompanying graphical package MYSTRO. In general, MYSTRO is designed to be easy to use for both simple and complex graphical processing.

As a pre-processor MYSTRO may be used interactively to generate full working finite element models. The pre-processing facilities include:

* Interactive model definition in terms of points, lines surfaces and volumes.
* Automatic or manual modelling scaling.
* Automatic regular and irregular line, surface, and volume mesh generation.
* Interactive definition and assignment of element properties, support and loading conditions.
* Generalised load generation and visualisation.
* Printing, labelling and interactive modifying of the components of the model.
* Load and support condition visualisation.
* Automatic generation of the LUSAS datafile.

As a post-processor MYSTRO possesses a range of manipulative and graphical facilities which allow the effective interpretation and display of the analysis results. These facilities include:

* Manipulation of displacements, velocities, accelerations, strains and stresses, field potentials, gradients and fluxes.
* Graphical display of results as vectors, smoothed or element by element contours, or X-Y graphs.
* Layer by layer representation of composite or nonlinear shells.
* Printing of selected numerical results.
* Bending moment and shear force diagrams for frame structures
* Yield flag and crack pattern plots for materially nonlinear elsto-plastic and concrete analyses.
* Colour fill for elements and contours with full or selective colour definition.
* Use of multiple windows with line and text annotations to create impressive compound pictures.
* Read and write access to existing model and picture files.

The relationship between MYSTRO and LUSAS and the various types of interface files used are shown in Figure 5.1

In the current study, the analysis was performed on an IBM compatible with an 80486 processor.

5.4 MODELLING PROCEDURES

A number of models have been built up using the finite element package LUSAS. These models were simulating the stainless steel welded joint before and after the application of PWHT. To study the effect of welding length and width, during the joint service, different models have also been built up to determine the stress field for these type of welded joints for both before and after PWHT.

Because of the symmetry of the welded component, substantial reduction in computational time will be achieved by considering just half of the welded component. For the example of the welded joint of a full welding length a mesh system has been created with 300 elements

connected together with 611 nodes as illustrated in Figure 5.2. Finer mesh has been considered in and around the HAZ.

5.4.1 MATERIAL PROPERTIES

Material property specification is required in order to define the constitutive relationship for each element. Because of the difference in the structure and the hardness of the HAZ and the base metal, the modulus of elasticity has been determined for both the base metal and the HAZ.

In this study the poisson's ratio has been assumed to be 0.3 for all different conditions due to the difficulties of determining this value experimentally, considering that the poisson's ratio will not change significantly. The poisson's ratio usually ranges between 0.27 to 0.3 for most types of steels [142].

However the modulus of elasticity has been determined for these different conditions. The following determined values have been considered in defining the material properties into the finite element model.

Modulus of Elasticity = 200000 N/mm² for the base metal before and after PWHT.

Modulus of Elasticity = 230000 N/mm² for the HAZ before PWHT.

Modulus of elasticity = 210000 N/mm² for the HAZ after PWHT.

5.4.2 SUPPORT CONDITIONS

Support conditions describe the way in which the model is grounded and are specified for individual nodal freedoms. All nodes in the symmetry line in these models have been constrained in X-direction.

5.4.3 LOADINGS

Two types of loads have been applied for as-welded condition. First load is the assumed service load, which is applied as prescribed displacement along the side of the welded joint. The displacement value was 0.15% of the total length of the welded component. Second load is the residual stresses, where the calculated residual stresses and their directions (as described in Appendix A) are applied in these different models for as-welded condition. However, the prescribed displacement only has been applied for the different models after PWHT, considering that the residual stresses have been totally relieved.

5.5 RESULTS AND DISCUSSIONS

As described before, many models have been built up to simulate the welded component before and after PWHT. The modelling was first done with welding width of 20 mm, considering the HAZ as the welding width and a full welding length. Figures 5.3 and 5.4 show the stress field in X and Y direction respectively.

It can be seen from Figure 5.3 that there is a considerable higher stress value at the transfer line between the base metal and the HAZ. These results show that the difference in the stress values reach about 140 N/mm^2 for the stress in X-direction. However, the results show that there is also a concentrated stress in Y-direction near the HAZ. The variation of these

stresses reach a value of about 130 N/mm² as illustrated in Figure 5.4.

It is evident from the above described results that there is substantial concentrated stress on the transfer line between the base metal and the HAZ. These results emphasize the need of reducing or eliminating the variation in the stress field as a result of the welding process, which introduced the existence of the residual stresses.

After the application of PWHT for the same above example, the stress field has been changed, considering that the residual stresses were relieved and the HAZ has been tempered. Figures 5.5 and 5.6 shows the stress field in X and Y direction respectively. It is evident from these results that the concentrated stress values have been eliminated and the component has about the same stress value of about 335 N/mm² in X-direction. Moreover, The stress in Y-direction is about zero as a result of eliminating the residual stresses.

In order to study the effect of welding length on the stress distribution of the welded joint, three models have been built up for the same previous welding component but with welding length of 1, 5 and 20% from the total length of the component. The width of the HAZ assumed as 20 mm.

Figures 5.7 and 5.8 show the stress distribution in X and Y direction respectively, for welding length of 20% of the total length of the welded joint. It can be seen from Figure 5.7 that there is a concentrated stress around the welding line and the stress distribution in x-direction was varied by about 100 N/mm² in this joint. However, the stress distribution in Y-direction shows that there is also concentrated stress around the welding line. The stress field was ranging between -20 N/mm² and 70 N/mm² as illustrated in Figure 5.8.

Figures 5.9 and 5.10 show the stress distribution in X and Y direction respectively, for welding length of 5% of the total length of the welded joint. It can be seen from Figure 5.9 that

there is a concentrated stress around the welding line and the stress distribution was varied by about 100 N/mm² in the welded joint. But, the stress distribution in Y-direction was varied by less than 50 N/mm². The stress distribution in Y-direction is illustrated in Figure 5.10.

Another model with welding length of 1% of the total length of the welded joint has been built up. The results show that the stress variations in both directions X and Y were decreased for about 65 and 30 N/mm² respectively. It can be seen from Figure 5.11 that the stress in X-direction was varied between 295 and 362 N/mm², and the maximum value was near the welding line. However, the stress distribution in Y-direction was about zero for most of the welded joint except the HAZ, where the stress reaches a value of less than 30 N/mm². These results are illustrated in Figure 5.12.

It is evident from the above described results that considerable level of concentrated stress exists around the HAZ for these different types of welded joints. It can also be seen that when the welding length decreased the stress variation in the welded joint was also decreased. These concentrated stresses in all these welded joint could have serious effect on the service life and a macrocrack could be introduced as a result of these variations in the stress field. This emphasize the necessity of eliminating the residual stresses in this type of welded components.

Figures 5.13 to 5.18 show the stress distribution in X and Y direction after the application of PWHT for these above welded joints. It can be seen from these results that after the application of PWHT the stress variation has been virtually eliminated for all these different welding lengths. It is obvious that the stress value in X-direction was about 330 N/mm² with a very negligible variation of less than 10 N/mm² for these different welded joints. However, The stress value in Y-direction was about ranging between -9 and 3 N/mm². It is evident from these results that a substantial effect on eliminating the stress variation and the concentrated stress for these welded joints has been obtained after the application of PWHT.

To study the effect of welding width on the stress field for this type of welded joint, three joints which have different welding widths were modeled. These widths were 5, 20 and 40 mm with welding length of 100 mm. Whilst, the component width and length are 500 and 1000 mm respectively.

It can be seen from Figure 5.19 that the stress distribution in X-direction for welding width of 40 mm is varied by about 120 N/mm^2 and the concentrated stresses were existed around the welding line. However, the stress distribution in Y-direction was varied by about 100 N/mm^2 and again the concentrated stresses were around the welding line. these results are illustrated in Figure 5.20

Figures 5.7 and 5.8 shows the stress field for welding width of 20 mm in X and Y direction respectively. It can be seen that there is a stress variation of about 100 N/mm^2 in X-direction and there is also stress variation of more than 100 N/mm^2 in Y-direction. It is evident from these results that there is a substantial concentrated stress around the welding line, for this type of welded joint.

Finally, after executing the welding with welding width of 5 mm, the stress distribution was varied by about 55 N/mm^2 in X-direction. These results are illustrated in Figure 5.21. However, the stress distribution in Y-direction was varied by less than 70 N/mm^2. It can be seen from Figure 5.22 that the welded component has a negligible stress value except the area near the welding line, where the stress reached a value of about 70 N/mm^2. It is evident from these results that there are still substantial values of concentrated stresses around the welding zone which could have a serious negative effect on this welded joint during service period.

Again after the application of PWHT for these above different welded joints which varied in their welding width, the stress variation was eliminated. It can be seen from Figures 5.7, 5.23 and 5.25 that the stress distribution in X-direction was about 330 N/mm^2 with a variation of less

than 10 N/mm². However, the stress distribution in Y-direction was about zero as illustrated in Figures 5.8, 5.24 and 5.26. It is evident from these results that PWHT has considerable benefits on these different welding joints, where the concentrated stress was eliminated and homogenous welded joints have been obtained.

It is still uncertain as to the level of stress variation for which the welded joint can be satisfactory without the application of PWHT. It would always be advisable that it is important to apply PWHT especially when the safety factor is very important. In the case of relatively smaller welding zone, the local heat treatment could be a very good solution to relieve the residual stresses for relatively large welded component [88] for which heat treatment of the whole component is unnecessary and expensive.

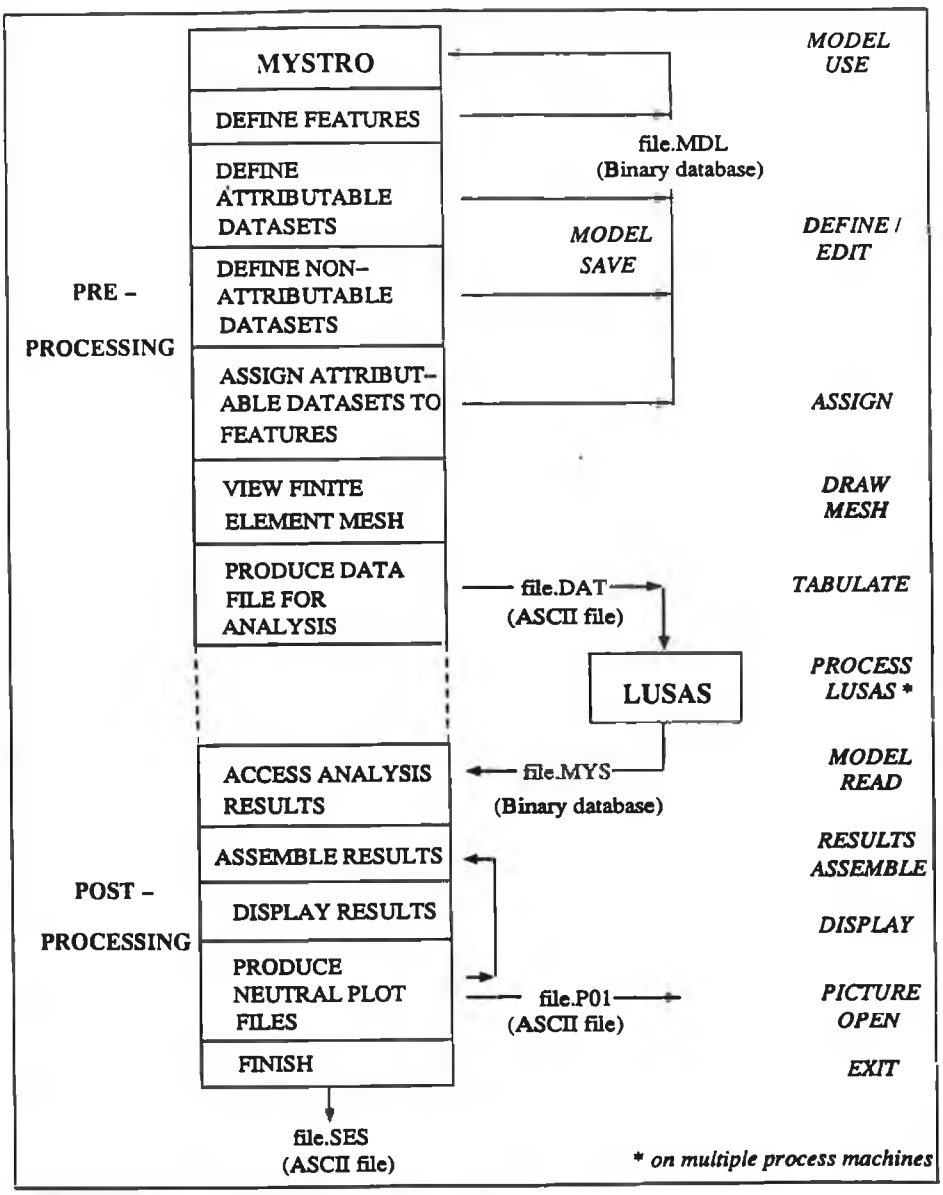

FIGURE 5.1 THE RELATIONSHIP BETWEEN MYSTRO AND LUSAS.

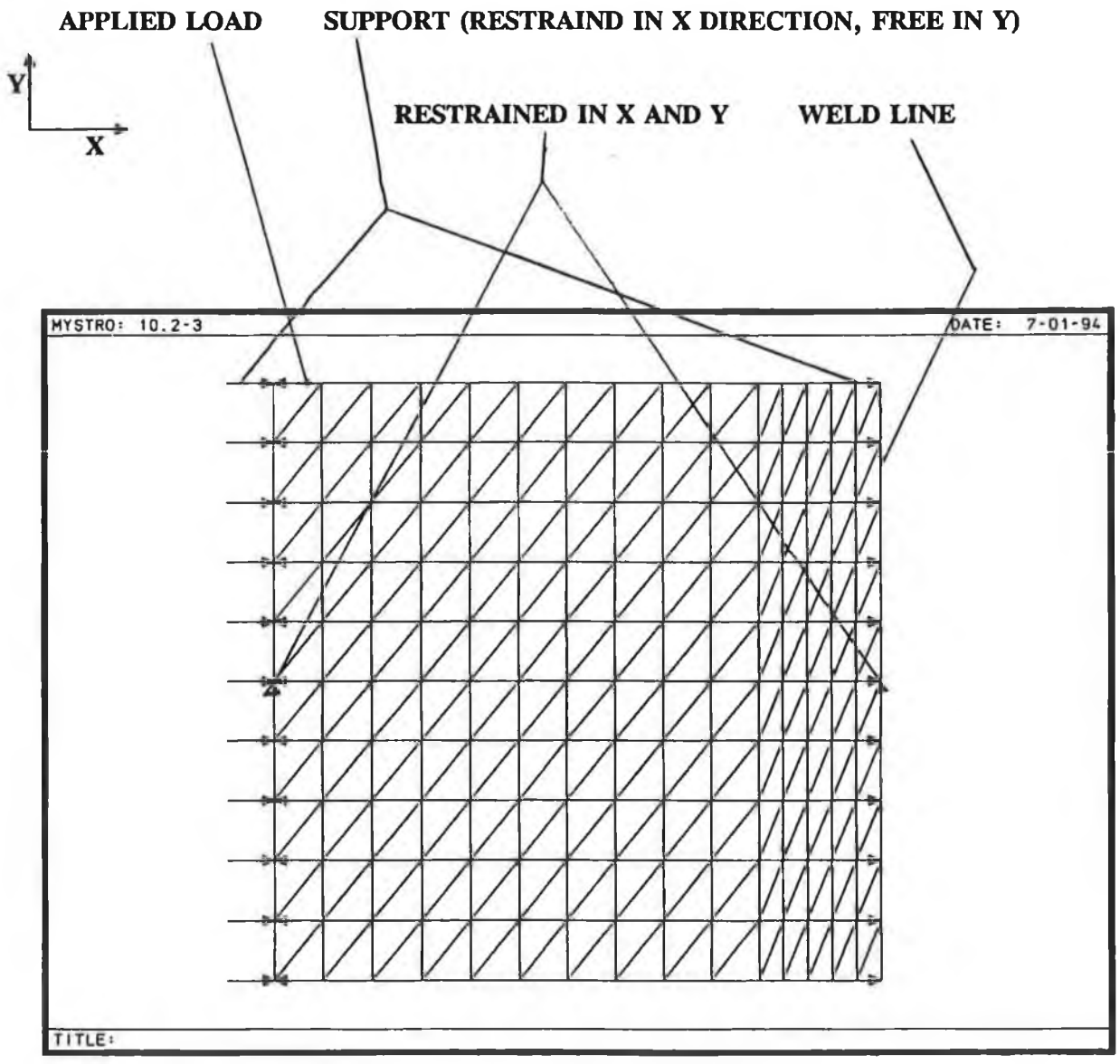

FIGURE 5.2 THE WELDED COMPONENT MODEL AFTER MESHING, FOR FULL WELDING LENGTH.

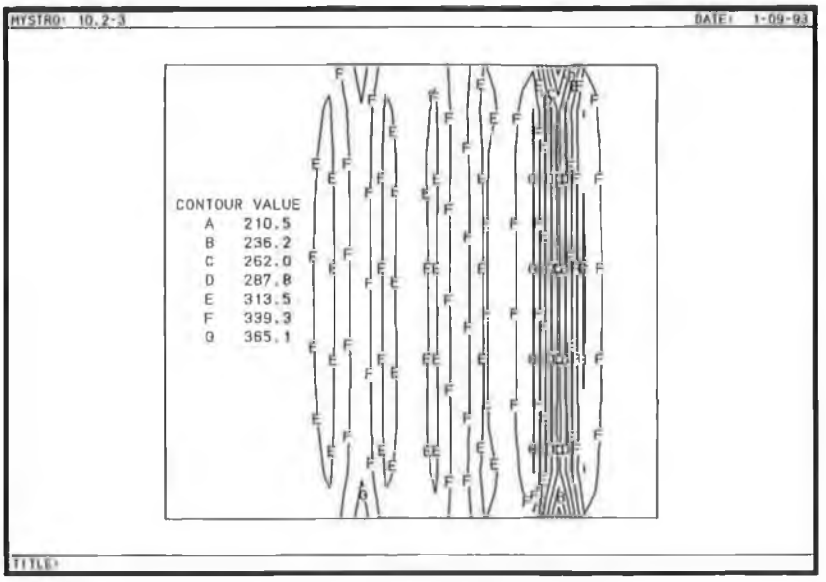

FIGURE 5.3 DISTRIBUTION OF σx, FOR FULL WELDING LENGTH, BEFORE PWHT.

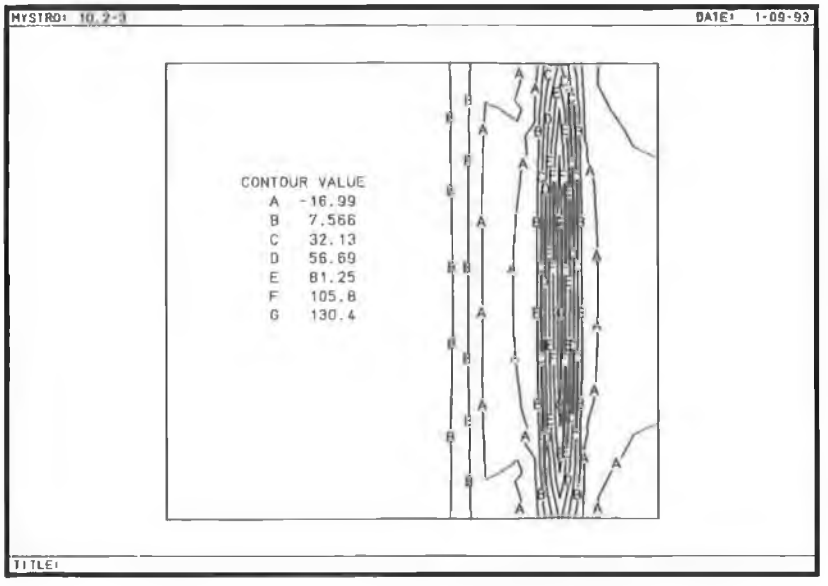

FIGURE 5.4 DISTRIBUTION OF σy, WITH FULL WELDING LENGTH, BEFORE PWHT.

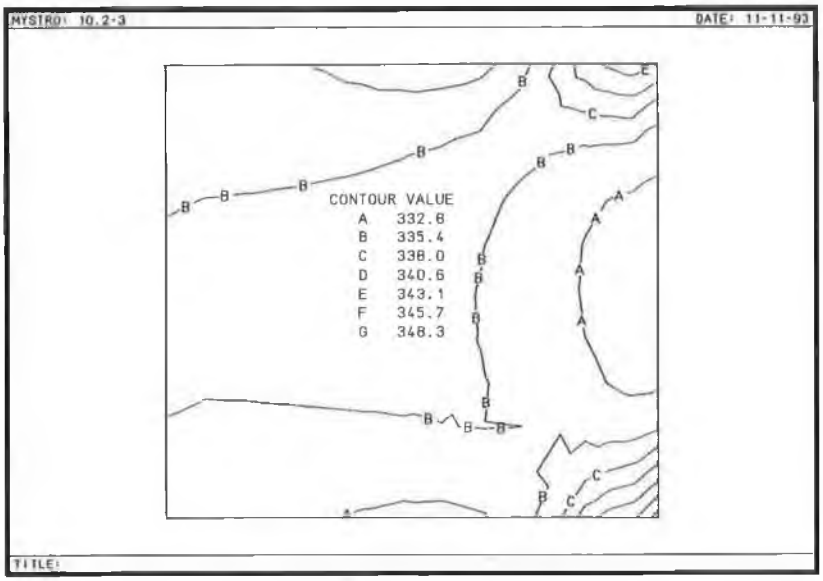

FIGURE 5.5 DISTRIBUTION OF σx, FOR FULL WELDING LENGTH, AFTER PWHT.

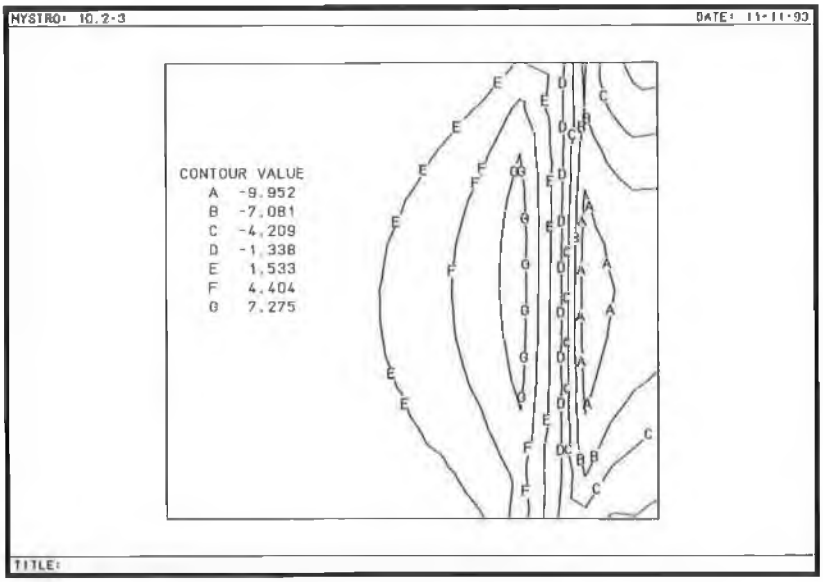

FIGURE 5.6 DISTRIBUTION OF σy, FOR FULL WELDING LENGTH, AFTER PWHT.

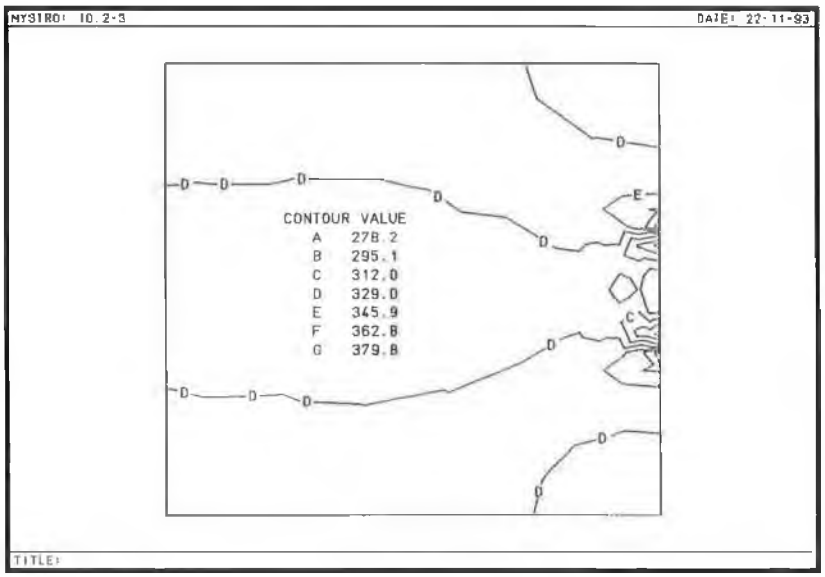

FIGURE 5.7 DISTRIBUTION OF σx, FOR WELDING LENGTH OF 20% OF THE SPECIMEN LENGTH, BEFORE PWHT.

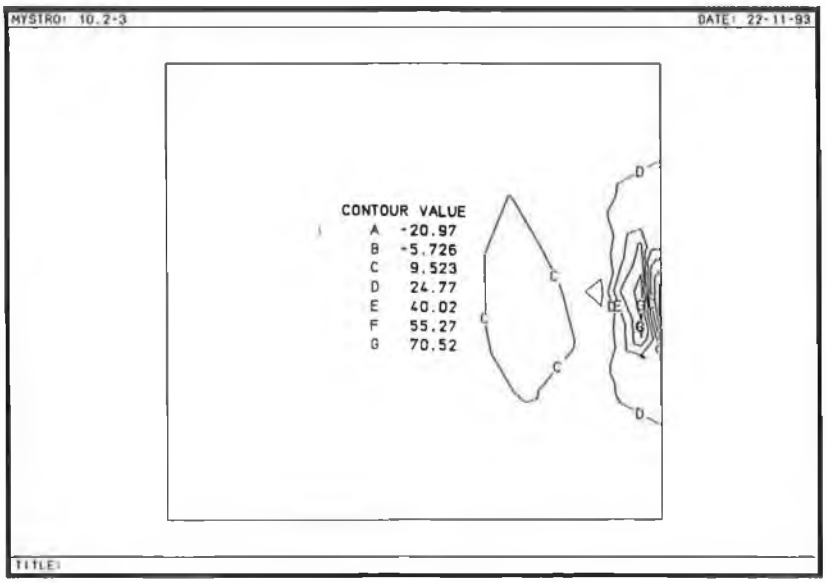

FIGURE 5.8 DISTRIBUTION OF σy, FOR WELDING LENGTH OF 20% OF THE SPECIMEN LENGTH, BEFORE PWHT.

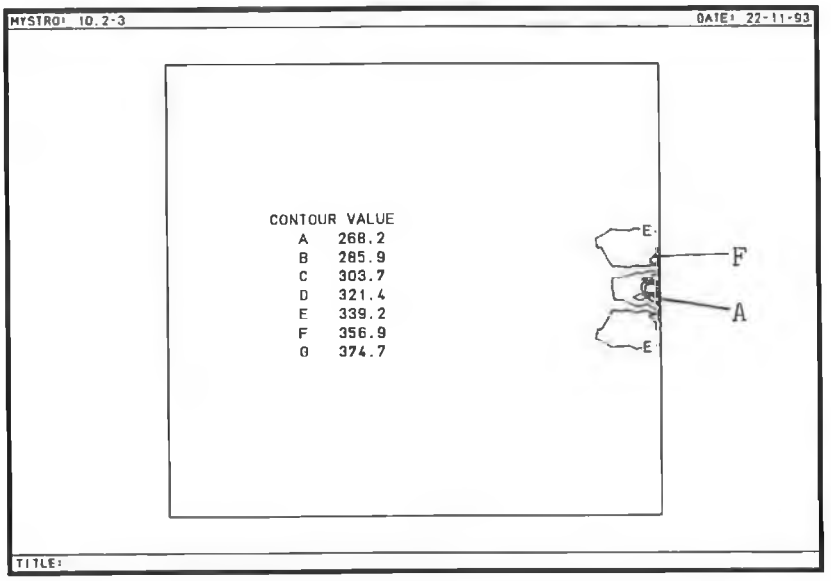

FIGURE 5.9 DISTRIBUTION OF σx, FOR WELDING LENGTH OF 5% OF THE SPECIMEN LENGTH, BEFORE PWHT.

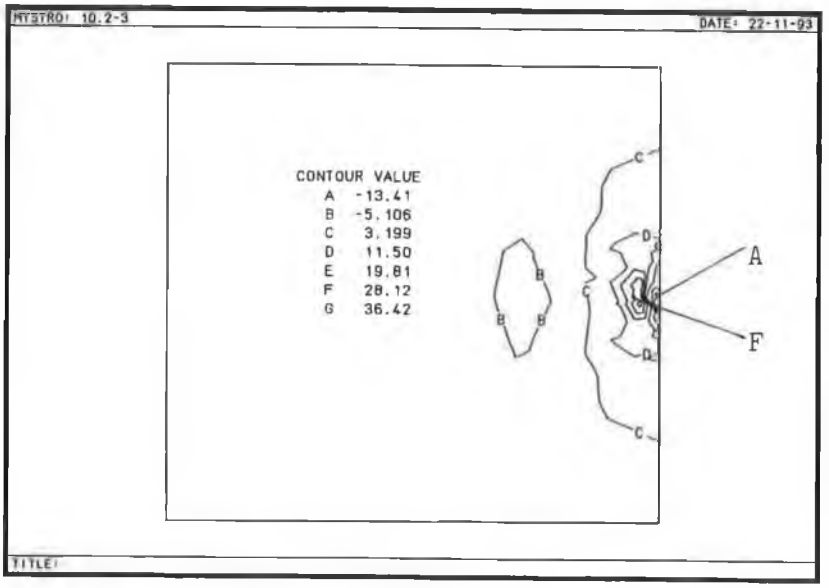

FIGURE 5.10 DISTRIBUTION OF σy, FOR WELDING LENGTH OF 5% OF THE SPECIMEN LENGTH, BEFORE PWHT.

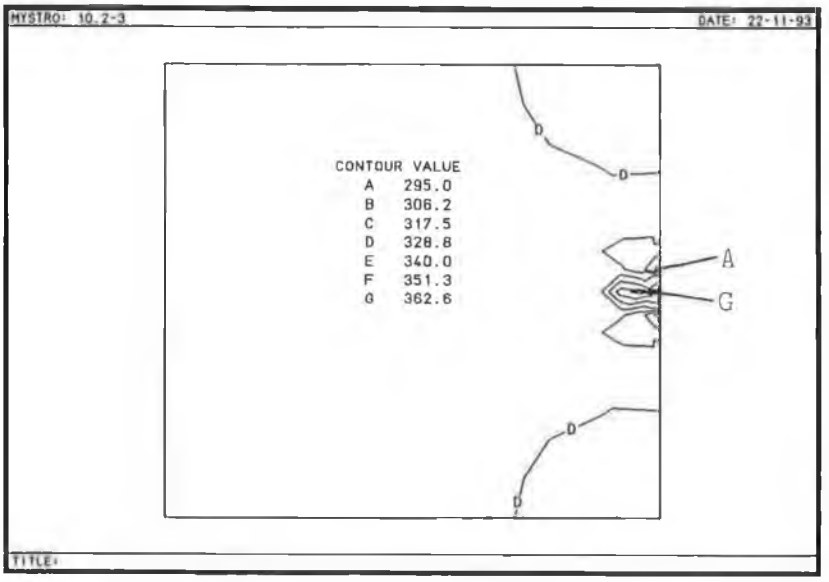

FIGURE 5.11 DISTRIBUTION OF σx, FOR WELDING LENGTH OF 1% OF THE SPECIMEN LENGTH, BEFORE PWHT.

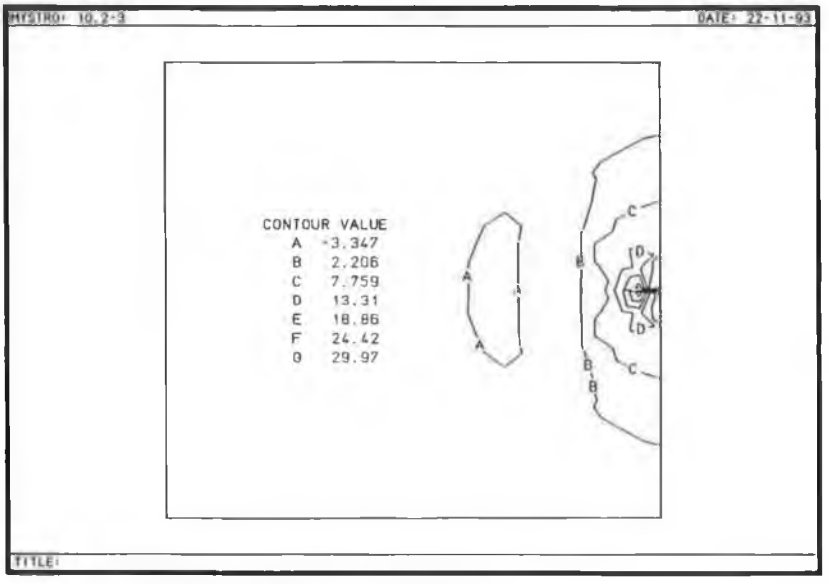

FIGURE 5.12 DISTRIBUTION OF σy, FOR WELDING LENGTH OF 1% OF THE SPECIMEN LENGTH, BEFORE PWHT.

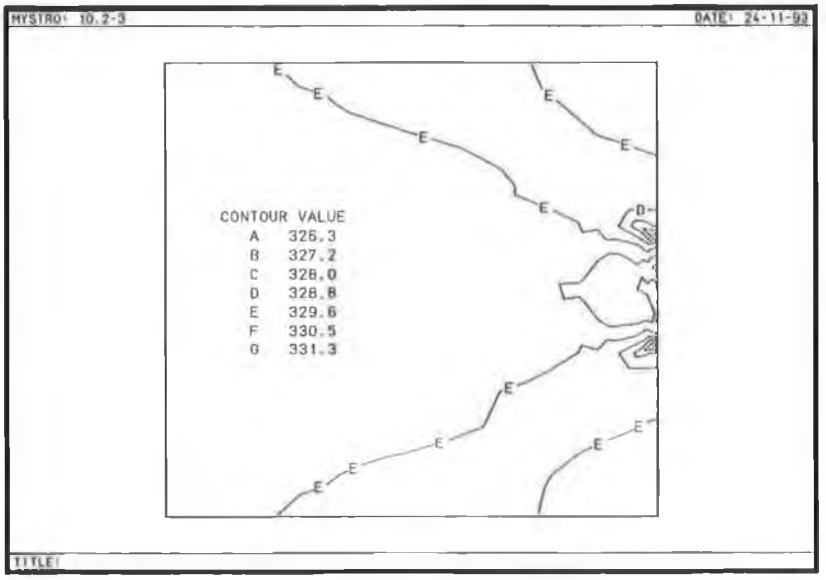

FIGURE 5.13 DISTRIBUTION OF σx, FOR WELDING LENGTH OF 20% OF THE SPECIMEN LENGTH, AFTER PWHT.

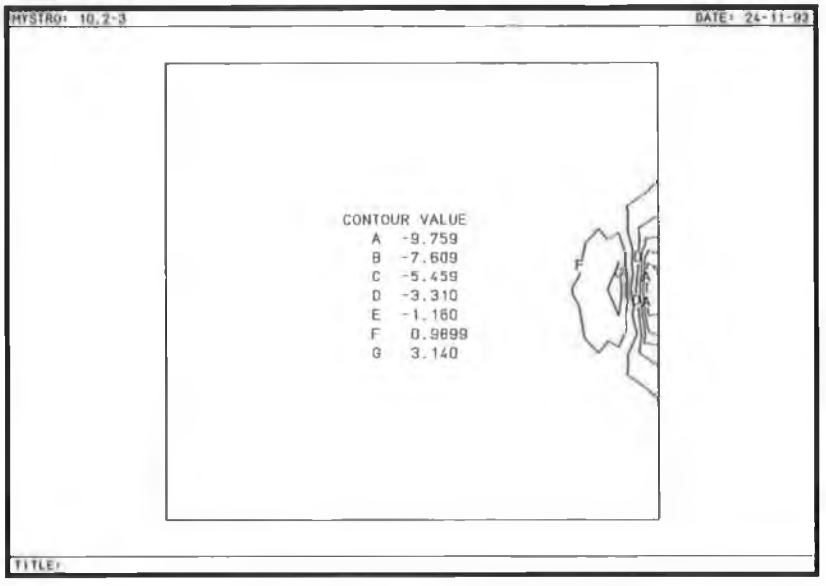

FIGURE 5.14 DISTRIBUTION OF σy, FOR WELDING LENGTH OF 20% OF THE SPECIMEN LENGTH, AFTER PWHT.

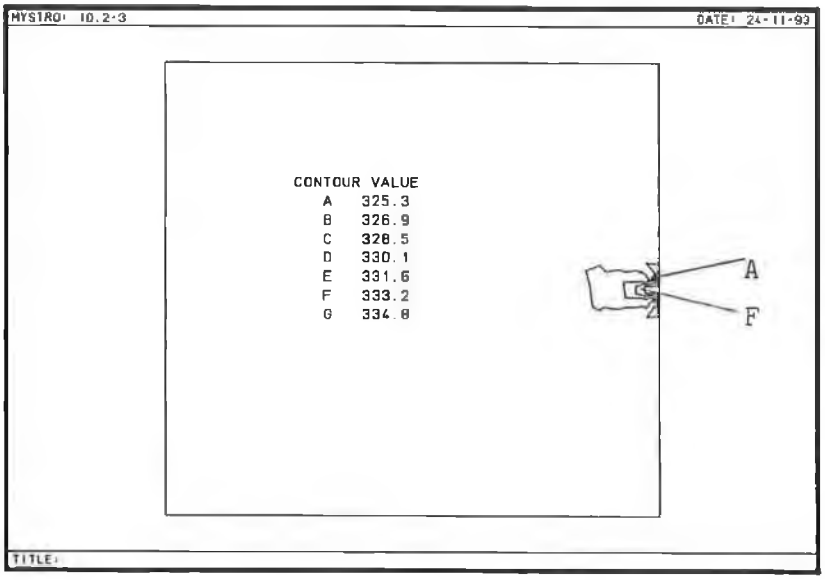

FIGURE 5.15 DISTRIBUTION OF σx, FOR WELDING LENGTH OF 5% OF THE SPECIMEN LENGTH, AFTER PWHT.

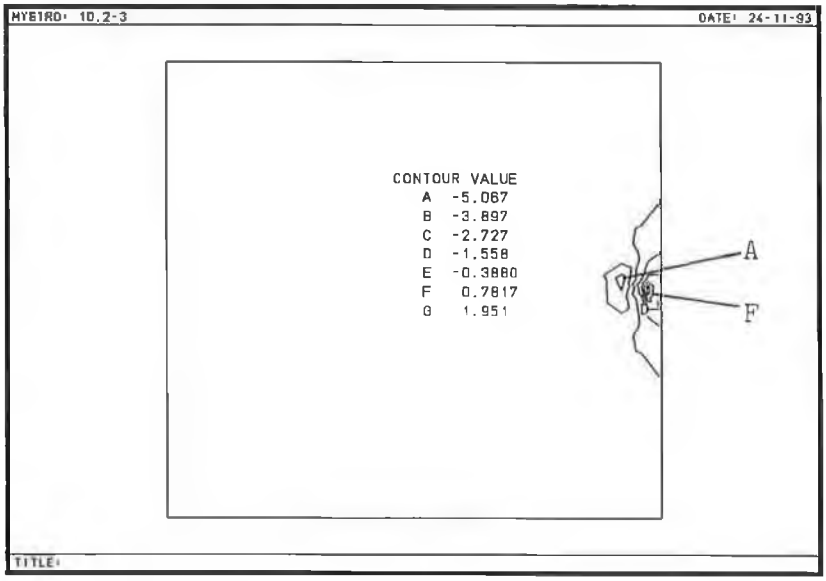

FIGURE 5.16 DISTRIBUTION OF σy, FOR WELDING LENGTH OF 5% OF THE SPECIMEN LENGTH, AFTER PWHT.

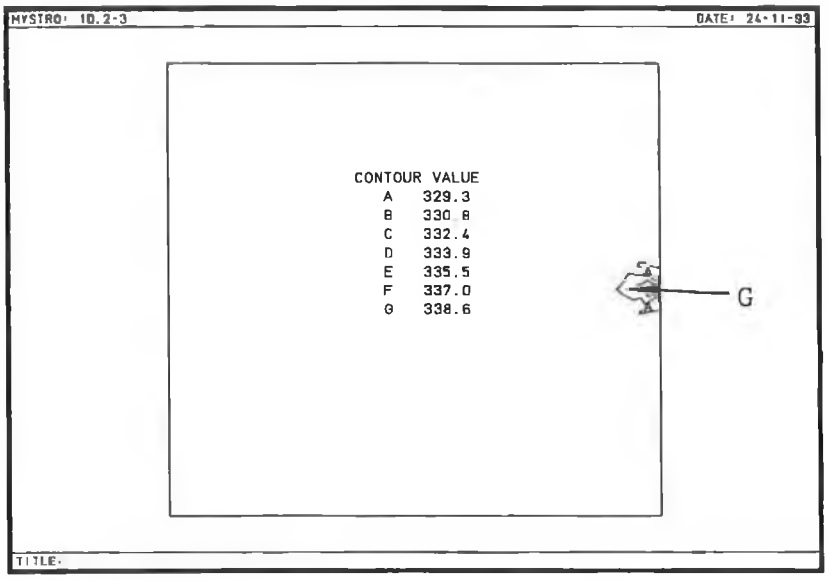

FIGURE 5.17 DISTRIBUTION OF σx, FOR WELDING LENGTH OF 1% OF THE SPECIMEN LENGTH, AFTER PWHT.

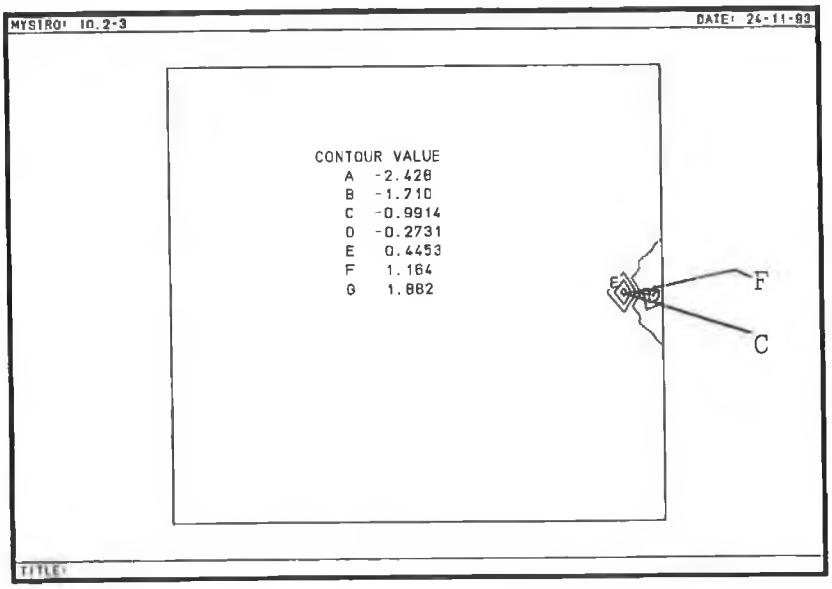

FIGURE 5.18 DISTRIBUTION OF σy, FOR WELDING LENGTH OF 1% OF THE SPECIMEN LENGTH, AFTER PWHT.

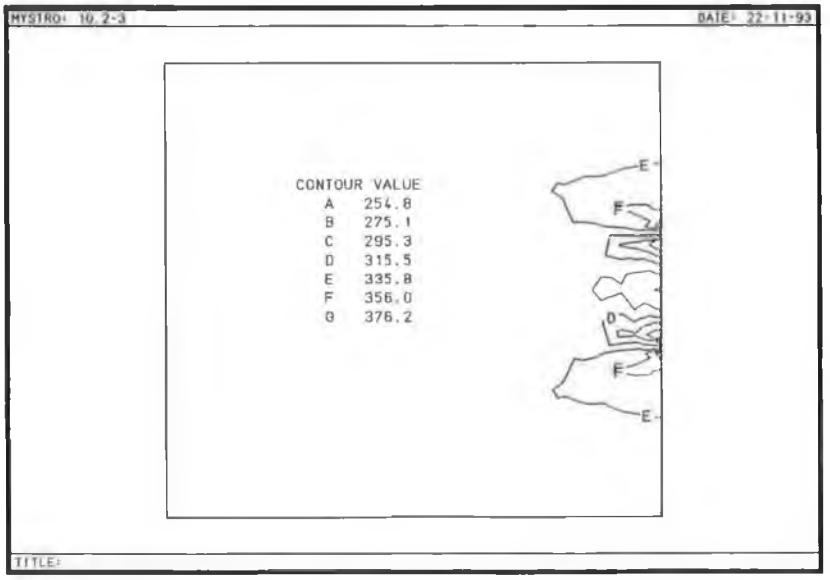

FIGURE 5.19 DISTRIBUTION OF σx, FOR WELDING WIDTH OF 40 mm AND WELDING LENGTH OF 20%, BEFORE PWHT.

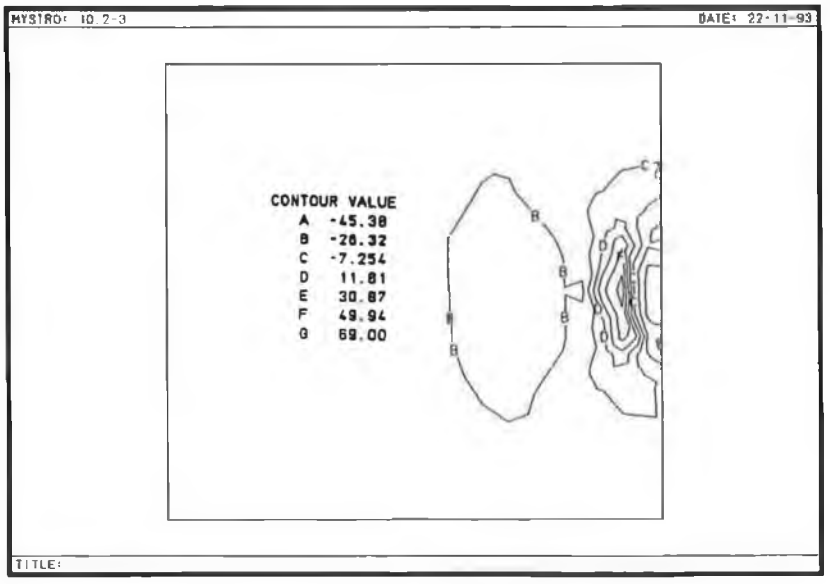

FIGURE 5.20 DISTRIBUTION OF σy, FOR WELDING WIDTH OF 40 mm AND LENGTH OF 20%, BEFORE PWHT.

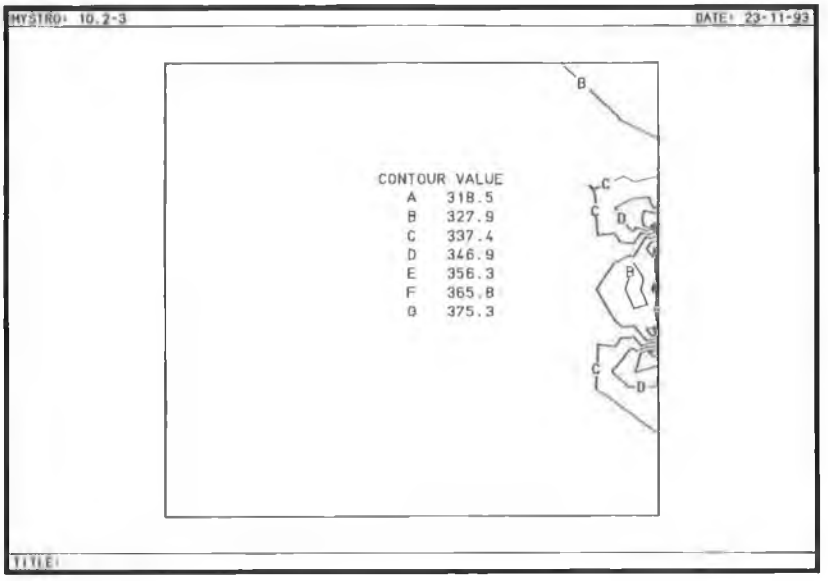

FIGURE 5.21 DISTRIBUTION OF σx, FOR WELDING WIDTH OF 5 mm AND LENGTH OF 20%, BEFORE PWHT.

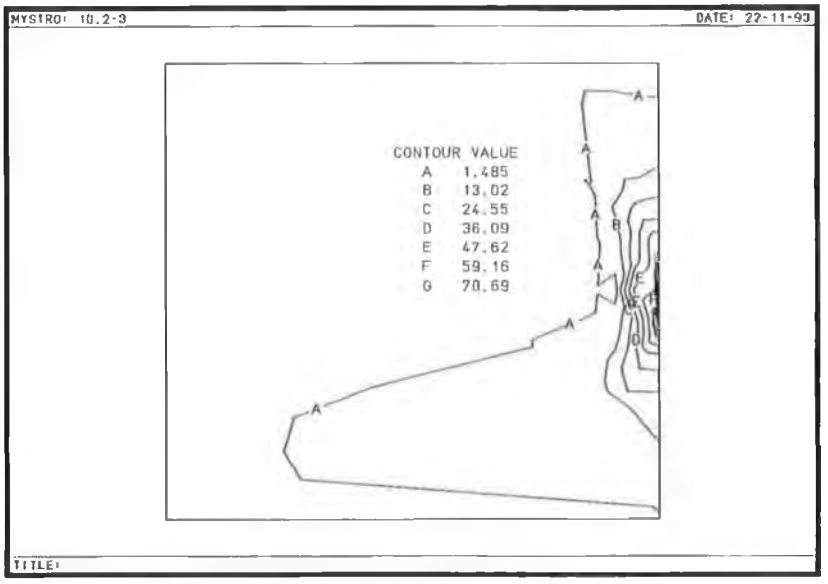

FIGURE 5.22 DISTRIBUTION OF σy, FOR WELDING WIDTH OF 5 mm AND LENGTH OF 20%, BEFORE PWHT.

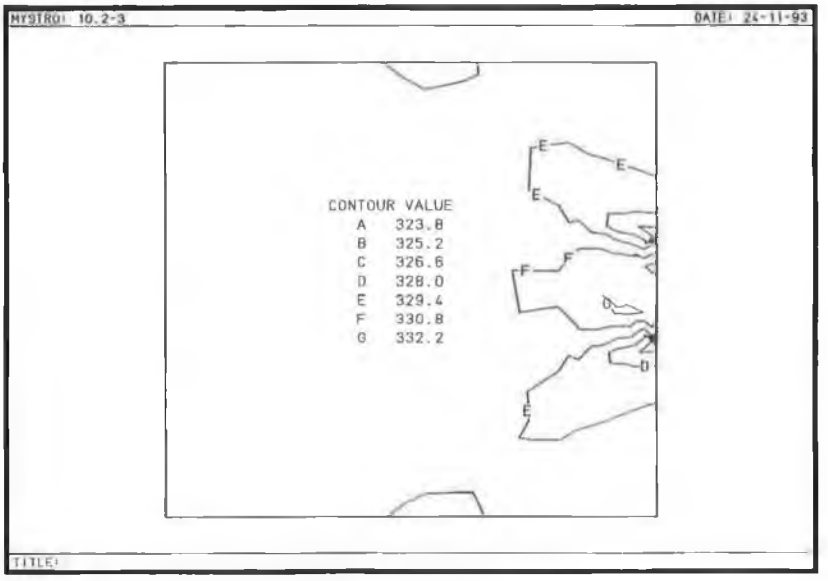

FIGURE 5.23 DISTRIBUTION OF σx, FOR WELDING WIDTH OF 40 mm AND LENGTH OF 20%, AFTER PWHT.

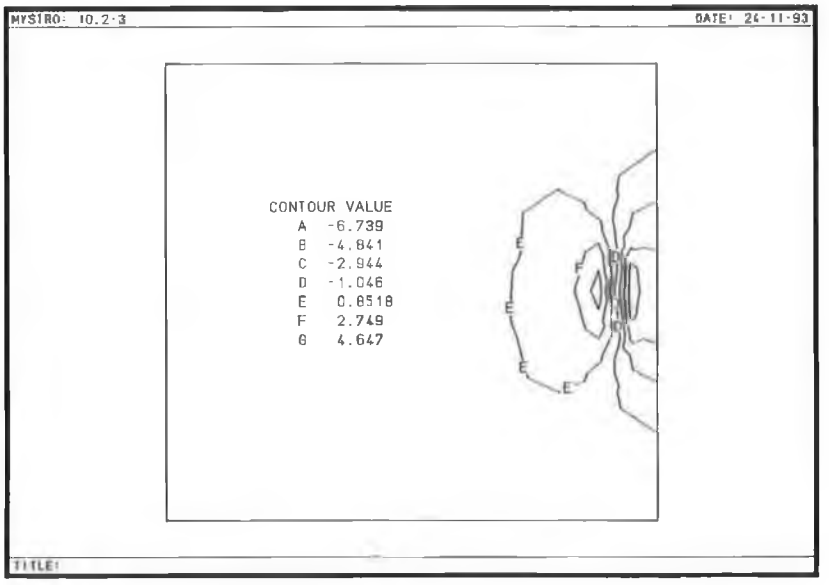

FIGURE 5.24 DISTRIBUTION OF σy, FOR WELDING WIDTH OF 40 mm AND LENGTH OF 20%, AFTER PWHT.

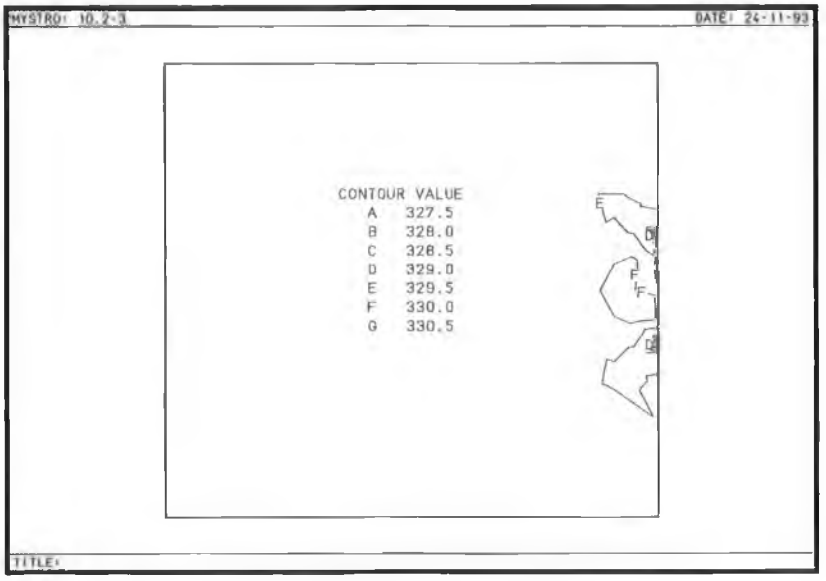

FIGURE 5.25 DISTRIBUTION OF σx, FOR WELDING WIDTH OF 5 mm AND LENGTH OF 20%, AFTER PWHT.

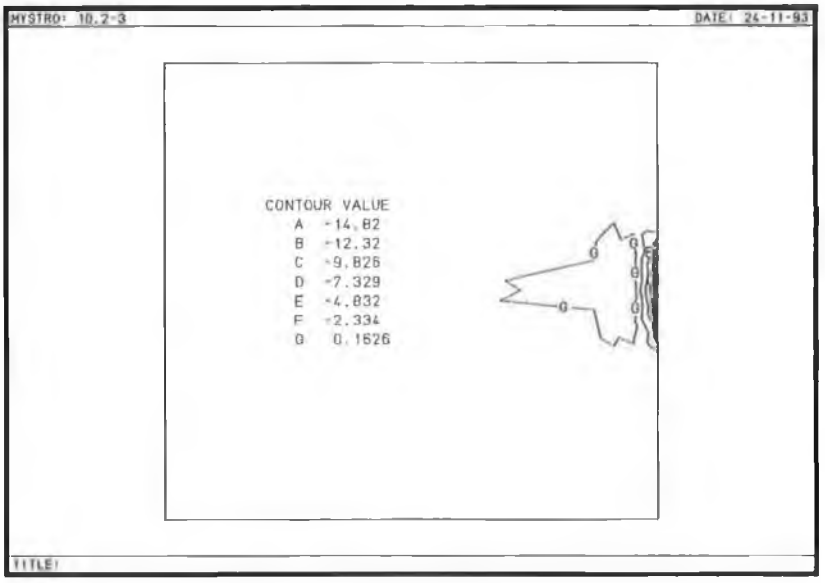

FIGURE 5.26 DISTRIBUTION OF σy, FOR WELDING WIDTH OF 5 mm AND LENGTH OF 20%, AFTER PWHT.

CHAPTER SIX

DISCUSSIONS

6.1 THE LOW CARBON STEEL COMPONENT

6.1.1 THE METAL MICROSTRUCTURE

In this project, the metal microstructure of the low carbon steel welded component was studied. The results of this inspection point out that after executing the welding, the structure of the HAZ is bainite as a result of the relatively fast cooling, from the melting point to the room temperature. These obtained results coincide with the result of the hardness measurements where the hardness value is higher in the HAZ than the base metal. It was also found that the HAZ has a homogeneous structure. It is evident from these results that the difference in the hardness value in the HAZ between the surface and the middle of the specimen does not have any noticeable difference on the microstructure of this zone.

After the application of these different heat treatment schemes the metal microstructure of the HAZ became tempered for different levels depending on the heat treatment procedures. These results show that the microstructure of the HAZ consists of tempered bainite, ferrite and very low percentage of precipitated carbide. It is evident from these results that the higher PWHT soaking temperature, the more effective on tempering the bainite and increasing the percentage of the ferrite in the structure of HAZ. These results coincide with the hardness test results, where the hardness value has been decreased in the HAZ and the maximum reduction was obtained after the application of PWHT with higher soaking temperature.

As described in the previous Chapter, different PWHTs were applied by varying the heating rate, time duration and cooling rate with soaking temperature of 450°C as illustrated in Table 3.1. It is evident that after the application of these different heat treatment schemes the microstructure of the HAZ has been tempered for different levels and the maximum effect has been obtained after the application of PWHT with longer time duration and slower cooling rate. Meanwhile, there is no significant effect by varying the heating rates. These results also coincide with the hardness measurements where the maximum reduction in the hardness value has resulted after the application of PWHTs with longer time duration (10 hours) and slower cooling rate (10 °C/h).

It can be noticed from these results that there is no considerable effect on the structure of the base metal for both as-welded condition and after the application of these heat treatment schemes, and it consists of pearlite and ferrite. It is evident that the softening in the base metal after PWHTs does not show any change on the structure of this zone.

6.1.2 THE HARDNESS TEST

As described before, the results of this test point out that the hardness value for the as-welded condition has a higher value of about 50 HV in the HAZ than the base metal of this type of welded component and this HAZ was extending to about 20 mm in the middle of the welded component. These results coincide with the microstructure results where a bainite structure is formed in the HAZ. Whilst, the base metal of the welded component has softer structure (pearlite and ferrite), this difference in the structure has resulted in the difference in the hardness between the HAZ and the base metal. It can be also noticed that the hardness value at the depth of 5 mm is slightly reduced and the HAZ becomes smaller by about 6 mm for both box-section and double-V welded components.

After the application of these different schemes of PWHT, the bainite structure in the

HAZ became tempered for different levels depending on the heat treatment scheme and a softer HAZ has been obtained. The hardness value in the HAZ is reduced for different levels ranging between 5 to 60 HV depending on the heat treatment scheme, which varied in the soaking temperature, heating rate, time duration and cooling rate. Figures 4.4, 4.5, 4.11, 4.12, 4.15, 4.16, 4.19, 4.20, 4.23 and 4.24 compare these different schemes with as-welded conditions.

The effect of soaking heat treatment temperatures were investigated. Three soaking temperatures were applied 450, 550 and 650 °C. The heating rate, time duration and cooling rate were fixed as 400 °C/h, 2 hours and 40 °C/h respectively.

It can be seen from these results that after the application of PWHT with different soaking temperatures, the hardness value is reduced in the HAZ for different levels depending on the heating temperature. But the base metal becomes slightly softer. It is obvious from the comparison diagram in Figure 4.11 that the hardness value in the HAZ is decreased by about 20 HV after the application of PWHT with soaking temperature of 450°C and by about 40 HV after PWHT with soaking temperature of 550°C and by about 60 HV after PWHT with soaking temperature of 650°C. Whilst the hardness value is slightly decreased in the base metal, this reduction ranged between 5 and 30 HV after the application of these three different soaking temperature. Moreover, it can also be noticed that the HAZ becomes smaller by about 8 mm after PWHT with soaking temperature of 450 °C and by about 10 mm after PWHT with soaking temperature of 550 °C and by about 12 mm after PWHT with soaking temperature of 650 °C. It is evident from these results that the hardness value in the HAZ decreases when the soaking temperature of PWHT increases. At the same time, a slightly softer base metal has resulted after the application of these different heating temperatures. It can be noticed that after the application of PWHT with soaking temperature of 650 °C, a softer structure has resulted and the difference in the hardness between the HAZ and the base metal has been reduced to a low level.

Three different heating rates 50, 100 and 400 °C/h were investigated. Meanwhile, the

soaking temperature, time duration and cooling rate have been kept as 450 °C, 2 hours and 40 °C/h respectively. After the application of PWHT with these heating rates the hardness value is decreased for about the same level. It can be seen from the comparison diagrams in Figure 4.15 that the hardness value in the HAZ is decreased to about 250 HV after the application of PWHT with heating rate of 50°C/h and to about 250-255 HV after the application of PWHT with heating rate of 100°C/h and to about 260 HV after PWHT with heating rate of 400°C/h. However, the base metal becomes softer with reduction in the hardness value of about 10 HV. It is clearly evident from these results that the hardness value is decreased to about the same level after the application of these different schemes of PWHTs, and there is a negligible change in the hardness value by varying the heating rate of PWHT. These results correspond with the microstructure inspection which reveal that there is no difference in the structure of the HAZ after the application of PWHT with these different heating rates.

Three PWHT schemes were applied by varying their time duration 0.5, 2 and 10 hours. Whilst, the soaking temperature, heating and cooling rate have been fixed as 450 °C, 400 °C/h and 40 °C/h respectively.

It can be seen from the comparison diagrams in Figure 4.19 that the hardness value in the HAZ is slightly decreased after the application of PWHT with time duration of 0.5 h. Meanwhile, after PWHT with time duration of 2 h the hardness value is reduced by about 20 HV. Finally, a lower hardness value was obtained after the application of PWHT with time duration of 10 h. It is evident from these results that the hardness value decreases by applying PWHT with longer time duration. It can also be noticed that the HAZ becomes smaller by about 8 to 12 mm after the application of PWHT with soaking duration between 0.5 and 10 hours.

In this investigation, the effects of the cooling rates of PWHT were studied. Three different cooling rates 10, 40 and 125 °C/h were applied. The soaking temperature, heating rate and time duration have been fixed as 450 °C, 400 °C/h and 2 hours respectively.

The obtained results show that after the application of PWHT with cooling rate of 10°C/h the hardness value in the HAZ is reduced by about 35 HV and by about 20 HV after PWHT with cooling rate of 40°C/h and by less than 10 HV after PWHT with cooling rate of 125°C/h. Meanwhile, the hardness value of the base metal becomes softer by about 5 to 15 HV after the application of these schemes of PWHT. It is evident from these results that the hardness value decreases by applying PWHT with slower cooling rate. These results reveal that there is a good agreement between the hardness test and the microstructure inspection where the structure has been tempered after the application of these heat treatment schemes.

It can be seen from Figures 4.4, 4.12, 4.16, 4.20 and 4.24 that the hardness value near the specimen surface is higher than the hardness value in the middle of the thickness. These results point out that the hardness value in the welding zone decreases as the distance from the surface increases due to probably the faster cooling rate. But this difference in the hardness variation does not have any noticeable effect on the microstructure of the HAZ.

6.1.3 THE TENSILE TEST

The initial test was carried out on the I-beam box-section component. The results revealed that the tensile strength has been improved by about 28 N/mm° after the application of PWHT (580 °C for 18 hours).

After the above initial test different PWHT schemes were applied. It can be seen from the results (Table 4.1) of this test that the tensile strength has been improved after the application of these different schemes of PWHT. This improvement in the tensile strength value is ranging between 5 and 38 N/mm². It is evident from these results that the maximum improvement in the tensile strength has been obtained after the application of PWHT with soaking temperature of 650°C.

It is also evident that there is no significant difference in the tensile strength by varying the heating rate of PWHT. Meanwhile, the results show that by varying the soaking temperature of PWHT the tensile strength is improved between 12 and 38 N/mm² and as the soaking temperature increased the improvement in the tensile strength increased.

These results point out that there is also an improvement in the tensile strength after the application of PWHT with different soaking time duration, these improvements were ranging between 5 and 24 N/mm², the maximum improvement has been obtained by applying PWHT with longer soaking time duration (10 hours).

An improvement in the tensile strength has also been obtained after the application of PWHT with different cooling rates, these improvements were ranging between 10 and 25 N/mm² and the tensile strength is increased by applying slower cooling rate.

It is evident from these results that when the structure is tempered the tensile strength has slightly improved after the application of these different types of heat treatments. These results also reveal that the tensile strength of the original metal is about 410 N\mm², which is slightly lower than the tensile strength for all these different conditions (before and after PWHTs).

In this test the specimens were loaded to fracture and the fracture was outside the HAZ. There is no noticeable reduction in the area of the HAZ and the fracture occurred outside this zone. These results correspond with the hardness test which showed that the HAZ still has higher hardness value with different structure from the base metal for both before and after PWHTs.

It is evident that the tensile strength of the HAZ has improved by 15% after the application of PWHT-3 (soaking temperature = 650 °C).

6.1.4 NOTCHED-IMPACT TEST

As described before, the initial test was applied on the I-beam box-section component. This test was made before and after the application of PWHT. The specimen was kept in the furnace for 18 hrs at soaking temperature of 580°C. It is evident from this initial test that a considerable improvement in the impact toughness has been gained after the application of PWHT. The toughness has increased by about 20 J after this type of heat treatment.

After this initial test, different PWHT schemes were applied which varied in their soaking temperature, heating rate, time duration and cooling rate. The results of this test are demonstrated in Table 4.3. It can be seen from these results that there is a substantial improvement in the impact toughness after the application of these different schemes of heat treatments.

It is evident from these results that after the application of PWHT with different soaking temperatures an improvement between 16 and 26 J in the toughness was gained. These results also proved that a better improvement in the toughness was combined with the application of PWHT with higher soaking temperature. These results correspond with the change in the structure after the application of these heat treatment schemes, where the toughness improved and the structure is tempered.

Meanwhile, it can be clearly noticed that after the application of PWHT with different heating rates, an improvement of about 16 J has been obtained. But there is no significant change by varying the heating rate. These results correspond with other microstructure and mechanical test results which showed that there is no significant effect on the structure, the hardness or the strength by varying the heating rate.

It is also evident that an improvement in the impact energy has been gained after the

application of PWHT with different soaking time durations. These improvements were ranging between 8 and 18 J. It can be noticed that by increasing the soaking time duration the impact energy increases.

After the application of PWHT with different cooling rates, a considerable improvement in the impact energy has also been obtained. These improvements were ranging between 11 and 19 J. It is evident from these results that the impact energy increases after the application of PWHT with slower cooling rate.

These above results show that the maximum improvement in the toughness has been gained after the application of PWHT with soaking temperature of 650 °C. The longer time duration (10 hours) and the slower cooling rates (10 °C/h) also have considerable effect on improving the toughness.

6.2 THE STAINLESS-STEEL WELDED COMPONENT

6.2.1 THE METAL MICROSTRUCTURE

The metal microstructure of the stainless-steel welded component has been inspected for as-welded condition and after the application of these different schemes of PWHT. This test was made on the HAZ and the base metal. The results of this investigation reveal that the metal microstructure is completely martensite in the HAZ. The structure of the base metal consists of tempered martensite, ferrite and low percentage of precipitated carbide. These results correspond with the hardness test where the HAZ has considerably higher hardness values compared to the base metal. It is evident from these results that a hard structure has been formed in the HAZ as a result of the fast cooling from the melting point to the room temperature. This fast cooling rate has left the carbide and the other alloy in the steel atoms which resulted in a substantial hard

martensite structure.

It is evident that after the application of different heat treatment schemes the structure has been tempered for different levels depending on the heat treatment procedures. It can be seen that after the application of PWHT with different heat treatment soaking temperatures 550, 650 and 750 °C the structure of the HAZ has been tempered and the structure consists of mainly tempered martensite, low percentage of ferrite and precipitated carbide. It can also be noticed that as the soaking temperature increased the percentage of ferrite and precipitated carbide increased especially after PWHT with soaking temperatures 650 and 750°. These results are in agreement with the hardness results, where the hardness value of the HAZ has been reduced after the application of these heat treatments and the maximum reduction has been obtained after PWHT with soaking temperature of 750 °C. The considerable difference between the HAZ and the base metal has been substantially eliminated after the application of PWHT with higher soaking temperature (750 °C) and the structure becomes about the same across the welded joint.

After the application of PWHTs with different heating rates 50, 100 and 400 °C/h with soaking temperature of 550 °C the structure of the HAZ has been tempered and a tempered martensite has been formed which coincide with the reduction of the hardness value in the HAZ. It is also evident that there is no difference in the structure by varying the heating rate for this welded joint.

It can be noticed that after the application of PWHTs with different soaking time durations the structure of the HAZ has been tempered and the percentage of ferrite and precipitated carbide slightly increased as the soaking time duration increased. These results are in agreement with the hardness results, where the hardness value in the HAZ has decreased as time duration increased due to the formation of these tempered structures.

Different PWHT schemes were applied by varying the cooling rate 10, 40, 125 °C/h.

The soaking temperature, heating rate and time duration kept as 550 °C, 400 °C/h and 2 hours respectively. It is evident that after the application of these different schemes the structure of the HAZ has been tempered. These results coincide with hardness results where the hardness value has been reduced in the HAZ after the application of these heat treatment schemes.

6.2.2 THE HARDNESS TEST

Different PWHT schemes were also applied on this type of welded component. The effect of soaking temperature, heating rate, time duration and cooling rate were studied and compared to as-welded condition. The hardness value has been measured across the specimen axis at three different depths from the specimen surface for both as-welded condition and after the application of these different schemes of PWHT. The results point out that the hardness value at the depth of 1 mm from the surface for as-welded condition is about 510 HV in the HAZ and around 260 HV in the base metal and the HAZ extended to about 20 mm in the middle of the welded component. Meanwhile, the hardness value at depths of 5 and 12 mm has lower values 475 and 460 HV respectively, and the HAZ area becomes smaller by about 6 to 8 mm in the middle of the specimen thickness.

As mentioned before, three different soaking temperature 550, 650 and 750°C were applied and the hardness value has been reduced for different levels after the application of these different schemes of heat treatment. It can be seen from the comparison diagrams in Figure 4.31 that the hardness value in the HAZ is reduced to about 470 HV after the application of PWHT with soaking temperature of 550°C and to about 345 HV after PWHT with soaking temperature of 650°C and to around 300 HV after PWHT with soaking temperature of 750°C. Meanwhile, the hardness value outside the HAZ is still ranging between 255 and 260 HV. It is evident from these results that the hardness value in the HAZ decreases as the heat treatment soaking temperature increases and this reduction in the hardness value is combined with the shrinkage of the HAZ. The HAZ is reduced by about 2 mm after PWHT-1 and by about 8 mm after

PWHT-2 and finally, by about 10 mm after PWHT-3.

It can be noticed that there is a substantial difference in the hardness value between the HAZ and the base metal for as-welded condition as a result of the fast cooling from the melting point to the room temperature. It is clearly evident from these results that after the application of these different PWHT schemes, the sharp difference in the hardness value between the HAZ and the base metal has been reduced from about 250 HV to about 200 HV after PWHT 1 and about 85 HV after PWHT 2, but the maximum reduction has been obtained after PWHT 3 (soaking temperature = 750°C), where this difference is reduced to around 40 HV. These results are in agreement with the microstructure results where the structure has been tempered and a relatively homogenous structure across the welded joint has been obtained after the application of PWHT with soaking temperatures of 750 °C.

The effect of the heating rate has been studied, three different heating rates 50, 100 and 400°C/h were employed. A comparison diagram has been plotted in Figure 4.35 for the hardness variation between as-welded condition and after PWHT with these different heating rates. The results show that the hardness value is reduced to about the same level after the application of these above PWHT schemes. This reduction was ranging between 35 and 45 HV in the HAZ.

It is evident from these results that there is no significant effect on the hardness value in the HAZ by varying the heating rate of PWHT. The hardness value in the HAZ ranged between 470 and 475 HV after the application of these heat treatment schemes. It can be noticed that after the application of these heat treatment schemes the HAZ becomes slightly smaller by about 3 to 4 mm comparing to the HAZ for as-welded condition. These results coincide with the microstructure results which showed that there is no significant difference in the structure of the HAZ after the application of these PWHT schemes.

Three different PWHT schemes have been applied, these schemes were varied only in

their time duration, 0.5, 2 and 10 hours. It can be seen from Figure 4.39 that the hardness value in the HAZ is slightly reduced by about 15 HV after the application of PWHT with time duration of 0.5 h, and by about 35 HV after PWHT with time duration of 2 h and this reduction was increased to be about 100 HV after the application of PWHT with time duration of 10 h. However, there is no significant change in the hardness value of the base metal for this welded component. It is evident from these results that the hardness value in the HAZ is reduced as the time duration of PWHT increases due to the tempered structure which has been formed as a result of the application of these heat treatment schemes.

Finally, three different PWHT schemes were applied, which varied only in their cooling rate 10, 40 and 125°C/h. Figure 4.43 pointed out the maximum reduction in the hardness value can be obtained after the application of PWHT with cooling rate of 10°C/h. Meanwhile, the hardness value in the HAZ is reduced by about 35 and 20 HV after PWHT with cooling rates 40 and 125°C/h respectively. It is evident from these results that the hardness value of the HAZ is reduced by applying PWHT with slower cooling rate. It can also be noticed that there is no considerable difference in the hardness value by applying PWHT with cooling rate of 40 or 125°C/h.

It is also clearly evident from Figures 4.26, 4.27, 4.28, 4.29, 4.32, 4.33, 4.36, 4.37, 4.40 and 4.41 that the width of the HAZ becomes smaller as the distance from the specimen surface increases for all these above conditions.

Finally, comparison diagrams between the hardness value along the specimen axis have been plotted in Figures 4.30, 4.34, 4.38 and 4.42. It is evident from these results that the hardness value reduces as the distance from the specimen surface increases. It can be noticed from the microstructure inspection, that the small variation in the hardness value in the depth of the specimen of the HAZ does not have any substantial effect on varying the structure of the HAZ.

6.2.3 THE TENSILE TEST

The obtained results of this test showed that the tensile strength of as-welded condition has about the same value as the original metal. After the application of these different heat treatment schemes the tensile strength has been varied between a slight reduction and a considerable improvement depending on the heat treatment scheme.

Three PWHT schemes were applied which varied only in their soaking temperature. It is evident from these results that there is a considerable improvement in the tensile strength after the application of PWHT with soaking temperature of 550 °C. However, there is no significant change in the tensile strength after the application of PWHT with soaking temperature of 650 °C. It can be noticed (Table 4.3) that there is a slight reduction in the tensile strength after the application of PWHT with soaking temperature of 750 °C. It is evident from these results that the tempered martensite which has been formed after PWHT with soaking temperature of 550 °C has a significant effect on improving the strength of these welded joints. It can be pointed out that the formation of the precipitated carbide after PWHT with temperature of 750 °C has a deterioration effect on reducing the strength of this welded joint. These results are in full agreement with other studies [131, 132] which emphasize that the formation of the precipitated carbide would negatively effect the material strength.

After the application of PWHT with different heating rates the tensile strength has been improved and the maximum improvement has been obtained after the application of PWHT with heating rate of 400 °C/h. It is evident from these results that the faster heating rate has slightly improved the tensile strength of this welded joint.

After the application of PWHT with different time durations 0.5, 2 and 10 hours, with soaking temperature of 550 °C the strength has been improved and the maximum improvement was obtained after PWHT with time duration of 0.5 h. It is evident from these results that

shorter the time duration of PWHT the most effective is the improvement of the tensile strength.

Three PWHT schemes were applied which varied only in their cooling rate 10, 40 and 125 °C/h. It is evident from these results that the maximum improvement in the tensile strength has been obtained after the application of PWHT with cooling rate of 125 °C/h. It can be pointed out from these results that the faster cooling rate would have better effect on improving the tensile strength of this welded joint.

In this test, all the specimens were loaded to fracture and the fracture occurred outside the HAZ for as-welded and after PWHTs conditions. It is evident from this test that there is not any noticeable change in the HAZ area for all these different conditions. It is also evident that the size of the HAZ is decreased by increasing the soaking temperature and the fracture occurred closer to the welding zone. Plate 3.1 shows a photograph of different tensile specimens for as-welded condition and after the application of PWHT with soaking temperatures of 550, 650 and 750 °C. It was also found that there is no significant difference on the size of the HAZ by varying the heating rate, time duration and cooling rate.

It is also evident that the tensile strength of the HAZ has been slightly improved after the application of PWHT with soaking temperature of 750 °C.

6.2.4 NOTCHED-IMPACT TEST

This test was carried out before and after the application of PWHTs. Different PWHT schemes were employed which varied in their soaking temperature, heating rate, soaking time duration and cooling rate. The results of this test show that the impact toughness has been improved for different levels depending on the heat treatment condition. The results show that the impact energy of the original materials (18 J) is relatively higher than the toughness in the as-welded condition and after some of these heat treatment schemes.

It is evident from these results that after the application of PWHT with different soaking temperatures 550, 650 and 750 °C, the impact energy has been improved and the maximum improvement has been obtained after the application of PWHT with soaking temperature of 750 °C. It can be noticed that this soaking temperature (750 °C) has a higher tempering effect on reducing the sharp difference in the hardness variation and improving the impact toughness. However, the formation of the precipitated carbide has slight deterioration effect on reducing the tensile strength. It is evident from these results that the higher PWHT soaking temperature the most effective on improving the impact toughness.

Three different heat treatment schemes which have different heating rates were applied. The results show that there is no significant difference on the impact toughness by varying these heating rates. These results are in good agreement with the microstructure and the hardness tests which showed that there is no significant change on the microstructure or the mechanical properties by varying the heating rate for this welded joint.

The effect of the soaking time duration was studied, three different duration 0.5, 2 and 10 hours were applied. It is evident from these results that the maximum improvement in the toughness has been obtained after the application of PWHT with long time duration (10 hours). It can be pointed out that the longer PWHT time duration the most effective on improving the impact toughness for this welded joint.

Three PWHT schemes which varied only in their cooling rate 10, 40 and 125 °C/h were applied. It can be seen from these results that the impact toughness has been improved after the application of these heat treatment schemes and the maximum improvement has been obtained after PWHT with cooling rate of 10 °C/h. It is evident from these results that the slower cooling rate the most effective on improving the toughness of this welded joint.

6.3 THE RESIDUAL STRESS

As described in Chapter 4, the initial test was carried out to determine the residual stress in the welding zone. To carry out this test, a very thin layer from the surface of the welding zone was removed to produce a smooth surface for measuring the residual stress at the point in the middle of this zone (see Plate 4.13). It can also be seen from these results that the residual stress in the welding zone has about 10% higher value than the closest measurable point near the welding line. These results coincide with the residual stress distribution for different types of welded components which had been investigated by Masubuchi et al, [100]; Misra and Peterson [113] and Muraki et al, [104, 105].

With the objective of ensuring the accuracy of the above results, the residual stress was also measured at a very close point to the welding line, for both before and after this machining. It is evident from these results that there is no significant difference between the residual stress for both conditions, which means that the shallow machining did not contribute in relieving or increasing the residual stress in the welded component.

6.3.1 THE I-BEAM BOX-SECTION COMPONENT

After the above initial test, the residual stress measurements were made across the welded specimen at different distances (15, 35, 60, 80 mm) from the welding axis to determine the magnitude and distribution of the residual stress. These measurements were carried out for both before and after the application of PWHTs. The principal residual stresses were determined for each condition and the maximum and minimum residual stresses are plotted in Figures 4.45 and 4.46.

It is evident from these results that before the application of PWHT the maximum

residual stress has a high value near the welding line (about 330 N/mm² at a distance of 15 mm from the welding line). This high value of residual stress, especially near the welding line, emphasize the need of treating this welded joint to reduce or eliminate the residual stresses, which could have serious effects on the reliability of the welded joint [133].

It is evident that after the application of PWHT (580°C for 18 hrs) the maximum value of the residual stress is dropped by about 70%, which can be seen as a considerable reduction in the residual stress but at the same time there is still residual stress in the welded component which might affect the long term service life of the structure.

To assess the effect of both maximum and minimum residual stresses, the equivalent residual stress has been calculated at different points before and after PWHTs. The equivalent residual stress has been calculated from the following equation [126], which indicates the magnitude of the stress as compared to the yield stress in tension.

$$\sigma_{eq}=\sqrt{[\sigma_{max}^2+\sigma_{min}^2-\sigma_{max}\cdot\sigma_{min}]}$$

The equivalent residual stress shows that the maximum value of the residual stresses for as-welded condition is near the welding axis and it decreases as the distance from the welding increases. These results show that there is a substantial reduction in the hardness value after the application of this type of heat treatment. This comparison between the equivalent residual stresses for both before and after PWHT is illustrated in Figure 6.1.

6.3.2 THE LOW CARBON STEEL COMPONENT

It is evident from these results that after welding and before the application of PWHT the maximum residual stress reached a value of about 360 N/mm² near the welding line and it decreases as the distance from the welding line increases. These results coincide with those

reported by other researches [104, 105], which pointed out that the residual stress could reach the yield stress near the welding line. These high values of the residual stress emphasize the need for the application of PWHT to reduce or eliminate this residual stress in the welded component to avoid any failure in the structure during the service period.

It can be seen that after the application of PWHTs the residual stresses have been decreased for different levels depending on the heat treatment scheme. It is evident that after the application of PWHT with different soaking temperature, a substantial reduction in the maximum values of the residual stresses has been gained. Moreover, the residual stress was eliminated after the application of PWHT with soaking temperature of 650°C. Meanwhile, the maximum value of the residual stress is reduced by about 45% after the application of PWHT with soaking temperature of 450°C and by about 70% after PWHT with soaking temperature of 550°C. These results prove that the soaking temperature of PWHT is a very effective parameter in reducing the residual stress, and the maximum stress relief can be gained by increasing the soaking temperature of PWHT.

The distribution of the equivalent residual stresses are illustrated in Figures 6.2 to 6.5. Figure 6.2 shows the equivalent residual stresses before and after the application of PWHT with these different soaking temperatures. It is evident from these results that after PWHT with soaking temperature of 650 °C, the residual stresses have been virtually eliminated and the mechanical properties have been improved.

Different heat treatment schemes were applied which varied only in their heating rates. The results show that there is a good reduction in the residual stress value after the application of these heat treatment schemes, and the maximum value is reduced by about 45% after the application of these different schemes. It can be seen from these results that the residual stress is reduced to about the same value after the application of these different heat treatment schemes. It is evident from these results that there is no significant effect on the residual stress

by varying the heating rate of PWHT.

Figure 6.3 compares the equivalent residual stresses for these different conditions, before and after PWHT with different heating rates. It is evident from this figure that there is no significant difference in the residual stresses by varying their heating rates. These results coincide with the mechanical testing results which revealed that there is no difference in the mechanical properties by varying the heating rate.

To assess the effect of soaking time duration on the residual stress, three different soaking time durations were applied. Figure 6.4 shows a comparison diagram for the equivalent residual stresses before and after PWHT with these different soaking time durations. The results of this test show that there is a good reduction in the residual stress after the application of these schemes of heat treatments. It can be seen from these results that there is about 42% reduction in the maximum value of the residual stress after the application of PWHT with time duration of 0.5 h. This reduction is about 45% after PWHT with time duration of 2 h. Finally, the maximum residual stress is reduced by about 65% after the application of PWHT with soaking time duration of 10 h. It is evident from these results that the residual stress decreases as the soaking time duration increases.

Different PWHT schemes which varied in their cooling rates were applied. Figure 6.5 shows a comparison diagram for the equivalent residual stresses before and after PWHT with these different cooling rates. The results show that there is a substantial reduction in the residual stresses after the application of these different heat treatments schemes. It can be seen from these results that the maximum value of the residual stress is reduced by about 53% after the application of PWHT with cooling rate of 10°C/h. This value is reduced by about 45% after the application of PWHT with cooling rate of 40°C/h. Finally, the maximum value of the residual stress is reduced by about 42% after the application of PWHT with cooling rate of 125°C/h. It is evident from these results that a higher reduction in the residual stress can be obtained by

applying heat treatment with slow cooling rate. Whilst, there is a similar effect on the residual stress after the application of PWHT with cooling rates of 40 and 125 °C/h.

It is evident from these results that after the application of PWHT with soaking temperature of 650 °C the residual stresses have been virtually relieved. However, after the application of PWHT with long time duration (10 hours) and slow cooling rate (10 °C/h) the residual stresses have been reduced to a relatively low level.

6.3.3 THE STAINLESS-STEEL COMPONENT

The magnitude and distribution of the residual stress were determined for these types of welded components. These results show that before the application of PWHT the maximum residual stress value is about 220 N/mm² near the welding line and it decreases as the distance from the welding line increases. These results coincide with other researches which showed that the maximum value of the residual stresses will be in and near to the welding zone.

It is evident that the residual stress of the welding zone has about 15% higher value than the residual stress at a point close to the welding line. These residual stresses would affect the reliability of the welded component and have a deteriorating effect on long term service of this welded joint. PWHTs have been applied to reduce or eliminate these residual stresses and their harm effects.

As mentioned before, different PWHT schemes were applied which varied in their soaking temperature, heating rate, soaking time duration and cooling rate. It can be seen from these results that there is a considerable reduction in the residual stress value after the application of these schemes. The residual stresses have been reduced for different levels depending on the heat treatment scheme.

It can be seen from these results that after the application of PWHTs with different soaking temperature the maximum value of the residual stress is reduced by about 120 to 220 N/mm^2. After the application of PWHT with soaking temperature of 550°C, a reduction of about 55% in the maximum value of the residual stress was obtained. The maximum value of the residual stress is reduced by about 72% after the application of PWHT with soaking temperature of 650°C. Finally, a total residual stress relief has been obtained after the application of PWHT with soaking temperature of 750°C. Figure 6.6 shows a comparison diagram for the equivalent residual stresses before and after PWHTs with these different soaking temperatures. It is evident from these results that a higher reduction in the residual stress can be obtained by increasing the soaking temperature of PWHT. The maximum improvement was recorded after the application of PWHT with soaking temperature of 750°C where the residual stresses were virtually eliminated.

Three different schemes of PWHT were applied which varied only in their heating rates 50, 100 and 400 °C/h. While, the soaking temperature, time duration and cooling rate have been fixed as 550 °C, 2 hours and 40 °C/h respectively. The results show that there is a substantial reduction in the residual stress values after the application of these different schemes of PWHT where the reduction in the maximum value of the residual stress was about 55%. Figure 6.7 shows the distribution of the equivalent residual stresses before and after PWHT with different heating rates. It is evident from these results that there is no significant difference in the residual stress value by varying the heating rates of PWHT.

To study the effect of soaking time duration on the residual stresses, three different PWHT schemes were applied with different soaking time duration 0.5, 2 and 10 hours. While, the soaking temperature, heating and cooling rates have been fixed as 550 °C, 400 and 40 °C/h respectively. It can be seen from the results of this test that the maximum value of the residual stress is reduced by about 47% after the application of PWHT with soaking time duration of 0.5 h. However, it is reduced by about 55% after the application of PWHT with soaking time

duration of 2 hrs. Finally, after the application of PWHT with soaking time duration of 10 hrs the maximum value of the residual stress is reduced by about 68%. Figure 6.8 shows the distribution of the equivalent residual stresses before and after PWHTs with these different time durations. It is evident from these results that a higher stress relief can be obtained by applying PWHT with longer soaking time duration.

Three different cooling rates 10, 40 and 125 °C/h were investigated. The soaking temperature, heating rate and time duration were fixed as 550 °C, 400 °C/h and 2 hours respectively. A considerable reduction in the residual stresses was obtained after the application of PWHT with these different cooling rates. It can be seen from these results that there is about 65% reduction in the maximum value of the residual stress after the application of PWHT with cooling rate of 10°C/h. A reduction of 55% is obtained after the application of PWHT with cooling rate of 40°C/h. Finally, the maximum value of the residual stress is reduced by about 47% after the application of PWHT with cooling rate of 125 °C/h. Figure 6.9 shows the distribution of the residual stresses before and after PWHT with these different cooling rates. It is evident from these results that a higher reduction in the residual stress value can be obtained by applying PWHT with slower cooling rate.

6.4 OPTIMIZATION

6.4.1 THE LOW CARBON STEEL COMPONENT

It can be noticed from the previous discussions that the soaking temperature of PWHT is the most effective parameter in eliminating the residual stresses and improving the mechanical properties for this type of welded component. It is also evident that the heating rate does not have any significant effect on the residual stress or the mechanical properties. For these reasons the soaking temperature and the heating rate were chosen as 650 °C and 400 °C/h respectively.

The time duration and the cooling rate have been changed to optimize the heat treatment procedures which can be applied by shorter time, with the purpose of eliminating the residual stresses and improving the mechanical properties.

Two heat treatment schemes were applied which varied in the soaking time duration 0.5 and 1 h. While the soaking temperature, heating and cooling rates have been kept as 650 °C, 400 and 40 °C/h respectively. The results revealed that there is no significant difference on the microstructure and the mechanical properties after the application of these types of PWHTs. The residual stresses were reduced to low level after PWHT with time duration of 0.5 h. Moreover, the residual stresses were virtually eliminated after PWHT with time duration of 1 h. It is evident from these results that the time duration of not less than 1 h is the optimum soaking time duration with the above soaking temperature, heating and cooling rates.

To reduce the operating time of the heat treatment cycle, the cooling rate was also investigated. Two different cooling rates were applied 125 and 100 °C/h. The soaking temperature, heating rate and time duration were kept as 650 °C, 400 °C/h and 1 h respectively. It is evident from the results that the mechanical properties have been improved after the application of these heat treatments schemes. It can also be noticed that there is no significant difference in the mechanical properties after the application of these above heat treatment schemes. These results also proved that the residual stresses were virtually eliminated after the application of PWHT with cooling rate of 100 °C/h. Whilst, the residual stresses were reduced to a low level after PWHT with cooling rate of 125 °C/h. Figure 6.10 shows a comparison diagram for the equivalent residual stresses after the application of all the above PWHT schemes.

It can be pointed out from the above results that residual stresses could be eliminated without compromising the mechanical properties after the application of PWHT with cooling rate of not less than 100 °C/h. Meanwhile, the soaking temperature, heating rate and time duration

have been optimized as 650 °C, 400 °C/h and 1 h respectively.

6.4.2 THE STAINLESS-STEEL WELDED COMPONENT

The results obtained reveal that the residual stresses have been totally relieved after the application of PWHT with soaking temperature of 750 °C. It can be seen from the previous results that there is no significant effect on the residual stress or the mechanical properties by varying the heating rate.

With the objective of optimizing the heat treatment procedures for this type of welded component, the soaking temperature and the heating rate were chosen as 750 °C and 400 °C/h respectively. The soaking time duration and the cooling rate were investigated to achieve the shortest PWHT cycle which could eliminate the residual stresses without compromising the mechanical properties.

Two soaking time durations were applied 0.5 and 1 h. The soaking temperature, heating and cooling rate have been kept as 750 °C, 400 and 40 °C/h respectively. The results showed that the sharp difference in the hardness value between the HAZ and the base metal has been eliminated to a very low level and the metal toughness has been improved after the application of these two PWHT schemes. The results also revealed that the residual stresses were reduced to a very low level after PWHT with time duration of 0.5 h. Meanwhile, the residual stresses were virtually eliminated after the application of PWHT with time duration of 1 h. It is evident from these results that the residual stresses can be eliminated with the above heat treatment procedures with time duration of not less than 1 h.

Two different cooling rates 70 and 100 °C/h were applied with the purpose of obtaining

a shorter heat treatment cycle which could eliminate the residual stresses. The soaking temperature, heating rate and time durations were kept as 750 °C, 400 °C/h and 1 hour respectively. The results revealed that the metal toughness has been improved after the application of these two heat treatment schemes. Also the sharp difference in the hardness between the HAZ and the base metal has been reduced to a relatively lower level. Meanwhile, the residual stresses have been reduced to a very low level after the application of the above heat treatment procedures with cooling rate of 100 °C/h. It can be seen that the residual stresses have been virtually eliminated after the application of PWHT with cooling rate of 70 °C/h. Figure 6.11 shows a comparison diagram for the equivalent residual stresses after the application of all the above heat treatment schemes. It is evident that a heat treatment with soaking temperature of 750 °C, heating rate of 400 °C/h, time duration of 1 hour and cooling rate not faster than 70 °C/h will eliminate the residual stresses and reducing the hardness variation between the HAZ and the base metal to a very low level without compromising the metal toughness for this type of welded joint.

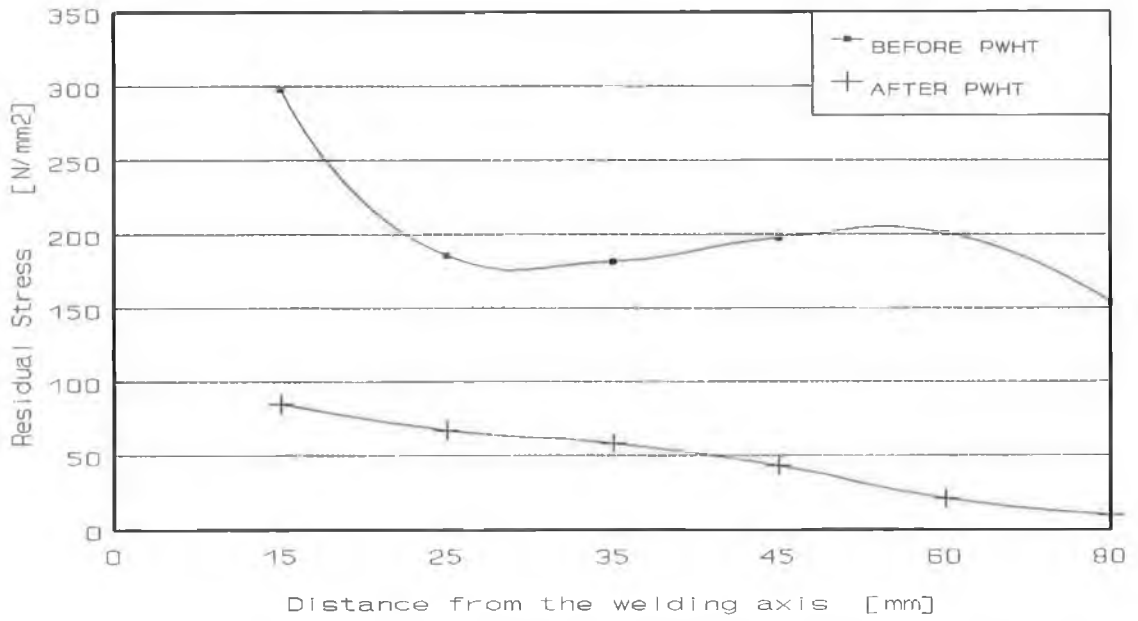

FIGURE 6.1 EQUIVALENT RESIDUAL STRESSES FOR I-BEAM BOX SECTION COMPONENT.

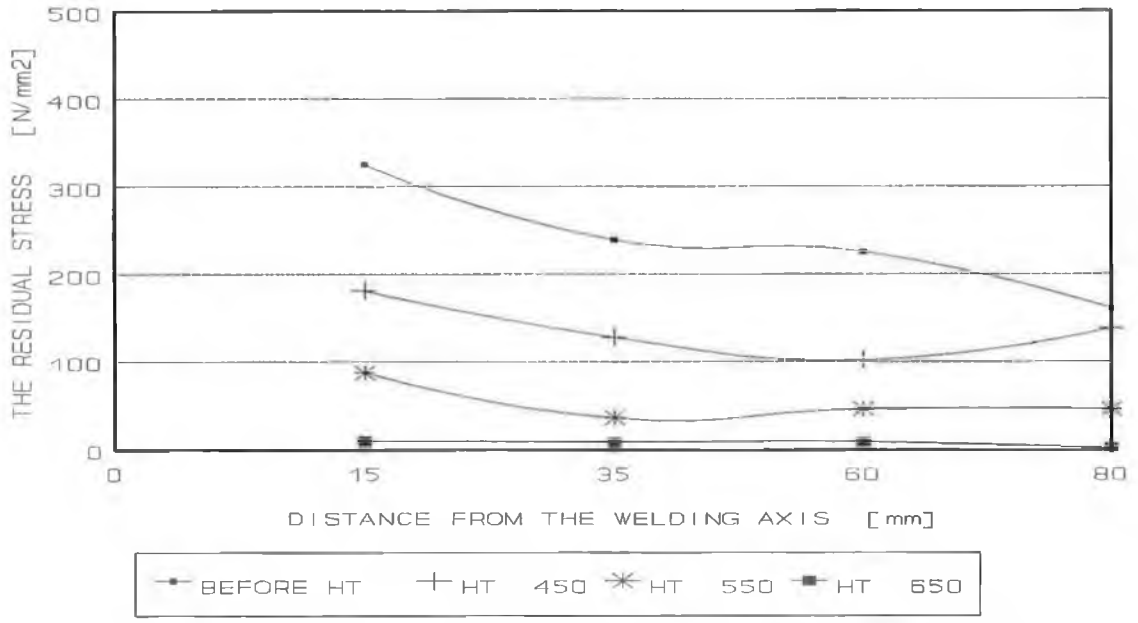

FIGURE 6.2 EQUIVALENT RESIDUAL STRESSES BEFORE AND AFTER PWHT WITH DIFFERENT SOAKING TEMPERATURES FOR AISI-1020 WELDED COMPONENT.

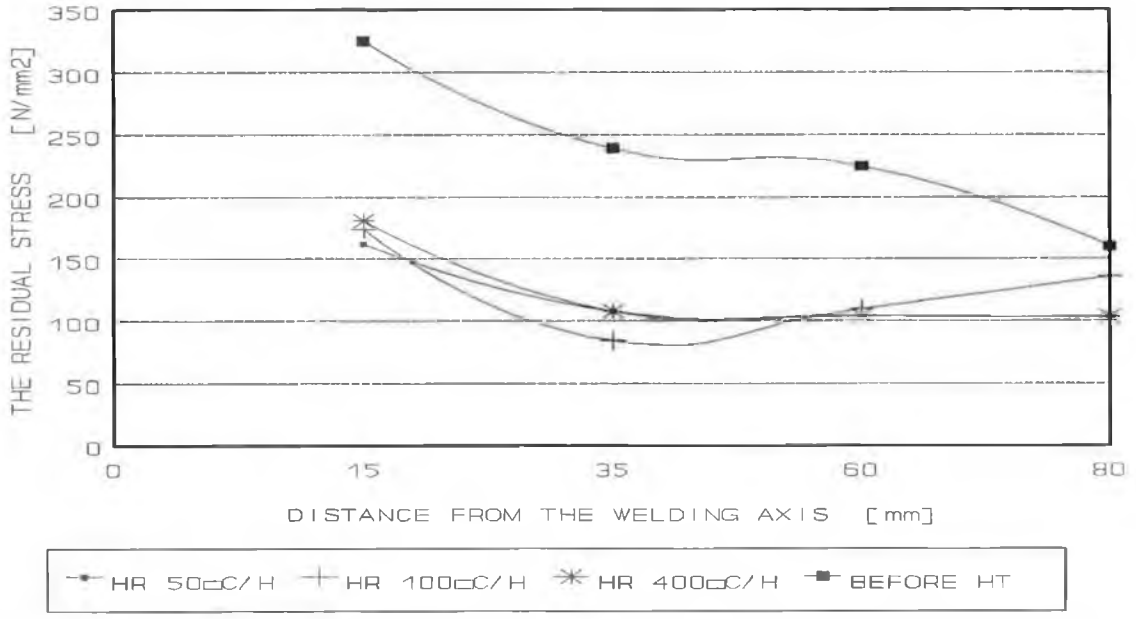

FIGURE 6.3 EQUIVALENT RESIDUAL STRESSES BEFORE AND AFTER PWHT WITH DIFFERENT HEATING RATES FOR AISI-1020 WELDED COMPONENT.

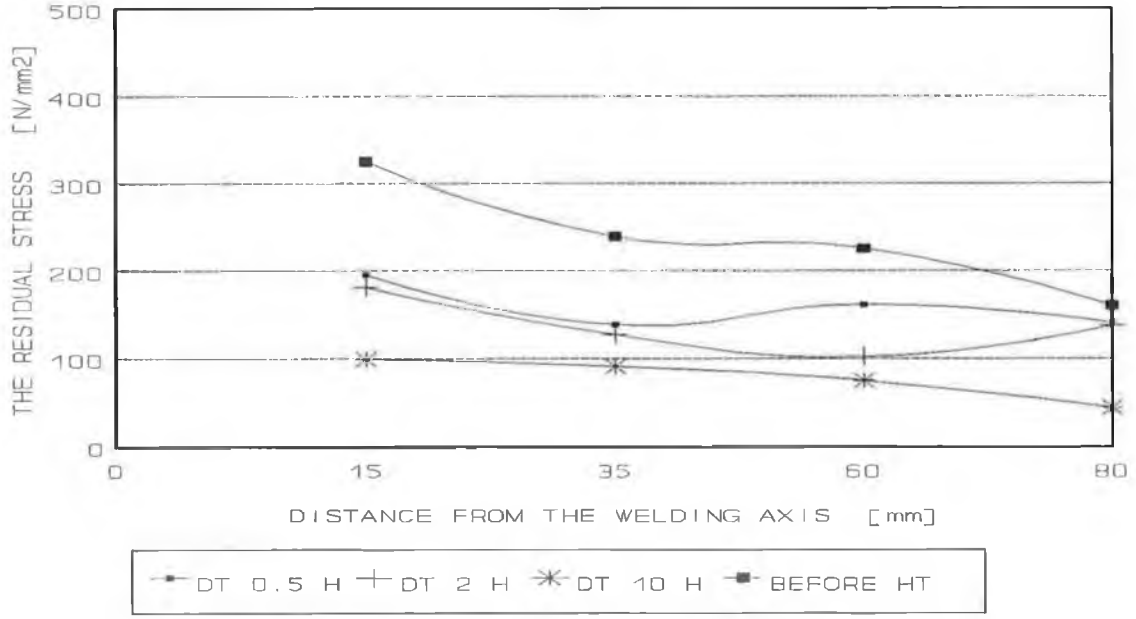

FIGURE 6.4 EQUIVALENT RESIDUAL STRESSES BEFORE AND AFTER PWHT WITH DIFFERENT TIME DURATIONS FOR AISI-1020 WELDED COMPONENT.

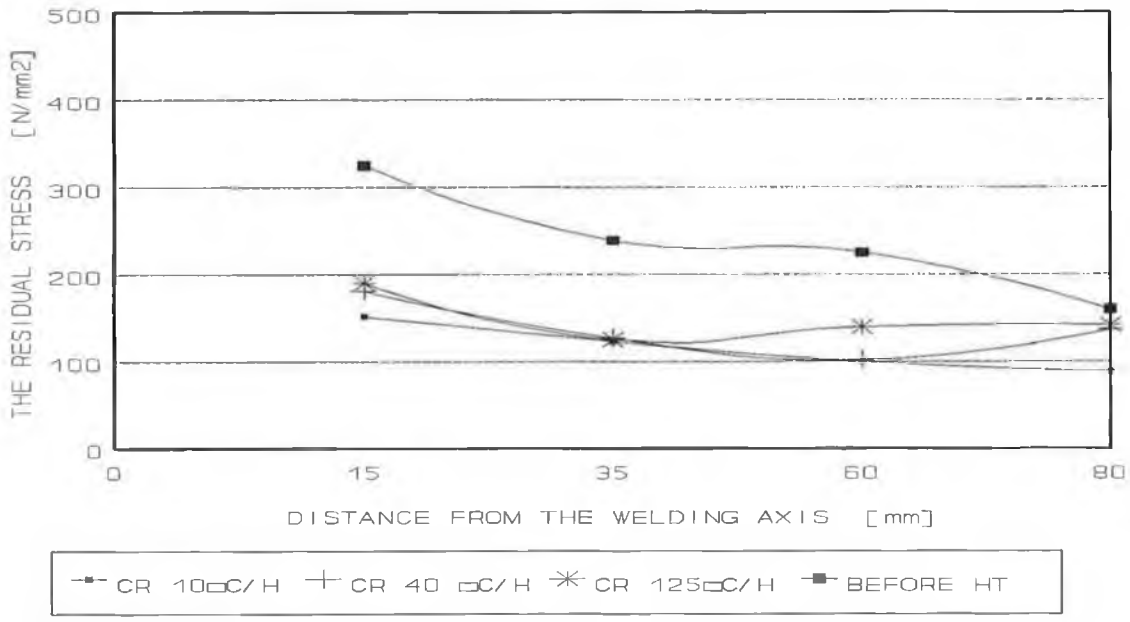

FIGURE 6.5 EQUIVALENT RESIDUAL STRESSES BEFORE AND AFTER PWHT WITH DIFFERENT COOLING RATES FOR AISI-1020 WELDED COMPONENT.

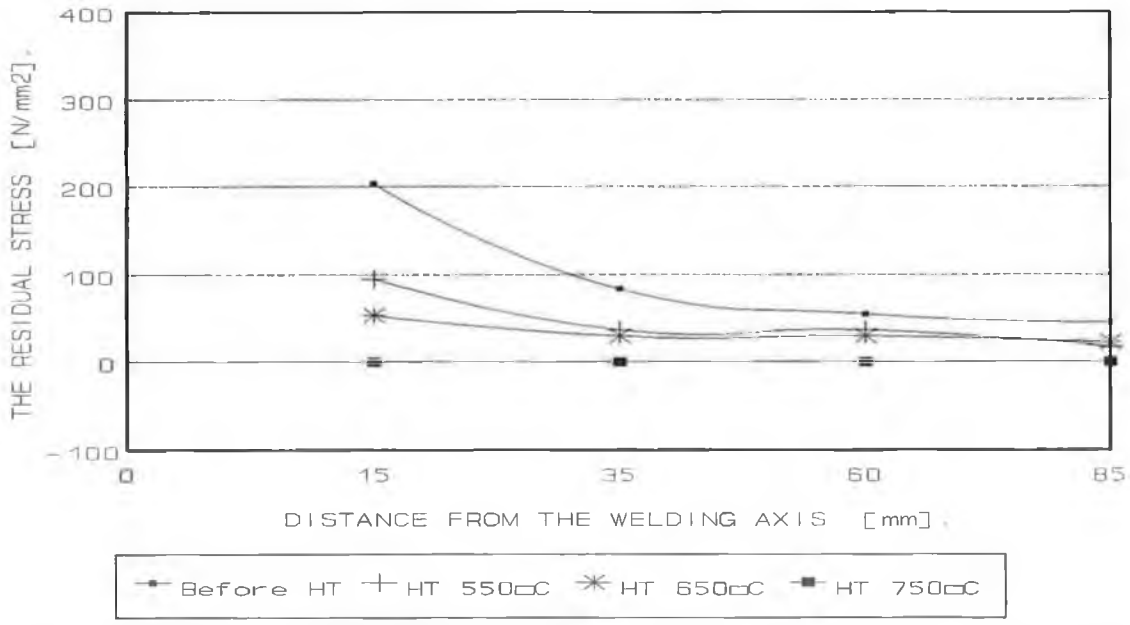

FIGURE 6.6 EQUIVALENT RESIDUAL STRESSES BEFORE AND AFTER PWHT WITH DIFFERENT SOAKING TEMPERATURES FOR AISI-410 WELDED COMPONENT.

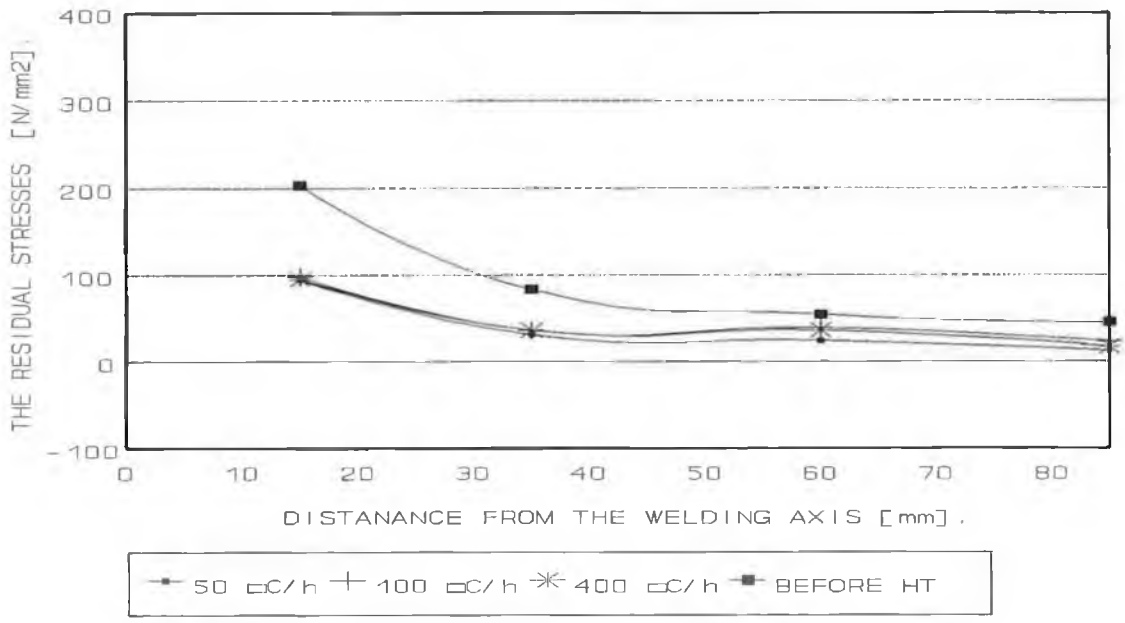

FIGURE 6.7 EQUIVALENT RESIDUAL STRESSES BEFORE AND AFTER PWHT WITH DIFFERENT HEATING RATES FOR AISI-410 WELDED COMPONENT.

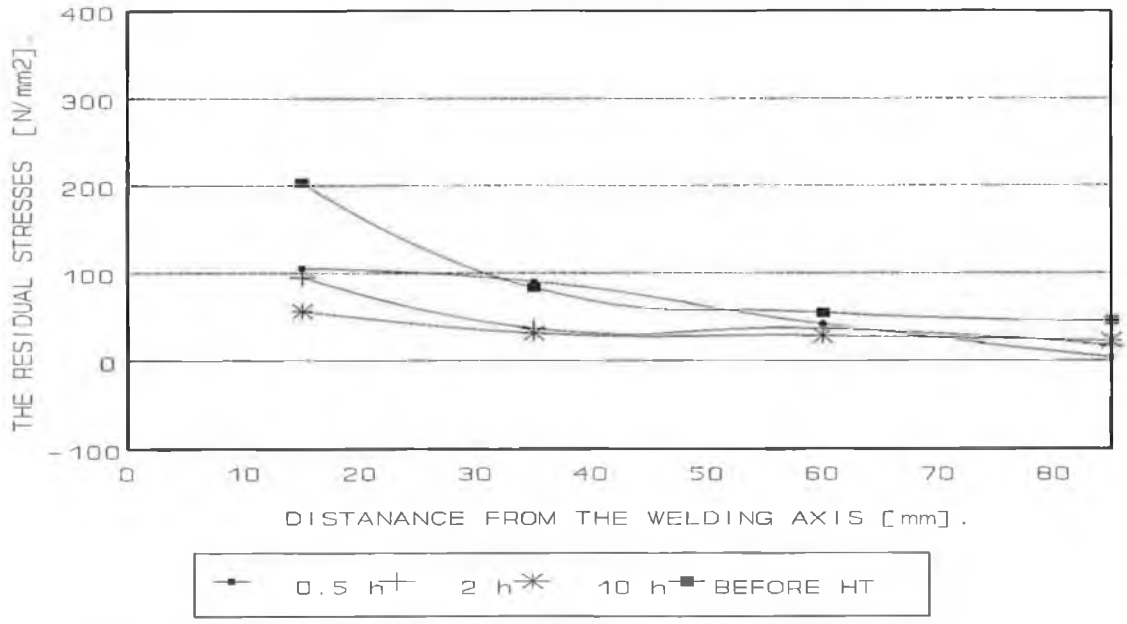

FIGURE 6.8 EQUIVALENT RESIDUAL STRESSES BEFORE AND AFTER PWHT WITH DIFFERENT TIME DURATIONS FOR AISI-410 WELDED COMPONENT.

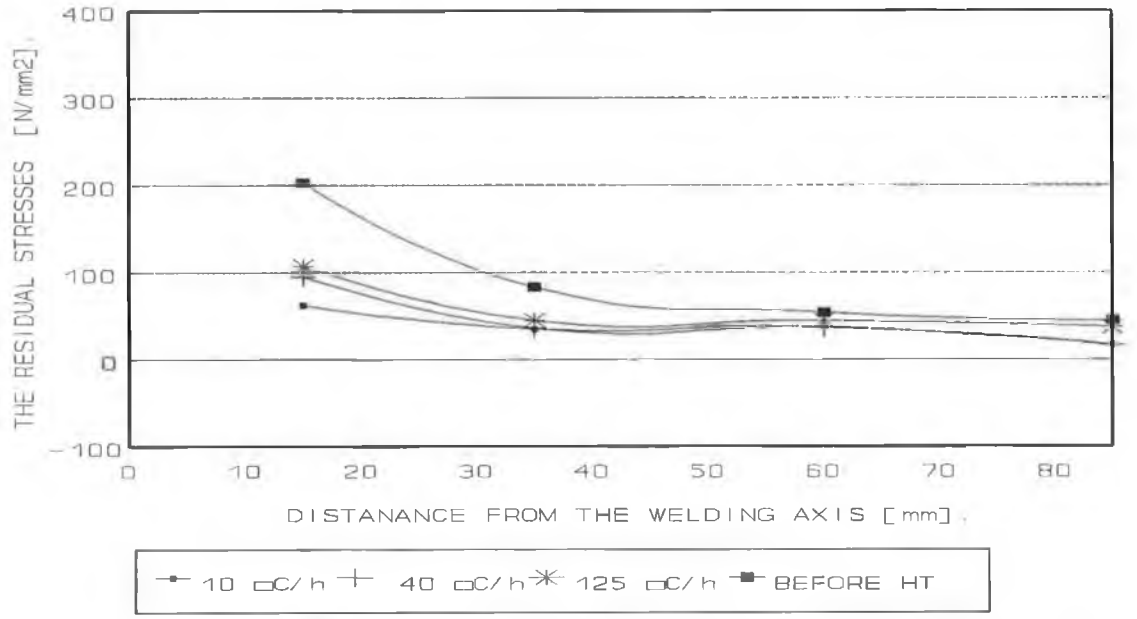

FIGURE 6.9 EQUIVALENT RESIDUAL STRESSES BEFORE AND AFTER PWHT WITH DIFFERENT COOLING RATES FOR AISI-410 WELDED COMPONENT.

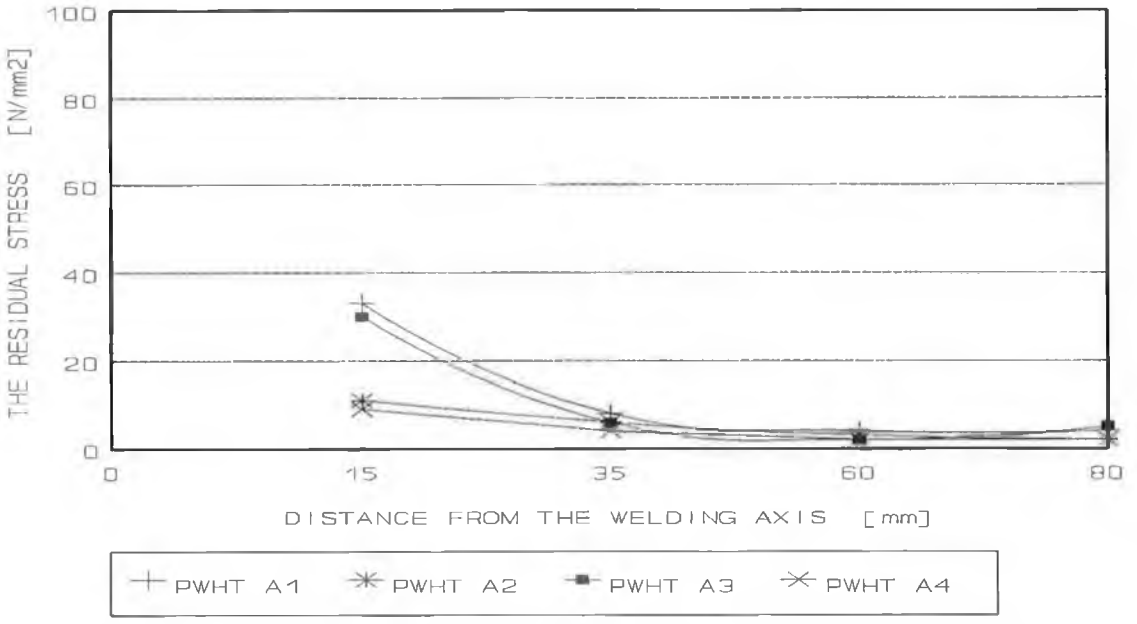

FIGURE 6.10 EQUIVALENT RESIDUAL STRESSES AFTER PWHTS (OPTIMIZATION) FOR AISI-1020 WELDED COMPONENT.

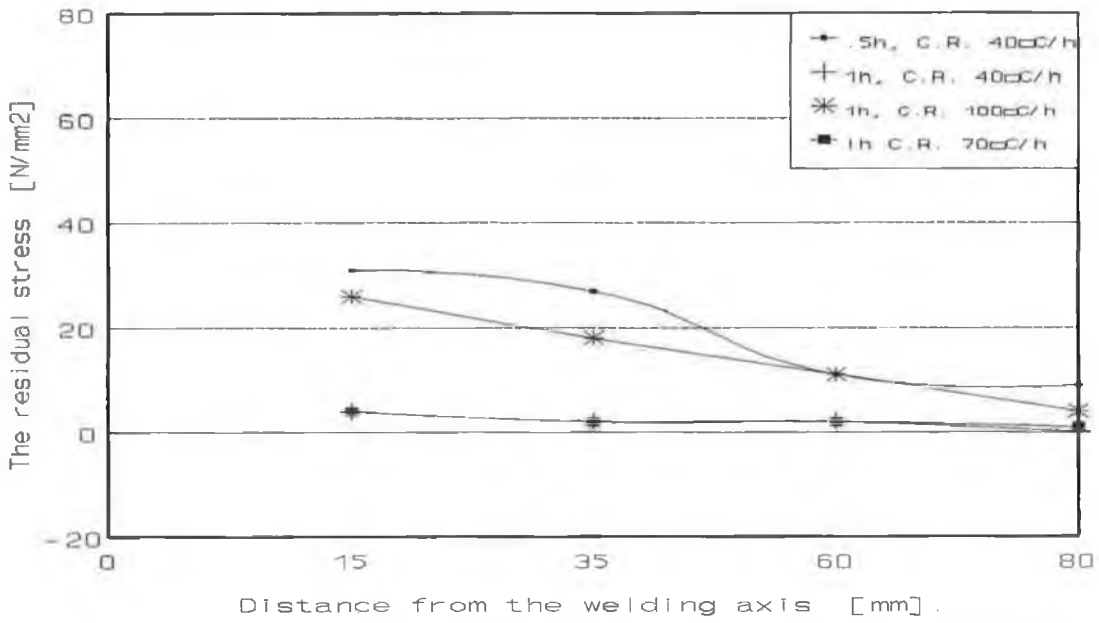

FIGURE 6.11 EQUIVALENT RESIDUAL STRESSES AFTER PWHTS (OPTIMIZATION) FOR AISI-410 WELDED COMPONENT.

CHAPTER SEVEN

CONCLUSION AND RECOMMENDATION

7.1 CONCLUSION

7.1.1 LOW CARBON STEEL COMPONENT

In this investigation, the effect of PWHT on low carbon AISI-1020 double-V welded joint has been studied. It can be concluded from this study that the PWHT has a substantial effect on reducing or eliminating the residual stresses with a good improvement in the mechanical properties. It has been found that the PWHT soaking temperature is the most effective parameter in the heat treatment cycle, and a soaking temperature of 650 °C is the most effective temperature for eliminating the residual stresses and improving the mechanical properties. It has also been found that there is no significant effect on the residual stresses and mechanical properties by varying the heating rate of PWHT. However, longer soaking time duration and the slower cooling rate have a considerable effect on reducing the residual stresses and improving the mechanical properties. For some components a minimum shorter soaking time is feasible which would give satisfactory and acceptable reduction in residual stress.

In this study, all heat treatment parameters have been optimized. It has been found that after the application of PWHT with soaking temperature, heating rate, time duration and cooling rate of 650 °C, 400 °C/h, 1 hour and 100 °C/h respectively the residual stresses have been virtually eliminated without compromising the mechanical properties.

7.1.2 STAINLESS-STEEL COMPONENT

The effect of PWHT on the microstructure, mechanical properties and residual stresses for double-V welded component of AISI-410 has been investigated. It can be concluded from this study that the PWHTs have considerable effect on reducing or eliminating the residual stresses without compromising the mechanical properties. It was found that the PWHT soaking temperature is the most important factor in the PWHT cycle, which can reduce the residual stress to a very low level. It was found that PWHT with a soaking temperature of 750 °C is the most effective temperature on eliminating the residual stress and reducing the hardness variation between the base metal and the HAZ to a low level and giving a homogeneous microstructure and improving the metal toughness.

It was found that there is no significant effect on the microstructure, mechanical properties and residual stresses by varying the heating rate of PWHT. However, there is a considerable effect on reducing the residual stress and improving the mechanical properties after the application of PWHT with longer soaking duration and slower cooling rate.

The heat treatment parameters have also been optimized. It was found that after the application of PWHT with soaking temperature of 750 °C, heating rate of 400 °C/h, soaking time duration of 1 hour and cooling rate of 70 °C/h, the residual stresses were virtually eliminated. The sharp difference in the hardness value between the base metal and the HAZ has been reduced to relatively very low level and a homogeneous microstructure has been obtained after the application of this type of heat treatment.

7.1.3 FINITE ELEMENT MODELLING

Finite element models have been developed to simulate stainless steel welded components in assumed ideal service condition. It was found from the finite element analysis that there is

considerable concentrated stress in and around the HAZ as a result of the existence of the residual stress in this type of welded component. This concentrated stress is virtually eliminated after the application of PWHT.

It was also found that this concentrated stress was decreased when the welding length or width were reduced. It can be pointed out that there is still concentrated stress in and around the welding line even with a very small welding zone. The PWHT could be very important procedure especially when the safety factor has a very important role during the component service.

It can also be suggested from this study that it is feasible to develop a mobile heat treatment device for localised heat treatment to a long beam structure manufactured by welding steel I-beam sections or any other large welded component.

7.2 FURTHER WORK

In any future work the following aspects may be considered:

1- Improved finite element models may be developed to predict the residual stresses for these types of welded components, which can be compared the current results which have been obtained in this research.

2- Other non-destructive residual stress measurement methods could be applied for the same conditions to compare the accuracy and effectiveness of hole-drilling method.

3- The same procedure of this research could be applied for different materials such as, ceramics and composites.

4- The effect of different welding processes on the residual stress may be investigated.

REFERENCES

1 - *A.D.Althouse, C.H.Turnquist, W.A.Bowditch and K.E.Bowditch.* **Modern welding.** Published by AWS. ISBN: 0 87006 668 4.

2 - *H.B.Cary.***Modern welding technology.** Published by AWS. ISBN: 0 13 599290 7.

3 - *K.Heindlhoffer.* **Evaluation of residual stress.** Published by McGraw - Hill, New York, 1948.

4 - *O.J.Horger.* **Residual stresses.** Handbook of experimental stress analysis, Edited by Hetenyi,M., New York, 1950.

5 - *R.G.Treuting, J.J.Lynch, H.B.Wishart, and D.G.Richards.* **Residual stress measurements.** Published by ASM 1952.

6 - *R.Gunnert.* **Measuring of residual stresses and strains.** Document No: X-286-62-0E, National Institute of Welding, 1962.

7 - *L.Mordfin.* **Measurement of residual stresses: problems and opportunities.** International Conf.on residual stress of designers and metallurgists, 9 - 10 April 1980, Chicago U.S.A. PP 189-210.

8 - *K.Masubuchi.* **Analysis of welded structures.** Published by Pergamon press, 1980, PP 114-115.

9 - *A.G.Olabi.* **The effect of PWHT and distribution of residual stress in weld repaired high chromium steel components.** M.Eng thesis, Dublin City University, 1990.

10 - *R.Kume, H.Okabayashi, and M.Amano.* **Mechanism of underclad cracking - combined effects of residual strain and heat affected zone ductility.** J. of eng. materials and technology, Oct 1976, PP 348-356.

11 - *W.A.Ellingson, and W.J.Shack.* **Residual stress measurements on multi pass weldments of stainless steel piping.** Experimental Mechanics, v:19 n:9 1979, PP 317-323.

12 - *J.Mathar.* **Determination of initial stresses by measuring the deformations around drilled holes.** Transactions of ASME v:56 n:4 1934, PP 249-254.

13 - *W.Soete.* **Measurement andrelaxation of residual stresses.** Welding Journal, v:28 n:8 1949, PP 354s-264s.

14 - *E.W.Suppiger, C.Riparbelli, and E.R.Ward.* **The determination of initial stresses and results of tests on steel plates.** Welding Journal, v:30 n:2 1951, PP 91s-104s.

15 - *N.J.Rendler, and I.Vigness.* **Hole drilling method on measuring residual stresses.** Experimental Mechanics v:6 n:12 1966, PP 577-586.

16 - *B.P.Gupta.* **Hole drilling technique: modifications in the analysis of residual stresses.** Experimental Mechanics v: 13 1973, PP 45-48.

17 - *A.M.Nawwar, K.McLachlan, and J.Shewchuk.* **A modified hole drilling technique for determining residual stresses in thin plate.** Experimental Mechanics v:16 n:6 1976, PP 226-232.

18 - *A.J.Bush, and F.J.Kromer.* **Simplification of the hole drilling method of residual stress measurement.** Transactions of ISA v:12 n:3 1973, PP 249-259.

19 - *E.Procter, and E.M.Beaney.* **Recent developement in the centre hole drilling technique for residual stress measurement.** Experimental Techniques v:6 1982, PP 10-15.

20 - *C.L.Chow, and C.H.Cundiff.* **On residual stress measurements in light truck wheels using the hole drilling method.** Experimental Mechanics v:25 n:1 1985, PP 54-59.

21 - *M.T.Flaman.* **Brief investigation of induced drilling stresses in the centre hole method of residual stress measurement.** Experimental Mechanics v:22 n:2 1982, PP 26-30.

22 - *A.Niku-lari, J.Lu, and J.F.Flavenot.* **Measurement of residual stress distribution by the incremental hole drilling method.** Experimental Mechanics v:25 n:2 1985, PP 175-185.

23 - *M.T.Flaman, and B.H.Manning.* **Determination of residual stress variation with depth by the hole drilling method.** Experimental Mechanics v:25 n:3 1985, PP 205-207.

24 - *M.T.Flaman, and J.M.Boag.* **Comparison of residual stress variation with depth analysis techniques for the hole drilling method.** Experimental Mechanics v:30 n:2 1990, PP 352-355.

25 - *J.E.Bynum.* **Modifications to the hole drilling technique of measuring residual**

stresses for improved accuracy and reproducibility. Experimental Mechanics v:21 n:1 1981, PP 21-31.

26 - *M.Kabiri.* **Measurement of residual stresses by the hole drilling method: influences of transverse sensitivity of the gages and relieved strain coefficients.** Experimental Mechanics v:24 n:3 1984, PP 252-256.

27 - *M.Kabiri.* **Nonuniform residual stress measurement by the hole drilling method.** Experimental Mechanics v:24 n:4 1984, PP 328-336.

28 - *J.Wang.* **Measurement of residual stress by the hole drilling method: general stress strain relationship and its solution.** Experimental Mechanics v:28 n:4 1988, PP 355-358.

29 - *J.Wang.* **Measurement of residual stress by the hole drilling method: on the direction of maximum residual stress.** Experimental Mechanics v:28 n:1 1988, PP 24-26.

30 - *J.H.Norton, and D.Rosenthal.* **Stress measurement by X-ray diffraction.** Proceedings of the society for experimental stress analysis v:1 n:2 1944, PP 73-76.

31 - *J.H.Norton, and D.Rosenthal.* **Applications of the X-ray diffraction method of stress measurement to problems involving residual stress in metals.** Proceedings of the society for experimental stress analysis v:1 n:2 1944, PP 81-90.

32 - *R.H.Marion, and J.B.Cohen.* **Anomalies in measurement of residual stress by x-ray diffraction.** Advances in X-Ray Analysis, v:18 1974, PP 34-45.

33 - *M.James, and J.B.Cohen.* **PARS - a portable X-ray analyzer for residual stresses.** Journal of Testing and Evaluation v:6 1978, PP 91-97.

34 - *C.O.Ruud, P.S.DiMascio, and D.M.Melcher.* **Nondestructive residual stress measurement on the inside surface of stainless steel pipe weldments.** Experimental Mechanics, v:24 n:2 1984, PP 162-168.

35 - *N.E.Dowling, R.W.Hendricks, and K.Ranganathan.* **X-ray residual stress measurements in notched test specimens.** Journal of Testing and Evaluation, v:16 n:5 1988, PP 456-460.

36 - *B.Eigenmann, B.Scholtes, and E.Macherauch.* **Determination of residual stresses in ceramics and ceramic-metal composites by x-ray diffraction methods.** Materials

Science and Engineering, v:118A n:1-2 1989, PP 1-17.

37 - *C.A.Peck.* **Practical aspects of residual stress measurement by x-ray diffraction.** Proceedings of ASM's conference on residual stress in design, Ohio USA, 1987, PP 7-9.

38 - *C.Glinka, and H.J.Prask.* **Neutron diffraction and small angle scattering as nondestructive testing probes of the microstructure of materials.** Mechanics of Nondestructive Testing, Plenum Press 1980, PP 143-164.

39 - *A.Allen, C.Andreani, M.T.Hutchings, and C.G.Windsor.* **Measurements of internal stresses within bulk materials using neutron diffraction.** NDT International, v:14 1981, PP 249-254.

40 - *T.Lorentzen.* **Nondestructive evaluation of residual stresses by neutron diffraction.** NDT International, v:21 n:6 1988, PP 385-388.

41 - *L.Pintschovius.* **Determination of residual stresses by neutron diffraction.** Memories et etudes Scientifiques revue de metallurgie, v:86 n:11 1989, PP 723-728.

42 - *G.F.Modlen, P.J.Webster, X.Wang, and G.Mills.* **An investigation of residual stresses in cold extruded and in cold drawn rods using neutron diffraction.** Proceedings of the International Conference of Sheet Metal, April 1992, UK, PP 171-180.

43 - *N.N.Hsu, and W.Sachse.* **Review of ultrasonic techniques for measuring residual stress.** 38th National ASNT Fall Conf, Oct 1978, Denver.

44 - *J.S.Heyman.* **A CW ultrasonic bolt strain monitor.** Experimental Mechanics, v:17 n:5 1977, PP 183-192.

45 - *N.N.Hsu.* **Acoustical birefringence and the use of ultrasonic waves for experimental stress analysis.** Experimental Mechanics, v:14 n:5 1974, PP 169-178.

46 - *J.J.Dike, and G.C.Johnson.* **Residual stress determination using acoustoelasticity.** Journal of Applied Mechanics, v:57 n:1 1990, PP 12-17.

47 - *R.L.Pashley.* **Barkhausen effect - an indication of stress.** Materials Evaluation, v:28 n:7 1970, PP 157-161.

48 - *R.Rautioaho.* **Influnce of tensile and cyclic loading upon Barkhausen noise in a mild steel.** Materials Evaluation, v:37 n:9 1979, PP 45-51.

49 - *K.Kashiwaya, H.Sakamoto, and Y.Inoue.* **Non-destructive measuring method of residual stress using magnetic sensors.** Materials Laboratory, v:29 n:3 1988, PP 126-133.

50 - *L.P.Karjalainen, M.Moilanen, and R.Rautioaho.* **Evaluating the residual stresses in welding from Barkhausen noise measurements.** Materialpruf, v:22 1980, PP 196-200.

51 - *K.Titto.* **Use of Barkhausen effect in testing for residual stresses and material defects.** Proceedings Of ASM's Conference on Residual Stress in Design, Ohio USA, 1987, PP 27-35.

52 - *V.A.Vinokurov.* **Mechanical aspect of stress reliaving by heat and non-heat treatment.** Proceedings of the International Conference on Stress Relieving Heat Treatments of Welded Steel Constructions, Bulgaria, 1987, PP. 1-11.

53 - *K.N.Krishnan, and K.P.Rao.* **Effect of post weld heat treatment on microstructural changes and ferrite content in austenitic weld metals.** Praktische Metallographic, 1990, v:27 n:10 PP. 524-532.

54 - *B.M.Bmankirski.* **Effect of vibration and heat treatment on the mechanical properties of the metal and welded joints in 20K steel.** Welding Production, v:32 n:3 1985, PP. 26-28.

55 - *G.Q.Zhou.* **Improvement of the mechanical properties of 2Cr13 steel welded joints.** Presented at the Ninth North American Manufacturing Research conference, 1981, Pennsylvania, USA. PP. 114-119

56 - *W.Burget, and J.Blauel.* **Comparison of procedure qualification test welds and weld joints in plates and pipes for offshore construction in COD tests.** Schweissen, v:40 n:4 1988, PP. E56-E59.

57 - *A.Akhtar.* **Field welding of stainless steel hydraulic turbines.** International Water Power and Dam Construction, 1985, v:37 n:8 PP. 21-25.

58 - *R.V.Salkin.* **The desirability of unifying ideas and codes on stress releif thermal heat treatments.** FWP Journal, 1988, v:28 n:11, PP. 27-34.

59 - *G.A.Adoyan, Y.S.Aldoshin, A.M.Gerchikov, and S.A.Shevchuk.* **Specimen for evaluating the distortion of metal under the effect of residual welding stresses.**

Welding Production, v:31 n:3 1984.

60 - *G.M.Evans.* **Effect of stress relieving on the microstructure and properties of C-Mn all welded metal deposits.** Welding Journal, v:65 n:12 1986, PP. 326s-334s.

61 - *G.M.Evans.* **The effect of carbon on the microstructure and properties of all weld metal deposits.** Welding Research Supplement, Nov. 1983, PP. 313s-320s.

62 - *G.M.Evans.* **Effects of Sulphur and Phosphorus on misrostructure and properties of C-Mn all welded metal deposits.** Metal Construction, v:18 n:10 1986, PP. 631R-636R.

63 - *G.M.Evans.* **Effects of Silicon on the microstructure and properties of C-Mn all welded metal deposits.** Metal Construction, v:18 n:7 1986, PP. 438R-444R.

64 - *G.M.Evans.* **The effect of heat input on the microstructure and properties of all weld metal deposits.** Welding Research Supplement, April 1982, PP. 125s-132s.

65 - *G.M.Evans.* **Factors affecting the microstructure and properties of all weld metal deposits Part1. Interpass temperature.** Welding Review, Feb. 1982, PP. 14-20.

66 - *G.M.Evans.* **Factors affecting the microstructure and properties of all weld metal deposits Part2. Electrod diameter.** Welding Review, May 1982, PP. 4-8.

67 - *G.M.Evans.* **Factors affecting the microstructure and properties of all weld metal deposits Part3. Welding position.** Welding Review, Aug. 1982, PP. 6-10.

68 - *Y.Toshioka.* **Heat treatment deformation, residual stress and their effects: An overview.** Adv. in Sur. Treat. Technol. 1986, v:3, PP. 1-24.

69 - *Anon* **Post weld treatments of steel pressure vessels.** Indian Welding Journal, v:17 n:3 1985, PP. 61-66.

70 - *J.Bonsansky, D.A.Porter, H.Astrom, and K.E.Easterling.* **Effects of stress annealing treatment on the structure of high heat-input welds containing Nb and Mo.** Scandinavian Journal of Metallurgy, v:6 n:3 1977, PP. 125-131.

71 - *R.Fidler.* **The effect of time and temperature on residual stresses in aus tenitic welds.** Presented at Pressure Vessels and Piping Conf. of ASME, 1982, Orlando, USA.

72 - *Y.Ito, M.Ikeda, K.Bessyo, M.Nakanishi.* **Bond brittleness of welded high strength steel.** Sumitomo Search, 1970 Nov., v:4 PP. 19-40.

73 - *I.Hrivnak.* **A review of the metallurgy of heat treatment of welded joints.** International Journal Pres. Ves. and Piping, 1985, v:20 PP. 223-237.

74 - *J.M.Vitek, N.H.Packan, and S.A.David.* **Microstructural evaluation of Fe-3Cr-1.5Mo-0.1V thick-section electron beam welds.** Proceedings of an International Conference on Trends in Welding Research, USA, 1986, PP. 203-207.

75 - *F.Gauzzi, and S.Missori.* **Microstructural transformations in austenitic-ferritic transition joints.** J. of Materials Science, 1988, v:23 n:3 PP. 782-789.

76 - *M.Takemoto, T.Shinohara, M.Shirai.* **Improvement of stress corrosion cracking resistance of weldments.** Presented at the 82 international corrosion forum, 1982, Houston TX. USA.

77 - *R.A.Farrar.* **Microstructure and phase transformations in duplex 316 manual metal arc weld metals.** J. of Materials Science 1987, v:22 n:1 PP. 363-373.

78 - *A.S.Zubchenko, and E.A.Suslove.* **Hardening and stress relaxation in reheating welded joints in 15Kh2MFA and 15Kh2NMFA steels.** Welding Production, v:33 n:1 1986, PP. 30-33.

79 - *I.Z.Mashinson.* **Examination of factors influencing the impact toughness of high-frequencywelded joints in pipes.** Welding Production, v:33 n:2 1986, PP.26-27.

80 - *T.P.S.Gill, and G.B.Gnanamoorthy.* **Effect of alloy composition on the transformation kinetics of delta ferrite in type 316 stainless steel weld metal.** Indian welding journal, 1986, v:18 n:2 PP. 61-64.

81 - *Anon* **Relieving stress without heat.** Tooling and Production, v:44 n:9 1978, PP. 62-63.

82 - *E.P.Olenin, A.S.Averin, E.V.Dobrotina, and O.K.Alekseev.* **Reducing the residual stresses in welded components by vibrational treatment.** Welding Production, v:30 n:5 1983, PP.10-21.

83 - *T.Hebel.* **Better way to relief stress.** Am. Mach. Autom. Manuf., v:130 n:12 1986, PP. 70-72.

84 - *D.S.Keller.* **Ultrasonic stress relieving.** Metal Treating, v:12 n:2 1970, PP.14-15.

85 - *B.V.Merrin, and E.P.Olenin.* **Reducing the residual welding stresses by the electrohydraulic treatment of welded joint.** Welding Production, v:28 n:1 1981,

PP. 1-2.

86 - *I.Hrivnak, and K.A.Yushchenko.* **Principles of mechanical stress-relief treatment.** Proceedings of the International Conference on Stress Relieving Heat Treatments of Welded Steel Constructions, Bulgaria, 1987, PP. 13-28.

87 - *E.A.Rikur, R.A.Zaripov, E.G.Starchenko, and N.A.Perlov.* **Flexible water-cooled inductor for local heating.** Chem. and Petol. Eng. 1991, v:26 n:7-8, PP. 385-387.

88 - *P.M.Korol'Kov.* **Local heat treatment of welded joints in large spherical tanks.** Chem. and Petrol. Eng. 1991, v:26 n:7-8, PP. 444-447.

89 - *A.A.Astaf'ev, L.I.Lepekhina, N.M.Batieva, M.Y.Khalikov, N.A.Viktorov, and S.N.Blozhko.* **The effect of heat treatment on the level of residual stresses and the properties of submerged-arc welded joints of steel 08KH18n10T.** Russian Metallurgy, 1986, v:2, PP. 114-119.

90 - *M.W.Wilson, and C.C.Hao.* **Residual stresses in welded structures.** Welding Research Supplement, May 1947,PP. 295s-320s.

91 - *P.M.Simpson.* **Residual stress analysis of type 304 austenitic stainless steel pipe weldments.** Presented at the International Conf. of Exposition on Fatigue, Corrosion, Cracking, Fracture Mechanics Failure Analysis." 1985, Salt Lake City, USA.

92 - *B.M.Botros.* **Temperature distribution in Arc welding metallic structures and its effect on the generated residual stresses.** 11th NAMRC, May 24-26, 1983, PP. 88-91.

93 - *M.Lamb, D.R.F.West, and W.M.Steen.* **Residual stresses in two laser surface melted stainless steels.** Materials Science and Technology, 1986, v:2 n:9 PP. 974-980.

94 - *D.G.Berghaus.* **Residual stresses at small diffusion welds.** Experimental Techniques, 1986, V.10 Pt.3 P 40-42.

95 - *R.D.Thomas JR.* **HAZ cracking in thick sections of austenitic stainless steel - part 1.** Welding Journal, 1984, v:63 n:12 PP. 24-32.

96 - *R.D.Thomas JR.* **HAZ cracking in thick sections of austenitic stainless steels - part 2.** Welding Journal, 1984, v:63 n:12 PP. 355 S-368 S.

97 - *C.D.Lundin, J.A.Henning, and R.Menon.* **Post weld heat treatment cracking in Cr-**

Mo steels. 67th American Welding Society Annual Meeting, April 1986, PP. 154-156.

98 - *W.E.Leyda, L.Katz, M.Gold, R.L.Synder.* **Stress rupture properties of C-Mo Cr-Mo, stainless steel, and Ni-Cr-Fe welds.** Presented at Winter Ann Meet of ASME 1978, San Fransisco, USA.

99 - *D.Rosenthal.* **Mathematical theory of heat distribution during welding and cutting.** Welding J., 1941, v:20 PP. 220s-234s.

100- *K.Masubuchi, M.Nishida, G.Yamamoto, K.Kitamura, and C.Taniguchi.* **Analysis of thermal stresses and metal movements of weldments: A basic study toward computer-aided analysis and control of welded structures.** Presented at the Annual Meeting for the Society of Naval Architects and Marine Engineers, New York USA, 1975, PP. 1-21.

101- *L.Tall.* **Residual stresses in welded plates-A theortical study.** Welding Journal, 1964, v:43 n:1, PP. 10s-23s.

102- *L.E.Lindgren.* **Temperature fields in simulation of butt- welding of large plates.** Commun. Appl. Num. Methods, 1986, v:2, PP.155-164.

103- *J.Goldak, A.Oddy, M.McDill, A.Chakravarti, M.Bibby, and R.House.* **Progress in computing residual stress and strain in welds.** Proceedings of an International Conference on Trends in Welding Research, USA, 1986, PP. 523-527.

104- *T.Muraki, J.J.Bryan, and K.Masubuchi.* **Analysis of thermal stresses and metal movement during welding, Part1 analytical study.** Journal of Engineering Materials and Technology, 1975, PP. 81-84.

105- *T.Muraki, J.J.Bryan, and K.Masubuchi.* **Analysis of thermal stresses and metal movement during welding, Part2 comparison of experimental data and analytical results.** Journal of Engineering Materials and Technology, 1975, PP. 85-91.

106- *L.A.Van Gulick.* **Finite element welding computations using general purpose nonlinear analysis codes.** Presented at Advanced Topics in Finite Element Analysis, 1988 Pittsburgh, USA.

107- *J.E.Agapakis, and K.Masubuchi.* **Thermal stress relieving of high strength and stainless steel weldments.** Int. Conf. on Computer Applications, Tokyo, Aug. 28-30,

1973.

108- K.Kussmaul, E.Roos, and W.Guth. **A contribution to the numerical and experimental determination of residual stresses in welds.** Nuclear Engineering and Design, 1989, v:112 PP. 337-348.

109- C.E.Majorana, G.Navarro, and B.A.Schrefler. **Numerical and experimental analysis of the residual stresses in welding processes.** International Journal of Computer Application in Technology, 1988, v:1 n:1-2 PP. 96-104.

110- V.Ramamurti, S.Suresh, B.Raghuraman, and G.Ravichandran. **Residual stress analysis in weldments.** Engineering Fracture Mechanics, 1991, v:38 n:6 PP. 385-391.

111- S.C.Tam, L.E.Lindgren, and L.Y.Yang. **Computer simulation of temperature fields in mechanised plasma Arc welding.** Journal of Mechanical Working Technology, 1989, v:19 PP. 23-33.

112- J.M.Argyris, J.Szimmat, and K.J.Willam. **Finite element analysis of Arc welding processes.** International Journal of Computer Application in Technology, 1988, v:1 PP. 249- 259.

113- A.Misra, and H.A.Peterson. **Examination of the ring method for determination of residual stresses.** Experimental Mechanics, 1981, v:21 n:3 PP.268-272.

114- N.A.Crites. **Today's strain gauges, Equipement and application.** Product Engineering, Mar 19 1962, PP. 85-93.

115- N.A.Crites. **Your guide to today's strain gauges.** Product Engineering, Feb 19 1962, PP. 69-81.

116- E.G.Wenski. **Small strain gauge applications.** Experimental Techniques, 1990, PP. 40-43.

117- Y.M.Cheong, and H.L.Marcus. **Residual stresses in composite materials: an overview of measurement methods used.** Materials Science and Engineering, 1987, PP. 115-127.

118- B.R.Lake, F.J.Appl, and C.W.Bert. **An investigation of the hole drilling technigue for measuring planar residual stress in rectangulary orthotropic materials.** Experimental Mechanics, 1970, v:10 n:6 PP. 233-239.

119- *J.P.Sandifer, and G.E.Bowie.* **Residual stress by blind hole method with off centre hole.** Experimental Mechanics, 1978, v:18 n:5, PP. 173-179.

120- *G.S.Schajer.* **Application of finite element calculations to residual stress measurements.** Journal of Engineering Materials and Technology, 1981, v:103 PP. 157-163.

121- *S.Rendner, and C.C.Perry.* **Factors affecting the accuracy of residual stress measurements using the blind-hole drilling method.** Int. Conf. on Experimental Stress Analysis, 1982, Haifa, PP. 604-616.

122- *A.Ajovalasit.* **The influence of hole eccentricity on the calibration constants of rosettes used in hole-drilling method.** Int. Conf. on Experimental Stress Analysis, 1982, Haifa, PP. 591-601.

123- *J.M.Boag, M.T.Flaman, and J.A.Herring.* **Considerations of using the hole drilling method for measuring residual stresses in engineering components.** Proceedings of ASM's Conference on Residual Stress in Design, Ohio USA, 1987, PP. 1-6.

124- *G.S.Schajer.* **Measurement of non - uniform residual stresses using the hole drilling method.** Presented at ASME Mater Div publ MDV7 Advances in Mechanical behaviour and properties evaluations, 1988, USA.

125- **Determining residual stresses by the hole-drilling strain gauge method.** Published by ASTM Standard E 837-85.

126- *E.P.Popov.* **Mechanics of materials.** Published by Prentice-Hall Inc. ISBN: 0-13-571299-8

127- **Measurements of residual stresses by the hole-drilling strain gauge method.** Published by Measurements Group TECH NOT, TN-503-3.

128- *W.M.Wilson and C.C.Hao.* **Residual stresses in welded structures.** The Welding Journal, 1974, v:25 n:5, PP. 295s-320s.

129- *T.Yodahida, H.Onoue and Y.Kurihara.* **Study on stress on groove welded joint.** Journal of the Japan Welding Society, 1963, v:32 n:5, PP. 434-442.

130- *R.D.Stout.* **Weldability of steels.** Published by the Welding Research Council, 1987.

131- *J.E.M.Braid and J.A.Gianetto.* **The effects of PWHT on the toughness of shielded metal arc weld metals for use in Canadian offshore structure fabrication.**

International Conference on Welding, Toronto, Canada, 1985, PP. 145-157.

132- F.B.Pickering. **The metallurgical evaluation of stainless steels.** 1980, ISBN: 0-87170-077-8.

133- H.P.Lieurade. **Effect of residual stresses and stress ratio on the fatigue strength of welded components.** Welding In The World, 1988, v:26 n:7-8, PP. 158-187.

134- G.M.Evans. **Factors affecting the microstructure and properties of ferritic all-weld metal deposits.** Welding Research Abroad, v:37 n:2-3, 1991, PP.2-102.

135- O.C.Zienkiewicz. **The finite element method.** Published by McGraw-Hill, 1977. ISBN: 0-07-084072-5.

136- T.R.Chandrupatla and A.D.Belegundu. **Introduction to finite elements in engineering.** Published by Prentice-Hall International, 1991. ISBN: 0-13-481722-2

137- Y.K.Cheung and M.F.Yeo. **A practical introduction to finite element analysis.** Published by Pitman, 1979. ISBN: 0-273-01083-2.

138- D.R.J.Owen and E.Hinton. **Finite elements in plasticity.** Published by Pineridge Press Limited, 1980. ISBN: 0-906674-05-2.

139- Lusas User Manual. **Finite Element Analysis LTD. 1990.**

140- Mystro User Manual. **Finite Element Analysis LTD. 1990.**

141- Lusas Theory Manual. **Finite Element Analysis LTD. 1990.**

142- Metals Handbook. Published by ASM, v:1, 1990, ISBN: 0-87170-377-7.

APPENDIX-A

Specimen condition	distance from the welding line [mm]	σ_{max} [N/mm²]	σ_{min} [N/mm²]	Direction α[°]
Before PWHT	15	330	80	20
Before PWHT	25	200	30	15
Before PWHT	35	175	-15	18
Before PWHT	45	165	-55	22
Before PWHT	60	160	-66	26
Before PWHT	80	143	-20	14
After PWHT	15	91	30	12
After PWHT	25	72	10	20
After PWHT	35	50	-15	28
After PWHT	45	20	-20	16
After PWHT	60	10	-15	18
After PWHT	80	1	-10	24

RESIDUAL STRESSES MAGNITUDES AND THEIR DIRECTION FOR I-BEAM BOX-SECTION COMPONENT.

Specimen condition	distance from the welding line [mm]	σ_{max} [N/mm²]	σ_{min} [N/mm²]	Direction α[°]
Before PWHT	15	360	86	23
Before PWHT	35	241	3	18
Before PWHT	60	191	-58	22
Before PWHT	80	164	8	25
After PWHT-a	15	203	55	16
After PWHT-a	35	131	7	14
After PWHT-a	60	115	33	22
After PWHT-a	80	110	-44	20
After PWHT-b	15	95	18	28
After PWHT-b	35	35	-2	17
After PWHT-b	60	34	-19	24
After PWHT-b	80	35	-17	24
After PWHT-c	15	11	8	20
After PWHT-c	35	6	-5	26
After PWHT-c	60	-4	-6	29
After PWHT-c	80	0	-2	24
After PWHT-d	15	178	38	18
After PWHT-d	35	118	23	12
After PWHT-d	60	108	8	22
After PWHT-d	80	112	19	29

RESIDUAL STRESSES MAGNITUDES AND THEIR DIRECTION FOR DOUBLE-V AISI-1020 WELDED COMPONENT.

Specimen condition	distance from the welding line [mm]	σ_{max} [N/mm²]	σ_{min} [N/mm²]	Direction α[°]
After PWHT-e	15	193	46	10
After PWHT-e	35	91	14	14
After PWHT-e	60	86	-39	18
After PWHT-e	80	100	-55	13
After PWHT-g	15	220	65	27
After PWHT-g	35	122	-28	29
After PWHT-g	60	110	-75	25
After PWHT-g	80	100	-61	18
After PWHT-i	15	112	35	13
After PWHT-i	35	85	-11	18
After PWHT-i	60	68	-13	20
After PWHT-i	80	50	16	25
After PWHT-j	15	169	40	23
After PWHT-j	35	122	-2	16
After PWHT-j	60	93	-13	28
After PWHT-j	80	97	20	21
After PWHT-l	15	215	67	28
After PWHT-l	35	115	-19	20
After PWHT-l	60	87	-75	23
After PWHT-l	80	84	-80	26

RESIDUAL STRESSES MAGNITUDES AND THEIR DIRECTION FOR DOUBLE-V AISI-1020 WELDED COMPONENT.

Specimen condition	distance from the welding line [mm]	σ_{max} [N/mm²]	σ_{min} [N/mm²]	Direction α[°]
Before PWHT	15	221	42	29
Before PWHT	35	7	-80	26
Before PWHT	60	-35	-63	21
Before PWHT	80	-22	-52	20
After PWHT-1	15	110	49	24
After PWHT-1	35	34	-4	19
After PWHT-1	60	25	-20	25
After PWHT-1	80	20	11	21
After PWHT-2	15	61	25	21
After PWHT-2	35	-8	-32	12
After PWHT-2	60	-17	-34	22
After PWHT-2	80	-18	-25	19
After PWHT-3	15	0	0	0
After PWHT-3	35	0	0	0
After PWHT-3	60	0	0	0
After PWHT-3	80	0	0	0
After PWHT-4	15	106	30	30
After PWHT-4	35	-8	-35	21
After PWHT-4	60	-21	-27	18
After PWHT-4	80	-10	-15	24

RESIDUAL STRESSES MAGNITUDES AND THEIR DIRECTION FOR DOUBLE-V AISI-410 WELDED COMPONENT.

Specimen condition	distance from the welding line [mm]	σ_{max} [N/mm²]	σ_{min} [N/mm²]	Direction α[°]
After PWHT-5	15	112	42	22
After PWHT-5	35	30	-10	17
After PWHT-5	60	25	-20	23
After PWHT-5	80	26	8	15
After PWHT-7	15	121	54	28
After PWHT-7	35	64	-40	24
After PWHT-7	60	40	-2	19
After PWHT-7	80	47	18	22
After PWHT-9	15	65	35	24
After PWHT-9	35	35	25	21
After PWHT-9	60	32	12	16
After PWHT-9	80	25	9	27
After PWHT-10	15	72	30	28
After PWHT-10	35	-19	-41	20
After PWHT-10	60	7	-35	25
After PWHT-10	80	-13	-20	22
After PWHT-12	15	123	50	27
After PWHT-12	35	-28	-52	14
After PWHT-12	60	-37	-51	22
After PWHT-12	80	-17	-43	20

RESIDUAL STRESSES MAGNITUDES AND THEIR DIRECTION FOR DOUBLE-V AISI-410 WELDED COMPONENT.

Specimen condition	distance from the welding line [mm]	σ_{max} [N/mm²]	σ_{min} [N/mm²]	Direction α[°]
After PWHT-A1	15	33	12	21
After PWHT-A1	35	8	6	15
After PWHT-A1	60	3	-2	17
After PWHT-A1	80	-5	-4	20
After PWHT-A2	15	11	3	22
After PWHT-A2	35	6	2	19
After PWHT-A2	60	3	-2	24
After PWHT-A2	80	-5	-4	18
After PWHT-A3	15	30	11	19
After PWHT-A3	35	6	5	25
After PWHT-A3	60	-2	-3	20
After PWHT-A3	80	2	-5	24
After PWHT-A4	15	10	3	22
After PWHT-A4	35	4	2	16
After PWHT-A4	60	-2	0	23
After PWHT-A4	80	1	-2	22

RESIDUAL STRESSES MAGNITUDES AND THEIR DIRECTION FOR DOUBLE-V AISI-1020 WELDED COMPONENT (OPTIMIZATION).

Specimen condition	distance from the welding line [mm]	σ_{max} [N/mm²]	σ_{min} [N/mm²]	Direction α[°]
After PWHT-B1	15	31	10	24
After PWHT-B1	35	20	-5	20
After PWHT-B1	60	15	0	17
After PWHT-B1	80	10	2	26
After PWHT-B2	15	4	2	25
After PWHT-B2	35	2	0	30
After PWHT-B2	60	1	-2	24
After PWHT-B2	80	0	0	0
After PWHT-B3	15	26	8	22
After PWHT-B3	35	18	5	25
After PWHT-B3	60	10	-2	21
After PWHT-B3	80	5	0	24
After PWHT-B4	15	4	3	24
After PWHT-B4	35	2	1	10
After PWHT-B4	60	2	2	13
After PWHT-B4	80	1	0	15

RESIDUAL STRESSES MAGNITUDES AND THEIR DIRECTION FOR DOUBLE-V AISI-410 WELDED COMPONENT (OPTIMIZATION).

APPENDIX-B

PUBLICATIONS

1 - **A.G.Olabi and M.S.J.Hashmi,** *The effect of post weld heat treatment in weld repaired components of AISI 410 materials.* Proc. of Int. Conf. of Sheet Metal 1992, 7-9 April 1992, Birmingham, UK. PP. 63-72.

2 - **A.G.Olabi and M.S.J.Hashmi,** *The effect of post weld heat treatment on the mechanical properties and residual stresses mapping in welded structural steel.* Proc. of the 9th Conference of the Irish Manufacturing Committee, 2-4 Sep 1992, Dublin,Ireland. PP. 521-532.

3 - **A.G.Olabi and M.S.J.Hashmi,** *Effects of post weld heat treatment soaking temperature on mechanical properties and residual stresses for martensite stainless steel welded components.* Journal of Materials Processing Technology, v:38 n:1-2 1993, PP. 387-398.

4 - **A.G.Olabi and M.S.J.Hashmi,** *Review of methods for measuring residual stresses in components.* Published in 9th NCMR Conf., 7-9 Sep 1993, Bath, UK. PP. 336-340.

5 - **A.G.Olabi and M.S.J.Hashmi,** *Effects of PWHT (heating, cooling rates and duration) on martensite stainless steel welded component.* Submitted to Journal of Material Science.

6 - **A.G.Olabi and M.S.J.Hashmi,** *The microstructure and mechanical properties of low carbon steel welded components after the application of PWHTs.* Published in Int. Conf. AMPT'93, 24-27 Aug 1993, Dublin, Ireland. PP. 591-602.

7 - **A.G.Olabi and M.S.J.Hashmi,** *Stress relief procedures for low carbon steel (1020) welded components.* Published in Int. Conf. AMPT'93, 24-27 Aug 1993, Dublin, Ireland. PP. 1289-1300.

8 - **A.G.Olabi and M.S.J.Hashmi,** *The optimum condition for PWHT of welded structural steel component.* Published in IMC-10, 8-10 Sep 1993, Galway, Ireland. PP. 411-422.

9 - **A.G.Olabi and M.S.J.Hashmi,** *Optimization of post weld heat treatment conditions for martensite stainless steel welded component.* Accepted to be Published in Int. Conf. 7-10 March 1994, Adelaide, Australia.